

**Alma Mater Studiorum – Università di Bologna**

**DOTTORATO DI RICERCA IN  
CHIMICA**

**Ciclo XXIX**

**Settore Concorsuale di afferenza: 03/B1 – FONDAMENTI DELLE SCIENZE  
CHIMICHE E SISTEMI INORGANICI**

**Settore Scientifico disciplinare: AREA 03 – CHIM/03 CHIMICA GENERALE  
E INORGANICA**

**NICKEL-PHOSPHORUS  
HOMOLEPTIC CARBONYL CLUSTERS**

**Presentata da:  
Chiara Capacci**

**Coordinatore Dottorato:  
Prof. Aldo Roda**

**Relatore:  
Prof.ssa Maria Carmela Iapalucci**

**Co-Relatore:  
Prof.ssa Cristina Femoni**

**Esame finale anno 2017**



## Abstract

This project is focused on the synthesis, the characterisation, and the study of the reactivity of a novel group of carbonyl clusters - nickel-phosphorus homoleptic carbonyl clusters.

The interest in this couple of elements has risen because of their peculiar characteristics - in the past years nickel-phosphorus binary phases and nanoparticles have been widely used both as hydroprocessing catalysts and for their ceramic properties. In fact, by now nickel is the best transition metal to use in form of phosphide if a catalytic behaviour is expected. A further investigation on nickel-phosphorus molecular compounds could help in understanding how these materials operate.

The first part of the work concerns the syntheses of new nickel-phosphorus homoleptic carbonyl clusters, and their structural and spectroscopical characterisations. Several new species will be introduced, as  $[\text{Ni}_{11}\text{P}(\text{CO})_{18}]^{3-}$ ,  $[\text{Ni}_{14}\text{P}_2(\text{CO})_{22}]^{2-}$ ,  $[\text{Ni}_{23-x}\text{P}_2(\text{CO})_{30-x}]^{4-}$  ( $x = 0, 1$ ),  $[\text{Ni}_{23-x}\text{P}_2(\text{CO})_{30-x}]^{6-}$  ( $x = 0, 1$ ),  $[\text{HNi}_{31}\text{P}_4(\text{CO})_{39}]^{5-}$ ,  $[\text{H}_2\text{Ni}_{31}\text{P}_4(\text{CO})_{39}]^{4-}$ ,  $[\text{Ni}_{29}\text{P}_5(\text{PO})(\text{CO})_{36}]^{4-}$ ,  $[\text{Ni}_{39}\text{P}_3(\text{CO})_{39}]^{6-}$ .

The second part of the work examines the reactivity and the behaviour of the new nickel-phosphorus homoleptic carbonyl clusters. The species were tested regarding their possible redox properties, their acid-base properties, and their response towards various reactants, and the corresponding results will be reported.

Eventually, a further structural analysis will be proposed, which was specifically designed for the comparison of these new nickel-phosphorus homoleptic carbonyl clusters with other heteroatomical nickel clusters, as well as with other transition metal-phosphorus clusters.

The collected data will be used to draw some conclusions concerning the characteristics of this novel family of compounds, as well as their possible future applications.



<b>Table of contents</b>	p.
<b>Introduction</b>	1
<i>State-of-the-art</i>	3
<i>Bimetallic nickel carbonyl clusters</i>	4
<i>Heteroatomical nickel carbonyl clusters</i>	7
<i>Group-15 elements in nickel carbonyl clusters</i>	10
Group-15 elements in heteroleptic nickel carbonyl clusters	10
Group-15 elements in homoleptic nickel carbonyl clusters	14
<i>Expected results</i>	21
<b>Results and Discussions</b>	23
<b><i>Chapter One - Reaction conditions and modus operandi</i></b>	23
<i>Reaction parameters</i>	23
Nickel cluster precursor	23
Counter-ions	23
Reaction solvents	24
Phosphorus reactants	25
<i>Further considerations and preventive measures</i>	26
<i>General modus operandi</i>	28
<b><i>Chapter Two - [Ni<sub>11</sub>P(CO)<sub>18</sub>]<sup>3-</sup></i></b>	34
<i>Synthetic approach and further considerations</i>	34
<i>Structural, spectroscopic, and spectrometric characterisations</i>	37
Structural characterisation	37
Spectroscopic and spectrometric characterisation	39
<i>Reactivity test</i>	43
<b><i>Chapter Three - [HNi<sub>31</sub>P<sub>4</sub>(CO)<sub>39</sub>]<sup>5-</sup> and [H<sub>2</sub>Ni<sub>31</sub>P<sub>4</sub>(CO)<sub>39</sub>]<sup>4-</sup></i></b>	47
<i>Synthetic approach and further considerations</i>	47

Table of contents

[H <sub>3</sub> Ni <sub>31</sub> P <sub>4</sub> (CO) <sub>39</sub> ] <sup>5-</sup> - penta-anionic form	47
[H <sub>2</sub> Ni <sub>31</sub> P <sub>4</sub> (CO) <sub>39</sub> ] <sup>4+</sup> - tetra-anionic form	50
<i>Structural, spectroscopic, and spectrometric characterisations</i>	51
Structural characterisation - premises	51
Structural characterisation of the penta-anion (symmetrical structures)	52
Structural characterisation of the penta-anion (non-symmetrical structure)	57
Structural characterisation of the tetra-anion	61
Spectroscopic and spectrometric characterisation	64
<i>Reactivity tests</i>	69
Reduction and oxidation	69
Deprotonation and protonation	74
Controlled decompositions	76
<i>Hydride nature of [H<sub>3</sub>Ni<sub>31</sub>P<sub>4</sub>(CO)<sub>39</sub>]<sup>5-</sup> and [H<sub>2</sub>Ni<sub>31</sub>P<sub>4</sub>(CO)<sub>39</sub>]<sup>4+</sup></i>	79
<b>Chapter Four - [Ni<sub>14</sub>P<sub>2</sub>(CO)<sub>22</sub>]<sup>2-</sup></b>	82
<i>Synthetic approach and further considerations</i>	82
<i>Structural, spectroscopic, and spectrometric characterisations</i>	84
Structural characterisation	84
Spectroscopic and spectrometric characterisation	86
<i>Reactivity tests</i>	90
Reduction and oxidation	90
Deprotonation and protonation	91
Controlled decompositions	92
<b>Chapter Five - [Ni<sub>23-x</sub>P<sub>2</sub>(CO)<sub>30-x</sub>]<sup>4-</sup> and [Ni<sub>23-x</sub>P<sub>2</sub>(CO)<sub>30-x</sub>]<sup>6-</sup> (x = 0, 1)</b>	95
<i>Synthetic approach and further considerations</i>	95
[Ni <sub>23-x</sub> P <sub>2</sub> (CO) <sub>30-x</sub> ] <sup>4-</sup> (x = 0, 1) - tetra-anionic form	95
[Ni <sub>23-x</sub> P <sub>2</sub> (CO) <sub>30-x</sub> ] <sup>6-</sup> (x = 0, 1) - hexa-anionic form	98
<i>Structural, spectroscopic, and spectrometric characterisations</i>	99
Structural characterisation of the tetra-anion	100
Structural characterisation of the hexa-anion	104
Spectroscopic and spectrometric characterisation	107

<i>Reactivity tests</i>	111
Reduction and oxidation	111
Controlled decompositions	114
<b><i>Chapter Six - Other nickel-phosphorus carbonyl clusters</i></b>	117
<b><i>[Ni<sub>29</sub>P<sub>5</sub>(PO)(CO)<sub>36</sub>]<sup>4-</sup></i></b>	118
<i>Synthesis</i>	118
<i>Structural characterisation</i>	119
<b><i>[Ni<sub>39</sub>P<sub>3</sub>(CO)<sub>44</sub>]<sup>6-</sup></i></b>	124
<i>Synthesis</i>	124
<i>Structural characterisation</i>	125
<b><i>Chapter Seven - Structural analyses and comparisons</i></b>	129
<i>Phosphorus-hosting cavities</i>	130
Ten-membered nickel cages - Ni <sub>10</sub> (μ <sub>10</sub> -P)	130
Nine-membered nickel cages - Ni <sub>9</sub> (μ <sub>9</sub> -P)	134
Closed nine-membered nickel cages	134
Open nine-membered nickel cages	138
Twelve-membered nickel cages - Ni <sub>12</sub> (μ <sub>12</sub> -P)	143
<i>Nickel-hosting cavities</i>	146
Fourteen-membered heteroatomical cages	148
Fourteen-membered heteroatomical cages - Ni <sub>11</sub> P <sub>3</sub> (μ <sub>14</sub> -Ni)	148
Fourteen-membered heteroatomical cages - Ni <sub>12</sub> P <sub>2</sub> (μ <sub>14</sub> -Ni), Ni <sub>10</sub> P <sub>3</sub> (μ <sub>13</sub> -Ni)	153
Fourteen-membered heteroatomical cages - Ni <sub>8</sub> P <sub>6</sub> (μ <sub>14</sub> -Ni)	157
Twelve-membered heteroatomical cages - Ni <sub>10</sub> P <sub>2</sub> (μ <sub>12</sub> -P)	159
<i>Elongations</i>	163
Elongation in phosphorus-hosting cavities	163
Elongation in nickel-hosting cavities	167
<b><i>Chapter Eight - Comparisons with other structures</i></b>	172
<i>Comparison with other heteroatomical nickel structures</i>	172

Heteroatom-centred nickel icosahedra	173
Heteroatomical icosahedra	176
$[\text{Ni}_{131}\text{Sb}_4(\text{CO})_{40}]^{6-}$ - sub-structures	183
<i>Comparison with other heteroatomical transition metals structures</i>	191
Squared anti-prismatic metallic cages	192
<i>Comparison with nickel-phosphorus binary phases</i>	198
Coordination polyhedra of LT- $\text{Ni}_5\text{P}_2$ and HT- $\text{Ni}_5\text{P}_2$	199
<b>Summary and conclusions</b>	201
<b>Summary</b>	201
<i>Syntheses</i>	201
<i>Nuclearities</i>	203
<i>Structural characteristics</i>	206
<i>Reactivity</i>	208
$[\text{Ni}_{11}\text{P}(\text{CO})_{18}]^{3-}$	210
$[\text{HNi}_{31}\text{P}_4(\text{CO})_{39}]^{5-}$	211
$[\text{Ni}_{14}\text{P}_2(\text{CO})_{22}]^{2-}$	213
$[\text{Ni}_{23-x}\text{P}_2(\text{CO})_{30-x}]^{4-}$ (x = 0, 1)	214
<b>Conclusions</b>	215
<b>Experimental section</b>	225
<i>Synthesis of <math>[\text{NEt}_4]_2[\text{Ni}_6(\text{CO})_{12}]</math></i>	226
<i>Synthesis of <math>[\text{NEt}_4]_3[\text{Ni}_{11}\text{P}(\text{CO})_{18}]</math></i>	227
<i>Synthesis of <math>[\text{NEt}_4]_5[\text{HNi}_{31}\text{P}_4(\text{CO})_{39}]</math></i>	228
<i>Synthesis of <math>[\text{NEt}_4]_4[\text{H}_2\text{Ni}_{31}\text{P}_4(\text{CO})_{39}]</math></i>	230
<i>Synthesis of <math>[\text{NBu}_4]_2[\text{Ni}_{14}\text{P}_2(\text{CO})_{22}]</math></i>	231
<i>Synthesis of <math>[\text{NEt}_4]_4[\text{Ni}_{23-x}\text{P}_2(\text{CO})_{30-x}]</math> (x = 0, 1)</i>	232
<i>Synthesis of <math>[\text{NEt}_4]_6[\text{Ni}_{23-x}\text{P}_2(\text{CO})_{30-x}]</math> (x = 0, 1)</i>	233



<i>Synthesis of [NEt<sub>4</sub>]<sub>4</sub>[Ni<sub>29</sub>P<sub>5</sub>(PO)(CO)<sub>36</sub>]</i>	234
<i>Synthesis of [NEt<sub>4</sub>]<sub>6</sub>[Ni<sub>39</sub>P<sub>3</sub>(CO)<sub>44</sub>]</i>	236



# Introduction

The aim of this work is to explore the chemistry of nickel and phosphorus in new heteroatomical molecular compounds: nickel-phosphorus homoleptic carbonyl clusters.

The interest in this couple of elements has risen because of their characteristics - in the past years nickel-phosphorus binary phases and nanoparticles have been widely used both as catalysts and for their ceramic properties.

Transition metal phosphides represent a new class of hydroprocessing catalysts, which have emerged as a promising group of high-activity, stable catalysts.<sup>1</sup> These phosphides have physical properties resembling those of ceramic materials, so are strong and hard, yet retain electronic and magnetic properties similar to those of metals.<sup>2</sup> Their crystal structures are based on trigonal prisms, yet they do not form layered structures. A further investigation could help in understanding how these materials operate.

Many metals form phosphides, and most are useful catalysts. It has been demonstrated that  $\text{MoP} < \text{WP} < \text{Fe}_2\text{P} < \text{Co}_2\text{P} < \text{Ni}_2\text{P}$  in terms of turn-over frequencies in hydrodeoxygenation reactions.<sup>3</sup> Also, the trend of catalytic activity for hydrodenitrogenation and hydrodesulfurization is  $\text{Fe}_2\text{P} < \text{CoP} < \text{MoP} < \text{WP} < \text{Ni}_2\text{P}$ .<sup>4</sup> So, to date nickel is the best transition metal to use in form of phosphide if a catalytic behaviour is expected.

Unfortunately, the nickel-phosphorus binary system is highly complex (Figure 0.1). Nickel tend to form a large number of phosphides, whose compositions are just trivially different -  $\text{Ni}_3\text{P}$ ,  $\text{Ni}_5\text{P}_2$ ,  $\text{Ni}_{12}\text{P}_5$ ,  $\text{Ni}_2\text{P}$ ,  $\text{Ni}_5\text{P}_4$ ,  $\text{NiP}$ ,  $\text{NiP}_2$ , and  $\text{NiP}_3$ .<sup>5,6</sup>

---

<sup>1</sup> R. Prins, M. E. Bussell; *Catal. Lett.*, **2012** (142) 1413-1436

<sup>2</sup> A. B. Hernandez, H. Ariga, S. Takakusagi, K. Kinoshita, S. Suzuki, S. Otani, S. T. Oyama, K. Asakura; *Chemical Physics Letters*, **2011** (513) 48-52

<sup>3</sup> H.Y. Zhaoa, D. Lia, P. Buia, S.T. Oyama; *Applied Catalysis A: General*, **2011** (391) 305-310

<sup>4</sup> S.T. Oyama; *Journal of Catalysis*, **2003** (216) 343-352

<sup>5</sup> H. Okamoto; *Journal of Phase Equilibria and Diffusion*, **2010** (31) 200-201

<sup>6</sup> C. Schmetterer, J. Vizdal, H. Ipser; *Intermetallics*, **2009** (17) 826-834

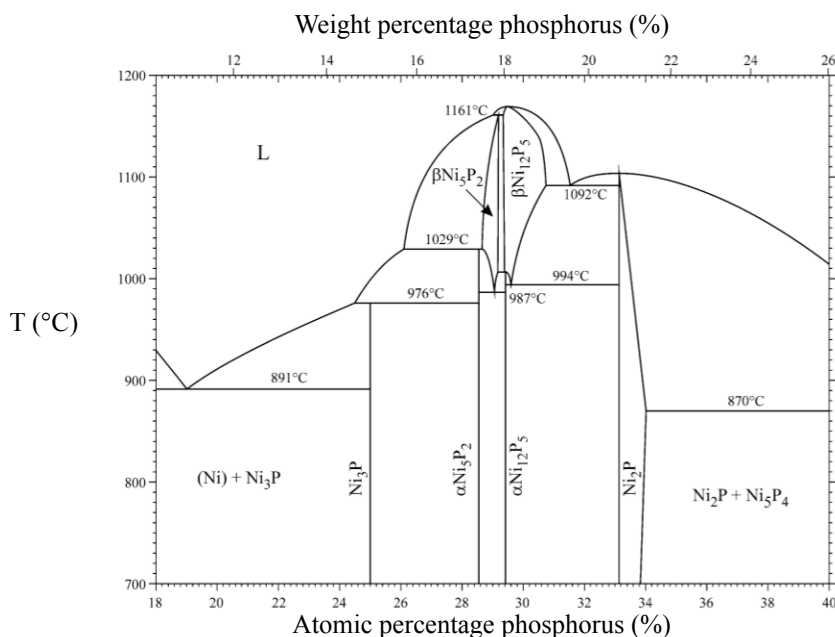


Figure 0.1 - Phase diagram for the nickel-phosphorus binary system. The diagram is a clear indication of the complexity of the system, even at low percentages of phosphorus.

Moreover, only few nickel-phosphorus phases have been structurally characterized, such as  $\text{Ni}_5\text{P}_2$ ,<sup>1, 2</sup>  $\text{Ni}_5\text{P}_4$ ,<sup>3</sup> and  $\text{Ni}_2\text{P}$ .<sup>4</sup> For instance, in  $\text{Ni}_5\text{P}_4$  the phosphorus atoms display four different types of connectivity, and are inside heteroatomical cages.  $\text{Ni}_5\text{P}_2$  has two structures and exists both as LT- $\text{Ni}_5\text{P}_2$  and HT- $\text{Ni}_5\text{P}_2$  - low and high temperature, respectively. Both display only three different coordination sites available for the phosphorus. In the former phase, one site is octahedral whilst the other two are bi-capped distorted anti-prisms - tetragonal or triangular (Figure 0.2). In the latter phase there is more homogeneity, as all the phosphorus atoms are inside bi-capped tetragonal prismatic cages (coordination number equal to ten). However, both in LT- $\text{Ni}_5\text{P}_2$  and HT- $\text{Ni}_5\text{P}_2$  there are no direct phosphorus-phosphorus interactions.

These information are not exhaustive, and a further structural characterization for nickel and phosphorus molecular compounds would be useful to better under-

- <sup>1</sup> S. Oryshchyn, V. Babizhetskyy, S. Chykhriy, L. Aksel'rud, S. Stoyko, J. Bauer, R. Guérin, Yu. Kuz'ma; *Inorganic Materials*, **2004** (40) 380-385
- <sup>2</sup> S. Oryshchyn, V. Babizhetskyy, O. Zhak, S. Stoyko, R. Guérin, A. Simon; *Intermetallics*, **2011** (19) 1041-1046
- <sup>3</sup> V. Babizhetskyy, B. Kotur, S. Oryshchyn, C. Zheng, F. Kneidinger, L. Leber, C. Simson, E. Bauer, H. Michor; *Solid State Communications*, **2013** (164) 1-5
- <sup>4</sup> S. Rundqvist; *Acta Chem. Scand.*, **1962** (16) 992-998

stand the mechanism with which these materials operate as catalysts.

Since nickel-phosphorus homoleptic carbonyl clusters have never been reported in the scientific literature so far, this work focused on the synthesis, the characterization, and the study of the reactivity of this new family of heteroatomical molecular compounds.

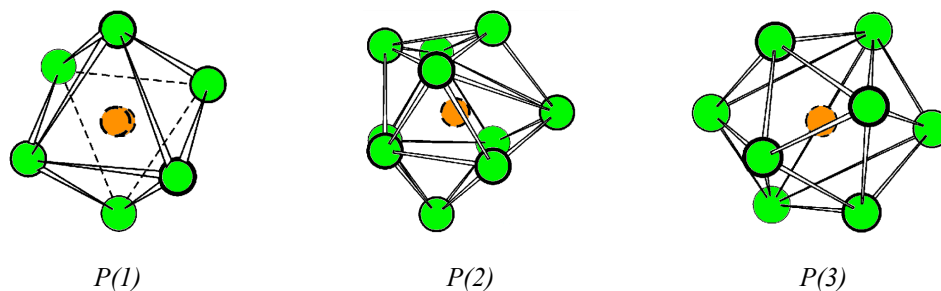


Figure 0.2 - Graphical representation of the three coordination polyhedra of phosphorus atoms in  $LT-Ni_5P_2$ . P(1) is inside an octahedral polyhedron. P(2) is inside a bi-capped tetragonal anti-prism. P(3) is inside a bi-capped triangular anti-prism. Nickel atoms are represented in green, phosphorus atoms in orange.

## State-of-the-art

Transition metal carbonyl clusters represent a vast family of compounds that can have a very wide set of characteristics.

In particular, nickel carbonyl clusters represent a large group of molecular compounds whose characteristics are very interesting.

For example, homometallic nickel carbonyl clusters can grow up to a nuclearity only equal to twelve - as in  $[H_{4-n}Ni_{12}(CO)_{21}]^{n-}$  ( $n = 2, 3, 4$ )<sup>1</sup> - but bimetallic and heteroatomical nickel cluster compounds can display higher nuclearities - as in  $[H_{6-n}Ni_{38}Pt_6(CO)_{48}]^{n-}$  ( $n = 4, 5, 6$ ),<sup>2, 3</sup>  $[Ag_{16}Ni_{24}(CO)_{40}]^{4-}$ ,<sup>4</sup>  $[HNi_{38}C_6(CO)_{42}]^{5-}$ ,<sup>5</sup> and

<sup>1</sup> A. Ceriotti, P. Chini, R. Della Pergola, G. Longoni; *Inorg. Chem.*, **1983** (22) 1595-1598

<sup>2</sup> A. Ceriotti, F. Dermartin, G. Longoni, M. Manassero, M. Marchionna, G. Piva, M. Sansoni; *Angew. Chem. Int. Ed. Engl.*, **1985** (24) 697-698

<sup>3</sup> F. Fabrizi de Biani, C. Femoni, M. C. Iapalucci, G. Longoni, P. Zanello, A. Ceriotti; *Inorg. Chem.*, **1999** (38) 3721-3724

<sup>4</sup> J. Zhang, L. F. Dahl; *J. Chem. Soc., Dalton Trans.*, **2002** (7) 1269-1274

<sup>5</sup> A. Ceriotti, A. Fait, G. Longoni, G. Piro; *J. Am. Chem. Soc.*, **1986** (108) 8091-8092

$[\text{H}_{6-n}\text{Ni}_{30}\text{C}_4(\text{CO})_{34}(\text{CdCl})_2]^{n-}$  ( $n = 3, 4, 5, 6$ ).<sup>1</sup> This behaviour is caused by the electron-rich nature of nickel, and also by its high affinity towards the carbonyl ligands.

If both these aspects are considered at once, it is possible to understand the behaviour of nickel in carbonyl cluster. On one hand nickel atoms tend to form the highest possible number of bonds - in order to delocalise the high electron density of the metal. On the other hand, each nickel atom strives for the highest number of carbonyl interactions. Therefore, homometallic nickel clusters have never been observed to grow up into high-nuclearity species - twelve is the threshold at which both metal-metal and metal-ligand interactions are concurrently maximised.

The presence of other elements, metallic or not, can overcome the lack of growth concerning homometallic nickel structures.

In bimetallic clusters it is possible to observe close-packed structures in the metallic skeletons of high-nuclearity compounds. For instance, this happens in many nickel-palladium<sup>2</sup> and nickel-platinum<sup>3</sup> carbonyl clusters. Also high-nuclearity nickel-carbide<sup>4</sup> carbonyl compounds have been reported, though not with close-packed structures.

### ***Bimetallic nickel carbonyl clusters***

In nickel-palladium compounds, it is possible to observe the synergy between two metals whose behaviour towards the carbonyl ligands is quite different. As aforementioned, the lighter metal has a high affinity towards the carbon monoxide, while the heavier presents a scarce tendency in bonding with the same ligand.<sup>5</sup> Thus, bimetallic nickel-palladium carbonyl clusters usually display close-

---

<sup>1</sup> A. Bernardi, C. Femoni, M. C. Iapalucci, G. Longoni, F. Ranuzzi, S. Zacchini, P. Zanello, S. Fedi; *Chem. Eur. J.*, **2008** (14) 1924-1934

<sup>2</sup> N. T. Tran, M. Kawano, D. R. Powell, L. F. Dahl; *J. Chem. Soc., Dalton Trans.*, **2000** (22) 4138-4144

<sup>3</sup> C. Femoni, M. C. Iapalucci, G. Longoni, P. H. Svensson; *Chem. Commun.*, **2001** (18) 1776-1777

<sup>4</sup> A. Bernardi, C. Femoni, M. C. Iapalucci, G. Longoni, F. Ranuzzi, S. Zacchini, P. Zanello, S. Fedi; *Chem. Eur. J.*, **2008** (14) 1924-1934

<sup>5</sup> N. T. Tran, M. Kawano, D. R. Powell, R. K. Hayashi, C. F. Campana, L. F. Dahl; *J. Am. Chem. Soc.*, **1999** (121) 5945-5952

packed structures, with a palladium core surrounded by nickel and further palladium atoms.

Some examples are  $[\text{Pd}_{33}\text{Ni}_9(\text{CO})_{41}(\text{PPh}_3)_6]^+$ ,<sup>1</sup>  $[\text{Pd}_{16}\text{Ni}_4(\text{CO})_{22}(\text{PPh}_3)_4]^{2-}$ ,<sup>2</sup>  $[\text{Ni}_{16}\text{Pd}_{16}(\text{CO})_{40}]^+$  and  $[\text{Ni}_{26}\text{Pd}_{20}(\text{CO})_{54}]^{6-}$ .<sup>3</sup> Their segregate structures (Figure 0.3) are clear examples of the synergy between the palladium lower affinity and the nickel higher affinity towards the carbonyl ligands.

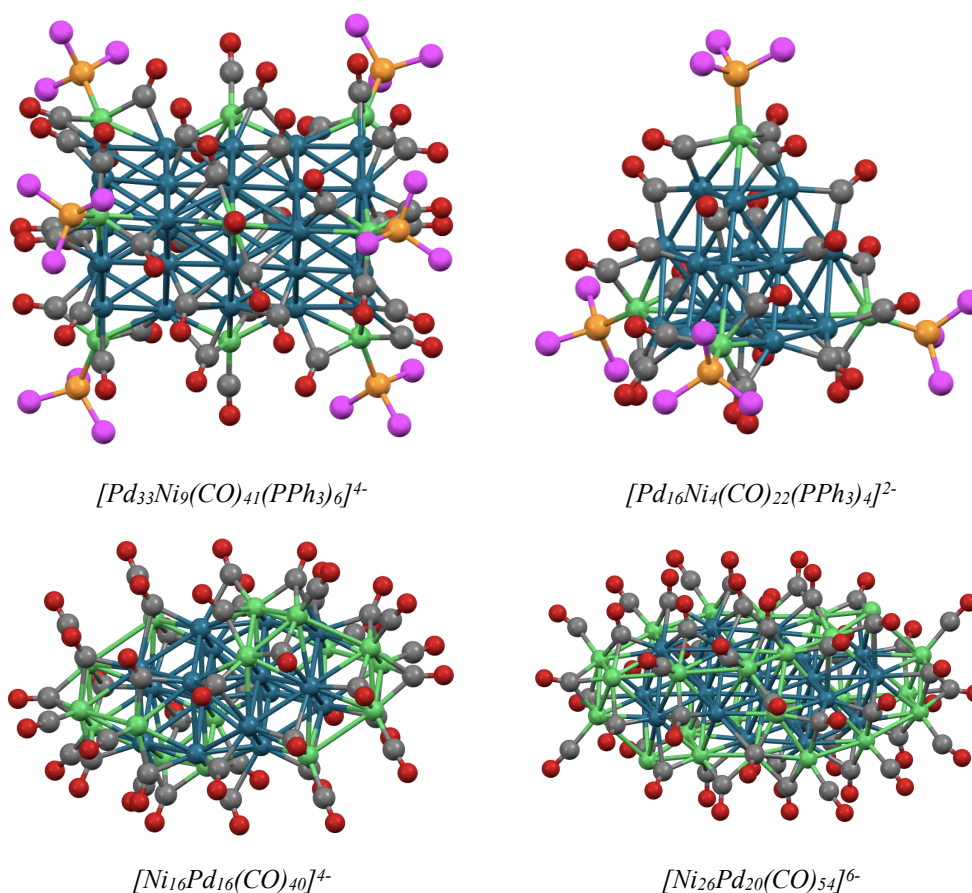


Figure 0.3 - Molecular structures of nickel-palladium clusters,  $[\text{Pd}_{33}\text{Ni}_9(\text{CO})_{41}(\text{PPh}_3)_6]^+$ ,  $[\text{Pd}_{16}\text{Ni}_4(\text{CO})_{22}(\text{PPh}_3)_4]^{2-}$ ,  $[\text{Ni}_{16}\text{Pd}_{16}(\text{CO})_{40}]^+$ , and  $[\text{Ni}_{26}\text{Pd}_{20}(\text{CO})_{54}]^{6-}$ . In these clusters it is possible to notice that nickel atoms are always on the surface of the metallic skeletons. Nickel atoms are represented in green, palladium atoms in blue, phosphorus atoms in orange, carbon atoms in grey, oxygen atoms in red. For clarity purposes, phenyl groups are represented as single magenta atoms.

- 
- <sup>1</sup> M. Kawano, J. W. Bacon, C. F. Campana, L. F. Dahl; *J. Am. Chem. Soc.*, **1996** (118) 7869-7870
  - <sup>2</sup> M. Kawano, J. W. Bacon, C. F. Campana, B. E. Winger, J. D. Dudek, S. A. Sirchio, S. L. Scruggs, U. Geiser, L. F. Dahl; *Inorg. Chem.*, **2001** (40) 2554-2569
  - <sup>3</sup> C. Femoni, M. C. Iapalucci, G. Longoni, P. H. Svensson, J. Wolowska; *Angew. Chem. Int. Ed.*, **2000** (39) 1635-1637

In some nickel-platinum clusters the segregation of the third-period transition metal is more evident (Figure 0.4). In  $[\text{Ni}_{136}\text{Pt}_4(\text{CO})_{45}]^{6-}$  and  $[\text{Ni}_{137}\text{Pt}_4(\text{CO})_{46}]^{6-}$ ,<sup>1,2</sup> as well as in  $[\text{H}_{6-n}\text{Ni}_{138}\text{Pt}_6(\text{CO})_{48}]^{n-}$  ( $n = 4, 5, 6$ ),<sup>3</sup> the platinum atoms respectively form a tetrahedron or a triangular anti-prism, which are entirely surrounded by nickel atoms. In these nickel-platinum bimetallic compounds the carbonyl ligands are exclusively coordinated to nickel atoms.

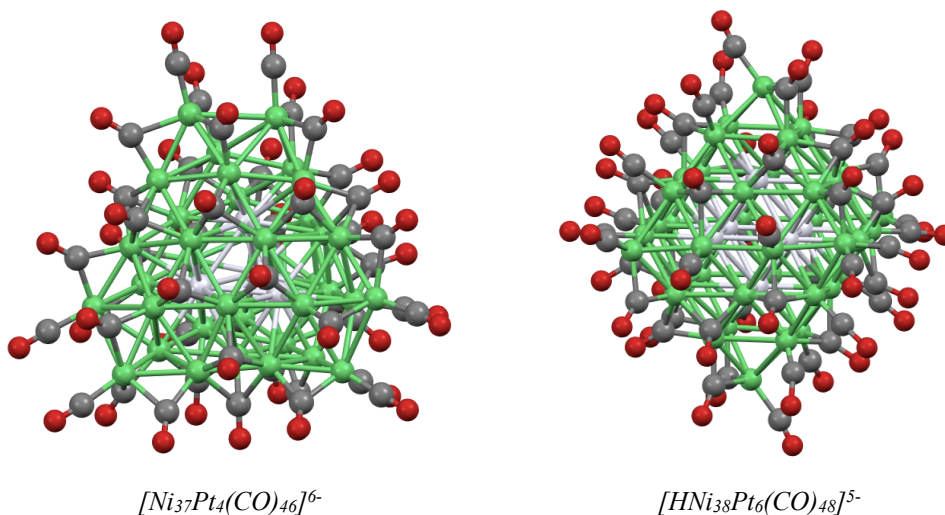


Figure 0.4 - Molecular structures of segregated nickel-platinum clusters,  $[\text{Ni}_{37}\text{Pt}_4(\text{CO})_{46}]^{6-}$  and  $[\text{HNi}_{38}\text{Pt}_6(\text{CO})_{48}]^{5-}$ . The platinum atoms constitute the core of the metallic skeleton. Nickel atoms are represented in green, platinum atoms in white, carbon atoms in grey, oxygen atoms in red.

However, there are also examples in which the platinum atoms are located on the cluster surface (Figure 0.5), as in  $[\text{Ni}_{135}\text{Pt}_9(\text{CO})_{48}]^{6-}$ ,<sup>4</sup>  $[\text{Ni}_{24}\text{Pt}_{14}(\text{CO})_{44}]^4$ ,  $[\text{Ni}_{14}\text{Pt}_{10}(\text{CO})_{30}]^4$ ,<sup>5</sup>  $[\text{HNi}_{24}\text{Pt}_{17}(\text{CO})_{46}]^{5-}$ , and  $[\text{Ni}_{32}\text{Pt}_{24}(\text{CO})_{56}]^{6-}$ .<sup>6</sup> Interestingly, the former also established a first structural similarity between nickel-platinum and nickel-palladium carbonyl clusters, compared to  $[\text{Ni}_{36}\text{Pd}_8(\text{CO})_{48}]^{6-}$ .

<sup>1</sup> F. Demartin, C. Femoni, M. C. Iapalucci, G. Longoni, P. Macchi; *Angew. Chem. Int. Ed.*, **1999** (38) 531-533

<sup>2</sup> F. Demartin, F. Fabrizi de Biani, C. Femoni, M. C. Iapalucci, G. Longoni, P. Macchi, P. Zanello; *Journal of Cluster Science*, **2001** (12) 61-74

<sup>3</sup> A. Ceriotti, F. Demartin, G. Longoni, M. Manassero, M. Marchionna, G. Piva, M. Sansoni; *Angew. Chem. Int. Ed. Engl.*, **1985** (24) 697-698

<sup>4</sup> C. Femoni, M. C. Iapalucci, G. Longoni, P. H. Svensson, P. Zanello, F. Fabrizi de Biani; *Chem. Eur. J.*, **2004** (10) 2318-2326

<sup>5</sup> C. Femoni, M. C. Iapalucci, G. Longoni, P. H. Svensson; *Chem. Commun.*, **2001** (18) 1776-1777

<sup>6</sup> C. Femoni, M. C. Iapalucci, G. Longoni, P. H. Svensson; *Chem. Commun.*, **2004** (20) 2274-2275



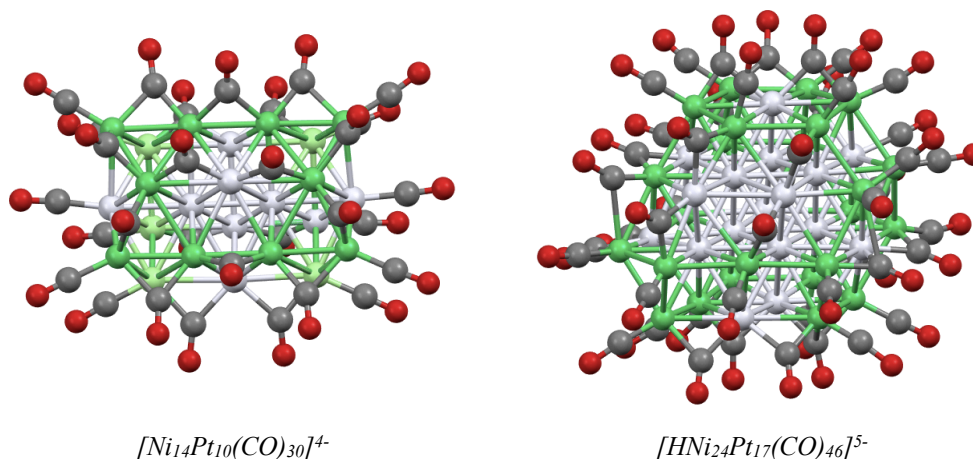


Figure 0.5 - Molecular structures of non-segregated nickel-platinum clusters,  $[Ni_{14}Pt_{10}(CO)_{30}]^{4+}$  and  $[HNi_{24}Pt_{17}(CO)_{46}]^{5-}$ . The platinum atoms are in interstitial as well as in superficial sites. Nickel atoms are represented in green, platinum atoms in white, the disordered nickel or platinum atoms of  $[Ni_{14}Pt_{10}(CO)_{30}]^{4+}$  in light green, carbon atoms in grey, and oxygen atoms in red.

### ***Heteroatomical nickel carbonyl clusters***

In presence of *p*-block elements, close-packed metal-frames are no longer common and the nickel atoms tend to form prismatic structures. Due to this, in these cases the nickel carbonyl clusters usually display a nuclearity comparable to that of homometallic nickel clusters.

Nonetheless, heteroatomical nickel compounds can sometimes grow into high-nuclearity structures, as nickel-carbides clusters do. Interestingly, this non-metallic element confers a high degree of variability to the overall structures, and it is possible to observe both low-nuclearity and high-nuclearity species belonging to this family of compounds (Figure 0.6).

For instance,  $[Ni_8C(CO)_{16}]^{2-}$  and  $[Ni_9C(CO)_{17}]^{2-}$ <sup>1</sup> display a low-nuclearity, and their non-complex metal cages are prismatic. However, there is plenty of known high-nuclearity compounds, as for example  $[Ni_{35}C_4(CO)_{39}]^{6-}$ ,  $[H_{6-n}Ni_{34}C_4(CO)_{38}]^{n-}$  (*n* = 6, 5),<sup>2</sup>  $[Ni_{32}C_6(CO)_{36}]^{6-}$  and  $[HNi_{38}C_6(CO)_{42}]^{5-}$ .<sup>3</sup> In these clusters it is possible

<sup>1</sup> A. Ceriotti, G. Longoni, M. Perego, M. Manassero, M. Sansoni; *Inorg. Chem.*, **1985** (24) 117-120

<sup>2</sup> A. Ceriotti, A. Fait, G. Longoni, G. Piro, L. Resconi; *J. Am. Chem. Soc.*, **1986** (108) 5370-5371

<sup>3</sup> F. Calderoni, F. Demartin, F. Fabrizi de Biani, C. Femoni, M. C. Iapalucci, G. Longoni, P. Zanello; *Eur. J. Inorg. Chem.*, **1999** (4) 663-671

to observe that the prismatic sub-units can be fused with each other, forming more elaborate, non-packed metal cages.

A similar behaviour can be observed in nickel-acetylides clusters, that generally are medium-nuclearity species (Figure 0.6). Few examples are  $[\text{Ni}_{16}(\text{C}_2)_2(\text{CO})_{23}]^{4-}$ ,<sup>1</sup>  $[\text{Ni}_{17}(\text{C}_2)_2(\text{CO})_{24}]^{4-}$ ,<sup>2</sup> and  $[\text{HNi}_{25}(\text{C}_2)_4(\text{CO})_{32}]^{3-}$ ,<sup>3</sup> whose apparently misshapen structures can be related to a squared orthobicupola (Johnson solid J28).<sup>4</sup>

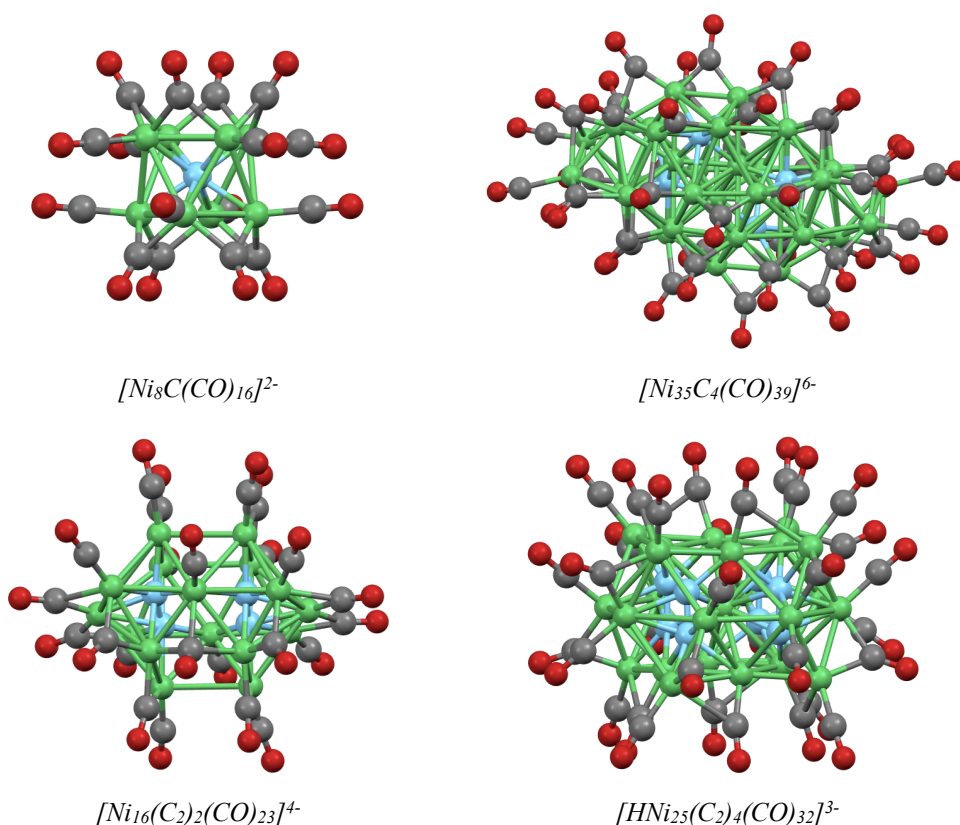


Figure 0.6 - Molecular structures of nickel-carbide and nickel-acetylide clusters,  $[\text{Ni}_8\text{C}(\text{CO})_{16}]^{2-}$ ,  $[\text{Ni}_{35}\text{C}_4(\text{CO})_{39}]^{6-}$ ,  $[\text{Ni}_{16}(\text{C}_2)_2(\text{CO})_{23}]^{4-}$ , and  $[\text{HNi}_{25}(\text{C}_2)_4(\text{CO})_{32}]^{3-}$ . They respectively display low, high, and medium nuclearities. Nickel atoms are represented in green, carbon atoms in grey, and oxygen atoms in red. For clarity purposes, carbide atoms and acetylide groups are represented in light blue.

<sup>1</sup> A. Ceriotti, G. Longoni, M. Manassero, N. Masciocchi, G. Piro, L. Resconi, M. Sansoni; *Chem. Commun.*, **1985** (20) 1402-1403

<sup>2</sup> C. Femoni, M. C. Iapalucci, G. Longoni, S. Zacchini, S. Fedi, F. Fabrizi de Biani; *Dalton Trans.*, **2012** (41) 4649-4663

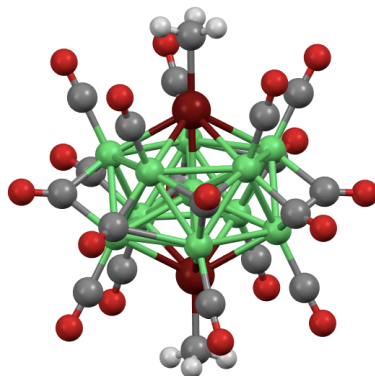
<sup>3</sup> C. Femoni, M. C. Iapalucci, G. Longoni, S. Zacchini; *Chem. Commun.*, **2008** (27) 3157-3159

<sup>4</sup> N. W. Johnson; *Canad. J. Math.*, **1966** (18) 169-200

Still, nickel-carbides and nickel-acetylides carbonyl clusters represent a minority, and it is possible to say that most heteroatomical nickel carbonyl clusters display low-nuclearity metal cages.

Nickel and *p*-block elements clusters usually adopt recurring structures, for what concerns both their geometry and their ligand coordination. The majority of these compounds is icosahedral,<sup>1</sup> or has a structure that can be related to an icosahedron. Fitting in this group there are several nickel carbonyl clusters with elements belonging to group-14, group-15, and group-16.

Moving along the tetragens group (*i.e.* group-14) there are scarce examples of nickel carbonyl clusters. Few nickel-germanium or nickel-tin species are reported in the literature - *e.g.*  $[\text{Ni}_{11}(\text{SnMe})_2(\text{CO})_{18}]^{2-}$ ,<sup>2</sup>  $[\text{Ni}_{12}\text{Sn}(\text{CO})_{22}]^{2-}$ ,  $[\text{Ni}_{12}\text{Ge}(\text{CO})_{22}]^{2-}$ , and  $[\text{Ni}_{10}\text{Ge}(\text{CO})_{20}]^{2-}$ .<sup>3</sup> The same remarks also applies to nickel-chalcogens (*i.e.* group-16) compounds, as  $[\text{Ni}_{11}\text{Se}_2(\text{CO})_{18}]^{2-}$  and  $[\text{Ni}_{10}\text{Te}_3(\text{CO})_{15}]^{2-}$ .<sup>4</sup> Still, all these cluster compounds display centred icosahedral structure (Figure 0.7), or relatable structures.



$[\text{Ni}_{11}(\text{SnMe})_2(\text{CO})_{18}]^{2-}$

Figure 0.7 - Molecular structure of an icosahedral nickel-tin cluster,  $[\text{Ni}_{11}(\text{SnMe})_2(\text{CO})_{18}]^{2-}$ . The heteroatoms are in apical positions, and each is coordinated to a stabilising methyl ligand. Nickel atoms are represented in green, tin atoms in maroon, carbon atoms in grey, oxygen atoms in red, hydrogen atoms in light grey.

- 
- <sup>1</sup> G. Longoni; *Pure & Appl. Chem.*, **1990** (62) 1183-1186
  - <sup>2</sup> J. P. Zebrowski, R. K. Hayashi, L. F. Dahl; *J. Am. Chem. Soc.*, **1993** (115) 1143-1144
  - <sup>3</sup> A. Ceriotti, F. Demartin, B. T. Heaton, P. Ingallina, G. Longoni, M. Manassero, M. Marchionna, N. Masciocchi; *J. Chem. Soc., Chem. Commun.*, **1989** (12) 786-787
  - <sup>4</sup> A. J. Kahaian, J. B. Thoden, L. F. Dahl; *J. Chem. Soc., Chem. Commun.*, **1992** (4) 353-355

## ***Group-15 elements in nickel carbonyl clusters***

Since this work will focus on nickel-phosphorus homoleptic carbonyl clusters, the state-of-the-art for nickel and group-15 elements heteroatomical compounds will be discussed in detail. Hence, a preliminary description of the different typologies of icosahedral structures would be useful.

An icosahedral cluster can be centred or non-centred. In both cases the apical positions of the structure are frequently - but not necessarily - occupied by two heteroatoms. The two pentagonal bases are usually formed by nickel atoms.

In non-centred icosahedra the cage remains void, whilst in centred icosahedra one additional metallic or non-metallic atom is hosted inside the cage. This further atom may or may not be present inside the cage depending on the dimensions of the atom, as well as on the electronegativity of the latter.<sup>1</sup>

### **♦ *Group-15 elements in heteroleptic nickel carbonyl clusters***

Considering heteroleptic species - *i.e.* in which both carbonyl and alkyl or other ligands are present - there is plenty of examples for each group-15 element. The whole family of icosahedral compounds with formula  $[\text{Ni}_{10}(\text{ER})_2(\text{CO})_{18}]^{2-}$  has been characterized - E = P and R = Me,<sup>2</sup> E = As and R = Me,<sup>3</sup> E = Sb and R = Me, Et, <sup>i</sup>Pr, <sup>t</sup>Bu, *p*-FC<sub>6</sub>H<sub>4</sub>,<sup>4</sup> E = Bi and R = Me, Et.<sup>5</sup>

All these species can be obtained through analogous synthetic pathways. By carrying out a reaction between the  $[\text{Ni}_6(\text{CO})_{12}]^{2-}$  di-anion<sup>6,7</sup> and a ER<sub>n</sub>X<sub>3-n</sub> halide

---

<sup>1</sup> A. Sironi; *J. Chem. Soc., Dalton Trans.*, **1993** (1) 173-178

<sup>2</sup> D. F. Rieck, J. A. Gavney, Jr., R. L. Norman, R. K. Hayashi, L. F. Dahl; *J. Am. Chem. Soc.*, **1992** (114) 10369-10379

<sup>3</sup> D. F. Rieck, R. A. Montag, T. S. McKechnie, L. F. Dahl; *J. Am. Chem. Soc.*, **1986** (108) 1330-1331

<sup>4</sup> P. D. Mlynek; L. F. Dahl; *Organometallics*, **1997** (16) 1641-1654

<sup>5</sup> P. D. Mlynek; L. F. Dahl; *Organometallics*, **1997** (16) 1655-1667

<sup>6</sup> J. C. Calabrese, L. F. Dahl, A. Cavalieri, P. Chini, G. Longoni, S. Martinengo; *J. Am. Chem. Soc.*, **1974** (96) 2616-2618.

<sup>7</sup> G. Longoni, P. Chini; *Inorg. Chem.*, **1976** (15) 3029-3031

(E = P, As, Sb, Bi)<sup>1</sup> it is possible to obtain the corresponding heteroatomical icosahedral cluster compound, with no exceptions.

Even if earlier attempts suggested that the  $[\text{Ni}_{10}(\text{BiR})_2(\text{CO})_{18}]^{2-}$  di-anion could not exist due to steric hindrance - caused by the excessively bulky bismuth atoms - this nickel-bismuth cluster was synthesised at last.

The  $[\text{Ni}_{10}(\text{ER})_2(\text{CO})_{18}]^{2-}$  di-anions share the same structural features, as all these compounds display a non-centred icosahedral geometry (Figure 0.8). The ten nickel atoms compose the two pentagonal bases, and the two heteroatoms are in apical positions. Bonded to the latter there are the alkyl or the aryl ligands, whilst the eighteen carbonyls are varyingly coordinated to the nickel atoms.

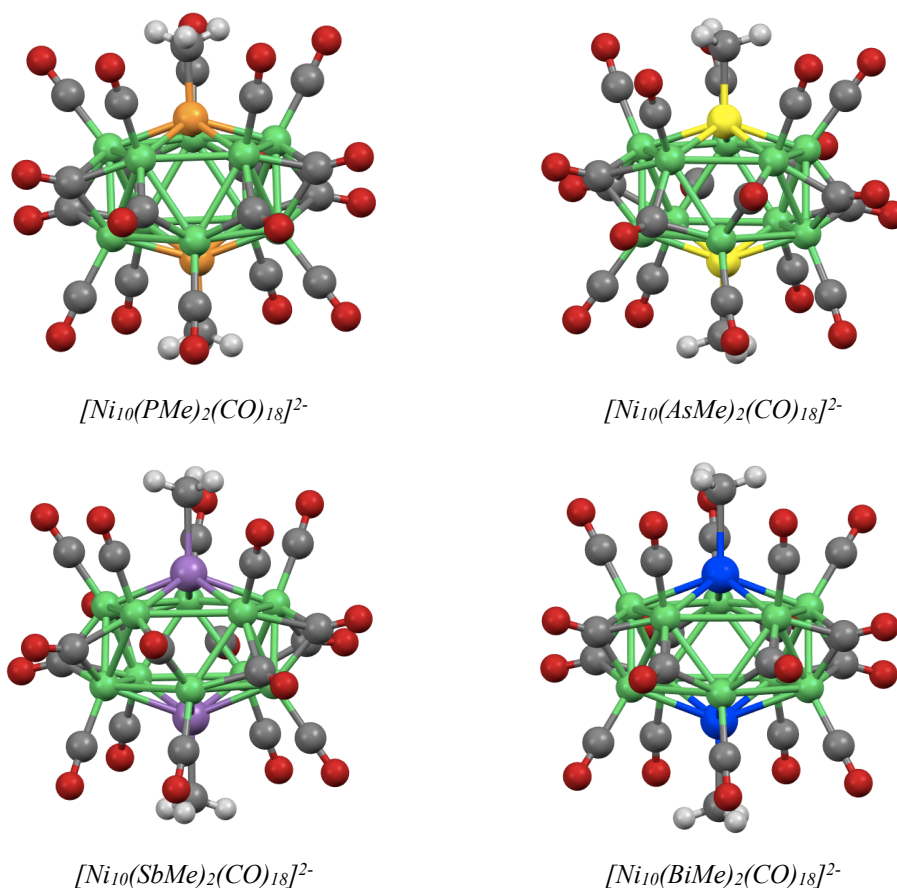


Figure 0.8 - Molecular structures of non-centred icosahedral nickel-pnictogen clusters. All  $[\text{Ni}_{10}(\text{EMe})_2(\text{CO})_{18}]^{2-}$  (E = P, As, Sb, Bi) species display remarkably similar configurations. Nickel atoms are represented in green, phosphorus atoms in orange, arsenic atoms in yellow, antimony atoms in purple, bismuth atoms in blue, hydrogen atoms in light grey, carbon atoms in grey, oxygen atoms in red.

<sup>1</sup> P. D. Mlynek; L. F. Dahl; *Organometallics*, **1997** (16) 1655-1667

The most interesting differences in this series of homologous clusters emerge on a deeper comparison between their respective metal-metal and metal-pnictogen bond lengths. Considering that these species are non-centred icosahedra, bond distances can be sorted into three categories - intra-pentagonal nickel-nickel, inter-pentagonal nickel-nickel, and apical nickel-heteroatom. The average values of the bond distances have been reported for the four different species (Table 0.1). To exclude in advance the possible effects of diverse non-carbonyl ligands, only species with methyl groups have been compared.

$[Ni_{10}(EMe)_2(CO)_{18}]^{2-}$	average bond lengths (Å)		
	intra-pentagonal nickel-nickel	inter-pentagonal nickel-nickel	nickel-pnictogen
$Ni_{10}P_2$	2.61	2.49	2.35
$Ni_{10}As_2$	2.69	2.49	2.43
$Ni_{10}Sb_2$	2.81	2.49	2.59
$Ni_{10}Bi_2$	2.88	2.50	2.63

Table 0.1 - Selected average values for bond distances in  $[Ni_{10}(EMe)_2(CO)_{18}]^{2-}$  clusters.

Observing the data, it is possible to make several considerations.

The elongation registered for the nickel-heteroatom interactions is clearly due to the increasing covalent radius of the pnictogen that is involved in the bond along with the metal. Interestingly, the increasing dimensions of the heteroatoms have an influence also on the nickel-nickel interactions. In fact, the average intra-pentagonal metal-metal bond distances grow along with the dimensions of heteroatoms, whilst the average inter-pentagonal metal-metal bond lengths remain consistent throughout the whole series.

These expansions, both for the nickel-pnictogen interactions and the nickel-nickel intra-pentagonal interactions, are not unexpected and conform to a non-arbitrary trend. The recorded experimental increase is the same observed for the covalent radii of the involved heteroatoms (Table 0.2).<sup>1,2</sup>

<sup>1</sup> B. Cordero, V. Gómez, A. E. Platero-Prats, M. Revés, J. Echeverría E. Cremades, F. Barragán, S. Alvarez; *Dalton Trans.*, **2008** (21) 2832-2838

<sup>2</sup> N. Agmon; *Chemical Physics Letters*, **2014** (595–596) 214-219

A graphical representation of the observed trends for the intra-pentagonal nickel-nickel bond lengths and the nickel-pnictogen bond lengths, along with the trend of the experimental covalent radii have been reported (Figure 0.9).

It is therefore clear that the nature and the characteristics of the heteroatoms in nickel clusters have a nontrivial role, and affect the formation and the arrangement of their icosahedral structures.

<i>covalent radii (Å)</i>	<i>P</i>	<i>As</i>	<i>Sb</i>	<i>Bi</i>
<i>calculated</i>	1.16	1.30	1.43	/
(*) <i>experimental</i>	1.07	1.19	1.39	1.48

Table 0.2 - Calculated (if available) and experimental covalent radii of group-15 elements.

(\*) In the following sections and graphs only experimental values will be considered.

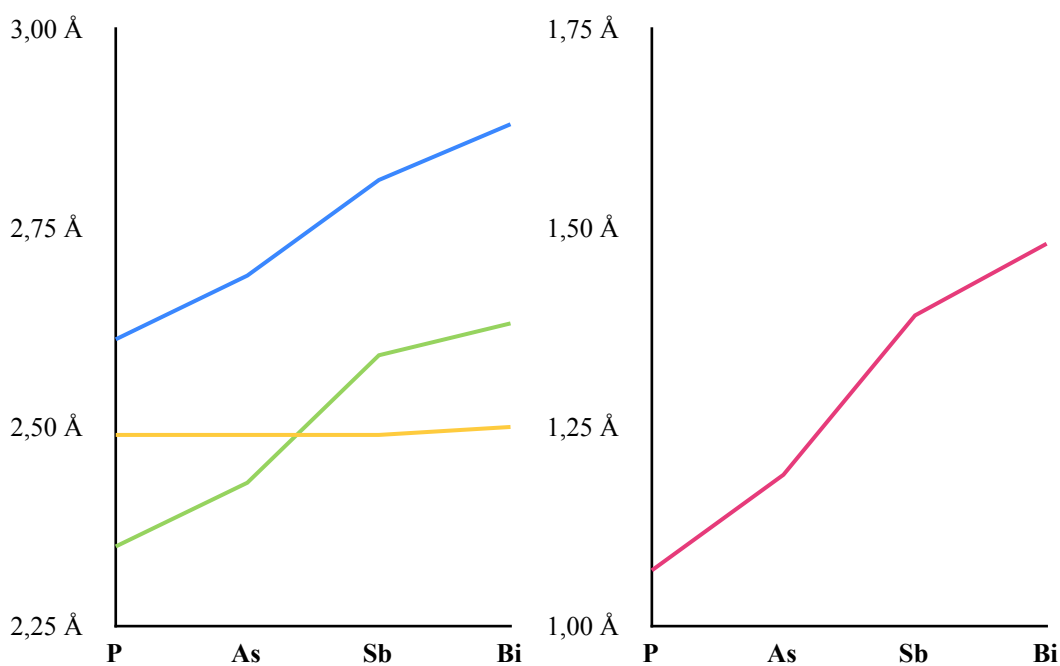


Figure 0.9 - On the left, plot showing the variation of the average bond distances for the three kinds of edges in the  $Ni_{10}E_2$  icosahedral cages, as a function of the congeneric element for each of the four members of the  $[Ni_{10}(EMe)_2(CO)_{18}]^{2-}$  series. Intra-pentagonal interactions have been reported in blue, inter-pentagonal interactions in yellow, nickel-pnictogen interactions in green. On the right, plot showing the variation of the experimental covalent radii of the heteroatoms, reported in red. It is clear that both the average intra-pentagonal nickel-nickel interactions and the nickel-pnictogen interactions follow the same trend, since the bond distances increase along with the size of the corresponding heteroatoms.

✦ **Group-15 elements in homoleptic nickel carbonyl clusters**

Considering homoleptic carbonyl clusters of nickel and group-15 elements, only for antimony and bismuth there are examples known in the literature (Table 0.3). Most of them, as the aforementioned  $[\text{Ni}_{10}(\text{ER})_2(\text{CO})_{18}]^{2-}$  compounds, are relatable to icosahedral structures.

*nickel-antimony homoleptic carbonyl clusters*      *nickel-bismuth homoleptic carbonyl clusters*

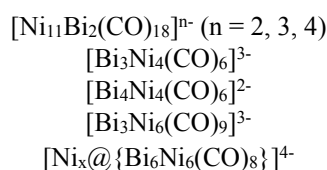
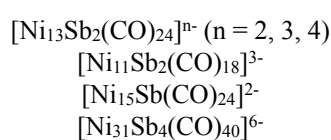


Table 0.3 - Series of known nickel-pnictogen clusters that exclusively bear carbonyl ligands.

Several carbonyl compounds belonging to this family can be synthesised by way of reactions between the  $[\text{Ni}_6(\text{CO})_{12}]^{2-}$  di-anion and a  $\text{EX}_3$  halide ( $\text{E} = \text{Sb}, \text{Bi}$ ), including all nickel-antimony carbonyl species.

By using different stoichiometric ratios between the nickel precursor and the antimony halide it is possible to obtain different heteroatomical clusters such as  $[\text{Ni}_{13}\text{Sb}_2(\text{CO})_{24}]^{n-}$  ( $n = 2, 3, 4$ ),<sup>1,2</sup>  $[\text{Ni}_{11}\text{Sb}_2(\text{CO})_{18}]^{3-}$ ,  $[\text{Ni}_{15}\text{Sb}(\text{CO})_{24}]^{2-}$ ,<sup>3</sup> and  $[\text{Ni}_{31}\text{Sb}_4(\text{CO})_{40}]^{6-}$ .<sup>4</sup> All but the latter share similar structural features, comparable to icosahedral geometries.

The first nickel-antimony homoleptic carbonyl cluster ever discovered was  $[\text{Ni}_{13}\text{Sb}_2(\text{CO})_{24}]^{3-}$ . It can be obtained carrying out the reaction between  $[\text{Ni}_6(\text{CO})_{12}]^{2-}$  and  $\text{SbCl}_3$  up to a 1.43 to 1 nickel per antimony molar ratio.

Its structure is closely related to those of  $[\text{Ni}_{10}(\text{ER})_2(\text{CO})_{18}]^{2-}$ , with the sole exception being the presence of an additional  $\mu_{12}$ -nickel atom at the centre of the

<sup>1</sup> V. G. Albano, F. Demartin, M. C. Iapalucci, G. Longoni, A. Sironi, V. Zanotti; *J. Chem. Soc., Chem. Commun.*, **1990** (7) 547-548

<sup>2</sup> V. G. Albano, F. Demartin, M. C. Iapalucci, F. Laschi, G. Longoni, A. Sironi, P. Zanello; *J. Chem. Soc., Dalton Trans.*, **1991** (S) 739-748

<sup>3</sup> V. G. Albano, F. Demartin, C. Femoni, M. C. Iapalucci, G. Longoni, M. Monari, P. Zanello; *Journal of Organometallic Chemistry*, **2000** (593-594) 325-334

<sup>4</sup> C. Femoni, M. C. Iapalucci, G. Longoni, P. H. Svensson; *Chem. Commun.*, **2000** (8) 655-656



structure. Ten nickel atoms form the pentagonal bases, that are capped by the two antimony atoms in apical positions. Instead of alkyl or aryl ligands, there are two  $\text{Ni}(\text{CO})_3$  fragments coordinated to each heteroatom. These appendices complete the coordination sphere of the cluster (Figure 0.10).

Interestingly, these fragments are labile - their detachment is triggered by treating a solution of the cluster with two equivalents of triphenylphosphine. This way it is possible to synthesize the  $[\text{Ni}_{11}\text{Sb}_2(\text{CO})_{18}]^{3-}$  cluster, whose structure remains coherent with that of its precursor except for the missing apical  $\text{Ni}(\text{CO})_3$  moieties (Figure 0.10).

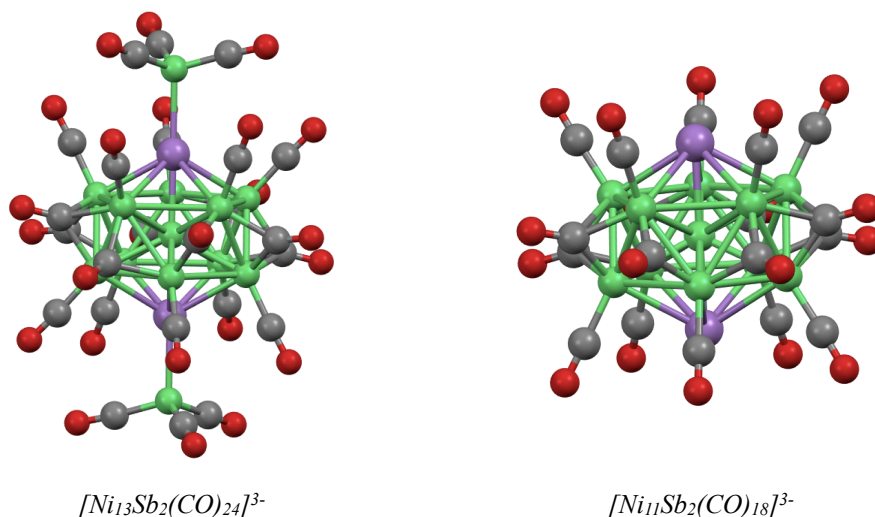


Figure 0.10 - Molecular structures of nickel-antimony carbonyl clusters,  $[\text{Ni}_{13}\text{Sb}_2(\text{CO})_{24}]^{3-}$  and  $[\text{Ni}_{11}\text{Sb}_2(\text{CO})_{18}]^{3-}$ . The metallic skeletons are remarkably similar, except for the apical  $\text{Ni}(\text{CO})_3$ . Nickel atoms are represented in green, antimony atoms in purple, carbon atoms in grey, and oxygen atoms in red.

If the same reaction is performed up to a 2.5 to 1 nickel per antimony molar ratio,  $[\text{Ni}_{15}\text{Sb}(\text{CO})_{24}]^{2-}$  is formed. The structure of this compound is heavily distorted, but its core still displays an antimony-centred icosahedral geometry. It is possible to individuate a  $\text{Ni}_{12}(\mu_{12}\text{-Sb})$  moiety, which is capped on three adjacent triangular faces by the remaining nickel atoms (Figure 0.11).

The distortion of the icosahedral cavity is probably triggered by the size of the encapsulated heteroatom, but cannot take place in a symmetrical fashion because the walls of the polyhedron are reinforced on only one side by the nickel capping

atoms. These results are nonetheless important, because they rebut the early thought that deterred from the possible existence of antimony-centred nickel icosahedral environments.<sup>1</sup>

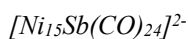
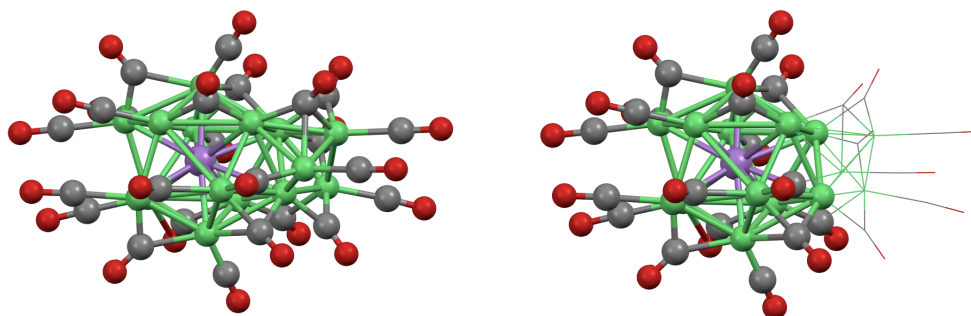


Figure 0.11 - Molecular structures of an heteroatom-centred icosahedral nickel-antimony carbonyl cluster,  $[\text{Ni}_{15}\text{Sb}(\text{CO})_{24}]^{2-}$ . On the right image, the icosahedral moiety has been highlighted. Nickel atoms are represented in green, antimony atoms in purple, carbon atoms in grey, and oxygen atoms in red.

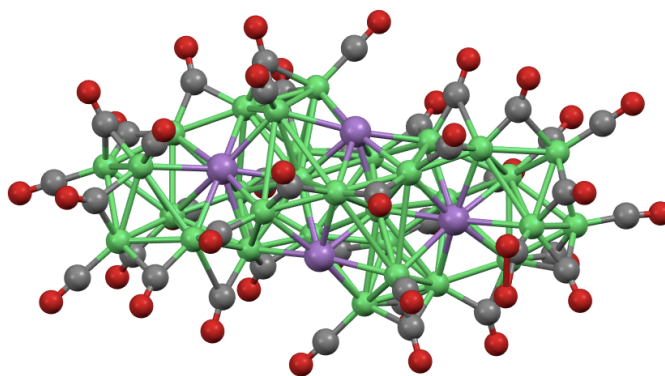
The size-effects of the antimony atoms are even more evident in the structure of the  $[\text{Ni}_{31}\text{Sb}_4(\text{CO})_{40}]^{6-}$  hexa-anion (Figure 0.12). This is the first cluster in which the group-15 heteroatoms are in semi-interstitial positions, nor apical nor enclosed. Moreover, in this compound there is no evidence of icosahedral fragments, and at first glance the structure does not display a specific geometry.

On a more detailed analysis, a pattern eventually emerges - the metallic frame core is in fact formed by two interpenetrating nickel-centred fourteen-hedra. These  $\text{Ni}_{11}\text{Sb}_3(\mu_{14}\text{-Ni})$  moieties have two heteroatomical hexagonal bases, each capped by a nickel atom. Their structure is therefore quite similar to that of an icosahedron whose pentagonal bases have been substituted by larger hexagonal bases.

By considering  $[\text{Ni}_{31}\text{Sb}_4(\text{CO})_{40}]^{6-}$  and  $[\text{Ni}_{15}\text{Sb}(\text{CO})_{24}]^{2-}$ , it is clear how the dimensions of the heteroatoms can affect the range of their possible interactions towards the nickel. While it is possible for the metal to be hosted inside a nickel-

<sup>1</sup> G. Longoni; *Pure & Appl. Chem.*, **1990** (62) 1183-1186

antimony icosahedral cage,<sup>1,2</sup> the same is not as likely for the post-transition element. Antimony atoms, which are considerably bulkier than nickel atoms, can be stabilised inside an icosahedral environment only with consistent distortions and symmetry losses, as seen in the  $[\text{Ni}_{15}\text{Sb}(\text{CO})_{24}]^{2-}$  di-anion.



$[\text{Ni}_{31}\text{Sb}_4(\text{CO})_{40}]^{6-}$

Figure 0.12 - Molecular structure of a high-nuclearity nickel-antimony carbonyl cluster,  $[\text{Ni}_{31}\text{Sb}_4(\text{CO})_{40}]^{6-}$ . It is possible to notice that the heteroatoms are in semi-interstitial positions. Nickel atoms are represented in green, antimony atoms in purple, carbon atoms in grey, and oxygen atoms in red.

With this in mind, it is evident that in nickel-bismuth homoleptic carbonyl clusters these size-triggered effects would probably be even more conspicuous. The nickel-bismuth family of clusters includes several compounds, amongst which  $[\text{Ni}_{11}\text{Bi}_2(\text{CO})_{18}]^{2-}$ .<sup>3</sup> This species can be obtained by performing the reaction between the  $[\text{Ni}_6(\text{CO})_{12}]^{2-}$  precursor and  $\text{BiCl}_3$ . Adding the reactant up to a 1.5 to 1 nickel per bismuth molar ratio, it is possible to obtain the di-anion in fair amounts.

This nickel-bismuth cluster belongs to the family of the nickel-centred icosahedral compounds, even if its structure is highly elongated (Figure 0.13). The considerations already listed regarding the non-centred  $[\text{Ni}_{10}(\text{BiE})_2(\text{CO})_{18}]^{2-}$  species are also applicable to this homoleptic species (Table 0.4).

- 
- <sup>1</sup> V. G. Albano, F. Demartin, M. C. Iapalucci, G. Longoni, A. Sironi, V. Zanotti; *J. Chem. Soc., Chem. Commun.*, **1990** (7) 547-548
  - <sup>2</sup> V. G. Albano, F. Demartin, M. C. Iapalucci, F. Laschi, G. Longoni, A. Sironi, P. Zanello; *J. Chem. Soc., Dalton Trans.*, **1991** (S) 739-748
  - <sup>3</sup> V. G. Albano, F. Demartin, M. C. Iapalucci, G. Longoni, M. Monari, P. Zanello; *J. Chem. Soc., Dalton Trans.*, **1992** (3) 497-502

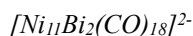
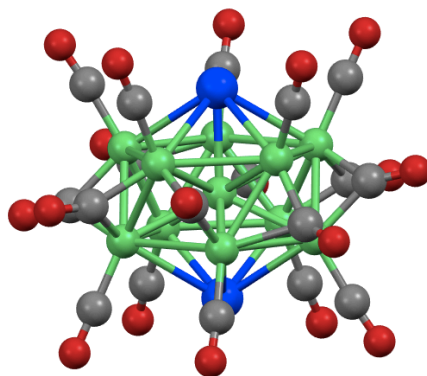


Figure 0.13 - Molecular structures of a nickel-centred icosahedral nickel-bismuth carbonyl cluster,  $[\text{Ni}_{11}\text{Bi}_2(\text{CO})_{18}]^{2-}$ . The presence of the interstitial nickel atom enlarges the whole metallic framework, and the intra-pentagonal interactions in particular. Nickel atoms are represented in green, bismuth atoms in blue, carbon atoms in grey, and oxygen atoms in red.

metallic cage	average bond lengths (Å)			
	interstitial	intra-pentagonal	inter-pentagonal	nickel-bismuth
$\text{Ni}_{11}\text{Bi}_2$	2.51	2.82	2.51	2.81
$\text{Ni}_{10}(\text{BiMe})_2$	/	2.63	2.50	2.88

Table 0.4 - Comparison between selected average values for bond distances in  $[\text{Ni}_{11}\text{Bi}_2(\text{CO})_{18}]^{2-}$  and  $[\text{Ni}_{10}(\text{BiMe})_2(\text{CO})_{18}]^{2-}$ .

By comparing the average bond distances for these two related species it is evident that the extensive dimensions of the bismuth atoms have the same general effect, both with and without the presence of the stabilising alkyl ligands. In  $[\text{Ni}_{11}\text{Bi}_2(\text{CO})_{18}]^{2-}$  the necessary extra-stabilisation - that in  $[\text{Ni}_{10}(\text{BiMe})_2(\text{CO})_{18}]^{2-}$  was provided by the organic fragments - is in all likelihood granted by the interstitial nickel atom.

Besides, other nickel-bismuth carbonyl clusters can be obtained performing a different type of reactions -  $[\text{Bi}_3\text{Ni}_4(\text{CO})_6]^{3-}$ ,  $[\text{Bi}_4\text{Ni}_4(\text{CO})_6]^{2-}$ ,  $[\text{Bi}_3\text{Ni}_6(\text{CO})_9]^{3-}$ , and  $[\text{Ni}_x@(\text{Bi}_6\text{Ni}_6(\text{CO})_8)]^{4-}$ .<sup>1</sup>

The syntheses listed so far involved the oxidation of a nickel carbonyl precu-

<sup>1</sup> J. M. Goicoechea, M. W. Hull, S. C. Sevov; *J. Am. Chem. Soc.*, **2007** (129) 7885-7893

sor triggered by a E(III) halide (E = P, As, Sb, Bi). An alternative synthetic pathway - fully described by Sevov *et al.* - involves the reaction between the  $K_4Bi_5$  Zintl-phase and a neutral nickel carbonyl complex - *e.g.*  $Ni(PPh_3)_2(CO)_2$ . In this situation the bismuth - which bears a formal oxidation state equal to -1 - acts as reductant towards the nickel, and so exhibits an opposite behaviour compared to the formerly described synthetic pathways (Table 0.5).

<i>synthesis of</i>	<i>nickel reactant and o.s.</i>	<i>bismuth reactant and o.s.</i>
$[Ni_{11}Bi_2(CO)_{18}]^{2-}$	$[Ni_6(CO)_{12}]^{2-}$ $-1/3$ <i>reducing agent</i>	$BiCl_3$ $+3$ <i>oxidising agent</i>
$[Bi_3Ni_4(CO)_6]^{3-}$	$Ni(PPh_3)_2(CO)_2$ $0$ <i>oxidising agent</i>	$K_4Bi_5$ $-1$ <i>reducing agent</i>

Table 0.5 - Schematisation of the formal oxidation states of the reactants in two different types of synthesis of nickel-bismuth carbonyl clusters. It is shown that by using different nickel and bismuth sources it is possible to trigger opposite redox effects.

$[Bi_3Ni_4(CO)_6]^{3-}$ ,  $[Bi_4Ni_4(CO)_6]^{2-}$ ,  $[Bi_3Ni_6(CO)_9]^{3-}$ , and  $[Ni_x@Bi_6Ni_6(CO)_8]^{4-}$  can all be obtained by using the same couple of reactants. In these cases, not the stoichiometric ratio between reactants but the sequestering agent present in solution with the Zintl-phase is the driving force towards the formation of one product rather than another.

In particular, the latter is a further example of an heteroatomical nickel-centred icosahedral cage - though with an occupancy factor equal to 0.334. Its metallic skeleton (Figure 0.14) presents interesting features, and can be interpreted with diverse approaches.

To compare this structure with that of  $[Ni_{10}(BiMe)_2(CO)_{18}]^{2-}$  and  $[Ni_{11}Bi_2(CO)_{18}]^{2-}$  it has to be assumed that two bismuth atoms are in apical position. With this premise, the two pentagonal base of the icosahedron are  $Ni_3Bi_2$  heteroatomical rings. The carbonyl ligands are solely bonded to nickel atoms - six are terminally coordinated to each nickel atom, and the other two  $\mu_3$ -COs are bridging over two symmetrical triangular nickel faces, on the opposite sides of the icosahedron.

On a less conventional interpretation, in this cluster it is possible to individuate a six-membered ring of bismuth atoms which is forming a cyclohexane-like chair conformation. Coordinated to each side of this chair there are two triangular nickel fragments along with their carbonyl ligands -  $\text{Ni}_3(\text{CO})_3(\mu_3\text{-CO})$ .

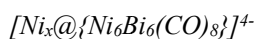
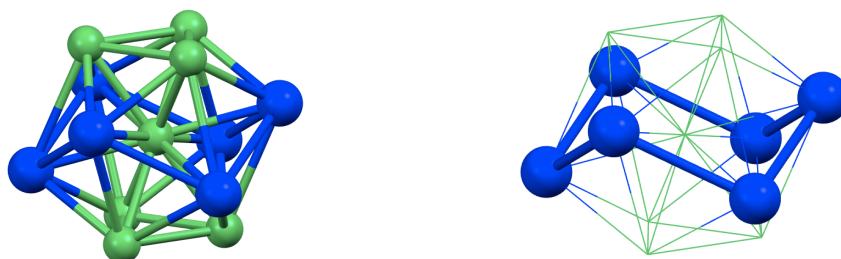


Figure 0.14 - Metallic skeleton of a nickel-bismuth clusters,  $[\text{Ni}_x@{\text{Ni}_6\text{Bi}_6(\text{CO})_8}]^{4-}$ . On the right image the cyclohexane-like chair conformation assumed by the bismuth atoms within the icosahedron has been highlighted. Nickel atoms are represented in green, and bismuth atoms in blue.

There are two main differences between the molecular structure of  $[\text{Ni}_x@{\text{Bi}_6\text{Ni}_6(\text{CO})_8}]^{4-}$  and that of the other nickel-bismuth carbonyl clusters. First, in this carbonyl-poor compound the ligand shell is loose and does not envelop the metallic skeleton. Moreover, its icosahedral geometry is far less distorted. This is clearly due to the effects of a lower nickel per bismuth ratio inside the structure. The heteroatomical pentagonal bases of  $[\text{Ni}_x@{\text{Bi}_6\text{Ni}_6(\text{CO})_8}]^{4-}$  are larger and can achieve a more efficient interaction with the apical atoms, without an excessive elongation of the intra-pentagonal bonds.

Finally,  $[\text{Bi}_3\text{Ni}_4(\text{CO})_6]^{3-}$ ,  $[\text{Bi}_4\text{Ni}_4(\text{CO})_6]^{2-}$ , and  $[\text{Bi}_3\text{Ni}_6(\text{CO})_9]^{3-}$  display different geometries. The latter can be viewed as derived from the  $[\text{Ni}_x@{\text{Bi}_6\text{Ni}_6(\text{CO})_8}]^{4-}$  cluster, by the removal of three bismuth atoms and one non-interstitial nickel atom. Therefore,  $[\text{Bi}_3\text{Ni}_6(\text{CO})_6]^{3-}$  could be forcibly included in the family of icosahedral nickel compounds.

The two lesser nuclearity compounds are not related to the others, and display *closo*-structures. The skeleton of  $[\text{Bi}_3\text{Ni}_4(\text{CO})_6]^{3-}$  is shaped as a pentagonal bipyramid, whilst the structure of  $[\text{Bi}_4\text{Ni}_4(\text{CO})_6]^{2-}$  is bis-disphenoidal.

## Expected results

With the information available in the literature, it is possible to venture in some hypotheses regarding the possible syntheses and structures of nickel-phosphorus homoleptic carbonyl clusters.

The more plausible synthetic pathway is homologous to the one already seen for the other nickel-pnictogen compounds. The reaction between the nickel precursor  $[\text{Ni}_6(\text{CO})_{12}]^{2-}$  and  $\text{PCl}_3$  would be a fine starting-point for the synthesis of new nickel-phosphorus homoleptic carbonyl clusters.

Concerning the possible structures of homoleptic nickel-phosphorus species, the existence of the heteroleptic  $[\text{Ni}_{10}(\text{PMe})_2(\text{CO})_{18}]^{2-}$  di-anion suggests that phosphorus atoms could be able to stabilise icosahedral nickel-based structures. However, the stabilisation provided by the alkyl ligands is not to be underestimated, as evinced from the comparison between  $[\text{Ni}_{10}(\text{SbR})_2(\text{CO})_{18}]^{2-}$  and nickel-antimony homoleptic carbonyl clusters. In this cases the absence of the organic fragments results in a lack of stabilisation, that is balanced by the inclusion of a  $\mu_{12}$ -nickel or a  $\mu_{12}$ -antimony inside the icosahedral cages.

Aside, not only the type of ligands but also the dimension of the heteroatoms - in terms of covalent radius - has a great importance. This aspect has already been thoroughly examined for increasing dimensions, as for the nickel-bismuth compounds. It is now important to forward some hypothesis considering an opposite trend.

Unfortunately, there is no evidence for nickel-arsenic carbonyl compounds in the literature. Along the group-15, arsenic is the closest element to phosphorus in terms of covalent radius, and a structural analysis of nickel-arsenic carbonyl compounds would have been useful.

A nickel-arsenic species actually exists, but does not bear nor carbonyl nor other ligands -  $[\text{As}@\text{Ni}_{12}@\text{As}_{20}]^{3-}$ .<sup>1</sup> Its structure is best described as an arsenic-centred nickel icosahedron -  $[\text{Ni}_{12}(\mu_{12}\text{-As})]^{3-}$  - encapsulated in an  $\text{As}_{20}$  pentagonal

---

<sup>1</sup> M. J. Moses, J. C. Fettinger, B. W. Eichhorn; *Science*, **2003** (300) 778-780

dodecahedron. Interestingly, the icosahedron and the pentagonal dodecahedron are reciprocal structures that switch faces for vertices. This means that each arsenic atom in the fuller-cage caps a Ni<sub>3</sub> face of the icosahedron and, conversely, there is a nickel atom centred below each As<sub>5</sub> ring.

This highly symmetrical compound scarcely shares any feature with the carbonyl clusters considered before. However, a structural analysis of the nickel-arsenic core could be useful, in order to understand if a nickel icosahedral cages could host arsenic atoms, or even smaller atoms. Experimental data show that the average values of the nickel-nickel and of the nickel-arsenic bond distances are comparable to that of carbonyl compounds. These results suggest that smaller pnictogen atoms, as arsenic and phosphorus atoms, could actually be hosted inside icosahedral nickel environments.

To conclude, it is difficult to foresee the nature of nickel-phosphorus homoleptic carbonyl clusters. In nickel-pnictogen compounds, both the type of ligands and the dimension of the heteroatoms play a vital role in the formation of a structure rather than another. Moreover, it is almost impossible to predict which effects a loss of stabilisation could cause, both in terms of geometry and nuclearity.

However, considering the modest covalent radius of the phosphorus compared to that of the other group-15 elements, it is reasonable to expect the formation of icosahedral structures or moieties in nickel-phosphorus carbonyl compounds. On the contrary, the formation of high-nuclearity species would be unexpected, since all the reported clusters - except [Ni<sub>39</sub>Sb<sub>4</sub>(CO)<sub>40</sub>]<sup>6-</sup> - display low-nuclearities.



# Results and Discussions

## Reaction conditions and modus operandi

The classical synthetic route for heteroatomical nickel clusters has already been mentioned in the introduction. Low-nuclearity homometallic nickel carbonyl clusters in presence of a post-transition element halide are usually subjected to redox processes, that lead to structural rearrangements that may originate new species. In order to do so, an according reaction pathway had been tentatively developed.

### *Reaction parameters*

The different aspects that needed to be considered were the nickel cluster precursor, its counter-ion, the reaction solvent, and the phosphorus reactant.

#### ✦ *Nickel cluster precursor*

$[\text{Ni}_6(\text{CO})_{12}]^{2-}$  is one of the most used nickel cluster precursors, due to its relatively high stability and its fairly simple - though lengthy - synthesis.<sup>1</sup> Moreover, its solubility can be easily tuned by choosing an appropriate counter-ion, thus designing the cluster to be soluble in both high-polarity and low-polarity organic environments.

#### ✦ *Counter-ions*

The most widely used counter-ions belong to the family of the tetra-alkylammonium cations. Although there was not an absolute rule, a general pattern

---

<sup>1</sup> J. C. Calabrese, L. F. Dahl, A. Cavalieri, P. Chini, G. Longoni, S. Martinengo; *J. Am. Chem. Soc.*, **1974** (96) 2616-2618

linked the nature of the ammonium counter-ion to the resulting solubility of the clusters.

Considering tetra-alkyl ammonium cations with four equal R-groups, the nickel salts should display higher solubilities with longer alkyl-chains, and *vice versa*. For example, a tetra-methyl-ammonium salt should be far less soluble compared to a tetra-butyl-ammonium salt - when paired with the same nickel carbonyl cluster. Thus, depending on which solvent was to be used, the choice of the appropriate ammonium cation was essential. It is worth to mention that the nature of the counter-ion affected not only the solubility of the cluster but also its potential crystallisation as well.

When considering both these aspects, the extensive use of tetra-ethyl-ammonium cations can be easily explained. On one hand, the alkyl chains were able to induce a reasonable solubility to low-charge species (*e.g.* the cluster precursor). On the other hand, this effect decreased when the charge-to-nuclearity ratio lowered, thus allowing the separation of any different product with the method of the subsequent extractions. Most importantly, a large number of carbonyl clusters appear to crystallise fairly easily in presence of this specific counter-ion.

For these reasons, in this work most reactivity trials were performed with tetra-ethyl-ammonium nickel carbonyl cluster salts. Only in a second time, if the need arose, different ammonium cations were used.

#### ✦ *Reaction solvents*

Whilst less predictable, the effects arising from the use of different solvents were not to be underestimated. In cluster chemistry, the most used organic solvents are dichloromethane, tetrahydrofuran (THF), methanol, acetone, acetonitrile, and dimethylformamide (DMF) - here listed from least to most solubilising. Their different intrinsic characteristics did have an impact on the reaction pathways, but the results were not easily foreseeable.

As a general rule, the only effect that was possible to control in advance was

linked to the nature of the counter-ion that was used. For example, when a short-chain ammonium cation was used, the salts of the cluster precursor were usually not soluble in dichloromethane, and poorly soluble in THF. The latter scenario may not be completely detrimental, as the products of the reaction should precipitate avoiding subsequent reactions and decomposition processes. However, a long-chain ammonium cation typically allowed to utilise every solvent. Moreover, it was also common for the products of the reaction to be still available in solution, thus undergoing themselves to further oxidation processes.

That being said, it was clear that the choice of the appropriate cation-solvent combination was fundamental in order to identify a high-yield, reproducible synthesis for the desired products. However, a long and empirical process was often required to choose the best cation-solvent couple for a specific synthesis, except for some rare strokes of serendipity.

#### ♦ *Phosphorus reactants*

Eventually, a parameter that had to be considered was the possible nature of the phosphorus reactant.

Phosphorus halides are not rare species, and there was plenty of possible compounds to choose from. Phosphorus forms halides in all of his positive oxidation states - namely +5, +3, and +2. The latter O.S. had not to be considered, as well as the former -  $P_2X_4$  compounds are generally extremely unstable, whilst  $PX_5$  species would have been too strongly oxidant.

$PX_3$  reactants therefore represented a valid choice, and in particular  $PCl_3$ . This was due to its chemical-physical characteristics - the species is liquid at room temperature, not extremely volatile, fairly stable, and inexpensive - and to the fact that chlorine is a typical good leaving group. Moreover, it has already been shown that  $EX_3$  (E = P, As, Sb, Bi) were the most used compounds in the syntheses of heteroleptic nickel-pnictogen clusters.

A reasonable alternative to  $PX_5$  compounds - where the phosphorus has an O.S. equal to +5 - was individuated in oxyhalides, also known as phosphoryl halides.

POX<sub>3</sub> compounds are in fact more oxidant than PX<sub>3</sub> ones - due to the higher O.S. of the phosphorus - but not as much as PX<sub>5</sub> species - due to the presence of the oxygen.

Taking these considerations into account, both PCl<sub>3</sub> and POCl<sub>3</sub> were selected as possible reactants for the synthesis of new nickel-phosphorus homoleptic carbonyl clusters.

The observations listed so far can be recapped as following: [Ni<sub>6</sub>(CO)<sub>12</sub>]<sup>2-</sup> was selected to be used as nickel precursor, and PCl<sub>3</sub> or POCl<sub>3</sub> were selected both as phosphorous sources and as oxidising agents. None of the organic solvents available were excluded in advance, and the ammonium cations were chosen each time to adjust and tune the solubility of the cluster precursor.

### ***Further considerations and preventive measures***

The first trials were made with the aim to identify and select a reduced range of cation-solvent couples to be further investigated.

In order for the [Ni<sub>6</sub>(CO)<sub>12</sub>]<sup>2-</sup> di-anion to be solubilised when dichloromethane was being used, only long-chain tetra-alkyl-ammonium cations as tetra-butyl-ammonium could be employed. Interestingly, the peculiar characteristics of dichloromethane - as, for example, its residual acidity and its low polarity index - caused the reactions conducted in this solvent to be remarkably different from all the others.

On the contrary the outcomes of the reactions were fairly alike when tetrahydrofuran, acetone, or acetonitrile were used, independently from the cation. However, acetone proved not to be a sound choice since the earlier attempts: the reaction yields were low - both with PCl<sub>3</sub> and with POCl<sub>3</sub> - due to an excessive formation of decomposition products, and the reaction outcomes were hardly reproducible.

Eventually, tetra-butyl-ammonium and CH<sub>2</sub>Cl<sub>2</sub>, tetra-ethyl-ammonium and THF, tetra-ethyl-ammonium and acetonitrile were selected as most promising

cation-solvent couples with which to proceed.

Along with the exclusion of the acetone from the pool of possible solvents, the preliminary series of tests also allowed to obtain other important information.

It is known that in presence of water both  $\text{PCl}_3$  and  $\text{POCl}_3$  are subjected to hydrolysis processes, thus releasing hydrochloric acid. An excessive quantity of HCl within the reaction environment would have led to the complete decomposition of the nickel cluster precursor, triggered by the low pH level.

Nonetheless, hydrochloric acid may be detrimental even in reduced proportions. It is in fact known that in mild acidic conditions the  $[\text{Ni}_6(\text{CO})_{12}]^{2-}$  di-anion is easily transformed into the  $[\text{Ni}_9(\text{CO})_{18}]^{2-}$  (Figure 1.1)<sup>1</sup> or the  $[\text{H}_2\text{Ni}_{12}(\text{CO})_{22}]^{2-}$  di-anions.<sup>2, 3</sup> The development of the latter did not interfere with the formation of new heteroatomical nickel-phosphorus clusters, yet the presence of  $[\text{Ni}_9(\text{CO})_{18}]^{2-}$  did, and had to be avoided.

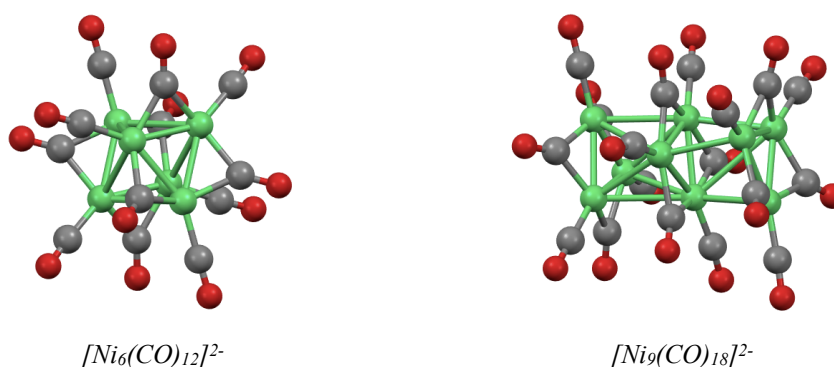


Figure 1.1 - Molecular structures of  $[\text{Ni}_6(\text{CO})_{12}]^{2-}$  and  $[\text{Ni}_9(\text{CO})_{18}]^{2-}$ . Despite their opposite reactivities with  $\text{PCl}_3$ , these two clusters present very similar metallic skeletons - the first is a trigonal anti-prism, and the second results from the merging of two trigonal anti-prisms.

The presence of this low-nuclearity species had adverse effects on the outcome of the reactions, mainly due to its null reactivity towards phosphorous halides. Whenever the nickel precursor was quantitatively transformed into the

- 
- <sup>1</sup> D. A. Nagaki, L. D. Lower, G. Longoni, P. Chini, L. F. Dahl; *Organometallics*, **1986** (5) 1764-1771
  - <sup>2</sup> R. W. Broach, L. F. Dahl, G. Longoni, P. Chini, A. J. Schultz, J. M. Williams; *Adv. Chem. Ser.*, **1978** (167) 93-110.
  - <sup>3</sup> A. Ceriotti, P. Chini, R. Della Pergola, G. Longoni; *Inorg. Chem.*, **1983** (22) 1595-1598

$[\text{Ni}_9(\text{CO})_{18}]^{2-}$  di-anion, nothing but decomposition products as  $\text{Ni}(\text{CO})_4$  or  $\text{NiCl}_2$  were obtainable.

However, even the formation of a small quantity of this cluster could result in undesired consequences. Actually, when both  $[\text{Ni}_6(\text{CO})_{12}]^{2-}$  and  $[\text{Ni}_9(\text{CO})_{18}]^{2-}$  were present in solution a solubility equilibrium established between them. In acetonitrile - a high-polarity, more solubilising solvent - the aforementioned equilibrium had no deleterious effects, apart from a slightly reduced yield. On the contrary, in THF the solubilisation of the  $[\text{Ni}_9(\text{CO})_{18}]^{2-}$  di-anion did actually prevail, triggering the precipitation of the other species and nullifying the reactivity of the designed cluster precursor.

This phenomenon happened since the characteristic charge-to-nuclearity ratio of  $[\text{Ni}_9(\text{CO})_{18}]^{2-}$  is lower than that of  $[\text{Ni}_6(\text{CO})_{12}]^{2-}$  - the ratios are respectively equal to  $-2/9$  and  $-1/3$ . Therefore the former cluster was solubilised at the other compound expenses.

These observations should have highlighted that the purity of the solvent, of the phosphorous reactants, and of the nickel cluster precursor had to be strictly controlled. The synthesis of  $[\text{Ni}_6(\text{CO})_{12}]^{2-}$  frequently allowed to obtain it with an adequate purity degree, yet  $[\text{Ni}_9(\text{CO})_{18}]^{2-}$  was rarely present. So not to waste the cluster precursor, the samples containing the impurity were used in acetonitrile-based synthesis, in order to avoid solubility problems.

Also, the solvents had to be anhydrous as well as the phosphorous reactants, to avoid hydrolysis processes and the consequent formation of HCl - whence further production of  $[\text{Ni}_9(\text{CO})_{18}]^{2-}$ .

### ***General modus operandi***

Once the best set of reaction conditions had been defined, the synthetic approach became more methodic, and was focused on the isolation and identification of whatever unknown products were detected via IR spectroscopy analyses. All reactions were initially performed following the same approach, evaluating

only in a second time if some parameters had to be changed.

Depending on the chosen solvent, an appropriate ammonium counter-ion was selected for the nickel precursor. During the earlier attempts tetra-butyl-ammonium was used in CH<sub>2</sub>Cl<sub>2</sub> solutions, whilst tetra-ethyl-ammonium was used both in THF and in acetonitrile. The corresponding [Ni<sub>6</sub>(CO)<sub>12</sub>]<sup>2-</sup> salts were dissolved in a minimum amount of solvent, in order to obtain a rather high cluster concentration in solution.

At the same time, low-concentration solutions of the phosphorous reactants - either PCl<sub>3</sub> or POCl<sub>3</sub> - were prepared. In fact, having a highly concentrated solution of cluster and a lowly concentrated solution of reactant allowed to minimise the potential onset of decomposition processes. These undesired processes tended to otherwise occur locally whenever adding one solution to the other - even in vigorously stirred environments.

IR spectra of the cluster solutions were always acquired before proceeding with the additions, in order to detect latent impurities or humidity. After that, if no problems had been noticed, the phosphorous reactants were drop-wise added in small portions, while regularly checking on the reaction development through IR spectroscopy analyses. As expected, it was noted that different solvents displayed different behaviours.

When the reactions were held in high-polarity environments, such as acetonitrile solutions, it was possible to fully follow the reaction progress. In fact, most products retained a good solubility and the rise of peaks at new absorption frequencies was detectable in the IR spectra.

On the contrary, in low-polarity environments most products were not soluble and precipitated, thereby any possibly new species was invisible towards IR analyses. An indirect form of control on those reactions was still available, as it was possible to observe that the characteristic IR absorption bands of [Ni<sub>6</sub>(CO)<sub>12</sub>]<sup>2-</sup> were decreasing in terms of intensity. At the same time, the possible presence of products of interest was confirmed by the formation of dark or black precipitates within the reaction mixtures. In both scenarios the additions of the phosphorous reactants usually continued until the characteristic absorption frequencies of

$[\text{Ni}_6(\text{CO})_{12}]^{2-}$  were no longer detectable in the IR spectra.

At that point the reaction mixtures were typically dried under vacuum to remove the solvent and  $\text{Ni}(\text{CO})_4$ , and then washed with water to eliminate organic and inorganic salts as nickel and ammonium chlorides - all being common decomposition by-products. After that, only nickel-phosphorus carbonyl clusters were supposed to be present in the reaction mixtures. The method of the subsequent extractions was applied as follows, in order to separate the potentially present different species.

Starting with a low-polarity solvent, the reaction mixtures were suspended in a minimal quantity of the chosen organic solvent. If solubilisation occurred the extract was filtered, and the solid residues were repeatedly washed until nothing soluble remained. The collected extraction was concentrated when needed, and saved for further purposes. The solid residues were again dried under vacuum. These steps were reiterated by using solvents with increasingly higher polarities, until nothing or metallic powders were left as solid residues.

At the end of this process different solutions were available, and supposedly the components of the reaction mixture had been isolated. By using  $\text{CH}_2\text{Cl}_2$  and THF a minor quantity of  $[\text{Ni}_6(\text{CO})_{12}]^{2-}$  or  $[\text{Ni}_9(\text{CO})_{18}]^{2-}$  was usually extracted, while the IR spectra acquired from the acetone and the acetonitrile solutions indicated the presence of several new heteroatomical carbonyl species.

As aforementioned, these isolated solutions were analysed via IR spectroscopy. In the best-case scenarios just one product was present in each extracted solution, so crystallisation essays were directly attempted. The solutions were otherwise treated to tentatively separate the coexisting species, and only then crystallisation was undertaken. X-ray diffraction analyses were performed whenever good-quality crystals were available, and the molecular structures of the compounds were eventually identified.

The general method that is used to induce the crystallisation of a cluster species involves a slow and gradual decrease of its solubility, hence triggering the precipitation of the compound in crystalline form. To do so, a miscible non-solvent is



usually layered over a well-concentrated solution of the cluster - while the non-solvent diffuses into the solution the cluster solubility lowers, eventually inducing its precipitation. If the process occurs at a suitable rate, and if the cation-solvent couple is appropriate, crystallisation may happen.

It is also fundamental to obtain suitable-quality crystals in order to perform X-ray diffraction analyses, and hence determine the full molecular structures of the new species. No more than partial molecular structures, or even bare metallic skeletons can be characterised if the quality of the crystals is mediocre.

The non-solvents that are most commonly employed are toluene over dichloromethane solutions, hexane over THF solutions, isopropanol or hexane over acetone solutions, and both hexane and diisopropyl ether over acetonitrile solutions. Anyway, every non-polar solvent that is less dense and at the same time miscible towards the cluster solution may potentially be used in order to attempt crystallisation.

Once a new nickel-phosphorus compound was structurally characterised and its IR spectrum was available, the refinement of its synthesis could begin. Few crystals were re-solubilised - usually in acetonitrile - and then the corresponding IR spectrum was acquired. This allowed to record the characteristic IR absorption frequencies of the new species, and most importantly allowed to unequivocally match the IR spectrum with that specific carbonyl cluster compound.

First, the correspondence between the IR spectra acquired before and after the crystallisation had to be checked. If the two spectra displayed the same absorption frequencies, it was safe to assume that the species did not undergo any transformation throughout the crystallisation process, and that the species that had been extracted at the end of the reaction was the same that had originated the crystals. At that point, the original reaction pathway was repeated as accurately as possible, reasonably expecting for the same outcome to happen.

A reproducible synthesis was successfully individuated whenever the crystallisation of the same compound occurred in at least two different independent occasions, by performing the reactions applying the same parameters.

Unfortunately, it is clear that many variables may affect the identification of a

reproducible synthetic pathway.

First, the crystallisation of a cluster compound is definitely not an effortless process. The acquisition of a suitable-quality crystalline sample may take a great number of attempts. By using combinations of different solvents, different cations, and different non-solvents the outcomes of the crystallisation may vary and eventually lead to positive results.

Second, it may be possible to notice that the IR spectrum acquired after the crystallisation does not correspond to the one acquired before. This unfortunate eventuality may be due to various complications. On the first hand, it may be possible that the reaction proceeded during the crystallisation process - triggered by some residual reactant or by an air-induced oxidation. On the second hand, there is another possible cause. For what concerns the solution before the crystallisation, it is not possible to totally exclude the coexistence of more than one species, despite the presence of just one couple of IR absorption bands in the corresponding spectrum. This can happen for species with similar or even overlapping absorption frequencies. Also, this can be due to a marked stoichiometric prevalence of one species over the other. In both cases, just one of the clusters that are present in the original solution may eventually crystallise, thus originating the differences between the spectra.

That being said, the tuning of a synthetic pathway for a sought-after cluster may be subjected to a great number of negative eventualities. Eventually most attempts are successful, but seldom it is impossible to define a certain synthesis for a species.

The previously mentioned considerations about crystallisation and identification were indeed experienced throughout this whole project. In this work about nickel-phosphorus carbonyl clusters, most species have had their synthesis identified, adjusted, and refined, with the aim of maximising the yield and the purity of the targeted compounds. However, few species were structurally and spectroscopically characterised, yet their syntheses were never optimised in spite of the numerous efforts made.

The new species belonging to the family of nickel-phosphorus homoleptic car-

bonyl clusters that had been structurally characterised were  $[\text{Ni}_{11}\text{P}(\text{CO})_{18}]^{3-}$ ,  $[\text{Ni}_{14}\text{P}_2(\text{CO})_{22}]^{2-}$ ,  $[\text{Ni}_{23-x}\text{P}_2(\text{CO})_{30-x}]^{4-}$  and  $[\text{Ni}_{23-x}\text{P}_2(\text{CO})_{30-x}]^{6-}$  ( $x = 0, 1$ ),  $[\text{HNi}_{31}\text{P}_4(\text{CO})_{39}]^{5-}$  and  $[\text{H}_2\text{Ni}_{31}\text{P}_4(\text{CO})_{39}]^{4-}$ ,  $[\text{Ni}_{29}\text{P}_5(\text{PO})(\text{CO})_{36}]^{4-}$ ,  $[\text{Ni}_{39}\text{P}_3(\text{CO})_{44}]^{6-}$ . For all but the last two species it was also possible to identify an adequate synthetic pathway.

The detailed synthetic approaches, the structural and spectroscopic characterisation, and a comprehensive reactivity study for each cluster will be reported in the following chapters.

## **[Ni<sub>11</sub>P(CO)<sub>18</sub>]<sup>3-</sup>** **Synthesis, characterisation, and reactivity**

### *Synthetic approach and further considerations*

Indeed, this was one of the most difficult synthesis to rationalise. This compound had a behaviour that was peculiar, and uncommonly difficult to understand.

It crystallised quite easily forming well-shaped crystals, from different solvents as well as with different cations. However, in most cases just few crystals developed, thus making it impossible to acquire a reference IR spectrum for the species. The only reference that could initially be used was the IR spectrum recorded before the crystallisation -  $\nu_{\text{CO}}$  equal to 2014s, 1873m  $\text{cm}^{-1}$ .

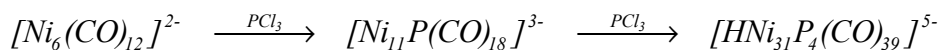
With the aim to overcome this problem the synthetic attempts continued, yet the co-crystallisation of [Ni<sub>11</sub>P(CO)<sub>18</sub>]<sup>3-</sup> and [HNi<sub>31</sub>P<sub>4</sub>(CO)<sub>39</sub>]<sup>5-</sup> - another nickel-phosphorus carbonyl cluster that will be later described - began to happen recurrently. It was therefore not clear to which cluster the recorded IR absorption frequencies corresponded.

These difficulties were ultimately overcome when a completely new set of IR absorption frequencies appeared throughout one of the synthetic attempts. At the end of a reaction carried out between [Ni<sub>6</sub>(CO)<sub>12</sub>]<sup>2-</sup> and PCl<sub>3</sub> in THF it was possible to extract an acetone solution from which was recorded a IR spectrum that had never been seen before -  $\nu_{\text{CO}}$  equal to 1980s, 1848m  $\text{cm}^{-1}$ .

The slow diffusion of hexane into that solution triggered the whole crystallisation of the sample, and an X-ray diffraction analysis confirmed that it was pure [Ni<sub>11</sub>P(CO)<sub>18</sub>]<sup>3-</sup>. Due to the suitable quantity of crystals that was available, it was eventually possible to acquire a reference IR spectrum for the species, that was coincident to the spectrum recorded before the crystallisation.

Once these important information had been obtained, a hypothesis was made in order to justify the frequent co-crystallisation of [Ni<sub>11</sub>P(CO)<sub>18</sub>]<sup>3-</sup> and [HNi<sub>31</sub>P<sub>4</sub>(CO)<sub>39</sub>]<sup>5-</sup>. It was assumed that [Ni<sub>11</sub>P(CO)<sub>18</sub>]<sup>3-</sup> could be an intermediate

product of the reaction between the nickel precursor and  $PCl_3$ . It was therefore suggested that its subsequent oxidation triggered by  $PCl_3$  could lead to the formation of the high-nuclearity  $[HNi_{31}P_4(CO)_{39}]^{5-}$  cluster (Scheme 2.1).



*Scheme 2.1 - Hypothetical scheme of the reaction between the  $[Ni_6(CO)_{12}]^{2-}$  precursor and  $PCl_3$ .*

To verify this hypothesis, the pure crystalline sample that had been collected was used to perform an oxidation test. This reactivity trial actually validated the hypothesis, and once that the fact that  $[Ni_{11}P(CO)_{18}]^{3-}$  was unstable towards oxidising environments had been discovered, its synthesis was adjusted. A complete account of this reactivity test will ensue in the dedicated chapter.

In the following paragraphs a more detailed description of the synthesis of  $[Ni_{11}P(CO)_{18}]^{3-}$  will be reported.

Once the nickel precursor  $[Ni_6(CO)_{12}]^{2-}$  had been prepared according to the procedure reported in the literature, its tetra-ethyl-ammonium salt was dissolved in a minimal quantity of tetrahydrofuran. The solution was placed inside a suitable round Schlenk flask and vigorously stirred. At the same time a 1:100 v/v  $PCl_3$  solution was prepared considering a 1 to 0.5 stoichiometric ratio - referred to the hexa-nuclear nickel cluster precursor - and then placed in a Schlenk tube. Before proceeding with the reaction, the nickel cluster solution was put under vacuum for not more than a minute, to eliminate any potential presence of air or nickel tetracarbonyl.

The addition of the diluted solution of  $PCl_3$  began after the IR spectrum of the starting solution of  $[Ni_6(CO)_{12}]^{2-}$  was acquired. Posterior to each addition an IR spectroscopy analysis was performed, to verify the actual decrement of the intensity of the  $[Ni_6(CO)_{12}]^{2-}$  characteristic absorption frequencies. Whenever an excessive amount of  $Ni(CO)_4$  was detected the nickel cluster solution was put under vacuum for one to five minutes before proceeding with further additions of  $PCl_3$ . Throughout the process it was possible to witness to the gradual formation of a

dark precipitate.

Once all the phosphorus reactant had been added, only  $\text{Ni}(\text{CO})_4$  along with traces of the  $[\text{Ni}_6(\text{CO})_{12}]^{2-}$  di-anion were left in solution, as confirmed via IR spectroscopy analysis. After the elimination of the volatile nickel tetracarbonyl and of the solvent under vacuum, the dried reaction mixture had to be thoroughly washed with water. This allowed to eliminate the organic and inorganic salts which formed during the reaction, such as nickel chlorides and ammonium chlorides. The aqueous solutions were usually colourless, yet sometimes the collected washings appeared greenish. The hue is a result of the presence of Ni(II) chloride salts - common by-products of the reaction - and its possible perceptibility is merely due to the concentration of the aqueous washing.

Posterior to that, the reaction mixture was deeply washed with THF to eliminate both  $[\text{Ni}_6(\text{CO})_{12}]^{2-}$  residues and potential traces of  $[\text{Ni}_9(\text{CO})_{18}]^{2-}$ . At last, the solid residue was extracted with acetone, thus allowing to obtain the product of interest,  $[\text{Ni}_{11}\text{P}(\text{CO})_{18}]^{3-}$ , as confirmed via IR spectroscopy analysis. Slow-diffusion of hexane into acetone concentrated solutions of the cluster usually originated good-quality crystals, though generally in small amounts.

The crystals were used to perform both an X-ray diffraction analysis and an IR spectroscopy analysis. The former allowed to determine the molecular structure of the cluster, and the latter granted to obtain the reference IR spectrum for  $[\text{Ni}_{11}\text{P}(\text{CO})_{18}]^{3-}$ . Its crystals were re-dissolved, and it was possible to notice that IR spectra collected in different solvents - acetone, and acetonitrile - did not display consistent differences -  $\nu_{\text{CO}}$  equal to 1980s, 1848m or 1982s, 1847m  $\text{cm}^{-1}$ .

This synthetic approach, although reproducible, has its flaws.  $[\text{Ni}_{11}\text{P}(\text{CO})_{18}]^{3-}$  is in fact the major product of the reaction, and the reported methodology usually allowed to obtain fair amounts of crystals. Still, this cluster was rarely obtained pure, and other species were commonly present in solution although in minor amounts. This was in all likelihood due to the high reactivity - as will be later discussed - of this cluster towards oxidising agents. Minimal amount of oxygen or of residual  $\text{PCl}_3$  could easily trigger the transformation of  $[\text{Ni}_{11}\text{P}(\text{CO})_{18}]^{3-}$  into higher-nuclearity, more oxidised species such as  $[\text{HNi}_{31}\text{P}_4(\text{CO})_{39}]^{5-}$ .

The low stability of this nickel-phosphorus cluster prevented all further reactivity studies, as it would have been impossible to determine whether  $[\text{Ni}_{11}\text{P}(\text{CO})_{18}]^{3-}$  or another related species was reacting.

### ***Structural, spectroscopic, and spectrometric characterisations***

$[\text{Ni}_{11}\text{P}(\text{CO})_{18}]^{3-}$  was thoroughly characterised despite its problematic synthesis. The regular although scarce formation of good-quality crystals allowed to obtain suitable samples for X-ray diffraction, IR spectroscopy, and electrospray ionisation - ESI - mass spectrometry analyses. The results that were obtained with each technique will be exposed in the following section.

#### ***✦ Structural characterisation***

The molecular structure of  $[\text{Ni}_{11}\text{P}(\text{CO})_{18}]^{3-}$  was discovered through a single-crystal X-ray diffraction analysis. Due to its low nuclearity, the structure of this nickel-phosphorus cluster is fairly uncomplicated (Figure 2.1).

Interestingly its metallic skeleton displayed a novel type of coordination compared to those of other nickel-pnictogen species, for phosphorus atoms as well as for nickel atoms. In other heteroleptic icosahedral species the phosphorus atoms were usually in apical position, yet in this case the post-transition element was interstitial and displayed a coordination number - C.N. - equal to ten.

More in detail, in the structure of this cluster the phosphorus atom was interstitial, and was hosted inside a ten-membered nickel cage. The cage was prismatic and had one squared base and one pentagonal base. Besides, the pentagonal base was capped by a further nickel atom. The last and eleventh nickel atom - the only one that was not coordinated to the post-transition element - capped one of the triangular faces of the prismatic cage.

There were no interstitial nickel atoms, clearly because of the reduced dimensions of the species.

The metallic core was surrounded by eighteen carbonyl ligands, which completed the coordination sphere of the cluster. Ten were linearly coordinated to one single nickel atom, and the remaining eight carbonyl ligands were bridging over nickel-nickel edges.

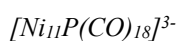
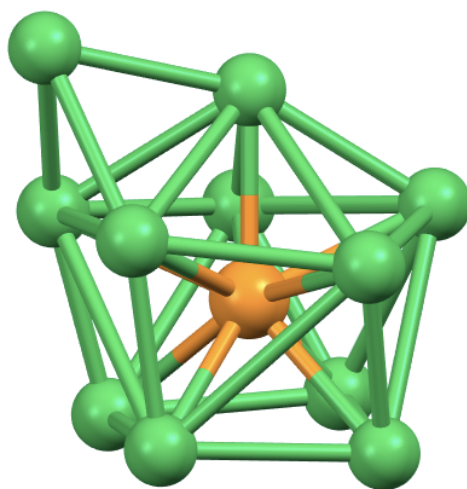
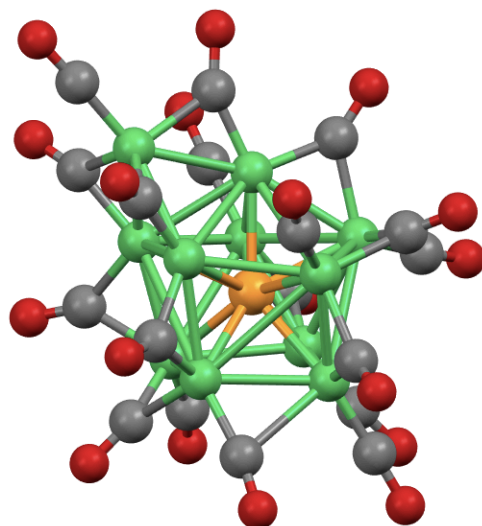


Figure 2.1 - Molecular structure and metallic skeleton of  $[\text{Ni}_{11}\text{P}(\text{CO})_{18}]^{3-}$ . The low nuclearity of the cluster allows to clearly distinguish the prismatic ten-membered nickel cage, the further capping atom, and the interstitial phosphorus atom. Nickel atoms are represented in green, phosphorus atoms in orange, carbon atoms in grey, oxygen atoms in red.

A selection of the crystal data that were collected for this cluster have been reported (Table 2.1). Its unit cell belonged to the  $\text{Pna}2_1$  space group of the orthorhombic C.S. - crystal system.

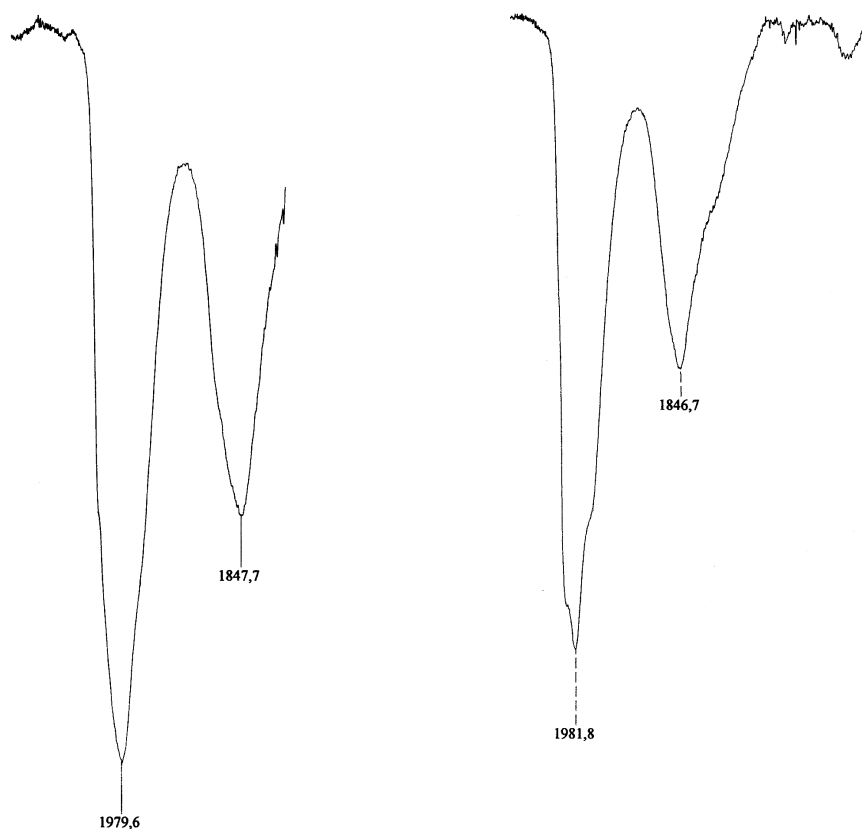


$a$ (Å)	25.313(2)	$\alpha$ (°)	90	<i>c.s.</i>	<i>orthorhombic</i>
$b$ (Å)	12.8319(11)	$\beta$ (°)	90	<b>space group</b>	$Pna2_1$
$c$ (Å)	16.8153(15)	$\gamma$ (°)	90	$U$ (Å <sup>3</sup> )	5461.8

Table 2.1 - Selected crystal data collected for  $[\text{Ni}_{11}\text{P}(\text{CO})_{18}]^{3-}$ .

#### ♦ Spectroscopic and spectrometric characterisation

As well as for a complete structural characterisation,  $[\text{Ni}_{11}\text{P}(\text{CO})_{18}]^{3-}$  crystals were dissolved and used for further purposes. The characteristic IR spectrum of this cluster did not change significantly either in acetone or acetonitrile (Figure 2.2). Its characteristic IR absorption frequencies have been reported (Table 2.2), with reference to different solvents.



IR spectra of  $[\text{Ni}_{11}\text{P}(\text{CO})_{18}]^{3-}$  in acetone and in acetonitrile

Figure 2.2 - IR spectra of  $[\text{Ni}_{11}\text{P}(\text{CO})_{18}]^{3-}$  recorded in different solvents. The spectra were coherent in terms of shape and IR absorption frequencies.

<i>solvent</i>	<i>THF</i>	<i>acetone</i>	<i>acetonitrile</i>
<b><i>IR absorption frequencies (cm<sup>-1</sup>)</i></b>	poorly soluble (with [NEt <sub>4</sub> ] <sup>+</sup> )	1980s 1848m	1982s 1847m

Table 2.2 - Characteristic IR absorption frequencies of [Ni<sub>11</sub>P(CO)<sub>18</sub>]<sup>3-</sup>.

\*\*\*

Also, a ESI mass spectrometry analysis was performed. An extremely diluted solution of the clusters was prepared by dissolving few crystals in acetonitrile. The sample was then analysed with an ESI mass spectroscope and the reference mass spectrum of [Ni<sub>11</sub>P(CO)<sub>18</sub>]<sup>3-</sup> was successfully acquired.

Mass spectra of cluster compounds may appear unusual, as the signal of the molecular ion - that usually corresponds to the base peak - is generally missing. On the contrary, this phenomenon is common for many carbonyl clusters. Clusters are in fact fragile species, and they generally do not endure unscathed the ionisation process. The attribution process that links each recorded peak to the corresponding original molecular fragment might seem difficult, due to the absence of the signal of the molecular ion, but this is a surmountable problem.

In the mass spectra of clusters it is typically possible to individuate at least one - but usually more - group of evenly spaced peaks. These signals are typically originated from the same cluster moiety which has progressively lost carbonyl ligands. The registered gap between each peak therefore allows to extrapolate the anionic charge of the original fragment, and so it is also possible to tentatively figure its formula. Being it known that a single carbonyl ligand bears a mass equal to 28 u, a group of peaks that are evenly spaced by 14 *m/z* units should indicate that the mother fragment bears a di-anionic charge. Likewise, a group of peaks that are evenly spaced by 9 *m/z* units should indicate the presence of a tri-anionic moiety, and so on. Once the anionic charge of the fragment has been individuated, it is possible to identify its formula by trial and error.

Finally, it is also important to remember that the ionised fragments may not be exclusively formed by cluster moieties. Throughout the ionisation processes the ruptured clusters may retain other atoms or even entire molecules - chlorine at-

oms, solvent molecules, or cation molecules.

$[Ni_{11}P(CO)_{18}]^{3-}$  is a low-nuclearity cluster, and this characteristics avoided an excessive fragmentation of the species. However, the interpretation of the mass spectra of nickel clusters is frequently challenging because of the intrinsic characteristics of this metal. In fact, nickel has five naturally-occurring stable isotopes<sup>1</sup> - the most abundant  $^{58}Ni$  plus  $^{60}Ni$ ,  $^{61}Ni$ ,  $^{62}Ni$ , and  $^{64}Ni$  - whose presence multiplies the number of peaks.

By comparing different theoretical mass spectra of hypothetical deca-nuclear metallic compounds -  $Co_{10}$ ,  $Rh_{10}$ ,  $Au_{10}$ ,  $Ni_{10}$ ,  $Pd_{10}$ , and  $Pt_{10}$  have been arbitrarily chosen - it is possible to notice two very distinct behaviours (Figure 2.3).

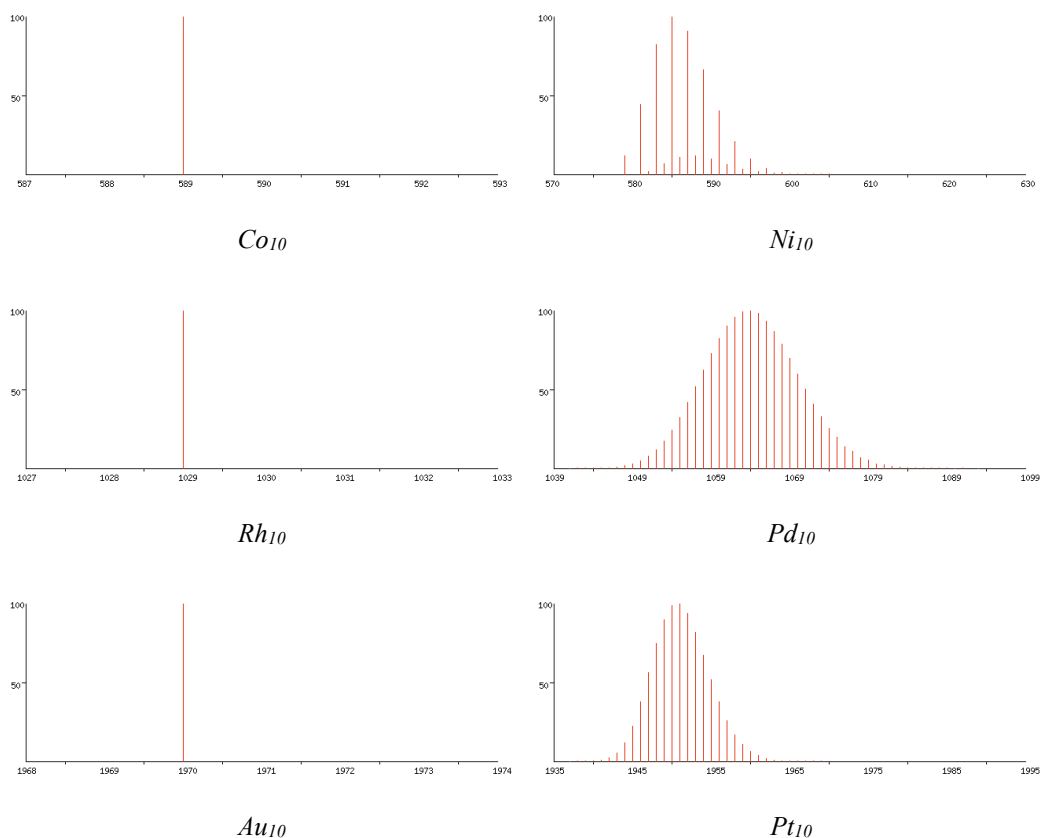


Figure 2.3 - Theoretical mass spectra of two series of hypothetical deca-nuclear metallic compounds. On the abscissa axes the mass over charge ( $m/z$ ) ratio is reported. On the ordinate axes the relative abundance (%) is reported. The series corresponding to mono-isotopic metals has been reported on the left, the series corresponding to poly-isotopic metals on the right.

<sup>1</sup> J. W. Gramlich, L. A. Machlan, I. L. Barnes, P. J. Paulsen; *J. Res. Natl. Inst. Stand. Technol.*, **1989** (94) 347-356

On one hand,  $d^{10}$  metals as nickel, palladium, and platinum have numerous stable isotopes. Therefore, these mass spectra tend to display a wide distribution of peaks around the base one, whose intensities reflect the natural abundance of each isotope. On the other hand, metals as cobalt, rhodium, and gold have just one naturally-occurring isotope. As a result, these mass spectra consist in one single peak. It is also worth to mention that the magnitude of this phenomenon increases along with the number of metallic atoms, and therefore it is more intense for clusters with higher nuclearities.

This phenomenon, along with the aforementioned fragmentation of the clusters, further complicated the interpretation of the recorded signals.

Nonetheless, by applying the presented approach - which is usually referred to as the carbonyl-loss method - to the  $[\text{Ni}_{11}\text{P}(\text{CO})_{18}]^{3-}$  mass spectra (Figure 2.4) it was possible to pair most of the registered peaks with their corresponding fragments, whose supposed formulae have been reported (Table 2.3).

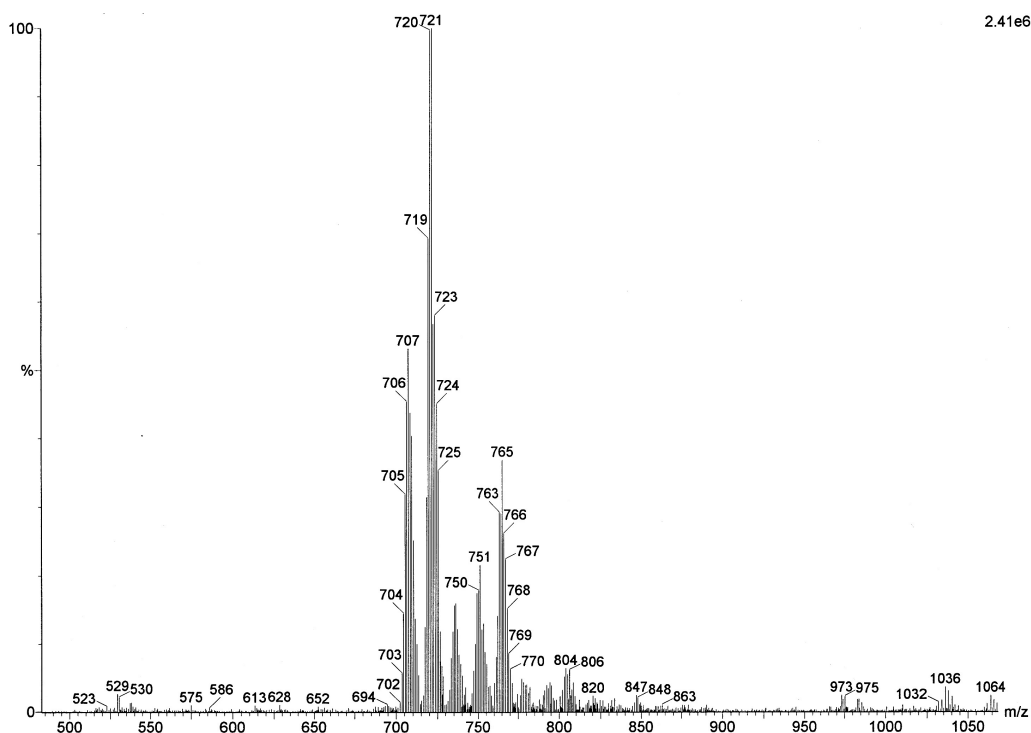


Figure 2.4 - ESI mass spectrum of  $[\text{Ni}_{11}\text{P}(\text{CO})_{18}]^{3-}$ . Due to the low nuclearity of the cluster the species did not undergo to excessive fragmentation processes, as evidenced by the moderate number of recorded peaks.

<i>peak (<math>m/z</math>)</i>	<i>corresponding cluster moiety</i>
765	$\{[Ni_{11}P(CO)_{18}][NEt_4]_2[CH_3CN]_2\}^{2-}$
751	$\{[Ni_{11}P(CO)_{17}][NEt_4]_2[CH_3CN]_2\}^{2-}$
736	$\{[Ni_{11}P(CO)_{16}][NEt_4]_2[CH_3CN]_2\}^{2-}$
720	$\{[Ni_{11}P(CO)_{18}][NEt_4]_2\}^{2-}$
707	$\{[Ni_{11}P(CO)_{17}][NEt_4]_2\}^{2-}$
530	$\{[Ni_{10}P(CO)_{16}]\}^{2-}$

Table 2.3 - Values of the characterised peaks and species to which they have been associated to during the interpretation of the ESI mass spectrum of  $[Ni_{11}P(CO)_{18}]^{3-}$ .

\*\*\*

It would have been interesting to perform a  $^{31}P$  NMR spectroscopy analysis on  $[Ni_{11}P(CO)_{18}]^{3-}$ , since its low nuclearity could have allowed to record a spectrum.

Unfortunately, it proved not to be the case. The other aforementioned characterisation techniques were successfully employed since they are usually performed on very diluted solutions or even on single-crystals. On the contrary, NMR analyses require samples whose concentration is rather high. The scarce stability of  $[Ni_{11}P(CO)_{18}]^{3-}$  excluded this possibility, as it proved to be extremely unlikely to obtain the cluster in large quantities with the required purity degree.

### ***Reactivity test***

As aforementioned, it was not possible to perform a comprehensive study on the reactivity of this nickel-phosphorus cluster. Despite crystalline samples being frequently obtained, the amounts available were never adequate in order to be properly used to conduct and follow a reaction.

On just one occasion the crystallisation process occurred quantitatively. Amongst all the possibilities, it was decided to perform an oxidation test. The aim was to validate the previously proposed reaction mechanism, for which  $[Ni_{11}P(CO)_{18}]^{3-}$  was an intermediate product - it had been supposed that the reac-

tion between  $[\text{Ni}_6(\text{CO})_{12}]^{2-}$  and  $\text{PCl}_3$  eventually led to the formation of  $[\text{HNi}_{31}\text{P}_4(\text{CO})_{39}]^{5-}$ . To do so, a non-phosphorous oxidant was used in order to trigger the oxidation of the cluster and at the same time avoid any possible interference caused by  $\text{PCl}_3$ . In case  $[\text{Ni}_{11}\text{P}(\text{CO})_{18}]^{3-}$  actually reacted to give  $[\text{HNi}_{31}\text{P}_4(\text{CO})_{39}]^{5-}$  the proposed mechanism would have been validated.

The oxidation trial was conducted as follows. Crystals of  $[\text{Ni}_{11}\text{P}(\text{CO})_{18}]^{3-}$  were dissolved into acetonitrile, and the purity of the sample was controlled via IR spectroscopy. After that, a freshly prepared 1:100  $\text{m}/\text{v}$  diluted solution of tropilium tetrafluoroborate was drop-wise added to the cluster solution.

By following the reaction progresses via IR spectroscopy it was possible to witness to the gradual decrease of the absorption frequencies of  $[\text{Ni}_{11}\text{P}(\text{CO})_{18}]^{3-}$ , along with the gradual increase of the characteristic absorption frequencies of  $[\text{HNi}_{31}\text{P}_4(\text{CO})_{39}]^{5-}$  (Figure 2.5).

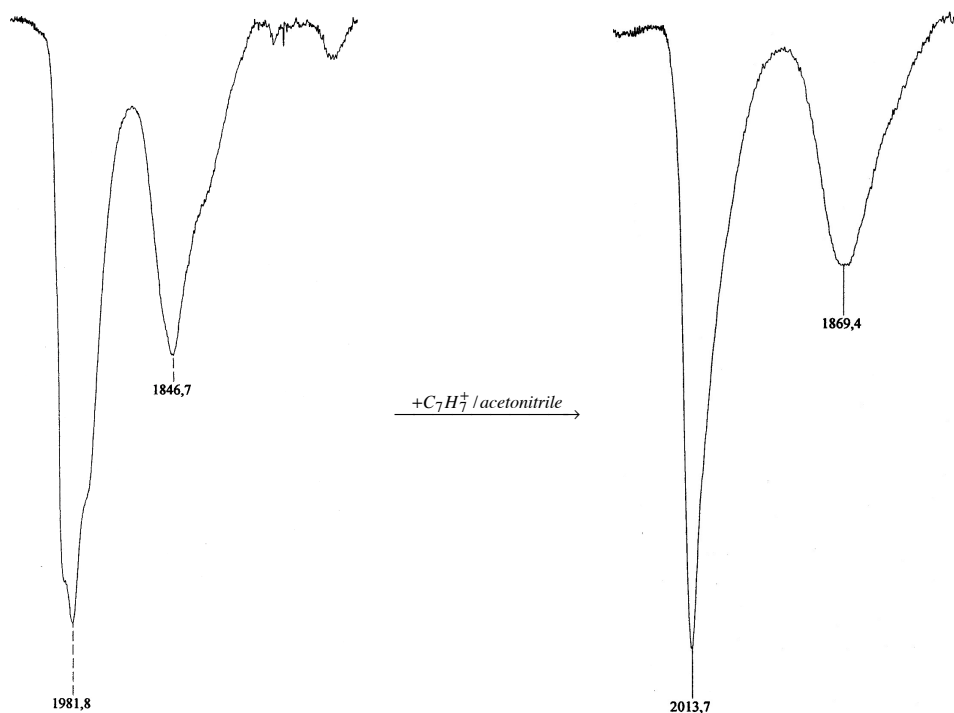


Figure 2.5 - IR spectra recorded in acetonitrile. On the left, spectrum of  $[\text{Ni}_{11}\text{P}(\text{CO})_{18}]^{3-}$  recorded before the oxidation reaction and, on the right, spectrum of the product of the reaction, the high-nuclearity  $[\text{HNi}_{31}\text{P}_4(\text{CO})_{39}]^{5-}$ .

At the end of the reaction, only the latter species was present in solution according to the IR spectrum. This confirmed the hypothesis and the proposed reaction mechanism (Figure 2.6).

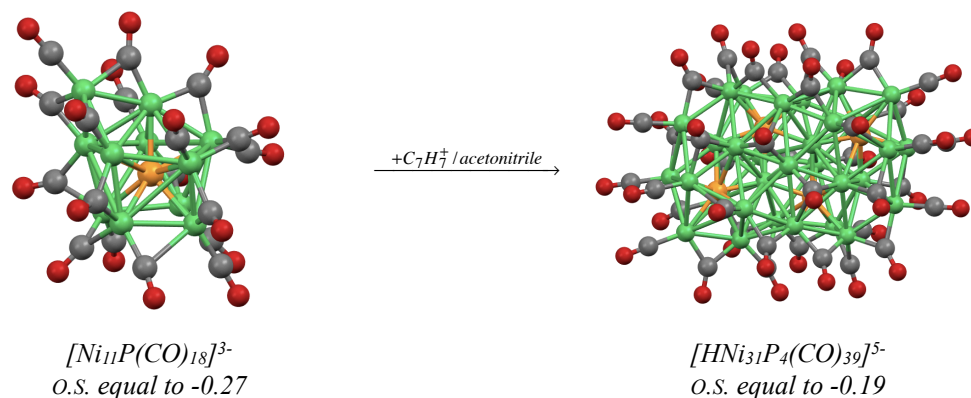


Figure 2.6 - Reaction scheme illustrating that  $[Ni_{11}P(CO)_{18}]^{3-}$  is oxidised to  $[HNi_{31}P_4(CO)_{39}]^{5-}$  when a mild oxidant is present. Nickel atoms are represented in green, phosphorus atoms in orange, carbon atoms in grey, oxygen atoms in red.

\*\*\*

Finally, these results were in part confirmed by the data obtained through some preliminary spectroelectrochemical analyses, performed along with cyclic voltammetry - C.V. - analyses. For what concerns the C.V. analyses, the information available at the moment are limited and non-conclusive. However, the data obtained from the spectroelectrochemical analyses were consistent with those obtained throughout the spectroscopic analyses. Therefore, it has been decided to report them, notwithstanding their ongoing development (Table 2.4).

$\nu_{CO} (cm^{-1})$	1980s 1846m	2015s 1861m	2023s 1873m
$E (V)$	-0.50	+0.10	+0.34
<i>associated species</i>	$[Ni_{11}P(CO)_{18}]^{3-}$	$[Ni_{31}P_4(CO)_{39}]^{5-}$	$[Ni_{31}P_4(CO)_{39}]^{4-}$

Table 2.4 - IR absorption frequencies recorded during the spectroelectrochemical analysis and corresponding potential  $E$ . The data were collected from an acetonitrile solution of the cluster.

The analysis was performed on an acetonitrile solution of the clusters in crystalline form. These preliminary data revealed an interesting behaviour, as they seem to be validating the previously proposed reaction mechanism.

In fact, by oxidising  $[\text{Ni}_{11}\text{P}(\text{CO})_{18}]^{3-}$  it was possible to record two distinct sets of IR absorption frequencies whose values were closely related to those of  $[\text{HNi}_{31}\text{P}_4(\text{CO})_{39}]^{5-}$  and  $[\text{H}_2\text{Ni}_{31}\text{P}_4(\text{CO})_{39}]^{4-}$ , respectively. It appeared as the original cluster had transformed into a different species rather than being oxidised. The minor variations that involved the signals of the bridging carbonyls were probably due to the different environments in which the analyses were performed.

These data are remarkably significant, as they seem to be supporting the hypothesised reaction mechanism between the  $[\text{Ni}_6(\text{CO})_{12}]^{2-}$  precursor, the  $[\text{Ni}_{11}\text{P}(\text{CO})_{18}]^{3-}$  intermediate product, and the  $[\text{HNi}_{31}\text{P}_4(\text{CO})_{39}]^{5-}$  final product. Still, a definitive validation of this process will possibly derive from the definitive results.

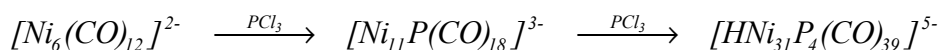


## $[\text{H}\text{Ni}_{31}\text{P}_4(\text{CO})_{39}]^{5-}$ and $[\text{H}_2\text{Ni}_{31}\text{P}_4(\text{CO})_{39}]^{4-}$ Synthesis, characterisation, and reactivity

### *Synthetic approach and further considerations*

#### ✦ $[\text{H}\text{Ni}_{31}\text{P}_4(\text{CO})_{39}]^{5-}$ - penta-anionic form

The major difficulties that needed to be overcome were due to the intrinsic mechanism of the synthetic reaction (Scheme 3.1). It has just been illustrated that  $[\text{Ni}_{11}\text{P}(\text{CO})_{18}]^{3-}$  and  $[\text{H}\text{Ni}_{31}\text{P}_4(\text{CO})_{39}]^{5-}$  are formed one after the other, as the first is an intermediate cluster product of the reaction.



*Scheme 3.1 - Schematisation of the oxidation reaction of  $[\text{Ni}_6(\text{CO})_{12}]^{2-}$  with  $\text{PCl}_3$ .*

Once the mechanism of the reaction between  $[\text{Ni}_6(\text{CO})_{12}]^{2-}$  and  $\text{PCl}_3$  had been clarified it was then possible to focus on refining the synthesis of the other species,  $[\text{H}\text{Ni}_{31}\text{P}_4(\text{CO})_{39}]^{5-}$ . In the following paragraphs the very same reaction between  $[\text{Ni}_6(\text{CO})_{12}]^{2-}$  and  $\text{PCl}_3$  will be completely re-imagined and reinvestigated, focusing on improving the yields, the selectivity, and the purity of  $[\text{H}\text{Ni}_{31}\text{P}_4(\text{CO})_{39}]^{5-}$ .

It has already been said that the co-crystallisation of this couple of heteroatomical compounds was a common phenomenon, and only after a significant amount of trials a recurrent behaviour became apparent. Co-crystallisation had been observed when the reactions were held both in acetonitrile and in tetrahydrofuran. Nonetheless, whenever the former was used this undesired phenomenon was significantly less frequent.

Due to this acetonitrile was selected as solvent in order to favour the formation of  $[\text{H}\text{Ni}_{31}\text{P}_4(\text{CO})_{39}]^{5-}$ . It was supposed that its higher polarity might have promoted the reactivity of the intermediate species, by retaining it in solution with

$\text{PCl}_3$  and therefore allowing it to be completely converted.

This choice allowed to reduce the occurring of co-crystallisation phenomena, and diverse pure crystalline samples of  $[\text{HNi}_{31}\text{P}_4(\text{CO})_{39}]^{5-}$  were obtained. Independent samples were used to perform both IR spectroscopy and X-ray diffraction analyses. The results were coherent, and thus it was possible to associate the molecular structure with its characteristic IR absorption frequencies -  $\nu_{\text{CO}}$  equal to 2014s, 1870m  $\text{cm}^{-1}$  in acetonitrile.

Eventually it was possible to refine a suitable synthetic route for  $[\text{HNi}_{31}\text{P}_4(\text{CO})_{39}]^{5-}$ , by using acetonitrile as solvent and changing the stoichiometric ratio between  $[\text{Ni}_6(\text{CO})_{12}]^{2-}$  and  $\text{PCl}_3$ .

The difficulties that were encountered were in fact due to the equivocality of the reaction mechanism rather than to the reaction conditions themselves. As already discussed, by using acetonitrile as solvent the problems related to the possible presence of  $[\text{Ni}_{11}\text{P}(\text{CO})_{18}]^{3-}$  impurities were promptly minimised.

By using this solvent it was also possible to prevent other undesired complications. For example, it was already mentioned how even traces of  $[\text{Ni}_9(\text{CO})_{18}]^{2-}$  could inhibit or reduce the solubility of the nickel precursor whenever THF or other low-polarity solvents were used. Acetonitrile is quite more polar and therefore problems related to this cluster impurity were less relevant. The handling of the  $\text{PCl}_3$  solutions was less restrained for the same reasons - humidity and the consequent formation of HCl had to be limited in any case, but traces could be tolerated.

The nickel cluster precursor was prepared in accord to the literature. The nature of the cation proved not have a sensitive influence neither on the solubility of  $[\text{Ni}_6(\text{CO})_{12}]^{2-}$  in acetonitrile nor on the overall reaction course, therefore any could be used. It was however noticed that crystallisation processes were favoured by using tetra-ethyl-ammonium as counter-ion.

The chosen nickel cluster salt was dissolved in the minimal amount of acetonitrile, and the solution was placed inside a suitable Schlenk tube. A 1:50 up to 1:100  $\text{V}/\text{V}$   $\text{PCl}_3$  solution was prepared in the same solvent, considering a 1 to 1 stoichiometric ratio. The actually needed proportion is lower, and usually the

nickel reactant was completely consumed at a 1 to 0.7 stoichiometric ratio. Still, a higher amount of  $\text{PCl}_3$  was seldom required to fulfil the reaction. This phenomenon could be explained by considering that in some instances the  $[\text{Ni}_6(\text{CO})_{12}]^{2-}$  was not completely pure - as well as the phosphorous trichloride.

The starting nickel cluster solution was analysed through IR spectroscopy, and then the  $\text{PCl}_3$  solution was gradually added to it. After each aliquot a IR spectrum of the reaction mixture was acquired. Due to the solubilising power of acetonitrile, throughout these reactions it was possible to witness to the rise of the IR absorption peaks of the cluster products, along with the decrease of the peaks associated to the nickel precursor.

Whenever an excessive quantity of nickel tetracarbonyl was detected, vacuum was applied in order to eliminate it. The products of the reaction were retained in solution, and the formation of dark or black precipitates was never detected. The reaction could be considered concluded once the characteristic signals of  $[\text{Ni}_6(\text{CO})_{12}]^{2-}$  were no longer visible in the IR spectrum.

The reaction mixture was then put under vacuum, so that  $\text{Ni}(\text{CO})_4$  and acetonitrile could be removed. The solid thus obtained was washed with water at first, and then with THF. In the aqueous solution it was possible to collect organic and inorganic waste - mostly nickel chlorides and organic chlorides. Within the tetrahydrofuran solution it was possible to extract  $[\text{Ni}_6(\text{CO})_{12}]^{2-}$  residues, along with occasional traces of  $[\text{Ni}_9(\text{CO})_{18}]^{2-}$ . In order for the reaction to be deemed successful this organic extraction had to be considerably diluted. The opposite would have indicated an insufficient degree of conversion for the nickel cluster precursor.

With acetone it was occasionally possible to extract  $[\text{Ni}_{11}\text{P}(\text{CO})_{18}]^{3-}$  in minor quantities. With acetonitrile it was possible to extract the product of interest -  $[\text{HNi}_{31}\text{P}_4(\text{CO})_{39}]^{5-}$  - as confirmed via IR spectroscopy analyses. However, by using cations different from tetra-ethyl-ammonium the cluster could be extracted with other solvents.

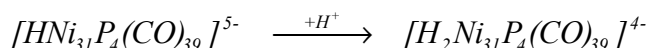
The crystallisation of the  $[\text{HNi}_{31}\text{P}_4(\text{CO})_{39}]^{5-}$  penta-anion occurred frequently, thus allowing a prompt structural characterisation of the species. However, whenever  $[\text{Ni}_{11}\text{P}(\text{CO})_{18}]^{3-}$  was still present in solution it would co-crystallise. Presuma-

bly, its lower nuclearity promoted the crystallisation of even minimal amounts of the cluster.

This synthetic approach was reproducible and by following these steps it was always possible to obtain good-quality samples of  $[\text{HNi}_{31}\text{P}_4(\text{CO})_{39}]^{5-}$  - save rare exceptions. As a consequence, for this nickel-phosphorus carbonyl cluster a comprehensive investigation was achieved, regarding both its intrinsic characteristics and its behaviour towards different reacting conditions. The full results will be reported in the ensuing chapters.

♦  **$[\text{H}_2\text{Ni}_{31}\text{P}_4(\text{CO})_{39}]^{4-}$  - tetra-anionic form**

Briefly, for what concerns the synthesis of  $[\text{H}_2\text{Ni}_{31}\text{P}_4(\text{CO})_{39}]^{4-}$  - *i.e.* the tetra-anionic form of the cluster - it involved a simple protonation reaction (Scheme 3.2). First the penta-anionic form had to be prepared, according to the previously reported methodology. Then, by treating the cluster solution with a mild protic acid solution it was possible to witness to a moderate rise of the IR absorption frequencies towards higher values. It was later assessed that the presence of the tetra-anionic cluster was confirmed whenever the IR absorption frequencies had stabilised at 2024s, 1885m  $\text{cm}^{-1}$ .



*Scheme 3.2 - Schematisation of the protonation reaction from the penta-anion to the tetra-anion.*

A crystalline sample was obtained by layering hexane over the acetone solution of the cluster. The species had been identified as  $[\text{H}_2\text{Ni}_{31}\text{P}_4(\text{CO})_{39}]^{4-}$  throughout an X-ray diffraction analysis.

Few crystals were re-dissolved in order to record a reference IR spectrum for the cluster, whose IR absorption frequencies in acetone and acetonitrile were coherent to those recorded before the crystallisation.

## ***Structural, spectroscopic, and spectrometric characterisations***

### ***♦ Structural characterisation - premises***

It was possible for  $[\text{HNi}_{31}\text{P}_4(\text{CO})_{39}]^{5-}$  to be characterised via X-ray diffraction analyses numerous times, by using crystals obtained from independent samples. These analysis provided unique data sets, each corresponding to a unique molecular structure.

Unsurprisingly, all the molecular structures were coherent and  $[\text{HNi}_{31}\text{P}_4(\text{CO})_{39}]^{5-}$  always displayed the same overall skeletal arrangement, not depending on the nature of the solvent or of the non-solvent. Some differences were actually uncovered, yet their entity was minimal.

At first only one of the molecular structures will be fully discussed, and later on considered as reference. The ensuing molecular structures will be compared to the reference one, and only their differences will be highlighted. The same comparative approach towards the structural analysis will be applied to the  $[\text{H}_2\text{Ni}_{31}\text{P}_4(\text{CO})_{39}]^{4-}$  tetra-anion, as its structure was as well coherent to those of the penta-anions.

\*\*\*

Before proceeding with the actual structural descriptions, it would be worthwhile to consider the coordination sites that could be available for the hydride hydrogen atoms. The empirical observations that led to the acknowledgement of the hydride nature of  $[\text{HNi}_{31}\text{P}_4(\text{CO})_{39}]^{5-}$  will be reported in the chapter dedicated to the reactivity of the cluster. In this paragraphs only the possible locations of the hydride atoms will be presented.

It is matter of fact that X-ray diffraction analyses can not give direct information about hydrogen atoms within large metallic clusters. Due to this, a rational survey of all the possibly available coordinative sites will be exposed.

On one hand, the hydride hydrogen atoms could be interstitial.<sup>1,2</sup> The metallic radius -  $r_M$  - of a nickel atom is equal to 1.24 Å.<sup>3</sup> The radius of a hydrogen atom that is coordinated to a metallic skeleton ranges from a minimum of 0.37 Å to a maximum of 1.30 Å - covalent radii of hydrogen and full-hydride hydrogen, respectively.<sup>4</sup> It can be calculated that  $0.228 \cdot r_M$  is the maximum radius value that permits to an interstitial atom to be hosted inside a tetrahedral cage. Analogously, for an atom to be enclosed in a metallic octahedral cage its radius have not to be larger than  $0.414 \cdot r_M$ . Given that, it follows that in nickel clusters as  $[\text{HNi}_{31}\text{P}_4(\text{CO})_{39}]^{5-}$  and its di-hydride derivative only octahedral cavities could host the hydride atoms.

On the other hand, the hydrogen atom could also be superficially coordinated to the outward metallic skeleton.<sup>5,6</sup> Squared or larger faces on the metallic surface should allow sufficient clearance for the hydrogen atom to be efficiently coordinated and not to be hindered by the carbonyl ligands.

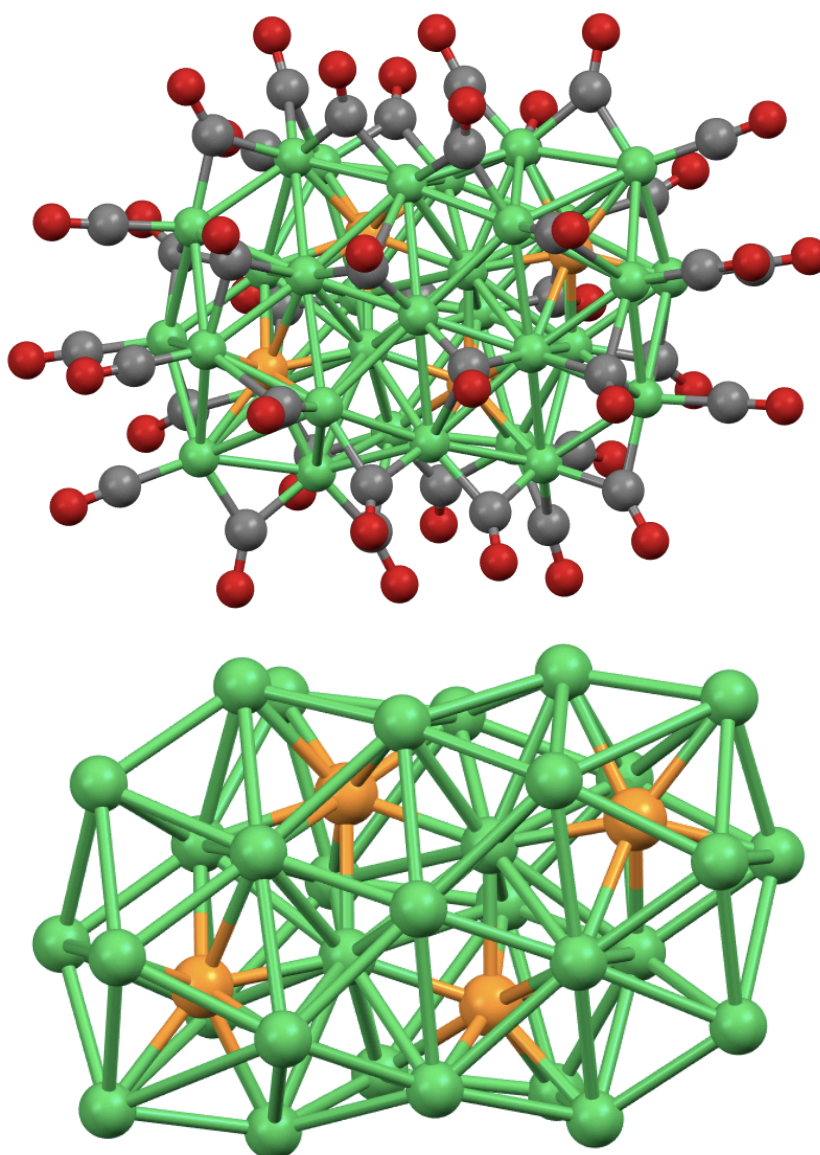
In the following descriptions any suitable cavity or superficial coordination site will be highlighted and detailed.

♦ ***Structural characterisation of the penta-anion (symmetrical structures)***

Two different crystalline samples of  $[\text{HNi}_{31}\text{P}_4(\text{CO})_{39}]^{5-}$  were obtained from acetone solutions of the cluster, one through slow diffusion of hexane and one through slow diffusion of isopropanol. The corresponding molecular structures differed over minor features and will be presented together.

- 
- <sup>1</sup> P. F. Jackson, B. F. G. Johnson, J. Lewis, P. R. Raithby, M. McPartlin, W. J. H. Nelson, K. D. Rouse, J. Allibon, S. A. Mason; *J. Chem. Soc., Chem. Commun.*, **1980** (7) 295-297
  - <sup>2</sup> D. W. Hart, R. G. Teller, C. Y. Wei, R. Bau, G. Longoni, S. Campanella, P. Chini, T. F. Koetzle; *J. Am. Chem. Soc.*, **1981** (103) 1458-1466
  - <sup>3</sup> B. Cordero, V. Gómez, A. E. Platero-Prats, M. Revés, J. Echeverría, E. Cremades, F. Barragán, S. Alvarez; *Dalton Trans.*, **2008** (21) 2832-2838
  - <sup>4</sup> R. Bau, M. H. Drabnis, L. Garlaschelli, W. T. Klooster, Z. Xie, T. F. Koetzle, S. Martinengo; *Science*, **1997** (275) 1099-1101
  - <sup>5</sup> S. A. R. Knox, J. W. Koepke, M. A. Andrews, H. D. Kaesz; *J. Am. Chem. Soc.*, **1975** (97) 3942-3947
  - <sup>6</sup> J. L. Vidal, W. E. Walker; *Inorg. Chem.*, **1981** (20) 249-254

These molecular structures were formed by a nickel-phosphorus core surrounded by the carbonyl ligands (Figure 3.1). The COs were varyingly coordinated, as twelve were singularly bonded, twenty-three were bridging over a nickel-nickel edge, and four were bridging over a triangular nickel face. Interestingly, these high-nuclearity frameworks were symmetrical and were composed by the two identical  $Ni_{16}P_2(CO)_{20}$  sub-units, which shared a nickel-carbonyl fragment.

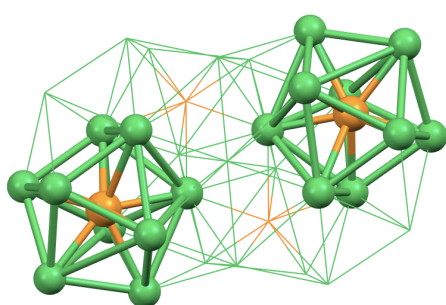


$[HNi_{31}P_4(CO)_{39}]^{5-}$

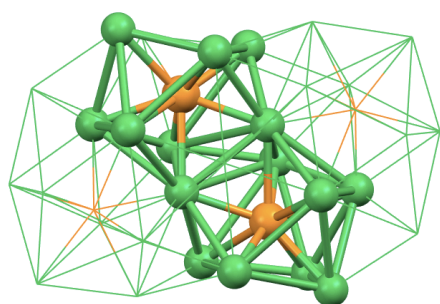
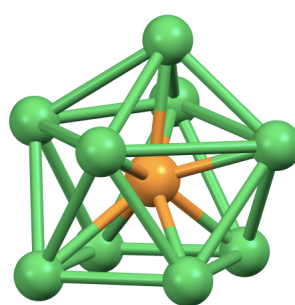
Figure 3.1 - Molecular structure and metallic skeleton of one of the symmetrical forms of the high-nuclearity  $[HNi_{31}P_4(CO)_{39}]^{5-}$  penta-anion. Nickel atoms are represented in green, phosphorus atoms in orange, carbon atoms in grey, oxygen atoms in red.

These metallic frameworks were prismatic rather than close-packed, in accord with the structure of  $[\text{Ni}_{11}\text{P}(\text{CO})_{18}]^{3-}$ . This suggested that this behaviour was not due to the low nuclearity of the species, but was possibly peculiar to the whole family of compounds.

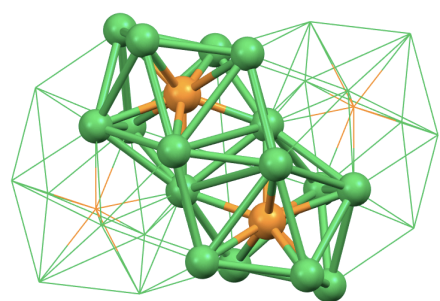
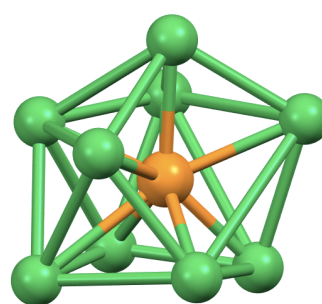
In these symmetrical molecular structures of  $[\text{HNi}_{31}\text{P}_4(\text{CO})_{39}]^{5-}$  the phosphorus atoms were in interstitial positions. The four heteroatoms formed two symmetrical couples, nonetheless they all displayed very similar coordinations. All had a C.N. equal to nine, and were inside prismatic nickel cages (Figure 3.2). In each molecular structure two open and two closed  $\text{Ni}_9(\mu_9\text{-P})$  moieties were present.



*Closed  $\text{Ni}_9(\mu_9\text{-P})$  moieties*



*Open  $\text{Ni}_9(\mu_9\text{-P})$  moieties*



*Open  $\text{Ni}_9(\mu_9\text{-P})$  moieties*

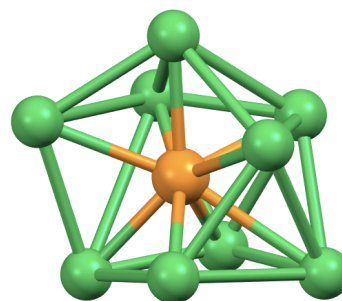


*Figure 3.2 - Structures of the two types of phosphorus-hosting cavities within the symmetrical metallic skeletons of  $[\text{HNi}_{31}\text{P}_4(\text{CO})_{39}]^{5-}$ . On the left the position of the symmetrical moieties has been highlighted. Nickel atoms are represented in green, phosphorus atoms in orange.*

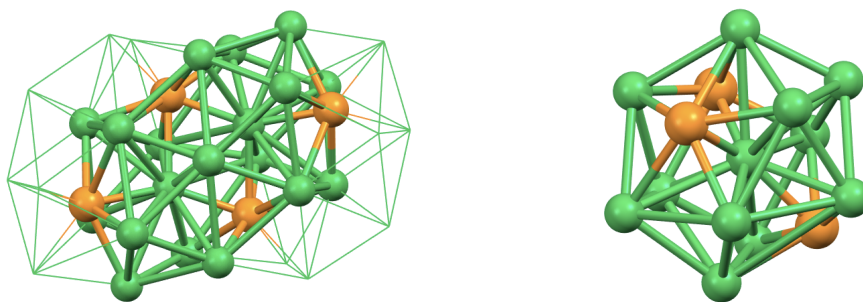


Each of the corresponding  $Ni_9(\mu_9-P)$  moieties was shaped as a monocapped squared anti-prism of nickel atoms, within which a phosphorus atom was hosted.

It is worth to mention that in both these metallic skeletons one of the two couples of nickel cavities was slightly distorted, despite maintaining the same general structure. The defect was located in the capped squared bases, which were in fact open four-membered rings. Due to this, one side of the two identical nickel anti-prisms was ajar, and a larger face was present instead of a triangular one.

In one of the two molecular structures only one nickel-nickel interaction was missing, and there was a squared lateral face on the side of the prisms. In the other molecular structure this defect was more pronounced - two nickel-nickel interactions were missing. Due to this, a pentagonal lateral aperture was present.

Two symmetrical interstitial nickel atoms were present inside these metallic skeletons of  $[HNi_{31}P_4(CO)_{39}]^{5-}$ , owing to the high nuclearity of the cluster. These interstitial nickel atoms displayed a coordination number equal to fourteen, and were located within two identical heteroatomical cages (Figure 3.3).



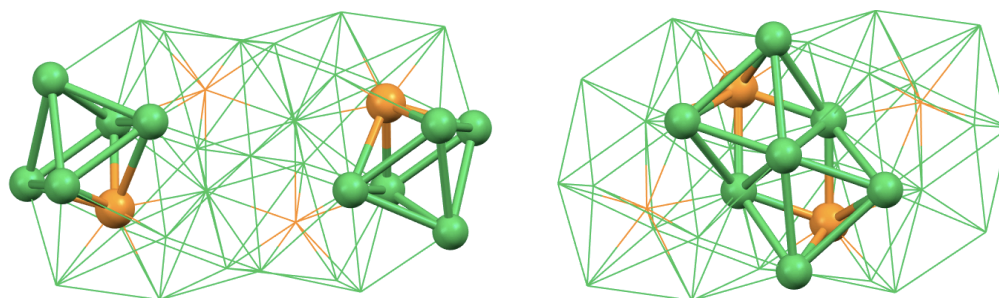
$Ni_{11}P_3(\mu_{14-Ni})$  moieties

*Figure 3.3 - Structure of the only type of nickel-hosting cavity within the symmetrical metallic skeletons of  $[HNi_{31}P_4(CO)_{39}]^{5-}$ . On the left the interpenetrating position of the moieties has been highlighted. Nickel atoms are represented in green, phosphorus atoms in orange.*

The resulting  $Ni_{11}P_3(\mu_{14-Ni})$  moieties were highly misshapen, and it was difficult to identify a geometry which could represent them. The presence of three phosphorus atoms - whose dimensions are significantly smaller than those of the nickel atoms - caused a considerable distortion. The whole cages were irregular,

yet a shape could be eventually identified. In each moiety, two opposing nickel atoms appeared to be in apical position, and to be capping a six-membered heteroatomical ring. Considering this, the two nickel-hosting  $\text{Ni}_{11}\text{P}_3(\mu_{14}\text{-Ni})$  structures could be described as a bi-capped hexagonal anti-prisms, or as anti-prismatic fourteen-hedra. Unfortunately the heteroatomical rings were not planar, and this depiction has a mostly theoretical value.

Finally, diverse possible location sites for the hydride hydrogen atom were present in the symmetrical molecular structures of  $[\text{HNi}_{31}\text{P}_4(\text{CO})_{39}]^{5-}$ . First, inside the metallic skeletons there were two symmetrical couples of octahedral cavities (Figure 3.4). Each cage was heteroatomical and comprehended one phosphorus atom, and all were fairly regular in shape. The  $\text{Ni}_5\text{P}$  octahedra were large enough to possibly host a hydride hydrogen atom.



*Ni<sub>5</sub>P octahedral cavities*

*Figure 3.4 - The two types of octahedral Ni<sub>5</sub>P cavities have been highlighted within the symmetrical metallic skeletons of  $[\text{HNi}_{31}\text{P}_4(\text{CO})_{39}]^{5-}$ . Nickel atoms are represented in green, phosphorus atoms in orange.*

Moreover, on the surface of these metallic skeletons there were two symmetrical nickel faces which were sufficiently large to coordinate the hydride hydrogen atom. In one of these symmetrical molecular structures there were two tetragonal faces, whilst in the other there were two non-planar pentagonal faces.

A selection of the two crystal data sets that were collected for the symmetrical forms of this cluster have been reported (Table 3.1). Both unit cells belonged to

the C2/c space group of the monoclinic crystal system, and displayed remarkably similar parameters.

In fact, neither isopropanol nor hexane molecules were individuated within the unit cells of these molecular structures, which therefore adopted similar packings. If non-solvent molecules had been present inside the unit cells, then these two molecular structures would have probably displayed two different crystal data sets.

$a$ (Å)	26.057(3) 26.104(4)	$\alpha$ (°)	90 90	<i>c.s.</i>	<i>monoclinic</i> <i>monoclinic</i>
$b$ (Å)	20.742(3) 21.179(3)	$\beta$ (°)	97.736(2) 98.268(2)	<i>space group</i>	<i>C2/c</i> <i>C2/c</i>
$c$ (Å)	23.666(3) 23.546(4)	$\gamma$ (°)	90 90	$U$ (Å <sup>3</sup> )	12674.3 12882.5

Table 3.1 - Selected crystal data collected for  $[HNi_{31}P_4(CO)_{39}]^{5-}$ . Data collected from the isopropanol-acetone crystals are reported in the upper rows, data collected from the hexane-acetone crystals in the lower rows.

✦ **Structural characterisation of the penta-anion (non-symmetrical structure)**

Another crystalline sample of  $[HNi_{31}P_4(CO)_{39}]^{5-}$  was obtained from an acetonitrile solution, via slow diffusion of diisopropyl ether through a thin layer of hexane. Whilst the previously described molecular structures of this cluster were closely related, this one was to a certain extent different.

Concerning this molecular structure (Figure 3.5), the main diverging aspect lies in the absence of symmetry. Nonetheless, it was still possible to consider this structure as *quasi*-symmetrical. For example, it was noticed that the nickel cages that hosted the heteroatoms were two by two closely related, and could therefore be considered as matching.

As well as in the other molecular structures, all the interstitial phosphorus atoms shared the same coordination number, which was equal to nine. Also, it was still possible to distinguish two types of phosphorus-hosting nickel cages, one

open and one closed. Their configurations (Figure 3.6) were corresponding to those previously seen, as they were shaped as mono-capped squared anti-prisms.

Another non-trivial difference could be individuated considering the interstitial nickel atoms and their surroundings (Figure 3.7). On one hand, two interstitial metallic atoms were present in this molecular structure of  $[\text{HNi}_{31}\text{P}_4(\text{CO})_{39}]^{5-}$ , in accord with the previous descriptions. On the other hand, the coordinations displayed by the two interstitial nickel atoms were slightly different.

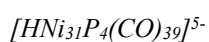
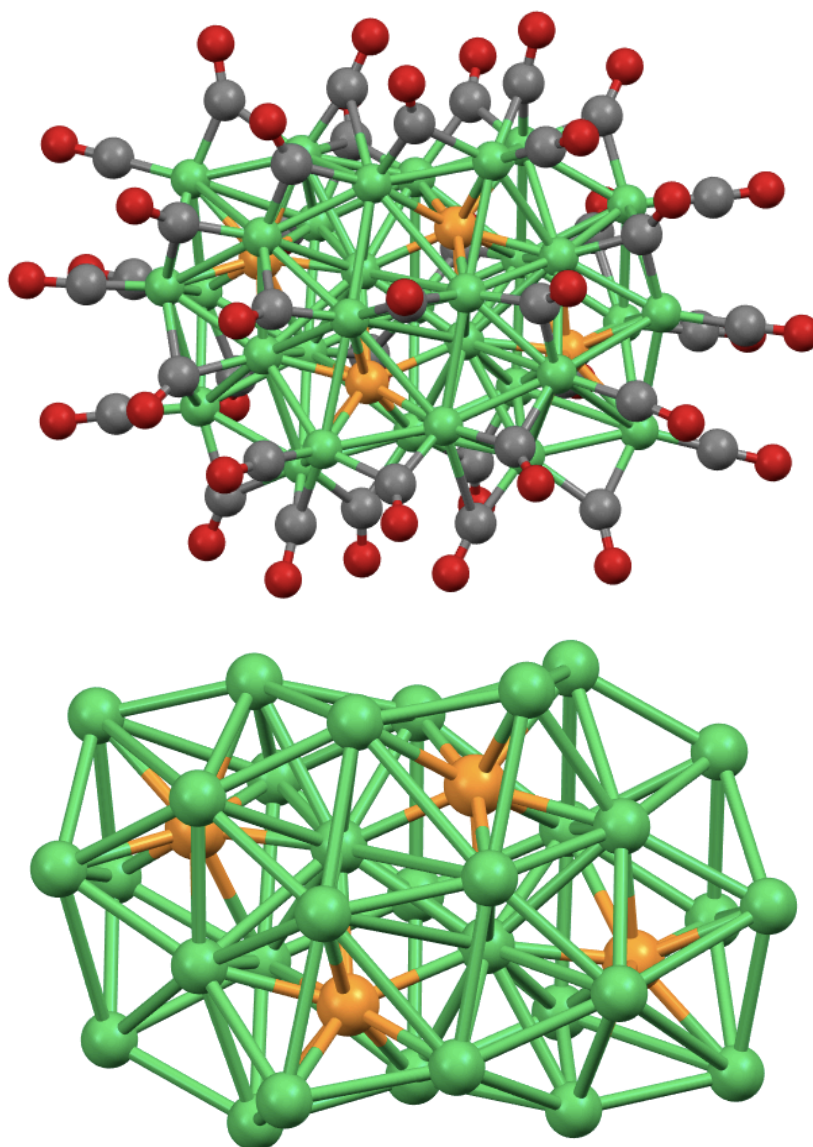
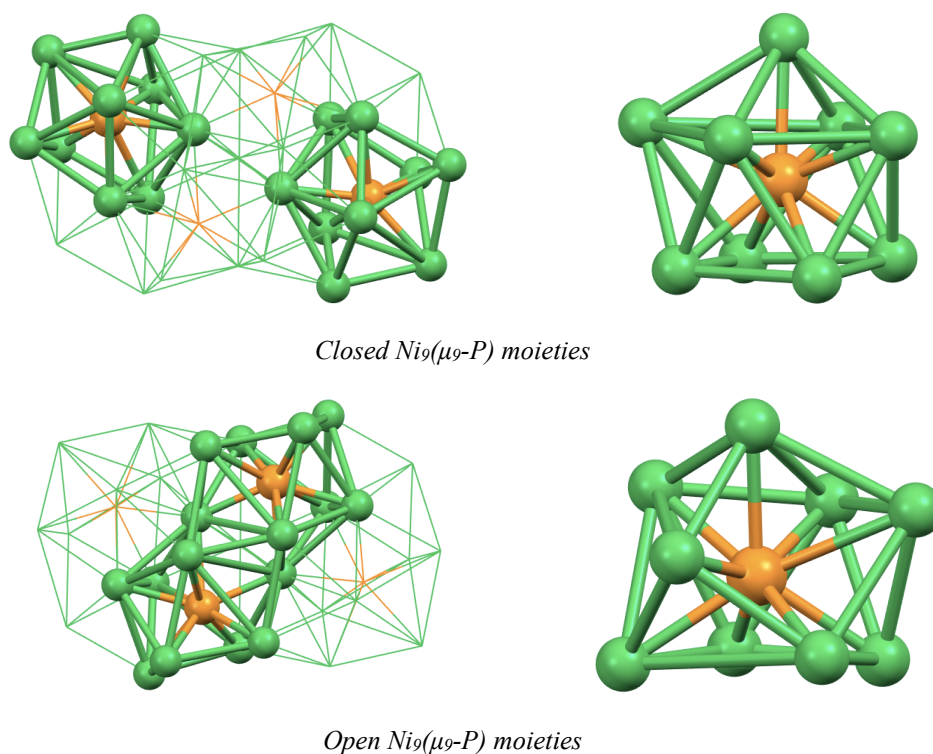


Figure 3.5 - Molecular structure and metallic skeleton of the non-symmetrical form of the  $[\text{HNi}_{31}\text{P}_4(\text{CO})_{39}]^{5-}$  penta-anion. Nickel atoms are represented in green, phosphorus atoms in orange, carbon atoms in grey, oxygen atoms in red.

One nickel atom was inside a fourteen-membered heteroatomical cage - therefore a  $Ni_{11}P_3(\mu_{14}-Ni)$  moiety was still present. This sub-unit was comparable to those already described for the symmetrical molecular structures. The other interstitial nickel atom displayed a lower coordination number, which was equal to thirteen. Surprisingly, the structure of the  $Ni_{10}P_3(\mu_{13}-Ni)$  sub-unit was in part relatable to an icosahedron. Two apical nickel atoms were individuated, each of which was capping a six-membered or a five-membered heteroatomical ring - one  $Ni_4P$  ring and one  $Ni_4P_2$  ring. The former was actually shaped as a pentagon, yet the latter was distorted and non-planar. This phenomenon was probably due to the presence of two phosphorus atoms within the  $Ni_4P_2$  base, and to the shortness of the corresponding nickel-phosphorus bonds.

Notwithstanding the distortion, this  $Ni_{10}P_3(\mu_{13}-Ni)$  sub-unit is relevant as this was the first structure that had been observed within a nickel-phosphorus homo-leptic carbonyl cluster that was similar to an icosahedron.



*Figure 3.6 - Structures of the two quasi-symmetrical types of phosphorus-hosting cavities within the non-symmetrical metallic skeleton of  $[HNi_{31}P_4(CO)_{39}]^{5-}$ . On the left the position of the moieties has been highlighted. Only one structure per type has been enlarged. Nickel atoms are represented in green, phosphorus atoms in orange.*

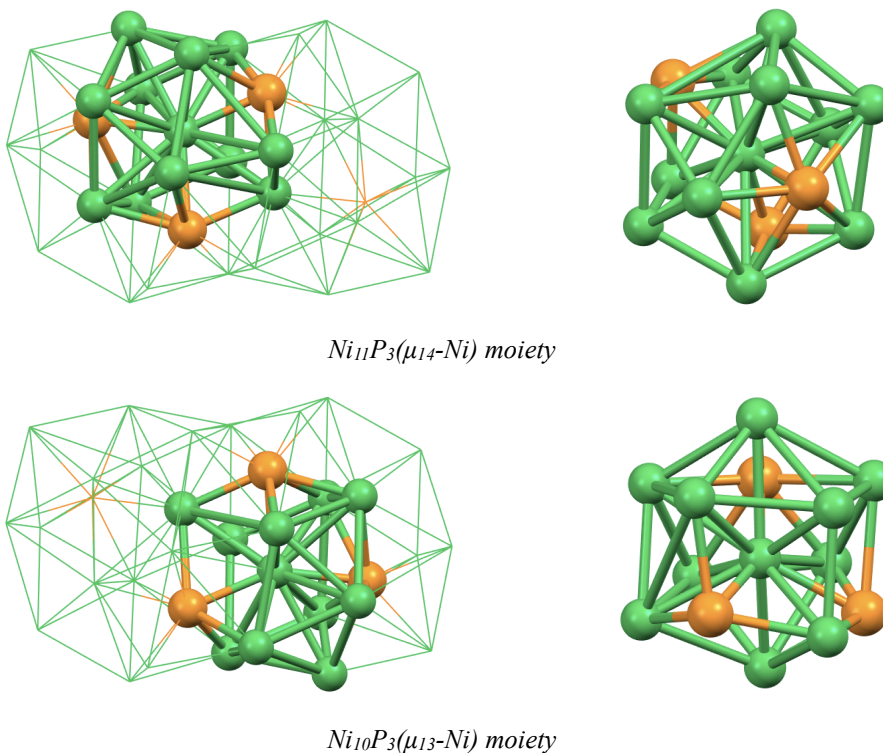


Figure 3.7 - Structure of the two types of nickel-hosting cavity within the non-symmetrical metallic skeleton of  $[HNi_{31}P_4(CO)_{39}]^{5-}$ . The position of the moieties has been highlighted in the left figures. Nickel atoms are represented in green, phosphorus atoms in orange.

In this molecular structure of  $[HNi_{31}P_4(CO)_{39}]^{5-}$  the available sites for the coordination of the hydride were the same that were present in the other molecular structures. Four independent - yet two by two related -  $Ni_5P$  octahedral sub-units (Figure 3.8) as well as two outer tetragonal nickel faces were available.

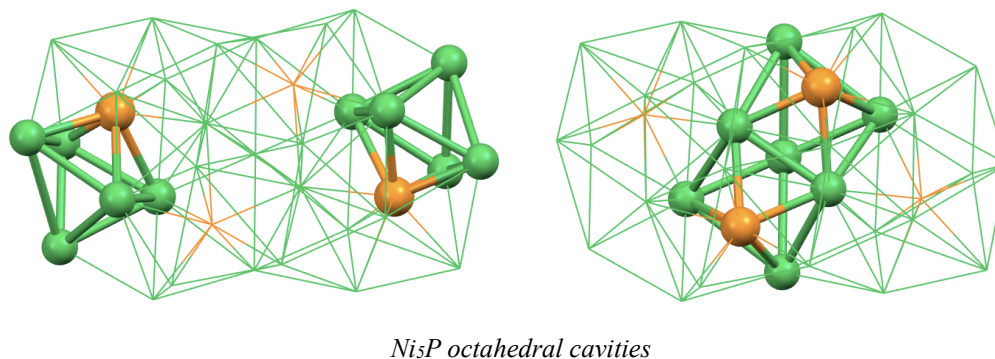


Figure 3.8 - The two types of quasi-symmetrical octahedral  $Ni_5P$  cavities have been highlighted within the non-symmetrical metallic skeleton of  $[HNi_{31}P_4(CO)_{39}]^{5-}$ . Nickel atoms are represented in green, phosphorus atoms in orange.

A selection of the crystal data that were collected for the non-symmetrical form of this cluster have been reported (Table 3.2). The unit cell of this molecular structure belonged to the  $P2_1/n$  space group of the monoclinic crystal system - whilst those of the symmetrical structures belonged to the  $C2/c$  space group.

$a$ (Å)	22.714(4)	$\alpha$ (°)	90	<i>c.s.</i>	<i>monoclinic</i>
$b$ (Å)	21.023(4)	$\beta$ (°)	98.416(2)	<i>space group</i>	$P2_1/n$
$c$ (Å)	26.309(5)	$\gamma$ (°)	90	$U$ (Å <sup>3</sup> )	12427.6

Table 3.2 - Selected crystal data for  $[HNi_{31}P_4(CO)_{39}]^{5-}$ , collected from the acetonitrile crystals.

#### ✦ *Structural characterisation of the tetra-anion*

A crystalline sample of  $[H_2Ni_{31}P_4(CO)_{39}]^{4-}$  was obtained after a protonation test that will be later described, and it was analysed via X-ray diffraction. This allowed to determine its molecular structure (Figure 3.9), that was consistent with those of its more reduced counterparts. The molecular structure was symmetrical, all phosphorus atoms were in interstitial positions, the phosphorus-hosting cages were coherent to the others in terms of coordination number and configuration, and there was a couple of interstitial nickel atoms.

However, the phosphorus-hosting nickel cages were slightly different in comparison to those within the previous structures. The coordination number of the two couples of symmetrical heteroatoms was the same, and the shape of the nickel cages was similar. Nonetheless, in all the other frameworks it had been possible to identify a closed type and an open type of nickel cavities. On the contrary, all the phosphorus-hosting nickel cages within the structure of  $[H_2Ni_{31}P_4(CO)_{39}]^{4-}$  were open (Figure 3.10).

One couple had a missing intra-square nickel-nickel edge, and the other had one intra-square and one inter-square missing edge. These deficiencies resulted in the substitution of one lateral triangular face with one squared and one pentagonal face, respectively.

For what concerns the interstitial nickel atoms (Figure 3.10), the Ni<sub>5</sub>P octahedral cavities (Figure 3.10), and the available superficial coordination sites for the hydride hydrogen atoms, all were present and did not display significant discrepancies compared to those accounted as reference.

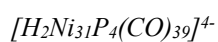
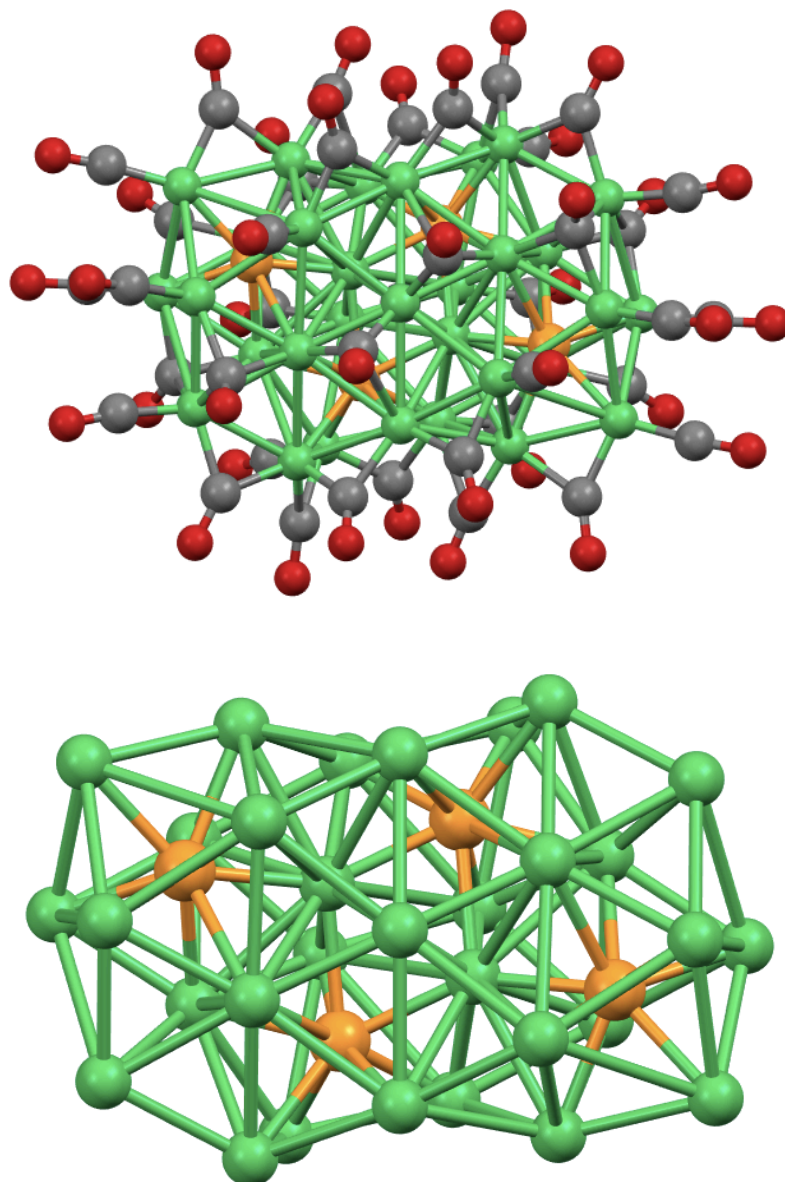
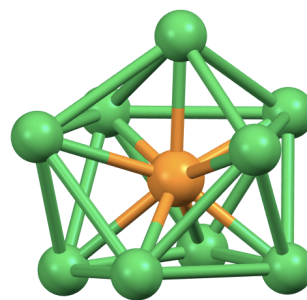
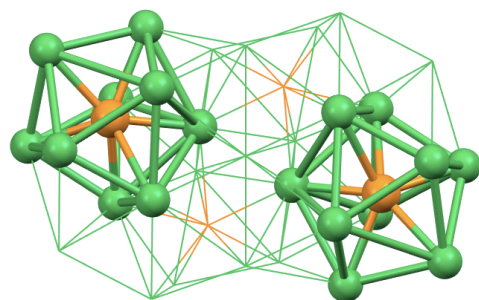
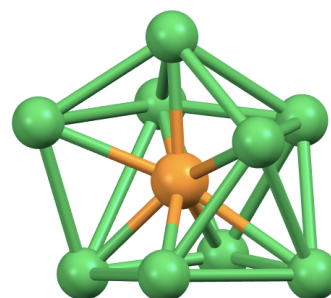
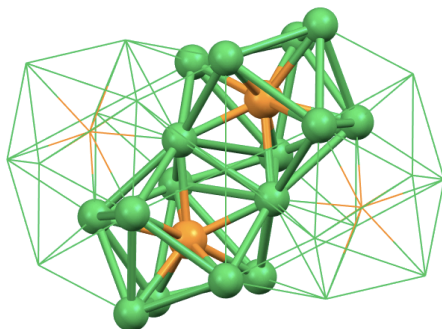


Figure 3.9 - Molecular structure and metallic skeleton of the high-nuclearity  $[H_2Ni_{31}P_4(CO)_{39}]^{4-}$  tetra-anion. Nickel atoms are represented in green, phosphorus atoms in orange, carbon atoms in grey, and oxygen atoms in red.

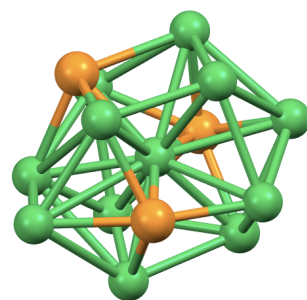
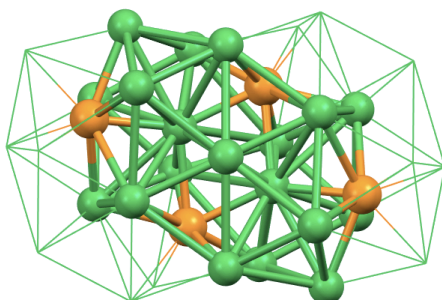




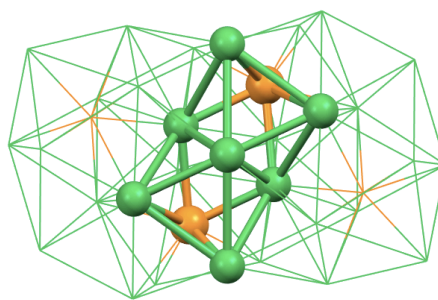
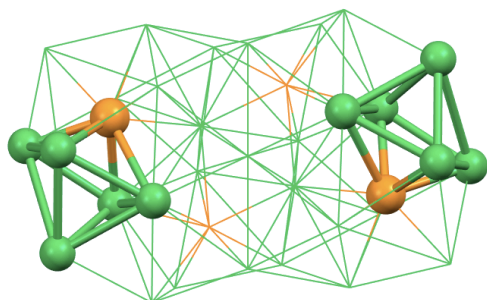
*Open Ni<sub>9</sub>(μ<sub>9</sub>-P) moieties*



*Open Ni<sub>9</sub>(μ<sub>9</sub>-P) moieties*



*Ni<sub>11</sub>P<sub>3</sub>(μ<sub>14</sub>-Ni) moieties*



*Ni<sub>5</sub>P octahedral cavities*

*Figure 3.10 - Symmetrical structures of the two types of phosphorus-hosting cavities, of the nickel-hosting cavities, and of the two types of octahedral cavities within the metallic skeleton of  $[H_2Ni_{31}P_4(CO)_{39}]^{4-}$ . The position of the moieties has been highlighted. Nickel atoms are represented in green, phosphorus atoms in orange.*

A selection of the crystal data that were collected for the tetra-anionic form of this cluster have been reported (Table 3.3). The unit cell of this molecular structure belonged to the C2/c space group of the monoclinic crystal system - as those of the symmetrical structures of the penta-anion.

<i>a</i> (Å)	27.263(2)	<i>α</i> (°)	90	<i>c.s.</i>	<i>monoclinic</i>
<i>b</i> (Å)	14.6645(13)	<i>β</i> (°)	107.513(1)	<b>space group</b>	<i>C2/c</i>
<i>c</i> (Å)	28.893(3)	<i>γ</i> (°)	90	<i>U</i> (Å <sup>3</sup> )	11016.3

Table 3.3 - Selected crystal data for  $[H_2Ni_{31}P_4(CO)_{39}]^{4-}$ .

#### ✦ *Spectroscopic and spectrometric characterisation*

As well as for a complete structural characterisation, crystals of  $[HNi_{31}P_4(CO)_{39}]^{5-}$  were dissolved and used for further purposes. A full IR spectroscopic analysis was performed, by solubilising a crystalline sample in different solvents. Tetra-ethyl-ammonium was used as cation so the cluster could be solubilised in acetone and more polar solvents.

Whether  $[HNi_{31}P_4(CO)_{39}]^{5-}$  was solubilised in acetone or acetonitrile there were no relevant differences between the spectra (Table 3.4, Figure 3.11). In these two solvents the shape and the recorded IR absorption frequencies were consistent with each other.

On the contrary, when  $[HNi_{31}P_4(CO)_{39}]^{5-}$  was solubilised in dimethylformamide - a basic, more polar solvent - the IR spectrum changed. Not only the relative intensity of the two signals was different, but also the IR absorption frequencies in the terminal region had clearly shifted towards lower values.

<i>solvent</i>	<i>acetone</i>	<i>acetonitrile</i>	<i>DMF</i>
<b><i>IR absorption frequencies (cm<sup>-1</sup>)</i></b>	2014s 1873m	2014s 1870m	2005s 1868m

Table 3.4 - Characteristic IR absorption frequencies of  $[HNi_{31}P_4(CO)_{39}]^{5-}$  in different solvents.

It is not uncommon for a cluster to display altered peak-shapes or varying IR absorption frequencies in spectra acquired in different solvents. Still, the shift was of about  $10\text{ cm}^{-1}$  for the signals corresponding to the terminal carbonyls. A variation of this magnitude could be due to a solvent-related effect, yet might also suggest that an actual deprotonation process - *i.e.* the loss of the hydride - took place.

In order to understand the behaviour of the cluster in DMF the solubilisation process had been reversed, that is to say that the cluster was precipitated from dimethylformamide with water and then re-dissolved in acetonitrile. If a deprotonation process had happened, then the IR absorption frequencies in acetonitrile would have remained those of the allegedly deprotonated cluster. Otherwise, the lowering of the frequencies would have probably been due to a solvent-related effect.

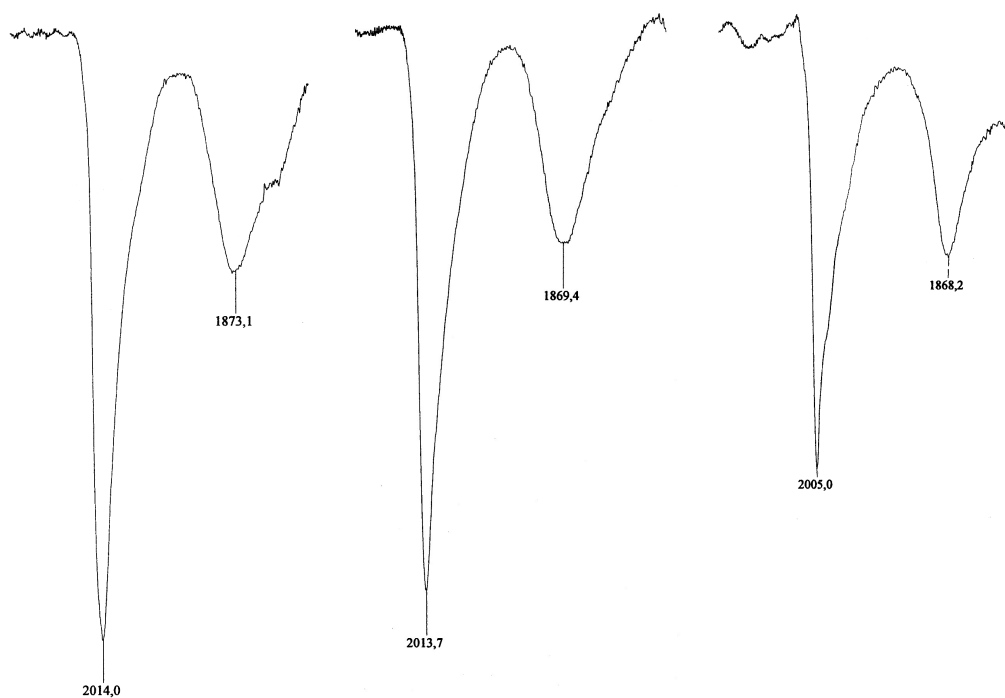
The trial suggested that the lowering of the IR absorption frequencies from 2014s, 1870m  $\text{cm}^{-1}$  in acetonitrile to 2005s, 1868m  $\text{cm}^{-1}$  in DMF was exclusively due to the solvent and that no deprotonation had happened. In fact, when the cluster was precipitated from the dimethylformamide solution and then re-dissolved in acetonitrile it was possible to notice that the IR absorption frequencies rose back to their original values.

Therefore, for this cluster the solvent-related effect of DMF has been estimated as equal to  $-9\text{ cm}^{-1}$  for the signals in the zone of the terminal carbonyls. This corrective factor was applied to all spectra that were recorded from dimethylformamide solutions, in order to compare them to those recorded from acetone or acetonitrile solutions.

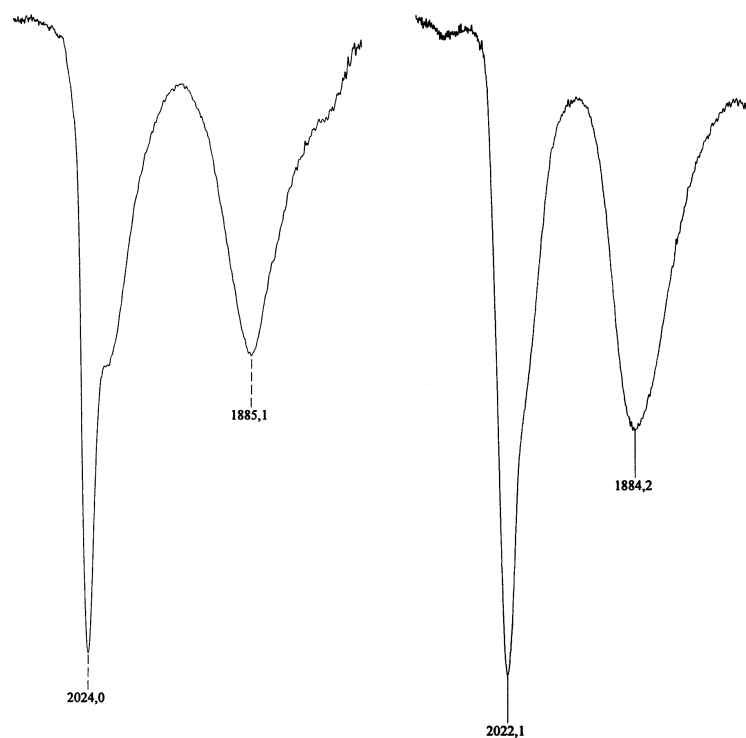
The IR spectroscopic analyses performed on  $[H_2Ni_{31}P_4(CO)_{39}]^{4-}$  (Table 3.5, Figure 3.11) indicated that the tetra-anion deprotonated in DMF, as the IR absorption frequencies lowered to values associated with  $[HNi_{31}P_4(CO)_{39}]^{5-}$ .

<i>solvent</i>	<i>acetone</i>	<i>acetonitrile</i>	<i>DMF</i>
<b><i>IR absorption frequencies (<math>\text{cm}^{-1}</math>)</i></b>	2024s 1885m	2022s 1884m	2005s 1868m

Table 3.5 - Characteristic IR absorption frequencies of  $[H_2Ni_{31}P_4(CO)_{39}]^{4-}$ .



IR spectra of  $[\text{HNi}_{31}\text{P}_4(\text{CO})_{39}]^{5-}$  in acetone, in acetonitrile, and in dimethylformamide



IR spectra of  $[\text{H}_2\text{Ni}_{31}\text{P}_4(\text{CO})_{39}]^{4+}$  in acetone and in acetonitrile

Figure 3.11 - IR spectra of  $[\text{HNi}_{31}\text{P}_4(\text{CO})_{39}]^{5-}$  and  $[\text{H}_2\text{Ni}_{31}\text{P}_4(\text{CO})_{39}]^{4+}$  in different solvents. Except for the one recorded in DMF, all spectra were coherent both in acetone and in acetonitrile for the two related species.

\*\*\*

Then, a ESI mass spectrometry analysis was performed. An extremely diluted acetonitrile solution of the cluster was prepared by dissolving few crystals in acetonitrile and then analysed.

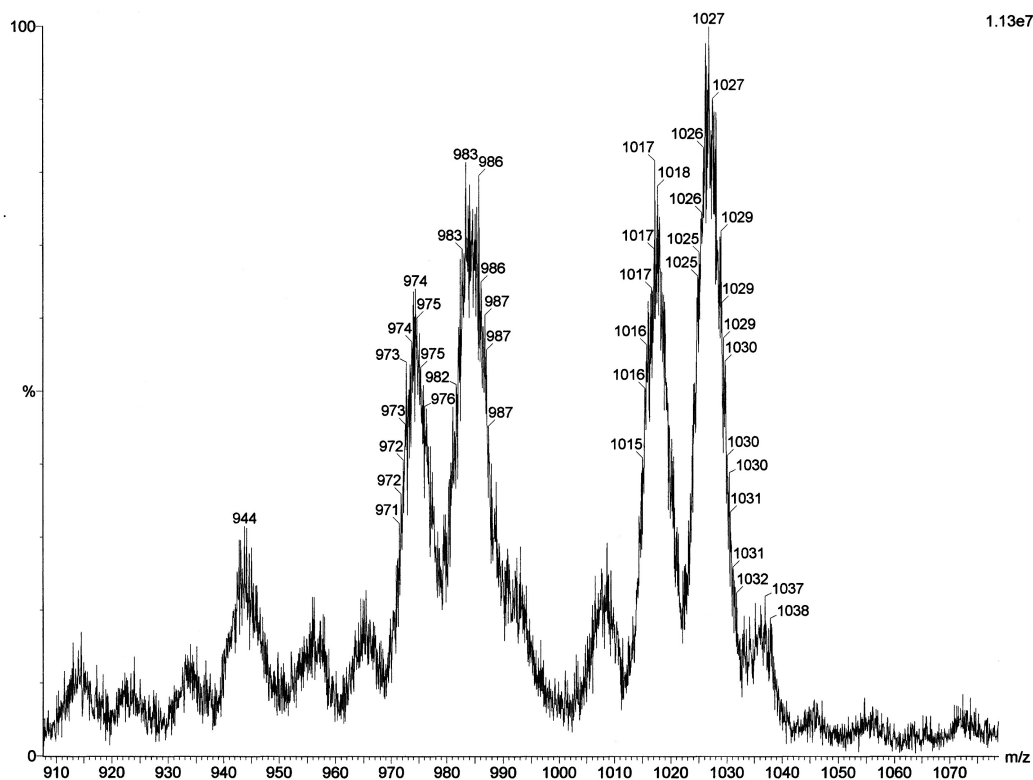
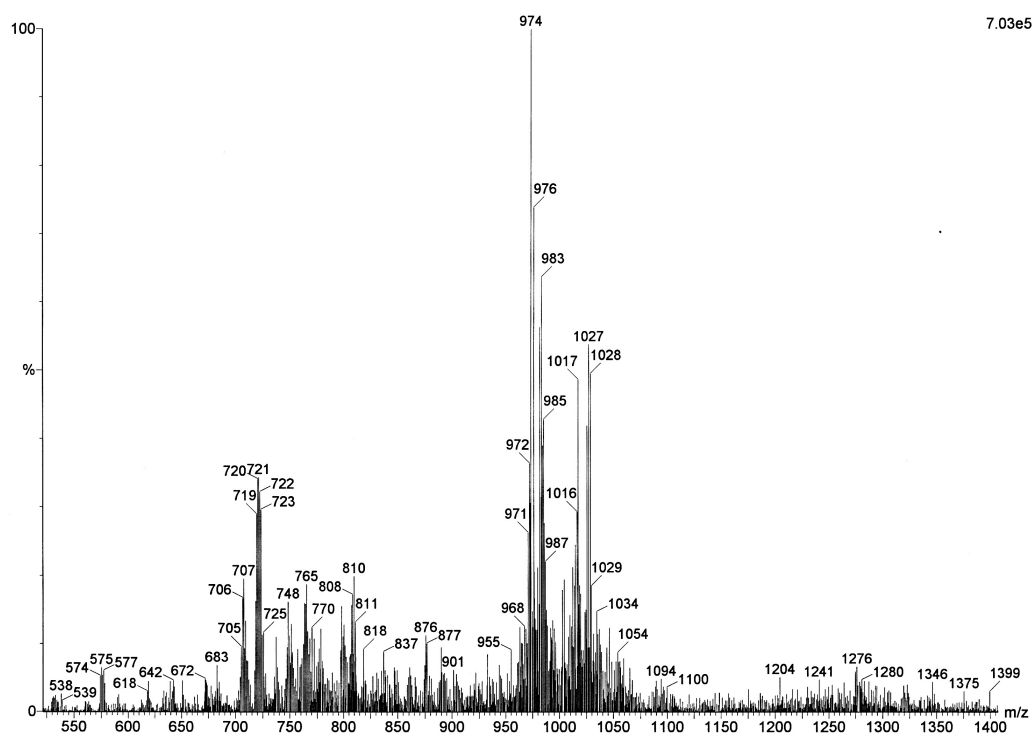
The results suggested that this compound was stable and resilient. Despite its high nuclearity, in all its spectra there were clear groups of peaks, and their number was not excessive. All but one group of signals had been successfully assigned to derivative species of  $[\text{HNi}_{31}\text{P}_4(\text{CO})_{39}]^{5-}$  (Table 3.6, Figure 3.12). The sole exception consisted in the peaks recorded at 720  $m/z$  and 707  $m/z$ , that were also present in the mass spectrum of  $[\text{Ni}_{11}\text{P}(\text{CO})_{18}]^{3-}$ .

The presence of the smaller cluster can be explained by recalling the previously proposed reaction mechanism and that co-crystallisation phenomena were common for these two species. The IR absorption frequencies of the smaller species were not detected in the IR spectrum that was recorded before the mass spectrometry analysis, yet a minor amount of  $[\text{Ni}_{11}\text{P}(\text{CO})_{18}]^{3-}$  might have been present nonetheless.

<i>peak (<math>m/z</math>)</i>	<i>corresponding cluster moiety</i>
1036	$\{[\text{HNi}_{31}\text{P}_4(\text{CO})_{37}][\text{NEt}_4]\}^{3-}$
1027	$\{[\text{HNi}_{31}\text{P}_4(\text{CO})_{36}][\text{NEt}_4]\}^{3-}$
1018	$\{[\text{HNi}_{31}\text{P}_4(\text{CO})_{35}][\text{NEt}_4]\}^{3-}$
1009	$\{[\text{HNi}_{31}\text{P}_4(\text{CO})_{34}][\text{NEt}_4]\}^{3-}$ or $\{[\text{HNi}_{31}\text{P}_4(\text{CO})_{39}]\}^{3-}$
983	$\{[\text{HNi}_{31}\text{P}_4(\text{CO})_{36}]\}^{3-}$
974	$\{[\text{HNi}_{31}\text{P}_4(\text{CO})_{35}]\}^{3-}$
(*) 720	$\{[\text{Ni}_{11}\text{P}(\text{CO})_{18}][\text{NEt}_4]_2\}^{2-}$
(*) 707	$\{[\text{Ni}_{11}\text{P}(\text{CO})_{17}][\text{NEt}_4]_2\}^{2-}$

Table 3.6 - Values of the characterised peaks and species to which they have been associated to during the interpretation of the ESI mass spectrum of  $[\text{HNi}_{31}\text{P}_4(\text{CO})_{39}]^{5-}$ .

(\*) Indicates fragments that were attributed to the  $[\text{Ni}_{11}\text{P}(\text{CO})_{18}]^{3-}$  cluster. A minor quantity of the cluster might have been present in the sample. Alternatively, the fragments might have originated after fragmentation processes.



Mass spectra of  $[HNi_{31}P_4(CO)_{39}]^{5-}$

Figure 3.12 - ESI mass spectra of  $[HNi_{31}P_4(CO)_{39}]^{5-}$ . Due to the stability of the cluster the species did not undergo excessive fragmentation processes despite its high nuclearity, as evidenced by the moderate number of recorded peaks. In the lower figure the detail of a MCA-ESI (multi-channel analysis - electrospray ionisation) mass spectrum has been reported.

\*\*\*

$^{31}\text{P}$  NMR and  $^1\text{H}$  NMR spectroscopy analyses were performed on this hydride nickel-phosphorus carbonyl cluster, with the dual objective of obtaining information regarding the phosphorus atoms and the hydride hydrogen atom. Unfortunately, both spectra were completely silent. These negative results were not unexpected, since to date the maximum nuclearity that allowed to successfully perform this type of spectroscopic analyses on clusters is equal to twenty-two - for  $[\text{H}_4\text{Rh}_{22}(\text{CO})_{35}]^{4-}$  and for  $[\text{H}_{4-n}\text{Ni}_{22}(\text{C}_2)_4(\text{CO})_{28}(\text{CdBr})_2]^{n-}$  ( $n = 2, 3, 4$ ).<sup>1, 2</sup>

This was therefore due to the high nuclearity of  $[\text{HNi}_{31}\text{P}_4(\text{CO})_{39}]^{5-}$ , as it is known that high numbers of metallic atoms exclude the possibility to record good-quality NMR spectra. In these cases the sought-after signals are as wide as to be indiscernible from the background noise. This detrimental behaviour is due to numerous effects, as dynamical site-exchange processes, and increasing metallisation and magnetism. This species behaved accordingly, and therefore it was not possible to obtain any information on the hydrogen atom or the phosphorus atoms.

### ***Reactivity tests***

As it was said,  $[\text{HNi}_{31}\text{P}_4(\text{CO})_{39}]^{5-}$  was easily obtained in good quantities, thus it was possible to deeply investigate its reactivity. The trials were aimed to discover its possible redox properties, to verify the supposed hydride nature of the species, and to assess the stability of the cluster in diverse environments.

#### **✦ *Reduction and oxidation***

The first reactions were focused on the study of the possible redox behaviour

---

<sup>1</sup> D. Collini, F. Fabrizi De Biani, D. S. Dolznicov, C. Femoni, M. C. Iapalucci, G. Longoni, C. Tiozzo, S. Zacchini, P. Zanello; *Inorg. Chem.*, **2011** (50) 2790-2798

<sup>2</sup> A. Bernardi, C. Femoni, M. C. Iapalucci, G. Longoni, S. Zacchini; *Dalton Trans.*, **2009** (21) 2217-2223

of  $[\text{HNi}_{31}\text{P}_4(\text{CO})_{39}]^{5-}$ . For clusters with comparable nuclearities it is common to display this characteristic.<sup>1</sup> Reduction and oxidation tests were performed both sequentially and independently, in order to check the possible reversibility of the redox processes as well.

For the reduction reactions, sodium naphthalenide was selected as reducing agent. The required amounts had been freshly prepared from naphthalene and metallic sodium in dimethylformamide, thus obtaining a dark green solution.

Small amounts of the solution of naphthalenide were drop-wise added to the cluster solution, and the progress of the reaction was frequently controlled via IR spectroscopy. Throughout the reactions it was possible to identify several possible oxidation states for the cluster.

It is important to remember that for medium- and high-nuclearity clusters a one-unit-charge increase is commonly associated to an approximate lowering of the IR absorption frequencies equal to  $10\text{ cm}^{-1}$  - conversely, a rise of circa  $10\text{ cm}^{-1}$  is usually linked to a one-unit-charge decrease. Also, it is important to remember to consider the solvent-related effects, since the trials had been performed in DMF.

In light of this, it was assumed that  $[\text{HNi}_{31}\text{P}_4(\text{CO})_{39}]^{5-}$  had been successfully reduced to its hepta-anionic state, and that also its hexa-anionic form had been individuated via IR spectroscopy analyses (Table 3.7).

<i>species</i>	$[\text{HNi}_{31}\text{P}_4(\text{CO})_{39}]^{5-}$		(*) $[\text{Ni}_{31}\text{P}_4(\text{CO})_{39}]^{6-}$	(*) $[\text{Ni}_{31}\text{P}_4(\text{CO})_{39}]^{7-}$
<i>solvent</i>	<i>acetonitrile</i>	<i>DMF</i>	<i>DMF</i>	<i>DMF</i>
<i><math>\nu_{\text{CO}}</math> (<math>\text{cm}^{-1}</math>)</i>	2014s 1870m	2005s 1868m	1990s 1859m	1977s 1841m
<i>shift (<math>\text{cm}^{-1}</math>)</i>	/	-9 -2	-24 -11	-37 -29
(§) <i>shift' (<math>\text{cm}^{-1}</math>)</i>	/	/ -2	-15 -11	-28 -29

Table 3.7 - IR absorption frequencies of the supposedly reduced forms of the  $[\text{HNi}_{31}\text{P}_4(\text{CO})_{39}]^{5-}$  nickel-phosphorus carbonyl clusters.

(\*) These species were identified via IR spectroscopy analyses only.

(§) Shift' is the corrected shift, calculated by considering the solvent-related effect of DMF.

<sup>1</sup> D. Collini, C. Femoni, M. C. Iapalucci, G. Longoni, P. Zanello; *Perspectives in Organometallic Chemistry*, C. G. Screttas, B. R. Steele, *The Royal Society of Chemistry*, **2003** (287) 183-195



It is worth to mention that the spectrum acquired at the end of the reduction reaction -  $\nu_{CO}$  equal to 1977s, 1841m  $cm^{-1}$  - was roughly similar to that of  $[Ni_{11}P(CO)_{18}]^{3-}$  -  $\nu_{CO}$  equal to 1980s, 1848m  $cm^{-1}$ . Since the latter could be oxidised to  $[HNi_{31}P_4(CO)_{39}]^{5-}$ , the opposite phenomenon might have occurred. It was therefore necessary to discern if the reduction process had led to formation of the hepta-anionic form of the original cluster or to formation of  $[Ni_{11}P(CO)_{18}]^{3-}$ .

In order to do so, the reduced DMF solution was precipitated by adding an aqueous solution of tetra-ethyl-ammonium bromide. The solid thus obtained was filtrated, washed with water, and accurately dried in vacuum. After that, the dark powder was re-dissolved in acetonitrile.

The IR spectrum displayed a different, higher couple of signals -  $\nu_{CO}$  equal to 1997s, 1861m  $cm^{-1}$ . Due to this, it was assumed that the reduction process led to the formation of the hepta-anionic form of  $[HNi_{31}P_4(CO)_{39}]^{5-}$  rather than to the formation of  $[Ni_{11}P(CO)_{18}]^{3-}$ . In fact, after an aqueous washing of a reduced species it is common to witness to a slight rise of the IR absorption frequencies that indicates a partial re-oxidation.

The acetonitrile solution obtained after the aqueous washing -  $\nu_{CO}$  equal to 1997s, 1861m  $cm^{-1}$  - was considered to be containing the deprotonated  $[Ni_{31}P_4(CO)_{39}]^{6-}$ , as the IR absorption frequencies were coherent with those individuated in dimethylformamide during the reduction process -  $\nu_{CO}$  equal to 1990s, 1859m  $cm^{-1}$  in DMF - provided to consider the shift equal to -9  $cm^{-1}$  associated with the solvent effect in the terminal region.

\*\*\*

Far less features emerged throughout the oxidation reactions.

Most importantly, it was verified that the reduction-oxidation processes were reversible. At the end of the reduction process - that is to say whenever the IR absorption frequencies of the hepta-anion were detectable - it was possible to revert the process by adding a mild oxidising agent. It was possible to witness to a rise of the IR absorption frequencies back to the characteristic values of  $[HNi_{31}P_4(CO)_{39}]^{5-}$ . The oxidising agent that was used was tropylium tetrafluoro-

rate, as a 1:100  $m/v$  diluted solution.

To further oxidise the pent-anionic form of the cluster was impossible. This species proved to be extremely stable towards oxidation, despite the many reactant used. Not only tropilium, but also metallic cations and even phosphorus trichloride were used, with no relevant effects. This was a further proof of the stability of this nickel-phosphorus carbonyl clusters.

\*\*\*

Finally, these results concerning the redox properties of  $[\text{HNi}_{31}\text{P}_4(\text{CO})_{39}]^{5-}$  were in part corresponding to the information obtained through some preliminary spectroelectrochemical analyses performed along with cyclic voltammetry - C.V. - analyses. For what concerns the C.V. analyses, the information available at the moment are limited and non-conclusive. However, the early data obtained from the spectroelectrochemical analyses were to some extent consistent with those obtained throughout the spectroscopic analyses. Therefore, it has been decided to report them, notwithstanding their ongoing development (Table 3.8, Figure 3.13). Still, it is important to consider these early data with reserve.

The analyses were performed on an acetonitrile solution of the clusters in crystalline form. The preliminary data revealed an interesting behaviour, as they seem to be validating the previously reported redox properties.

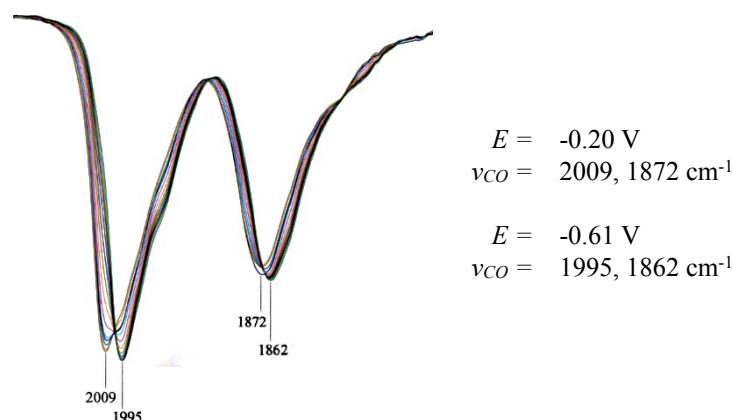


Figure 3.13 - One of the preliminary results of the spectroelectrochemical analyses has been reported, concerning the reduction process from  $[\text{HNi}_{31}\text{P}_4(\text{CO})_{39}]^{5-}$  to  $[\text{HNi}_{31}\text{P}_4(\text{CO})_{39}]^{6-}$ .

<i>cluster charge</i>	-4	-5	-6	-7	-8	-9
$\nu_{\text{CO}}$ ( $\text{cm}^{-1}$ )	2021s 1882m	2009s 1872m	1995s 1862m	1982s 1852m	1965s 1841m	1951s 1825m
<i>E (V)</i>	+0.19	-0.20	-0.61	-0.88	-1.12	-1.39

Table 3.8 - IR absorption frequencies recorded for  $[\text{HNi}_{31}\text{P}_4(\text{CO})_{39}]^{n-}$  during the spectroelectrochemical analysis, associated cluster charge and corresponding potential *E*. The data were collected from an acetonitrile solution of the cluster.

In fact, by reducing  $[\text{HNi}_{31}\text{P}_4(\text{CO})_{39}]^{5-}$  it was possible to record several distinct sets of IR absorption frequencies, whose values were in part related to those recorded throughout the spectroscopic analyses. It appeared as the original cluster had been reduced to its nona-anionic state, passing through the hexa-, hepta-, and octa-anionic states as well. However, it was possible to notice that in some instances the  $\nu_{\text{CO}}$  were moderately different from those previously reported (Table 3.9). These variations, that involved the more reduced species, were possibly due to the different environments within which the analyses were performed.

<i>species</i>	$[\text{H}_2\text{Ni}_{31}\text{P}_4(\text{CO})_{39}]^{4-}$	$[\text{HNi}_{31}\text{P}_4(\text{CO})_{39}]^{5-}$	$[\text{Ni}_{31}\text{P}_4(\text{CO})_{39}]^{6-}$	(*) $[\text{Ni}_{31}\text{P}_4(\text{CO})_{39}]^{7-}$
$\nu_{\text{CO}}$ ( $\text{cm}^{-1}$ )	2022s 1884m	2014s 1870m	1997s 1861m	1986s 1841m

Table 3.9 - IR absorption frequencies assigned to  $[\text{HNi}_{31}\text{P}_4(\text{CO})_{39}]^{5-}$  and its derivative species individuated during the reduction reactions, and IR absorption frequencies characteristic of  $[\text{H}_2\text{Ni}_{31}\text{P}_4(\text{CO})_{39}]^{4-}$ .

(\*) The reported values have been corrected by considering the  $-9 \text{ cm}^{-1}$  solvent effect of DMF.

Interestingly, during the spectroelectrochemical analysis it was possible to oxidise the  $[\text{HNi}_{31}\text{P}_4(\text{CO})_{39}]^{5-}$  cluster. The charge and the IR absorption frequencies of  $[\text{HNi}_{31}\text{P}_4(\text{CO})_{39}]^{4-}$  seem to be corresponding to those of  $[\text{H}_2\text{Ni}_{31}\text{P}_4(\text{CO})_{39}]^{4-}$ . However, during the reactivity trials it had not been possible to oxidise the penta-anionic species to its tetra-anionic state with any reactant.  $[\text{H}_2\text{Ni}_{31}\text{P}_4(\text{CO})_{39}]^{4-}$  was obtained just by protonating  $[\text{HNi}_{31}\text{P}_4(\text{CO})_{39}]^{5-}$ , and its corresponding  $\nu_{\text{CO}}$  were never observed in oxidising environments.

At the moment, it is not clear what could have inhibited the oxidation of the penta-anionic cluster during the study of its reactivity. Moreover, the potential associated to the oxidation process in the spectroelectrochemical analysis - E equal to +0.19 V - was not as high as to justify these contrasting behaviours.

Still, a more definitive evaluation of these data will occur after having received the complete and definitive results.

#### ✦ *Deprotonation and protonation*

Deprotonation and protonation tests were performed both sequentially and independently, in order to check the possible reversibility of these processes.

Sodium methoxide was used as deprotonating agent. This reactant was freshly prepared from methanol and metallic sodium. Some similarities emerged between the deprotonation and the reduction processes, probably because of phenomena related to the hydride nature of the cluster.

An acetonitrile solution of  $[\text{HNi}_{131}\text{P}_4(\text{CO})_{39}]^{5-}$  was treated by drop-wise adding to it small amounts of the solution of sodium methoxide. The first additions led to a prompt lowering of the IR absorption frequencies that stabilised at  $\nu_{\text{CO}}$  equal to 1997s, 1855m  $\text{cm}^{-1}$ . These frequencies strongly resembled those obtained after the precipitation of the reduced solution -  $\nu_{\text{CO}}$  equal to 1997s, 1861m  $\text{cm}^{-1}$  in acetonitrile - as well as those associated to  $[\text{Ni}_{131}\text{P}_4(\text{CO})_{39}]^{6-}$  in DMF -  $\nu_{\text{CO}}$  equal to 1990s, 1859m  $\text{cm}^{-1}$ . Therefore, the product of the reaction was accordingly considered to be the deprotonated hexa-anionic form of the cluster (Table 3.10).

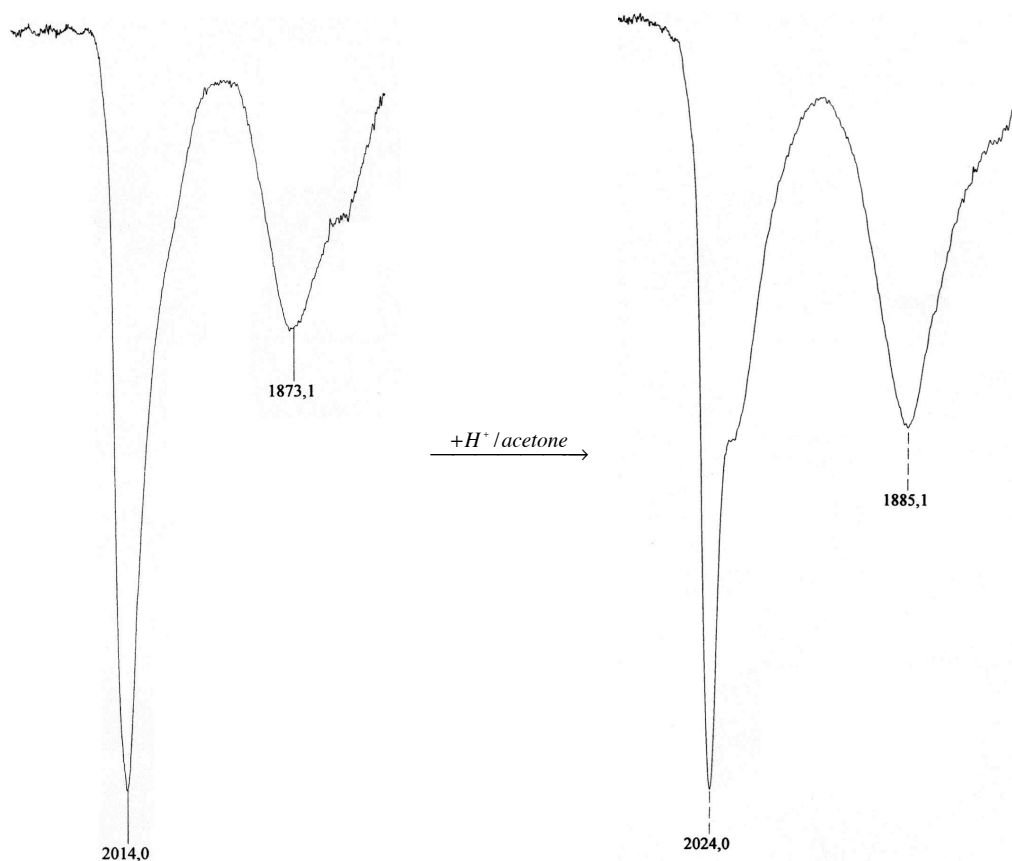
This phenomenon further supported the fact that  $[\text{HNi}_{131}\text{P}_4(\text{CO})_{39}]^{5-}$  had been formulated as a hydride species. At the moment there is no direct proof to support this hypothesis, yet the fact that both the deprotonation reaction and the reduction reaction led to the formation of the same product - as demonstrated through IR spectroscopy analyses - strongly suggest it.

\*\*\*

Interesting results emerged throughout the protonation reactions performed on  $[\text{HNi}_{31}\text{P}_4(\text{CO})_{39}]^{5-}$ . First, the reversibility of the deprotonation-protonation processes was demonstrated. By adding a 1:100  $\text{V}/\text{V}$  diluted solution of tetrafluoroboric acid to a previously deprotonated sample, it was possible to witness to the rise of the IR absorption frequencies back to their original values.

Then, a protonation reaction performed on  $[\text{HNi}_{31}\text{P}_4(\text{CO})_{39}]^{5-}$  led to the formation of a species that displayed higher IR absorption frequencies, whose values in acetone stabilised at 2024s, 1885m  $\text{cm}^{-1}$  (Table 3.10, Figure 3.14).

At first, this species was hypothetically formulated as the di-hydride derivative of  $[\text{HNi}_{31}\text{P}_4(\text{CO})_{39}]^{5-}$ . The hypothesis was confirmed as the compound was successfully characterised not only via IR spectroscopy, but also via single-crystal X-ray diffraction. A suitable crystalline sample was obtained by layering hexane over the acetone solution of the cluster.



*IR spectra in acetone acquired during the protonation reaction.*

*Figure 3.14 - IR spectra of the  $[\text{HNi}_{31}\text{P}_4(\text{CO})_{39}]^{5-}$  penta-anion before the protonation reaction and of the  $[\text{H}_2\text{Ni}_{31}\text{P}_4(\text{CO})_{39}]^{4-}$  tetra-anion after the protonation reaction.*

$[\text{H}_2\text{Ni}_{31}\text{P}_4(\text{CO})_{39}]^{4-}$  proved to be stable towards re-solubilisation in acetone or acetonitrile, and the IR spectrum acquired in acetonitrile after the crystallisation process displayed the same IR absorption frequencies of the spectrum that was acquired from the acetone solution of the cluster, as previously shown in the chapter dedicated to the spectroscopic characterisation.

It is important to note that the fact that no oxidising agent could trigger a reaction strongly supported the formulation of both this species and its precursor as hydride clusters.

<i><math>\nu_{\text{CO}}</math> (<math>\text{cm}^{-1}</math>) of the products obtained from <math>[\text{HNi}_{31}\text{P}_4(\text{CO})_{39}]^{5-}</math></i>	
$+\text{H}^+ \rightarrow [\text{H}_2\text{Ni}_{31}\text{P}_4(\text{CO})_{39}]^{4-}$	$+\text{OH}^- \rightarrow [\text{Ni}_{31}\text{P}_4(\text{CO})_{39}]^{6-}$
2024s	1997s
1885m	1855m
<i>in acetone</i>	<i>in acetonitrile</i>

Table 3.10 - IR absorption frequencies of the derivative forms of  $[\text{HNi}_{31}\text{P}_4(\text{CO})_{39}]^{5-}$ .

#### ✦ *Controlled decompositions*

Due to the elevated stability displayed by the  $[\text{HNi}_{31}\text{P}_4(\text{CO})_{39}]^{5-}$  cluster a few controlled decomposition trials were performed.

The first attempts were focused on controlled thermal decompositions. Heat can induce a carbonyl loss to clusters, which in turn can trigger a full or a partial skeletal rearrangement.

The reactions were performed on acetonitrile solutions of  $[\text{HNi}_{31}\text{P}_4(\text{CO})_{39}]^{5-}$ , which were put under reflux for one, two, or four hours. Unfortunately, these thermal treatments did not give remarkable results. Throughout the shorter trials no change could be detected via IR spectroscopy analyses.

By prolonging the duration of the thermal treatment up to four hours it was sometimes possible to witness to the formation of new IR absorption frequencies -  $\nu_{\text{CO}}$  equal to 1983vs, 1856s  $\text{cm}^{-1}$ . That IR spectrum was not associated to any known cluster compound but the identification of the product proved to be impossible, since no crystalline sample was obtained. An ESI mass spectroscopy analysis

was eventually performed on the unknown product, to tentatively deduce the nature of the species. Unfortunately, the mass spectrum (Figure 3.15) did not reveal significant information, apart from the large distribution of the peaks that suggested the possible presence of one, or more, sensibly fragile compounds.

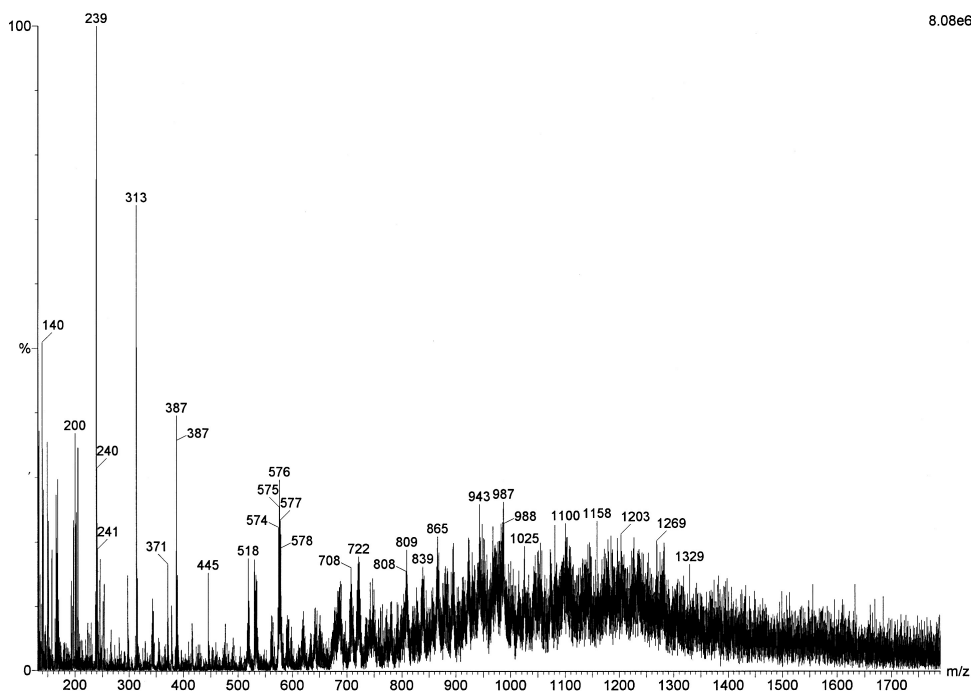


Figure 3.15 - ESI mass spectrum of the product of the controlled thermal decomposition of  $[\text{HNi}_{31}\text{P}_4(\text{CO})_{39}]^{5-}$ . The excessive fragmentation processes may indicate the fragility of the product as well as the coexistence of more species.

It is worth to mention that during one trial it was possible to supposedly trigger the deprotonation of  $[\text{HNi}_{31}\text{P}_4(\text{CO})_{39}]^{5-}$ , as disclosed via IR spectroscopy analysis. In fact, at the end of one thermal treatment it was possible to record an IR spectra -  $\nu_{\text{CO}}$  equal to 1998s, 1860m  $\text{cm}^{-1}$  - that was superimposable to the spectrum previously associated to  $[\text{Ni}_{31}\text{P}_4(\text{CO})_{39}]^{6-}$ .

\*\*\*

A second set of reactivity tests was performed employing a carbon monoxide atmosphere. Usually, when a nickel carbonyl cluster is kept under carbon monoxide it completely decomposes into nickel tetracarbonyl -  $\text{Ni}(\text{CO})_4$ . However, a

minimal exposure to carbon monoxide can lead to the detachment of small nickel-carbonyl fragments, without triggering a complete decomposition of the cluster. As a consequence, new species may originate through a nickel-carbonyl loss or through rearrangements of the bonds.

An acetonitrile solution of  $[\text{HNi}_{131}\text{P}_4(\text{CO})_{39}]^{5-}$  was put under a CO atmosphere while being vigorously stirred. Unsurprisingly, large amounts of  $\text{Ni}(\text{CO})_4$  began to form just after few minutes. In order to avoid an excessive loss of nickel the carbon monoxide atmosphere was removed as soon as the characteristic IR signal of nickel tetracarbonyl -  $\nu_{\text{CO}}$  equal to 2040s  $\text{cm}^{-1}$  - covered all other possible peaks in the IR spectrum.

This volatile decomposition product was removed under vacuum along with the solvent, and then the solid residue was re-dissolved in acetonitrile. Its IR spectrum displayed unknown absorption frequencies, equal to 2010s, 1842m  $\text{cm}^{-1}$ . The species could not be structurally characterised since it was not possible to obtain any suitable crystalline sample. The ESI mass spectrum (Figure 3.16) did not provide useful information either.

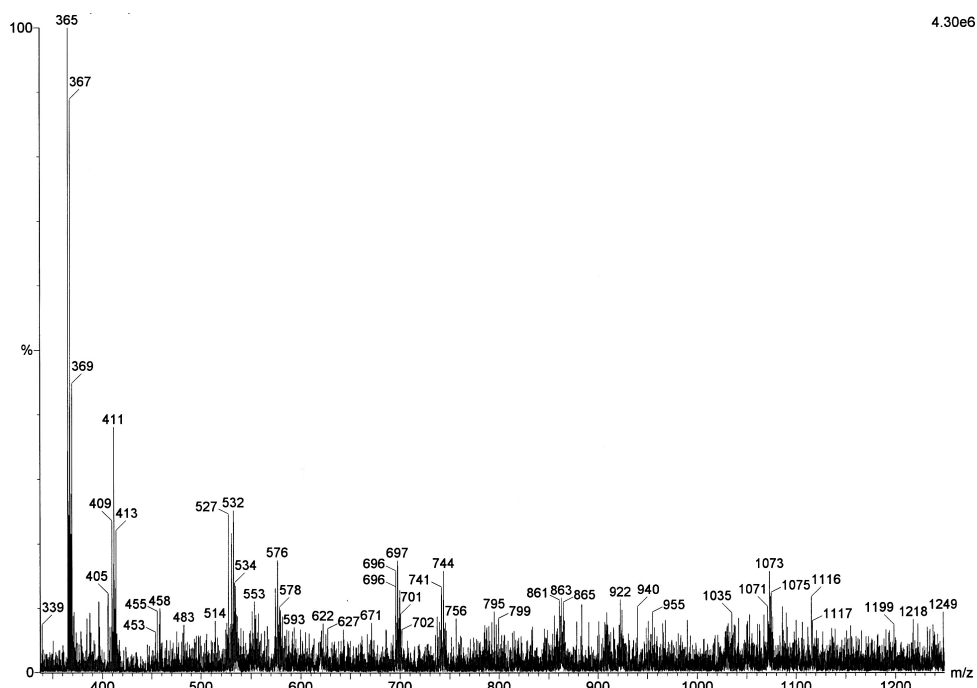


Figure 3.16 - ESI mass spectrum of the product of the controlled decomposition of  $[\text{HNi}_{131}\text{P}_4(\text{CO})_{39}]^{5-}$  under CO atmosphere. The excessive fragmentation processes may indicate the fragility of the product as well as the coexistence of more species.



***Hydride nature of  $[\text{HNi}_{31}\text{P}_4(\text{CO})_{39}]^{5-}$  and  $[\text{H}_2\text{Ni}_{31}\text{P}_4(\text{CO})_{39}]^{4-}$*** 

From the beginning of this discussion  $[\text{HNi}_{31}\text{P}_4(\text{CO})_{39}]^{5-}$  has been presented as a hydride species. It is worth to mention that this assumption was made *a posteriori*, after having discovered some peculiar behaviours of the species in various conditions.

The different signs that led to this deduction have already been exposed in the appropriate sections of this last chapter, yet it would be useful to report them together in a more coherent passage.

A first suspicion of the possible hydride nature of the cluster came while recording the IR spectra of  $[\text{HNi}_{31}\text{P}_4(\text{CO})_{39}]^{5-}$  in different solvents. The  $\nu_{\text{CO}}$  recorded in DMF were lower than those recorded in acetone and acetonitrile. The shift was in the order of  $10\text{ cm}^{-1}$  for the signals in the zone of the terminal carbonyls, and similar phenomena are commonly associated with the variation of a one-unit-charge for medium- and high-nuclearity clusters. Due to the characteristic of the solvent - dimethylformamide is moderately basic - a spontaneous deprotonation process might have occurred. This assumption was later disproved, and the lowering of the IR absorption frequencies was associated to a solvent-related effect.

Nonetheless, other evidences emerged while performing reactivity trials. First, it was noticed that the cluster could be protonated, yet it could not be oxidised. Eventually,  $[\text{H}_2\text{Ni}_{31}\text{P}_4(\text{CO})_{39}]^{4-}$  happened to be structurally characterised as product of a protonation trial, further supporting the presumed hydride nature of the cluster.

Most importantly, during the deprotonation reactions it was not possible to record IR absorption frequencies lower than  $1997\text{s}$ ,  $1855\text{m cm}^{-1}$ . Very similar  $\nu_{\text{CO}}$  were also registered after the aqueous washing performed on the product of the reduction reactions. These two aspects implicated that the same species was obtained as stable product after the reduction reaction as well as at the end of the deprotonation reaction.

Despite none of these proofs being conclusive by itself, as a whole they strongly suggested that the cluster under consideration could be an hydride species (Table 3.11).

$[\text{H}_2\text{Ni}_{31}\text{P}_4(\text{CO})_{39}]^{4-}$		$[\text{HNi}_{31}\text{P}_4(\text{CO})_{39}]^{5-}$		$[\text{Ni}_{31}\text{P}_4(\text{CO})_{39}]^{6-}$
2024s 1885m acetone	$\xleftarrow{+\text{H}^+}$	2014s 1873m acetone		
		2013s 1869m acetonitrile	$\xrightarrow{+\text{OH}^-}$	1997s 1855m acetonitrile
		2005s 1869m DMF	$\xrightarrow{+e^-/\text{H}_2\text{O}}$	1997s 1861m acetonitrile

Table 3.11 - Selected IR absorption frequencies of  $[\text{HNi}_{31}\text{P}_4(\text{CO})_{39}]^{5-}$  and its derivatives species, as observed throughout the reactivity tests. All values are reported in  $\text{cm}^{-1}$ . For spectra recorded from DMF solutions the values of the IR absorption frequencies have not been corrected by considering the solvent effect.

\*\*\*

After having assumed that both  $[\text{HNi}_{31}\text{P}_4(\text{CO})_{39}]^{5-}$  and  $[\text{H}_2\text{Ni}_{31}\text{P}_4(\text{CO})_{39}]^{4-}$  were hydride species, a survey on the possible coordination of the hydride hydrogen atoms was performed.

As aforementioned, in all the characterised molecular structures of these species there were several appropriate coordination sites. The hydride hydrogen atoms could have been interstitial - hosted inside the previously shown octahedral  $\text{Ni}_5\text{P}$  cavities - or superficial - coordinated to squared or pentagonal nickel faces on the surface of the metallic skeletons of the cluster.

In order to locate the hydride hydrogen atoms, the molecular structures of the penta-anions were compared to the molecular structure of the tetra-anion.  $[\text{H}_2\text{Ni}_{31}\text{P}_4(\text{CO})_{39}]^{4-}$  featured one hydrogen more than  $[\text{HNi}_{31}\text{P}_4(\text{CO})_{39}]^{5-}$ , and therefore any difference concerning the previously individuated sites - e.g. a significant enlargement of the octahedral cavities, or an inhomogeneous distribution of the carbonyl ligands - could have disclosed the actual location of the hydride hydrogen atoms. Unfortunately, by comparing the molecular structures it was not possible to highlight any remarkable dissimilarity.

Due to the lack of more consistent information, and in light of the available data, the hydride hydrogen atoms were allegedly considered to be superficially

coordinated to the metallic skeleton of the clusters (Figure 3.17). Further information would have been otherwise decisive.

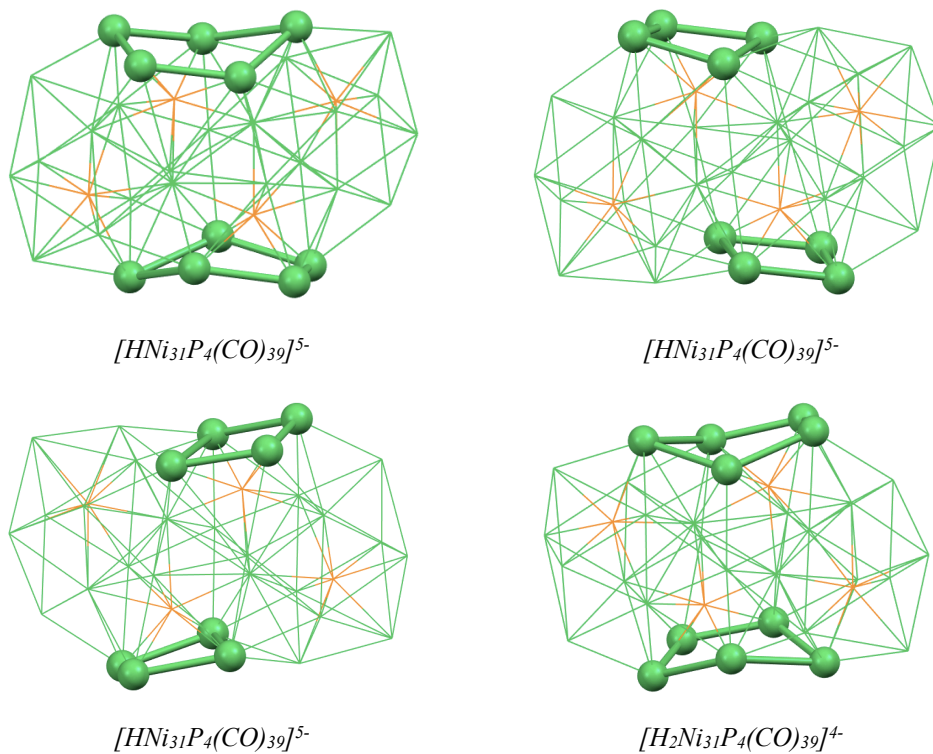


Figure 3.17 - The pentagonal and the squared superficial sites to which the hydride hydrogen atoms could be coordinated in the molecular structures of  $[HNi_{31}P_4(CO)_{39}]^{5-}$  and  $[H_2Ni_{31}P_4(CO)_{39}]^{4-}$  have been highlighted. Nickel atoms are represented in green, phosphorus atoms in orange.

## **[Ni<sub>14</sub>P<sub>2</sub>(CO)<sub>22</sub>]<sup>2-</sup>** **Synthesis, characterisation, and reactivity**

### *Synthetic approach and further considerations*

While the syntheses and the characterisations of the [Ni<sub>11</sub>P(CO)<sub>18</sub>]<sup>3-</sup> and the [HNi<sub>31</sub>P<sub>4</sub>(CO)<sub>39</sub>]<sup>5-</sup> clusters proved to be in some measures challenging, the behaviour of [Ni<sub>14</sub>P<sub>2</sub>(CO)<sub>22</sub>]<sup>2-</sup> was quite the opposite.

The tuning of the synthesis of [Ni<sub>14</sub>P<sub>2</sub>(CO)<sub>22</sub>]<sup>2-</sup> was almost effortless. Most of the times, at the end of the reactions that were conducted in CH<sub>2</sub>Cl<sub>2</sub> it was possible to obtain this product and to extract it by using the same solvent in which the reaction was carried out. The structural characterisation of the species was performed shortly after its synthesis, since this cluster regularly forms well-shaped crystals by layering toluene over a concentrated solution of the cluster in dichloromethane.

Interestingly, despite solutions of [Ni<sub>14</sub>P<sub>2</sub>(CO)<sub>22</sub>]<sup>2-</sup> being dark in coloration, the crystalline form of the cluster exhibited a peculiar hue and so it was possible for a trained eye to recognise this compound fairly easily. It is matter of fact that most medium-nuclearity and high-nuclearity clusters appear dark or black in crystalline form. On the contrary, it is more common for low-nuclearity species to originate coloured crystals - for example, [Ni<sub>6</sub>(CO)<sub>12</sub>]<sup>2-</sup> crystals are reddish and [Ni<sub>9</sub>(CO)<sub>18</sub>]<sup>2-</sup> crystals are orangish - whilst this rarely happens for bulkier clusters. Nonetheless, crystals of [Ni<sub>14</sub>P<sub>2</sub>(CO)<sub>22</sub>]<sup>2-</sup> were greenish and *quasi*-iridescent, despite giving the impression of being black at first sight.

Due to its proneness to crystallisation, to obtain a reference IR spectrum for the cluster was straightforward. Few crystals of the cluster were re-dissolved in dichloromethane, as well as in THF, and in acetonitrile. The IR absorption frequencies recorded in dichloromethane were coherent with those observed before the crystallisation, thus it was possible to use that spectra as reference for [Ni<sub>14</sub>P<sub>2</sub>(CO)<sub>22</sub>]<sup>2-</sup>. Moreover, the IR spectrum of the compound had an unusual

shape, thus it was easy to individuate this species.

In the following paragraphs a full description of the synthesis of this nickel-phosphorus carbonyl cluster will ensue.

As aforementioned, this compound could be easily synthesised throughout the reaction between the  $[Ni_6(CO)_{12}]^{2-}$  precursor and  $PCl_3$  in dichloromethane. In order for the nickel precursor to be soluble in this solvent, its counter-ion had to be tetra-butyl-ammonium. A tetra-butyl-ammonium salt of  $[Ni_6(CO)_{12}]^{2-}$  was prepared and then dissolved in a minimal quantity of dichloromethane. The thus obtained solution was placed inside a suitable Schlenk tube and vigorously stirred. At the same time a diluted solution of  $PCl_3$  in dichloromethane was prepared, considering a dilution from 1:100  $v/v$  up to 1:50  $v/v$ .

Before proceeding with the reaction, a IR spectrum of the solution of the cluster precursor was acquired in order to verify its purity, and only then the diluted solution of  $PCl_3$  was added. One up to three millilitres of reactants were added at a time, and IR spectroscopy analyses were performed after each aliquot had been incorporated. After having reached the defined stoichiometric ratio - 1 to 0.5 referred to the nickel cluster precursor - the reaction mixture was dried under vacuum, so that both the solvent and  $Ni(CO)_4$  could be eliminated. The thus obtained solid was thoroughly washed with water, and then again dried under vacuum. Finally, it was possible to extract the product of interest with  $CH_2Cl_2$ , as confirmed via IR spectroscopy.

Well-shaped crystals were frequently obtained through slow diffusion of toluene into a concentrated dichloromethane solution of the cluster. An X-ray diffraction analysis was performed, thus allowing to structurally characterise the compound. Then, few crystals were re-dissolved in dichloromethane, as well as in other solvents. The IR absorption frequencies recorded from  $CH_2Cl_2$  before and after the crystallisation were coherent with each other. However, it was also possible to notice that the IR spectra collected in different solvents displayed consistent differences. A more detailed comparison will ensue in the dedicated chapter.

It is worth to mention that other species were detected in the acetone and in the acetonitrile extractions of these reactions. These products were allegedly identi-

fied as  $[\text{Ni}_{23-x}\text{P}_2(\text{CO})_{30-x}]^{4-}$ ,  $[\text{HNi}_{131}\text{P}_4(\text{CO})_{39}]^{5-}$ , or other unknown species through spectroscopical characterisation. Still, their IR spectra were not sufficiently clear to confirm the hypothesis, and it was not possible to obtain any crystalline sample.

### ***Structural, spectroscopic, and spectrometric characterisations***

The  $[\text{Ni}_{14}\text{P}_2(\text{CO})_{22}]^{2-}$  cluster was fully characterised, as the previously mentioned synthetic approach allowed to obtain this species both in solution and in crystalline form with an adequate purity degree. Whilst cluster solutions had been used for reactivity tests - which will be later described - crystalline samples were used to fully characterise the compound.

An X-ray diffraction analysis was performed, as well as IR spectroscopy analyses, an ESI mass spectrometry analysis, and a  $^{31}\text{P}$  NMR spectroscopy analysis.

#### **♦ *Structural characterisation***

The molecular structure of this di-anion was determined via a single-crystal X-ray diffraction analysis (Figure 4.1). The metallic skeleton was composed by two symmetrical units - each of which was a phosphorus-hosting nickel cavity - and it was surrounded by twenty-two varyingly coordinated carbonyl ligands. Ten COs were linearly coordinated to a nickel atom, while twelve carbonyl ligands were bridging over a nickel-nickel edge.

As well as in the previously described structures, also in that of  $[\text{Ni}_{14}\text{P}_2(\text{CO})_{22}]^{2-}$  the post-transition element displayed a novel coordination number compared to standard nickel-phosphorus cluster chemistry. The two symmetrical phosphorous atoms were inside a nine-membered nickel cage, thus having a C.N. equal to nine. These cavities (Figure 4.2) consisted of two identical mono-capped squared anti-prisms, whose non-capped squared bases were fused together. Comparing these anti-prisms with those seen in  $[\text{HNi}_{131}\text{P}_4(\text{CO})_{39}]^{5-}$ , those within the molecular structure of  $[\text{Ni}_{14}\text{P}_2(\text{CO})_{22}]^{2-}$  appeared to be more regular in shape.

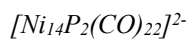
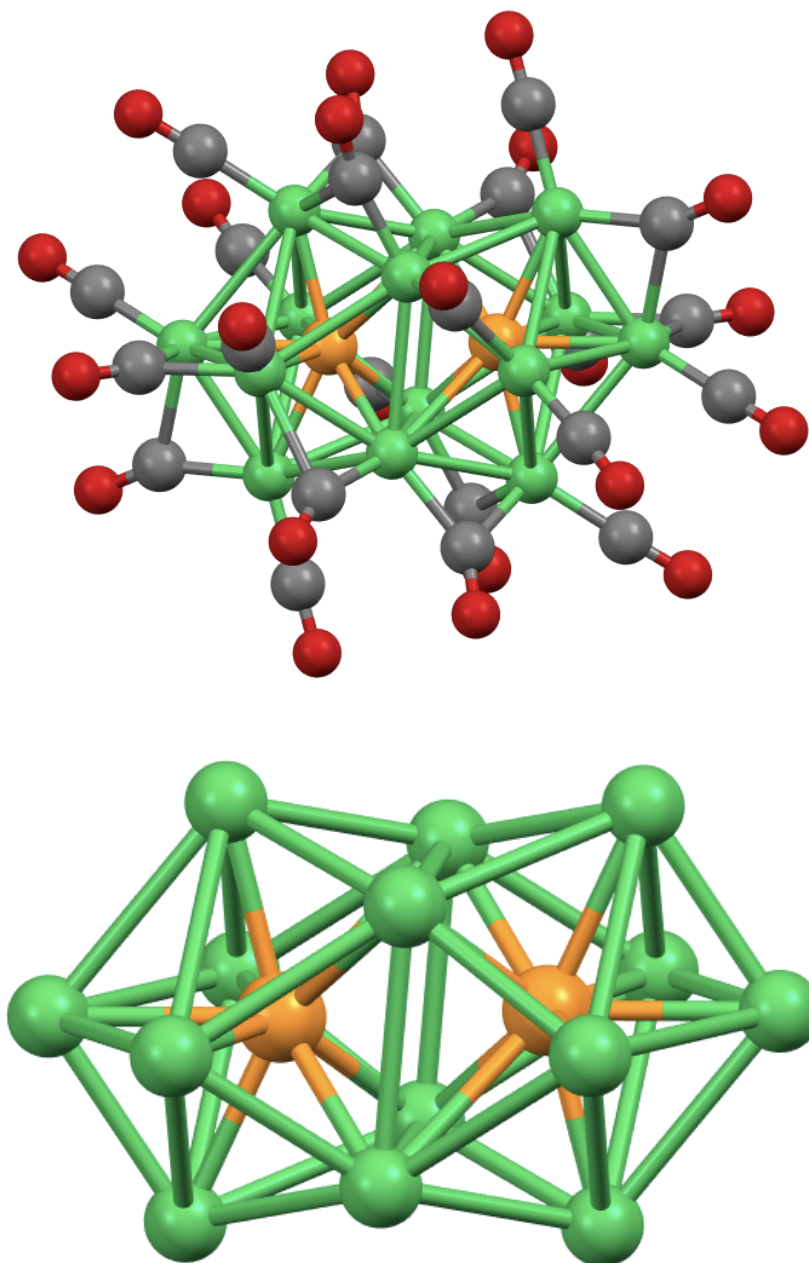
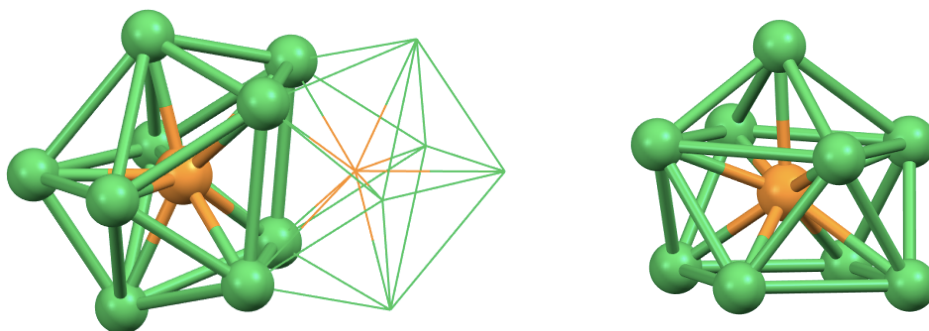


Figure 4.1 - Molecular structure and metallic skeleton of the  $[\text{Ni}_{14}\text{P}_2(\text{CO})_{22}]^{2-}$  di-anion. Nickel atoms are represented in green, phosphorus atoms in orange, carbon atoms in grey, and oxygen atoms in red.

In the molecular structure of this cluster there were neither interstitial metallic atoms nor nickel atoms non-coordinated to one of the two phosphorus atoms, probably because of the reduced nuclearity of the species.



$Ni_9(\mu_9-P)$  moiety

Figure 4.2 - Structure of the two symmetrical phosphorus-hosting cavities within the metallic skeleton of  $[Ni_{14}P_2(CO)_{22}]^{2-}$ . In the left image the position of one moiety has been highlighted. Nickel atoms are represented in green, phosphorus atoms in orange.

A selection of the crystal data that were collected for this cluster have been reported (Table 4.1). The unit cell of  $[Ni_{14}P_2(CO)_{22}]^{2-}$  belonged to the  $P2_1/n$  space group of the monoclinic crystal system.

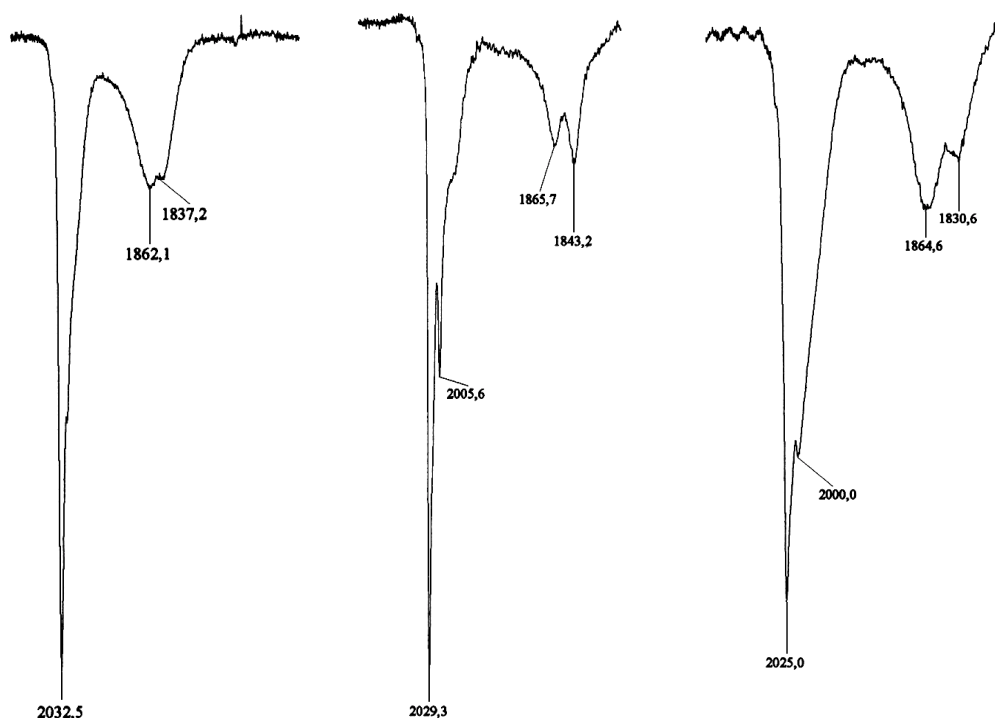
$a$ (Å)	11.2393(9)	$\alpha$ (°)	90	<i>c.s.</i>	<i>monoclinic</i>
$b$ (Å)	20.1941(15)	$\beta$ (°)	100.4700(10)	<b>space group</b>	$P2_1/n$
$c$ (Å)	16.8025(13)	$\gamma$ (°)	90	$U$ (Å <sup>3</sup> )	3750.13

Table 4.1 - Selected crystal data collected for  $[Ni_{14}P_2(CO)_{22}]^{2-}$ .

#### ♦ Spectroscopic and spectrometric characterisation

After the structural characterisation, crystals of  $[Ni_{14}P_2(CO)_{22}]^{2-}$  were redissolved and used for other purposes. A full IR spectroscopy analysis was performed, by solubilising a crystalline sample in different solvents (Table 4.2, Figure 4.3). Not only the magnitude of the shift of the IR absorption frequencies was relevant, but the overall shapes of the spectra were different as well. This behaviour - that was more intense of that displayed by the hydride  $[HNi_{31}P_4(CO)_{39}]^{5-}$  cluster - was related to the so-called solvent-effect. It is in fact not atypical for a cluster species to display altered peak-shapes or varying IR absorption frequencies in spectra acquired in different solvents.





IR spectra of  $[\text{Ni}_{14}\text{P}_2(\text{CO})_{22}]^{2-}$  in dichloromethane, in tetrahydrofuran, and in acetonitrile

Figure 4.3 - IR spectra of  $[\text{Ni}_{14}\text{P}_2(\text{CO})_{22}]^{2-}$  in different solvents. This cluster is a typical example of species whose spectra are affected by solvent-related effects, as its characteristic IR absorption frequencies - mostly in the zone characteristic of terminal carbonyls - as well as the shape of the peaks - mostly in the zone characteristic of bridging carbonyls - change by using different solvents.

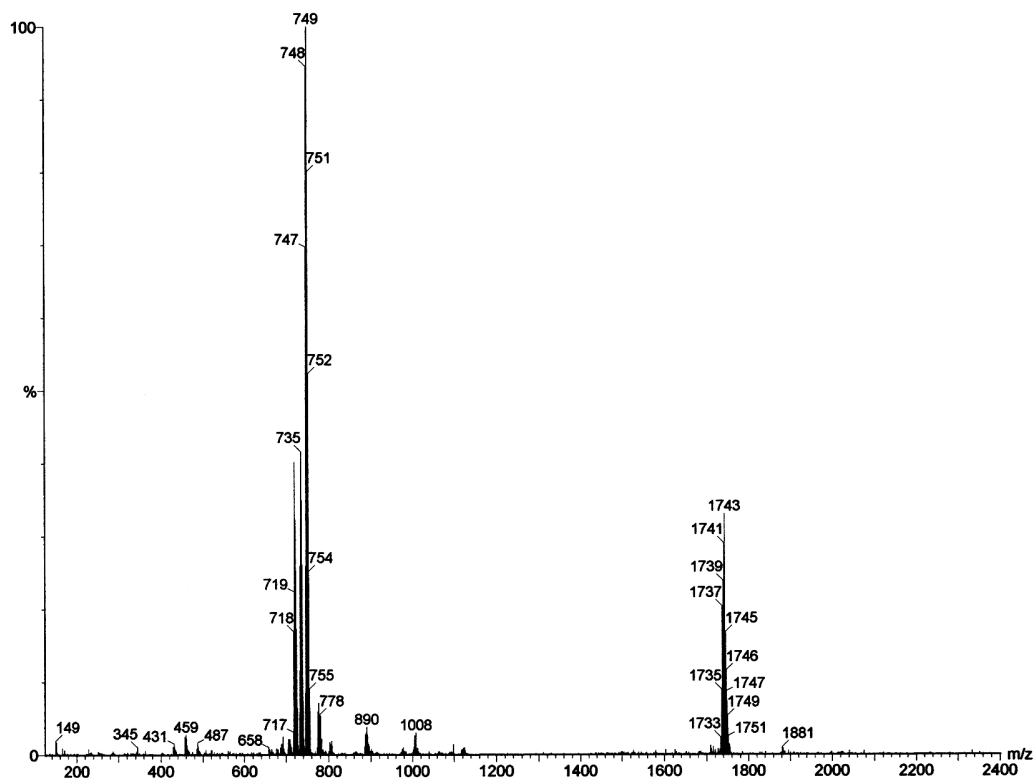
<i>solvent</i>	<i>dichloromethane</i>	<i>tetrahydrofuran</i>	<i>acetonitrile</i>
<b>IR absorption frequencies (<math>\text{cm}^{-1}</math>)</b>	2033vs 1862mw 1837sh	2029vs 2006m 1866w 1843mw	2025s 2000m 1865mw 1831w

Table 4.2 - IR absorption frequencies of  $[\text{Ni}_{14}\text{P}_2(\text{CO})_{22}]^{2-}$  in different solvents.

\*\*\*

After the IR spectroscopy analyses, a solution obtained by dissolving few crystals in acetonitrile was used to acquire the reference mass spectrum of  $[\text{Ni}_{14}\text{P}_2(\text{CO})_{22}]^{2-}$  (Figure 4.4). As in the case of  $[\text{Ni}_{11}\text{P}(\text{CO})_{18}]^{3-}$ , the low-nuclearity of the cluster allowed to avoid excessive fragmentation processes. In fact, in this

case this phenomena was not only reduced but essentially absent - all fragments appeared to have been originated from carbonyl losses and to have preserved the metallic skeleton intact (Table 4.3).



Mass spectrum of  $[\text{Ni}_{14}\text{P}_2(\text{CO})_{22}]^{2-}$

Figure 4.4 - ESI mass spectrum of  $[\text{Ni}_{14}\text{P}_2(\text{CO})_{22}]^{2-}$ . Due to the characteristics of the cluster, the species endured almost unscathed the ionisation process, as evidenced by the reduced number of recorded peaks. Interestingly, in this mass spectra all peaks appeared to correspond to fragments whose metallic skeletons remained that of the original cluster.

peak ( $m/z$ )	corresponding cluster moiety
1743	$\{[\text{Ni}_{14}\text{P}_2(\text{CO})_{22}][\text{NBu}_4]\}^-$
749	$\{[\text{Ni}_{14}\text{P}_2(\text{CO})_{22}]\}^{2-}$
735	$\{[\text{Ni}_{14}\text{P}_2(\text{CO})_{21}]\}^{2-}$
721	$\{[\text{Ni}_{14}\text{P}_2(\text{CO})_{20}]\}^{2-}$

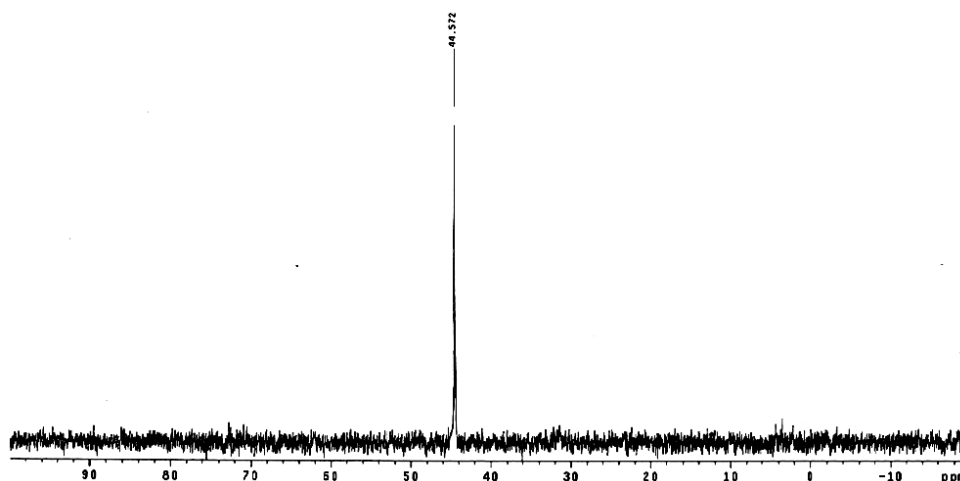
Table 4.3 - Values of the characterised peaks and species to which they have been associated to during the interpretation of the ESI mass spectrum of  $[\text{Ni}_{14}\text{P}_2(\text{CO})_{22}]^{2-}$ . The reduced number of fragments suggested that that species was remarkably stable towards the operating conditions.

Interestingly, along with a di-anionic species and its carbonyl-loss-related peaks -  $\{[\text{Ni}_{14}\text{P}_2(\text{CO})_{22}]\}^{2-}$ ,  $\{[\text{Ni}_{14}\text{P}_2(\text{CO})_{21}]\}^{2-}$ , and  $\{[\text{Ni}_{14}\text{P}_2(\text{CO})_{20}]\}^{2-}$  at 749  $m/z$ , 735  $m/z$ , and 721  $m/z$  - in this spectrum it was possible to discern the peak of the mono-anionic molecular ion -  $\{[\text{Ni}_{14}\text{P}_2(\text{CO})_{22}][\text{NBu}_4]\}^-$  at 1743  $m/z$ . Alike phenomena are quite rare to happen for nickel-phosphorus cluster compounds, as electro-spray-ionisation processes usually generates tri-anionic or di-anionic moieties.

\*\*\*

Due to the moderate nuclearity and to the proneness to crystallisation of this cluster, it was possible to perform a  $^{31}\text{P}$  NMR spectroscopy on  $[\text{Ni}_{14}\text{P}_2(\text{CO})_{22}]^{2-}$  (Figure 4.5). The analysis was performed on a concentrated solution of the cluster in dichloromethane, obtained by dissolving a fair amount of crystals.

In the spectrum it was possible to individuate one single, sharp signal -  $\delta$  equal to 44.57 ppm. The shape of the peak is coherent with those usually recorded in  $^{31}\text{P}$  NMR spectra. Moreover, the presence of just one single peak suggested that the two phosphorus atoms within the cluster were equivalent in solution as well as in the solid state - since the molecular structure was symmetrical.



$^{31}\text{P}$  NMR spectrum of  $[\text{Ni}_{14}\text{P}_2(\text{CO})_{22}]^{2-}$

Figure 4.5 - NMR spectrum of  $[\text{Ni}_{14}\text{P}_2(\text{CO})_{22}]^{2-}$ . Interestingly, in this spectrum a single peak is visible and therefore the two phosphorus atoms have to be considered as equivalent.

## ***Reactivity tests***

As the  $[\text{Ni}_{14}\text{P}_2(\text{CO})_{22}]^{2-}$  cluster was easily synthesised, it was possible to explore its behaviour in diverse environments. The tests investigated its possible redox or acid-base properties, and its ability to withstand controlled degradation-inducing atmospheres. All the reactions were performed by using as starting material solutions of the clusters as they were obtained at the end of aforementioned synthesis.

### **♦ *Reduction and oxidation***

The first reactions were focused on the study of the redox behaviour of  $[\text{Ni}_{14}\text{P}_2(\text{CO})_{22}]^{2-}$  (Table 4.4). Reduction and oxidation tests were performed both sequentially and independently, in order to check the possible reversibility of the processes. Sodium diphenylketyl was selected as reducing agent for the reduction reaction. The required amounts had been freshly prepared from benzophenone and metallic sodium in dimethylformamide, thus obtaining a dark blue solution.

Small amounts of the solution of diphenylketyl were added to the cluster solution, and the progress of the reaction was frequently controlled via IR spectroscopy. Throughout the reaction it was possible to notice that the IR absorption frequencies progressively lowered, down to 1974s, 1844m, 1832sh  $\text{cm}^{-1}$  in DMF.

\*\*\*

Then, a diluted solution of tropylium tetrafluoroborate was used as oxidising agent. The reactant was drop-wise added to the solution of  $[\text{Ni}_{14}\text{P}_2(\text{CO})_{22}]^{2-}$  in dichloromethane, and as expected the IR absorption frequencies shifted to higher values, up to 2040s, 1901mw  $\text{cm}^{-1}$ . In this case it was supposed that the  $[\text{Ni}_{14}\text{P}_2(\text{CO})_{22}]^-$  species might have been formed. It is worth to mention that by the end of the reaction it was necessary to remove  $\text{Ni}(\text{CO})_4$  that had formed throughout the oxidation and whose presence was altering the spectra.

Unfortunately, neither the species obtained after the reduction test nor the species obtained after the oxidation test crystallised. Due to that, it was not possible to characterise the product of the reactions.

$\nu_{\text{CO}} (\text{cm}^{-1})$ of the products obtained from $[\text{Ni}_{14}\text{P}_2(\text{CO})_{22}]^{2-}$	
+e <sup>-</sup>	-e <sup>-</sup>
1974s	2040s
1844m	1901mw
1832sh	in $\text{CH}_2\text{Cl}_2$
in DMF	

Table 4.4 - IR absorption frequencies of the supposedly derivative forms of the  $[\text{Ni}_{14}\text{P}_2(\text{CO})_{22}]^{2-}$  nickel-phosphorus carbonyl clusters.

#### ✦ Deprotonation and protonation

Protonation and deprotonation tests were performed both individually and subsequently, in order to check the possible reversibility of the processes. In both cases  $[\text{Ni}_{14}\text{P}_2(\text{CO})_{22}]^{2-}$  displayed a consistent behaviour (Table 4.5) with that of most medium-low nuclearity carbonyl clusters.

A diluted acidic solution of tetrafluoroboric acid was drop-wise added to the solution of the cluster, and the reaction pathway was followed via IR spectroscopy. The reaction was started in acetonitrile and then continued in dichloromethane. As expected, it was possible to register a gradual shift of the IR absorption frequencies towards higher values, up to 2044s, 1901mw  $\text{cm}^{-1}$ . Similar frequencies were recorded at the end of the oxidation process, and had already been tentatively assigned to  $[\text{Ni}_{14}\text{P}_2(\text{CO})_{22}]^-$ . It was not possible to obtain a crystalline sample from the solution, yet the species was tentatively formulated as  $[\text{HNi}_{14}\text{P}_2(\text{CO})_{22}]^-$ .

\*\*\*

Then, a diluted solution of tetra-ethyl-ammonium hydroxide was used as deprotonating agent. The reactant was drop-wise added to the protonated reaction

mixture. First, the IR absorption frequencies lowered back to the original values of the  $[\text{Ni}_{14}\text{P}_2(\text{CO})_{22}]^{2-}$  di-anion. Then, by proceeding with further additions it was possible to record progressively lower IR absorption frequencies -  $\nu_{\text{CO}}$  equal to 2011s, 1861m  $\text{cm}^{-1}$  in dichloromethane,  $\nu_{\text{CO}}$  equal to 1991s, 1981sh, 1852m, 1805sh  $\text{cm}^{-1}$  in acetonitrile. It is worth to mention that the deprotonation process could have been a mild reduction process instead, induced by the presence of the hydroxyl anion. Unfortunately, the deprotonated - or possibly reduced - species did not crystallise. Due to that, it was not possible to discover the real nature of the process and to characterise the product of the reactions.

<i><math>\nu_{\text{CO}}</math> (<math>\text{cm}^{-1}</math>) of the products obtained from <math>[\text{Ni}_{14}\text{P}_2(\text{CO})_{22}]^{2-}</math></i>		
<i>+H<sup>+</sup></i>	<i>+OH<sup>-</sup></i>	
		1991s
2044s	2011s	1981sh
1901mw	1861m	1852m
<i>in CH<sub>2</sub>Cl<sub>2</sub></i>	<i>in CH<sub>2</sub>Cl<sub>2</sub></i>	1805sh
		<i>in CH<sub>3</sub>CN</i>

Table 4.5 - IR absorption frequencies of the products of the protonation and the deprotonation trials performed on the  $[\text{Ni}_{14}\text{P}_2(\text{CO})_{22}]^{2-}$  nickel-phosphorus carbonyl clusters.

#### ✦ *Controlled decompositions*

Other reactivity tests were conducted in degrading environments, in order to verify if the compact structure of the cluster could provide some degree of stabilisation.

The first trial was performed with triphenylphosphine, as this compound displays a high affinity towards nickel atoms in carbonyl clusters. Its presence typically triggers the detachment of nickel-carbonyl fragments from the original cluster skeleton, which then form  $\text{Ni}(\text{CO})_x(\text{PPh}_3)_{4-x}$  neutral complexes. As a consequence, new species may originate via rearrangements of the metallic core.

A diluted solution of triphenylphosphine in acetone was prepared, and then drop-wise added to a solution of  $[\text{Ni}_{14}\text{P}_2(\text{CO})_{22}]^{2-}$ . Along with the additions it was possible to witness to the development of peaks at the characteristic IR absorption

frequencies of  $Ni(CO)_x(PPh_3)_{4-x}$  species -  $\nu_{CO}$  of  $Ni(CO)_3(PPh_3)$  equal to 2070s, 1990vs  $cm^{-1}$ ,  $\nu_{CO}$  of  $Ni(CO)_2(PPh_3)_2$  equal to 2000s, 1940vs  $cm^{-1}$ .

Once all the original cluster had reacted, the reaction mixture was dried and then thoroughly washed with toluene in order to eliminate the neutral nickel-carbonyl-triphenylphosphine complexes. At the end of the process it was possible to extract a new compound with acetonitrile, whose IR absorption frequencies were equal to 2000s, 1871m  $cm^{-1}$ . This yet-unknown species never originated crystalline samples, and so it still has to be structurally characterised.

\*\*\*

The second trial was carried out under carbon monoxide atmosphere. As previously described, nickel has an extremely high affinity towards this molecule, and could trigger a mechanism similar to that of triphenylphosphine.

An acetone solution of  $[Ni_{14}P_2(CO)_{22}]^{2-}$  was prepared inside a suitable Schlenk tube, and then vacuum was applied in order to replace the inert nitrogen atmosphere with a degrading carbon monoxide atmosphere. The solution was kept under vigour stirring for just few minutes, and then again put under vacuum to eliminate both the solvent and the  $Ni(CO)_4$  - along with the carbon monoxide atmosphere.

The thus obtained solid residue was then extracted with acetonitrile, and analysed through IR spectroscopy. The results were truly remarkable, as the IR spectrum was in fact coincident to that of  $[HNi_{31}P_4(CO)_{39}]^{5-}$ .

It was therefore reasonable to assume that the loss of several nickel-carbonyl fragments from the skeleton of  $[Ni_{14}P_2(CO)_{22}]^{2-}$  - triggered by the carbon monoxide atmosphere - induced a structural rearrangement of the original species, that possibly transformed into  $[HNi_{31}P_4(CO)_{39}]^{5-}$  (Figure 4.6). Unfortunately, it was not possible to obtain a crystalline sample of the product, therefore the hypothesis could not be confirmed.

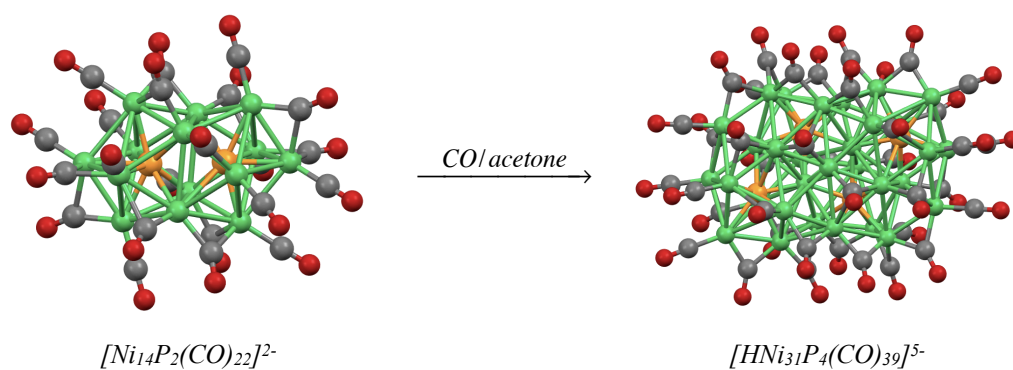


Figure 4.6 - Reaction scheme illustrating that, when  $[Ni_{14}P_2(CO)_{22}]^{2-}$  is kept under carbon monoxide for a brief lapse of time, it is transformed into  $[HNi_{31}P_4(CO)_{39}]^{5-}$ . Nickel atoms are represented in green, phosphorus atoms in orange, carbon atoms in grey, and oxygen atoms in red.



## **$[\text{Ni}_{23-x}\text{P}_2(\text{CO})_{30-x}]^{4-}$ and $[\text{Ni}_{23-x}\text{P}_2(\text{CO})_{30-x}]^{6-}$ ( $x = 0, 1$ ) Synthesis, characterisation, and reactivity**

### *Synthetic approach and further considerations*

$[\text{Ni}_{23}\text{P}_2(\text{CO})_{30}]^{4-}$  and  $[\text{Ni}_{22}\text{P}_2(\text{CO})_{29}]^{4-}$  formally are two distinct species, yet they have never been separately identified in any of the analysed samples. They will be therefore referred to as a single cluster in the ensuing chapters, for comprehension purposes.

#### **★ $[\text{Ni}_{23-x}\text{P}_2(\text{CO})_{30-x}]^{4-}$ ( $x = 0, 1$ ) - tetra-anionic form**

This cluster was the first species ever isolated and characterised after having used  $\text{POCl}_3$  as reactant. This phosphoryl chloride was selected in order to extend the pool of possible synthetic pathways, since these family of reactants -  $\text{EOX}_3$  - had never been employed in the literature of heteroatomical nickel clusters.

Whilst the reaction between  $[\text{Ni}_6(\text{CO})_{12}]^{2-}$  and  $\text{POCl}_3$  regularly gave the same reproducible outcomes, the identification and the structural characterisation of the  $[\text{Ni}_{23-x}\text{P}_2(\text{CO})_{30-x}]^{4-}$  tetra-anion were challenging. During the earlier attempts, the nature of the cluster products of the aforementioned synthetic reaction was not clear. In fact, at the end of most syntheses it was possible to identify two different products - one was extracted with acetone and one was extracted with acetonitrile. However, during the earlier attempts these allegedly new nickel-phosphorus clusters did not crystallise in any environment.

In order to induce more favourable conditions, both the acetone and the acetonitrile samples were treated with various reactants, in order to achieve the crystallisation of a derivative form of the sought-after compounds. Crystallisation trials were performed with a variety of solvent/non-solvent combinations, as well as in acidic, basic, oxidising, or reducing environments.

Most endeavours did not give the hoped results, yet crystals eventually formed from one of the acetone solutions, after having it treated with a mild reducing solution of sodium methoxide. The quality of the crystalline sample was barely adequate to perform an X-ray diffraction analysis, nonetheless it was possible to structurally characterise the  $[\text{Ni}_{23-x}\text{P}_2(\text{CO})_{30-x}]^{6-}$  hexa-anion.

Then, the thus obtained crystals were re-dissolved in acetonitrile in order to acquire a reference IR spectrum of the cluster. However, the spectra registered before and after the crystallisation process were consistent in shape, although different in terms of IR absorption frequencies - before the crystallisation  $\nu_{\text{CO}}$  were equal to 1985s, 1848m  $\text{cm}^{-1}$ , and after the crystallisation  $\nu_{\text{CO}}$  were equal to 2005s, 1869m  $\text{cm}^{-1}$ . This suggested that the two species could have been the same cluster bearing different oxidation states, and the phenomenon was tentatively explained with two different hypotheses.

In the first hypothesis, it had been supposed that the species had been reduced beyond its hexa-anionic state during the reduction process. So, the IR spectrum recorded before the crystallisation would have been that of a more negatively charged compound, presumably an hepta-anion or an octa-anion. This more-reduced form of the cluster did not endure the crystallisation, and throughout the process was partially re-oxidised to the structurally and spectroscopically characterised hexa-anionic form.

In the second possible scenario, it had been presumed that the structurally characterised hexa-anion was the actual product of the reduction reaction. At that point, the reduced  $[\text{Ni}_{23-x}\text{P}_2(\text{CO})_{30-x}]^{6-}$  did not withstand the re-dissolution process, therefore the IR spectroscopy analysis had individuated a less negatively charged species - presumingly a penta-anion or a tetra-anion.

In other words, it was assumed that the two spectra portrayed the IR absorption frequencies of the same cluster bearing different negative charges - *i.e.* the same cluster in different oxidation states. Nonetheless, it was not possible to ascertain which of the two spectra was that of the structurally characterised hexa-anion.

These information were still relevant, since by using the recorded IR spectra as references it was eventually possible to tune the synthesis and to identify purer solutions. Several crystallisation attempts were made, and finally another suitable

crystalline sample was directly obtained from the acetone extraction.

The structural characterisation of these crystals allowed to identify the species as being the  $[Ni_{23-x}P_2(CO)_{30-x}]^{4-}$  tetra-anion. Most importantly, in this case the IR spectra acquired before and after the crystallisation process were corresponding to each other -  $\nu_{CO}$  equal to 2001s, 1872m  $cm^{-1}$  in acetone,  $\nu_{CO}$  equal to 2005s, 1869m  $cm^{-1}$  in acetonitrile. Moreover, both these spectra were coherent with that obtained from the re-dissolution of the previously obtained crystalline sample -  $\nu_{CO}$  equal to 2005s, 1869m  $cm^{-1}$ .

With these results it was therefore possible to clarify the outcomes of the reduction process, and to assess which hypothesis was correct. Considering that the IR absorption frequencies that were recorded after the crystallisation process were that of the tetra-anionic cluster, it was possible to deduce that the IR absorption frequencies of the hexa-anionic form of the cluster were those of the spectrum acquired at the end of the reduction reaction -  $\nu_{CO}$  equal to 1985s, 1848m  $cm^{-1}$ .

To summarise, the  $[Ni_{23-x}P_2(CO)_{30-x}]^{4-}$  tetra-anion was formed at the end of the reaction between  $[Ni_6(CO)_{12}]^{2-}$  and  $POCl_3$ , and extracted with acetone. Then, the reduction process reduced the cluster to its hexa-anionic form, that was the first to be structurally characterised. Once re-dissolved, the cluster eventually returned to its original oxidation state, thus leading to the recording of mismatching IR spectra. The ambiguity was eventually overcome when crystals of the cluster in its tetra-anionic form were obtained, and structurally and spectroscopically characterised.

In the following paragraphs a full description of the synthesis of this nickel-phosphorus carbonyl cluster will ensue.

$[Ni_{23-x}P_2(CO)_{30-x}]^{4-}$  is obtained throughout the reaction between the  $[Ni_6(CO)_{12}]^{2-}$  cluster and  $POCl_3$ , by using THF or acetonitrile as solvents. Tetra-ethyl-ammonium was generally used as cation, but also tetra-methyl-ammonium and tri-methyl-butyl-ammonium proved to be fitting choices. A concentrated solution of  $[Ni_6(CO)_{12}]^{2-}$  with any soluble counter-ion was prepared, and placed inside a suitable Schlenk tube. In order to obtain this cluster the oxidising phosphorus source had to be  $POCl_3$  and not  $PCl_3$ . A fresh solution of the reactant was pre-

pared, with a 1:100 up to 1:50 <sup>v/v</sup> concentration.

An IR spectroscopy analysis was performed to verify the purity of the nickel cluster precursor before proceeding with the reaction. After that, the diluted phosphoryl chloride was drop-wise added to the solution of the cluster, one to three millilitres at a time, periodically checking on the reaction progresses via IR spectroscopy. When the reaction was performed in acetonitrile it was possible to witness to the rise of peaks at new IR absorption frequencies. Otherwise, the good advancement of the reactions in THF was confirmed by the progressive formation of a dark precipitate. Whenever an excessive amount of Ni(CO)<sub>4</sub> was detected in solution, this by-product was eliminated by applying vacuum.

Once the required stoichiometric ratio had been reached - 1 to 0.8 referred to the nickel cluster precursor - the reaction mixture was dried under vacuum and thoroughly washed with water. The solid thus obtained was then accurately dried and prepared to be extracted.

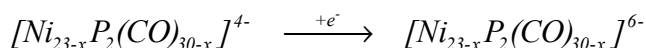
As expected, with tetrahydrofuran it was usually possible to extract residues of [Ni<sub>6</sub>(CO)<sub>12</sub>]<sup>2-</sup> or [Ni<sub>9</sub>(CO)<sub>18</sub>]<sup>2-</sup>. The cluster product of interest [Ni<sub>23-x</sub>P<sub>2</sub>(CO)<sub>30-x</sub>]<sup>4-</sup> could be extracted with acetone or acetonitrile, depending on the chosen counterion. Layering a film of hexane over a concentrated acetone solution of the cluster allowed to seldom obtain few crystals, whose quality was unfortunately rarely adequate for X-ray diffraction analyses.

It is worth to restate that the pairing of the molecular structure with its corresponding IR spectrum was achieved after a great number of tentatives. The assignation of the correct characteristic  $\nu_{CO}$  was a lengthy process, due to the poor tendency of the cluster to crystallise, along with the registration of some ambiguous IR spectra.

♦ [Ni<sub>23-x</sub>P<sub>2</sub>(CO)<sub>30-x</sub>]<sup>6-</sup> (x = 0, 1) - hexa-anionic form

As aforementioned, for what concerns the synthesis of [Ni<sub>23-x</sub>P<sub>2</sub>(CO)<sub>30-x</sub>]<sup>6-</sup> - *i.e.* the hexa-anionic form of the cluster - it involved a simple reduction reaction (Scheme 5.1). First the tetra-anionic form had to be prepared, according to the

previously reported methodology. Then, by treating an acetonitrile solution of the cluster with a mild reducing solution it was possible to witness to a moderate shift of the IR absorption frequencies towards lower values. It was assumed that the presence of the hexa-anionic cluster was confirmed whenever the IR absorption frequencies had stabilised at 1985s, 1848m  $cm^{-1}$ .



*Scheme 5.1 - Schematisation of the reduction reaction from the tetra-anion to the hexa-anion.*

A crystalline sample was obtained by layering diisopropyl ether through a thin film of hexane over an acetonitrile solution of the cluster. This species had been characterised as  $[Ni_{23-x}P_2(CO)_{30-x}]^{6-}$  throughout an X-ray diffraction analysis, despite the poor quality of the sample. Few crystals were re-dissolved in order to record a reference IR spectrum for the cluster, yet this reduced cluster proved to be re-oxidised in non-reducing environments. In acetonitrile only the IR absorption frequencies associated to the tetra-anionic form of the cluster were recorded.

### ***Structural, spectroscopic, and spectrometric characterisations***

The full characterisation of  $[Ni_{23-x}P_2(CO)_{30-x}]^{4-}$  was challenging but was eventually accomplished. This cluster was not prone to crystallise, however it was possible to collect few suitable samples for an X-ray diffraction analysis, as well as for an ESI mass spectroscopy analysis. The IR spectroscopy analyses were performed on re-dissolved crystals and on solutions of the cluster directly obtained at the end of the synthesis.

The tetra-anionic form and the hexa-anionic form displayed extremely similar molecular structures, and just minor differences were present. The molecular structure of the  $[Ni_{23-x}P_2(CO)_{30-x}]^{4-}$  tetra-anion will be described at first, and then will be compared to that of the hexa-anion.

#### ***♦ Structural characterisation of the tetra-anion***

The  $[\text{Ni}_{23-x}\text{P}_2(\text{CO})_{30-x}]^{4-}$  nickel-phosphorus cluster was structurally characterised via single-crystal X-ray diffraction analysis. Both  $[\text{Ni}_{23}\text{P}_2(\text{CO})_{30}]^{4-}$  and  $[\text{Ni}_{22}\text{P}_2(\text{CO})_{29}]^{4-}$  co-crystallised inside the unit cell - with a 1 to 1 ratio - and were neither isolated nor observed in other proportions.

The only difference between these two nickel-phosphorus species consisted in one apical nickel-carbonyl fragment (Figure 5.1) - which was present in one of the molecular structures and absent in the other. In the following descriptions these species will be addressed to as one, for clarity purposes.

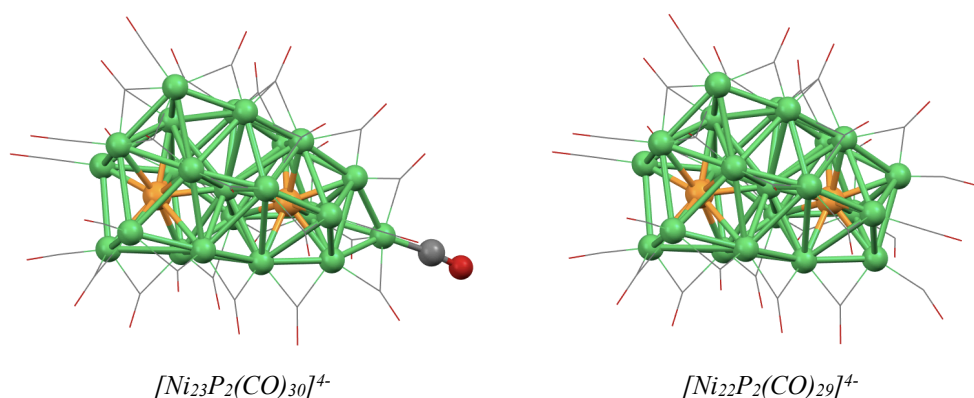


Figure 5.1 - Structures of the two co-existing species in  $[\text{Ni}_{23-x}\text{P}_2(\text{CO})_{30-x}]^{4-}$  ( $x = 0, 1$ ). The carbonyl ligands have been faded in order to better individuate the apical nickel-carbonyl fragment that is missing from one of the structures. Nickel atoms are represented in green, phosphorus atoms in orange, carbon atoms in grey, and oxygen atoms in red.

The metallic skeleton of the cluster was asymmetrical (Figure 5.2), and the two phosphorous atoms were hosted inside two distinct and different nickel cavities.

Both cavities were similar to those already seen in other nickel-phosphorus clusters (Figure 5.3). One was a ten-membered prismatic nickel cage, with one squared and one capped pentagonal base. The other nickel cage was shaped as a mono-capped squared open anti-prism, whose capped base was distorted by a missing edge. The former cavity had the same arrangement seen for the phosphorus-hosting cavity of  $[\text{Ni}_{11}\text{P}(\text{CO})_{18}]^{3-}$ , whilst the latter had the same arrangement of some of the cavities seen in  $[\text{HNi}_{31}\text{P}_4(\text{CO})_{39}]^{5-}$  and  $[\text{H}_2\text{Ni}_{31}\text{P}_4(\text{CO})_{39}]^{4-}$ . Thereby, also in this cluster both phosphorous atoms dis-

played a coordination number equal to nine or ten, and no icosahedral moiety was present.

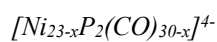
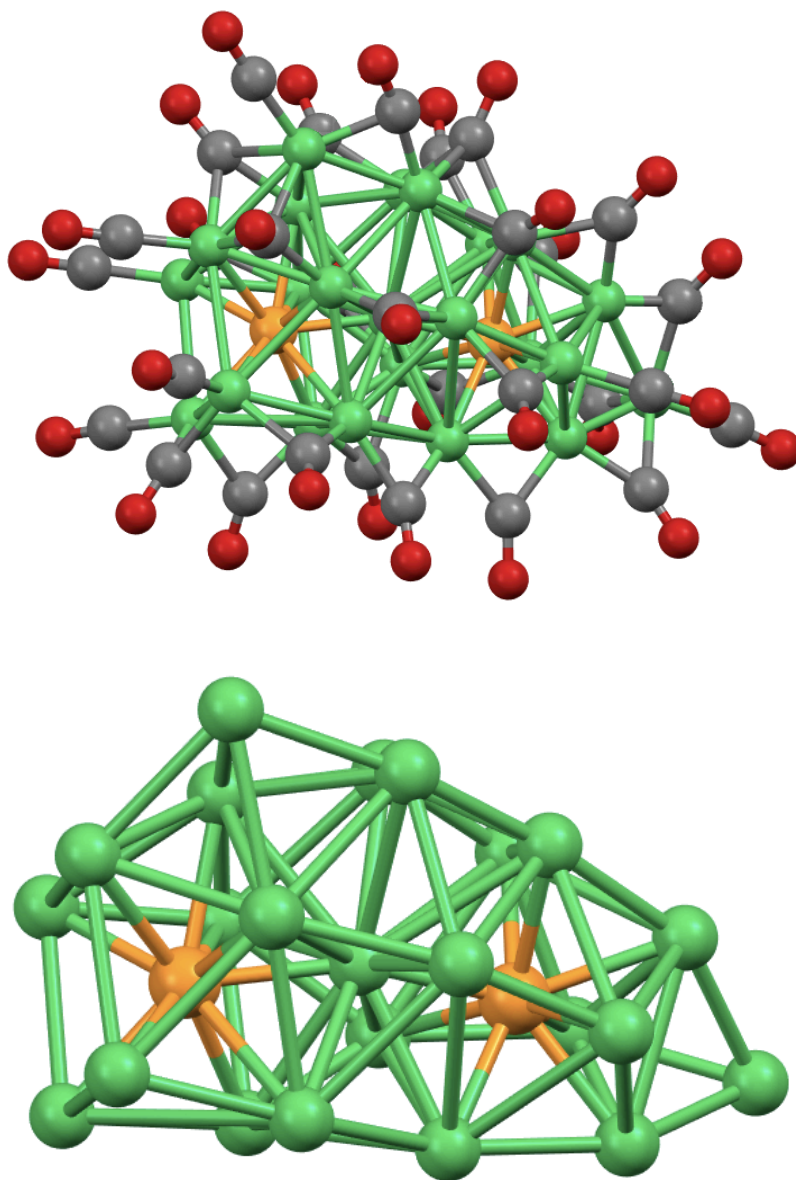


Figure 5.2 - Molecular structure and metallic skeleton of the  $[Ni_{23-x}P_2(CO)_{30-x}]^{4+}$  ( $x = 0, 1$ ) tetra-anion. The rightmost apical nickel-carbonyl fragment is only present in the structure of  $[Ni_{23}P_2(CO)_{30}]^{4+}$ . Nickel atoms are represented in green, phosphorus atoms in orange, carbon atoms in grey, oxygen atoms in red.

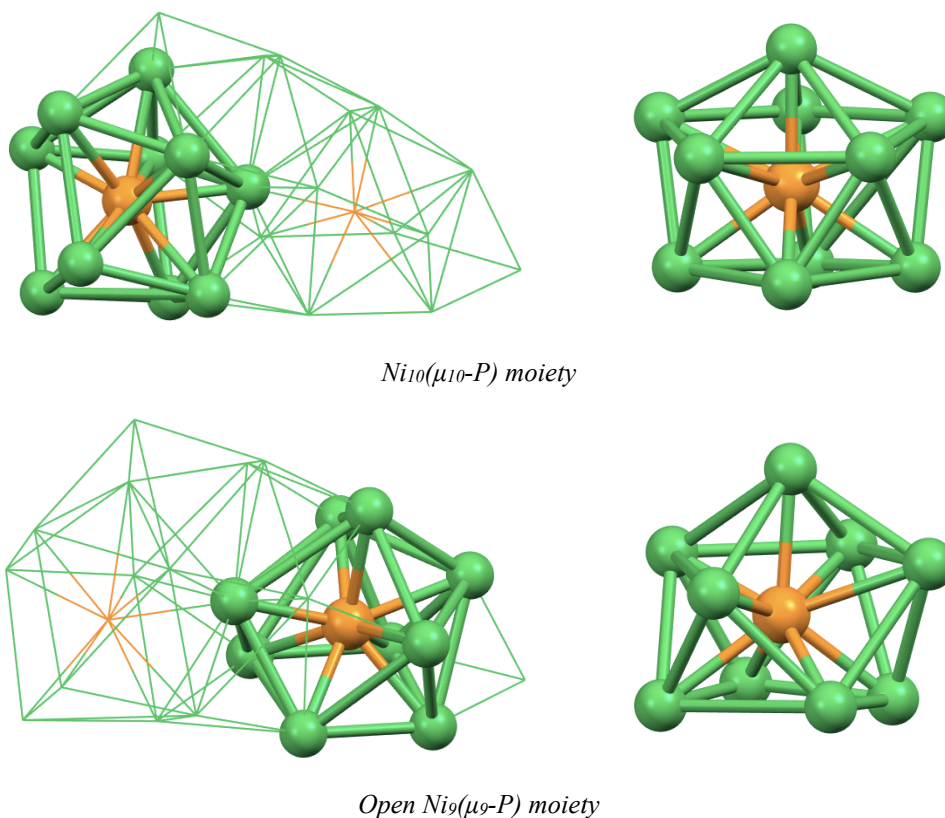


Figure 5.3 - Structures of the two types of phosphorus-hosting cavities within the metallic skeleton of  $[Ni_{23-x}P_2(CO)_{30-x}]^+$  ( $x = 0, 1$ ). On the left the position of the moieties has been highlighted. Nickel atoms are represented in green, phosphorus atoms in orange.

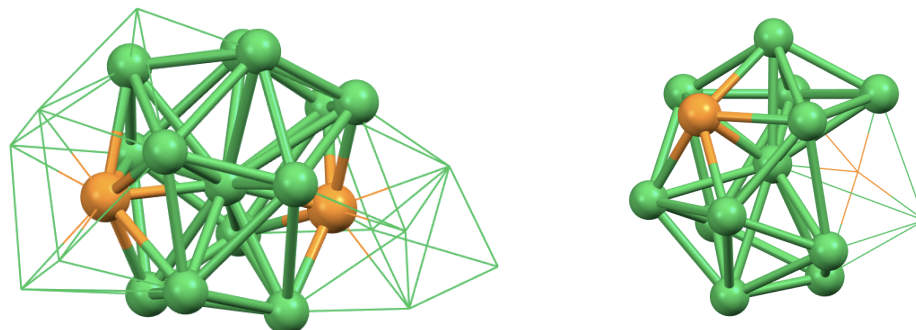
An interstitial nickel atom was individuated within the metallic skeleton of the cluster (Figure 5.4). It was hosted inside an heteroatomical cage, forming a  $Ni_{12}P_2(\mu_{14}-Ni)$  moiety. The coordination number of the nickel was equal to fourteen, as in the  $Ni_{11}P_3(\mu_{14}-Ni)$  moieties individuated within most of the molecular structures of  $[HNi_{31}P_4(CO)_{39}]^{5-}$ .

It was not possible to identify a clear arrangement for this distorted fragment. However, one nickel atom and one phosphorous atom appeared to be particularly in disarray. Assuming not to consider them, the then-fictional coordination number lowered to twelve and, more interestingly, it was possible to visualise an icosahedron.

This hypothetical icosahedral fragment had one heteroatomical  $Ni_4P$  base and one  $Ni_5$  base, each capped by a further nickel atom. The two bases were angled and divergent. Due to this, it would be misleading to consider this moiety as supporting evidence for the existence of icosahedral moieties in homoleptic nickel-



phosphorus carbonyl clusters. It is also important to consider that the original cavity was excessively distorted, and that two atoms had to be *a priori* excluded.



$Ni_{12}P_2(\mu_{14}-Ni)$  moiety

Figure 5.4 - Structure of the nickel-hosting cavity in the metallic skeleton of  $[Ni_{23-x}P_2(CO)_{30-x}]^{4-}$  ( $x = 0, 1$ ). On the left, the position of the moiety within the metallic skeleton has been highlighted. On the right, the disarrayed atoms have been faded. Nickel atoms are represented in green, phosphorus atoms in orange.

Finally, the metallic skeleton of  $[Ni_{23-x}P_2(CO)_{30-x}]^{4-}$  was surrounded by thirty - or twenty-nine - varyingly coordinated carbonyl ligands. Seven - or six - were singularly coordinated to one nickel atom, twenty-one were bridging over a nickel-nickel edge, and two were bridging over a triangular nickel face.

A selection of the crystal data that were collected for this cluster have been reported (Table 5.1). The unit cell of  $[Ni_{23-x}P_2(CO)_{30-x}]^{4-}$  belonged to the  $P2_1/n$  space group of the monoclinic crystal system. A comparison with the crystal data collected for the hexa-anionic form of the cluster will be proposed in the following section.

$a$ (Å)	14.9034(18)	$\alpha$ (°)	90	<i>c.s.</i>	<i>monoclinic</i>
$b$ (Å)	23.394(3)	$\beta$ (°)	99.202(2)	<i>space group</i>	$P2_1/n$
$c$ (Å)	26.186(3)	$\gamma$ (°)	90	$U$ (Å <sup>3</sup> )	9012.26

Table 5.1 - Selected crystal data collected for  $[Ni_{23-x}P_2(CO)_{30-x}]^{4-}$  ( $x = 0, 1$ ).

✦ **Structural characterisation of the hexa-anion**

A crystalline sample of  $[\text{Ni}_{23-x}\text{P}_2(\text{CO})_{30-x}]^{6-}$  was obtained after having performed a reduction test, and it was analysed via X-ray diffraction. This allowed to determine its molecular structure (Figure 5.5, Figure 5.6), that was coherent with that of its less reduced counterpart.

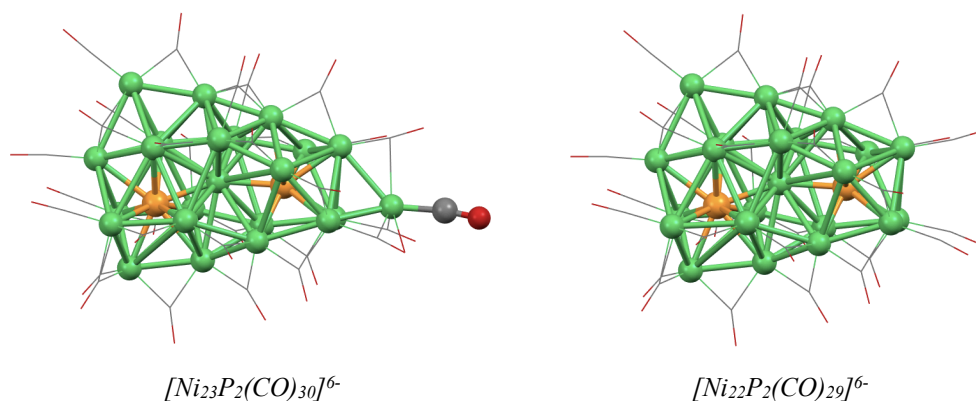


Figure 5.5 - Structures of the two co-existing species in  $[\text{Ni}_{23-x}\text{P}_2(\text{CO})_{30-x}]^{6-}$  ( $x = 0, 1$ ). The carbonyl ligands have been faded in order to better individuate the apical nickel-carbonyl fragment that is missing from one of the structures. Nickel atoms are represented in green, phosphorus atoms in orange, carbon atoms in grey, oxygen atoms in red.

As usual, the phosphorus atoms were in interstitial positions. The geometries of these phosphorus-hosting cavities were comparable to those already seen in the tetra-anionic form of the cluster. Moreover, it was also possible to individuate an interstitial nickel atom within a  $\text{Ni}_{12}\text{P}_2(\mu_{14}\text{-Ni})$  moiety.

For what concerns the phosphorus atoms, one had a coordination number equal to ten, whilst the other had a coordination number equal to nine (Figure 5.7). The first heteroatom was inside a prismatic nickel cage with one squared base and one capped pentagonal base. The second heteroatom was inside a mono-capped squared anti-prismatic nickel cage, open on one side.

A minor difference between the structures of the hexa-anion and the tetra-anion could be found considering the interstitial nickel atom and its surrounding cavity (Figure 5.7). The type of coordination of the interstitial metallic atom was the same, meaning that a  $\text{Ni}_{12}\text{P}_2(\mu_{14}\text{-Ni})$  moiety was still present. Moreover, one

nickel atom and one phosphorous atom were in disarray as well. Assuming not to consider them, a hypothetical  $Ni_{11}P(\mu_{12}-Ni)$  fragment was individuated, whose arrangement was similar to that individuated within the tetra-anionic form of the cluster. However, the geometry of the heteroatomical cage was slightly different, and the structure appeared to be even more distorted.

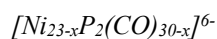
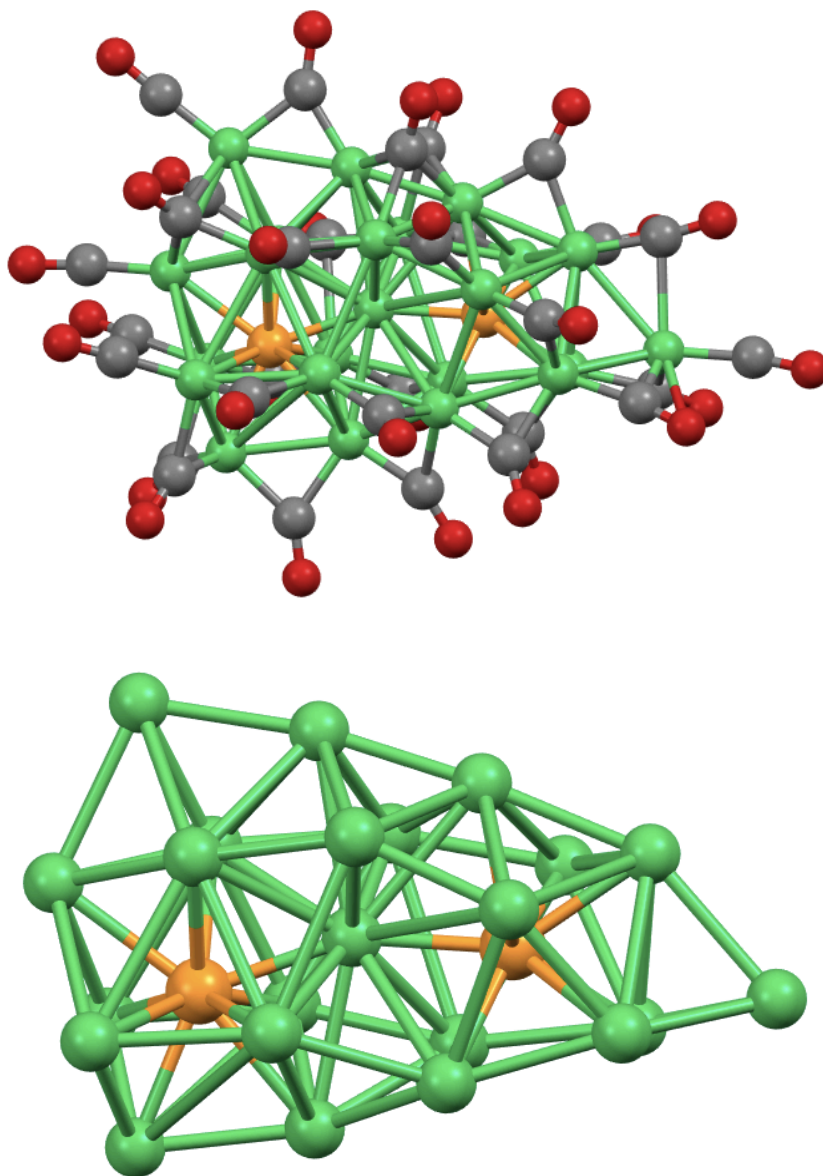


Figure 5.6 - Molecular structure and metallic skeleton of the  $[Ni_{23-x}P_2(CO)_{30-x}]^{6-}$  ( $x = 0, 1$ ) hexa-anion. Nickel atoms are represented in green, phosphorus atoms in orange, carbon atoms in grey, oxygen atoms in red.

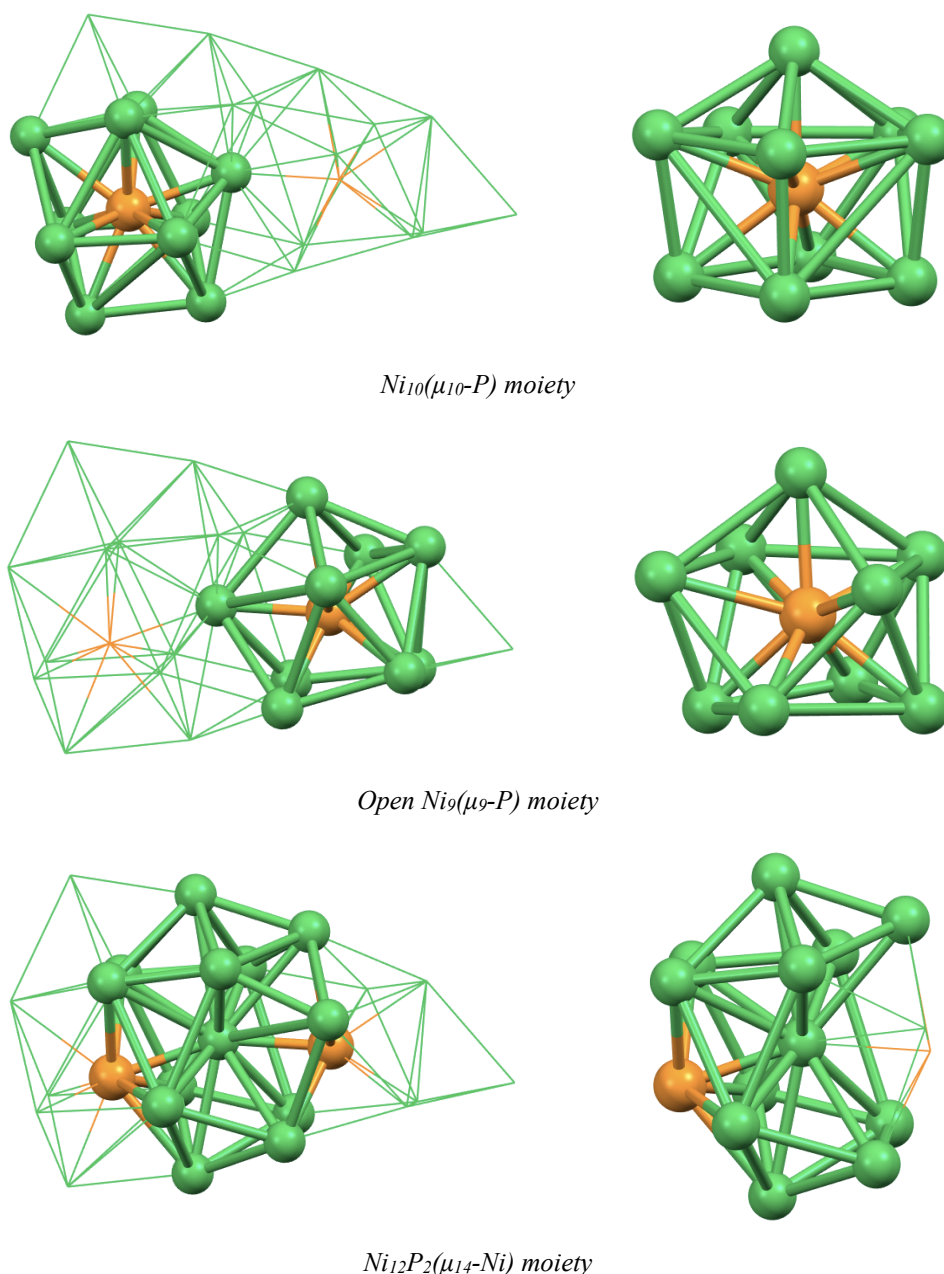


Figure 5.7 - Structures of the two phosphorus-hosting cavities and structure of the nickel-hosting cavity within the metallic skeleton of  $[Ni_{23-x}P_2(CO)_{30-x}]^{6-}$  ( $x = 0, 1$ ). On the left the position of the moieties has been highlighted. Nickel atoms are represented in green, phosphorus atoms in orange.

A selection of the crystal data that were collected for this cluster have been reported (Table 5.2). Its unit cell belonged to the  $Pna2_1$  space group of the orthorhombic crystal system.  $[Ni_{23-x}P_2(CO)_{30-x}]^{4-}$  and  $[Ni_{23-x}P_2(CO)_{30-x}]^{6-}$  displayed remarkably different crystal data, despite having closely related structures. This was probably due to the different number of cations within the unit cell.

$a$ (Å)	31.274(8)	$\alpha$ (°)	90	<i>c.s.</i>	<i>orthorhombic</i>
$b$ (Å)	24.562(6)	$\beta$ (°)	90	<b>space group</b>	$Pna2_1$
$c$ (Å)	15.752(4)	$\gamma$ (°)	90	$U$ (Å <sup>3</sup> )	12100.3

Table 5.2 - Selected crystal data collected for  $[Ni_{23-x}P_2(CO)_{30-x}]^{6-}$  ( $x = 0, 1$ ).

#### ♦ Spectroscopic and spectrometric characterisation

$[Ni_{23-x}P_2(CO)_{30-x}]^{4+}$  was dissolved in different solvents in order to collect its reference IR spectra in diverse environments (Table 5.3, Figure 5.8). It was not possible to perform the same comprehensive study on the hexa-anionic form of the cluster, as it was re-oxidised in non-reducing environments (Figure 5.9).

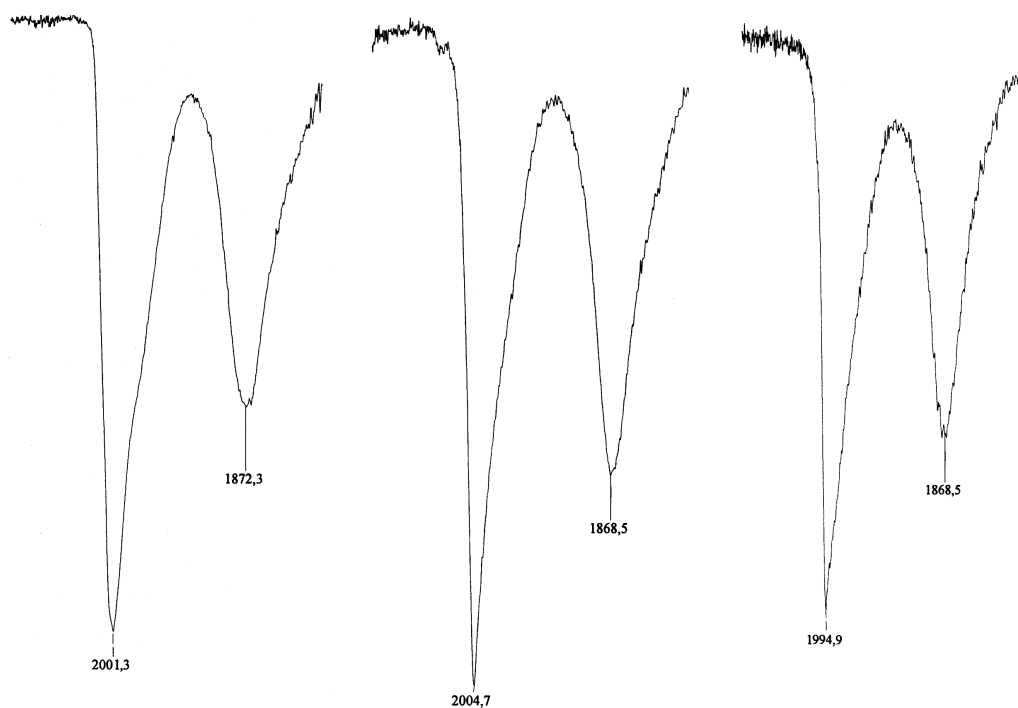
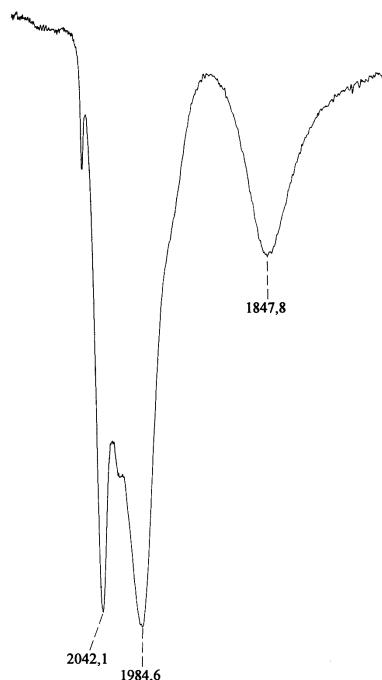
IR spectra of  $[Ni_{23-x}P_2(CO)_{30-x}]^{4+}$  in acetone, in acetonitrile, and in DMF

Figure 5.8 - The IR spectra of the cluster in different solvents were coherent with each other.

<i>solvent</i>	<i>acetone</i>	<i>acetonitrile</i>	<i>DMF</i>
<b>IR absorption frequencies (cm<sup>-1</sup>)</b>	2001s 1872m	2005s 1869m	1995s 1869m

Table 5.3 - Characteristic IR absorption frequencies of  $[Ni_{23-x}P_2(CO)_{30-x}]^{4+}$  ( $x = 0, 1$ ).



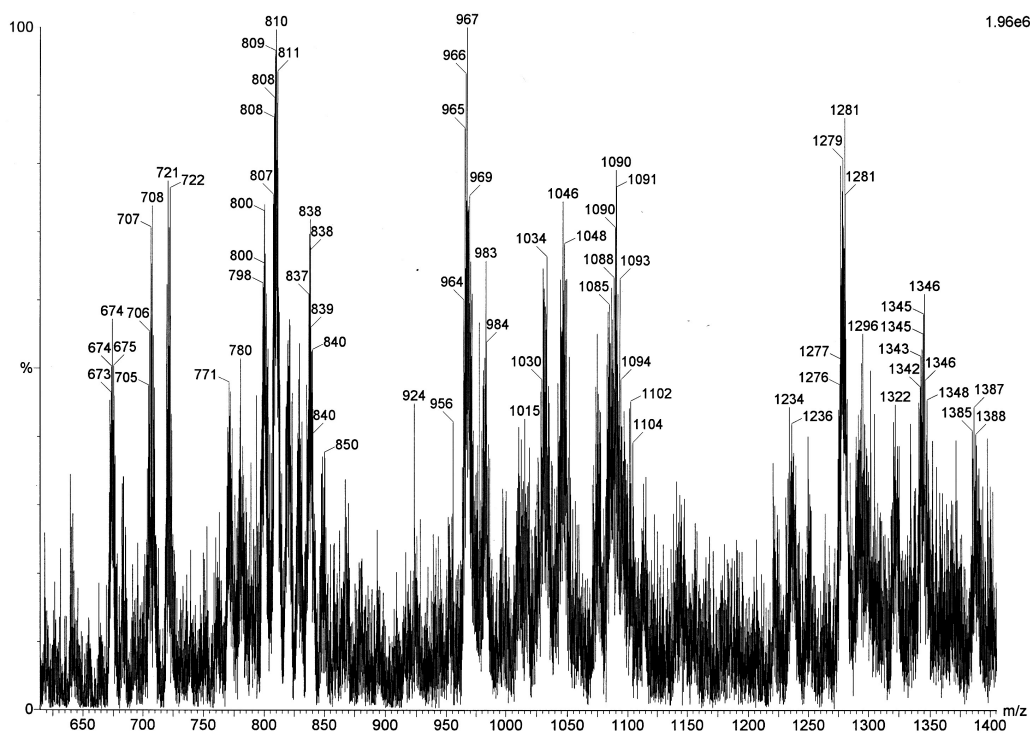
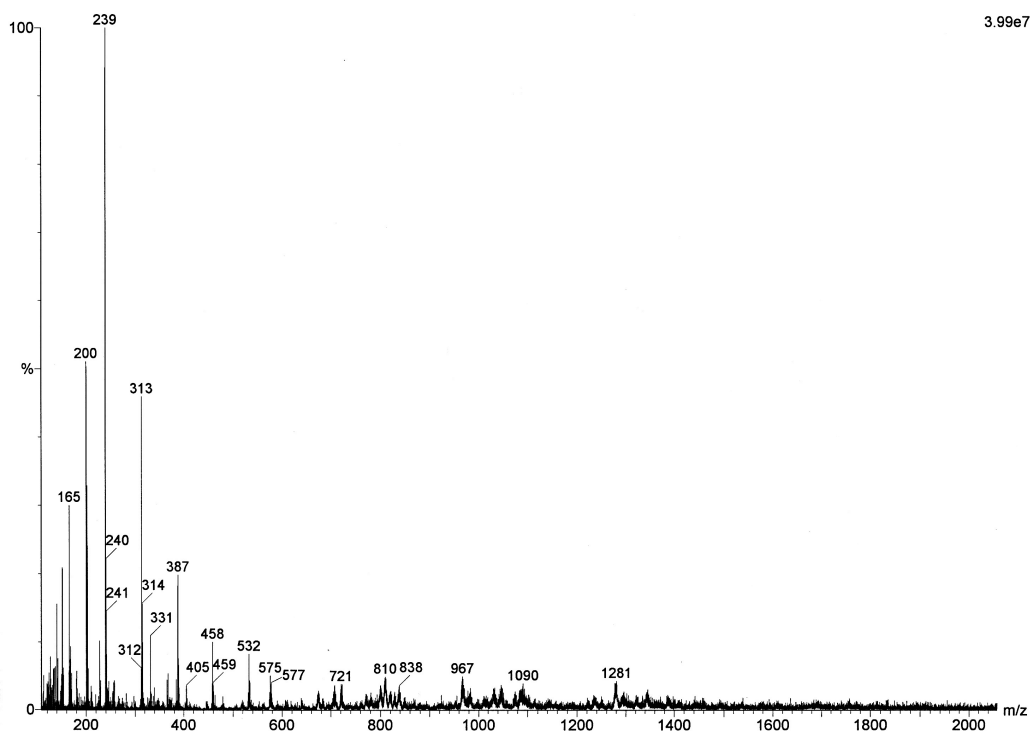
IR spectrum of  $[Ni_{23-x}P_2(CO)_{30-x}]^{6-}$  in acetonitrile

Figure 5.9 - The hexa-anion was re-oxidised when re-dissolved after the crystallisation, and its only spectrum was recorded at the end of a reduction reaction - thus the presence of  $Ni(CO)_4$  at  $2042\text{ cm}^{-1}$ .

\*\*\*

Apart from the aforementioned IR spectroscopy analyses, an ESI mass spectrometry analysis was performed on  $[Ni_{23-x}P_2(CO)_{30-x}]^{4-}$  as well. Unfortunately, for this nickel-phosphorus compound it was not possible to register a spectrum as clear as those recorded for  $[Ni_{11}P(CO)_{18}]^{3-}$ ,  $[Ni_{14}P_2(CO)_{22}]^{2-}$ , and  $[HNi_{31}P_4(CO)_{39}]^{5-}$ .

The collected data suggested that this species was probably unstable towards the operating conditions applied in this analytical process. In fact, there were several peaks related to decomposition and fragmentation processes - in the spectral zone below  $750\text{ m/z}$ . Notwithstanding the difficult interpretation process, it was eventually possible to assign to various peaks their corresponding mother-fragments (Table 5.4, Figure 5.10). This analysis highlighted the intrinsic lability of the cluster. Along with the co-existence of two actually distinct carbonyl compounds, this characteristic could justify the difficulties related to its crystallisation.



Mass spectra of  $[Ni_{23-x}P_2(CO)_{30-x}]^+$

Figure 5.10 - ESI mass spectra of  $[Ni_{23-x}P_2(CO)_{30-x}]^+$ . Due to the low stability of the cluster the species underwent to extensive fragmentation processes, as evidenced by the high number of recorded peaks at lower  $m/z$  values. In the lower figure a detail of the mass spectrum is reported.

<i>peak (m/z)</i>	<i>corresponding cluster moiety</i>
1277	{[Ni <sub>23</sub> P <sub>2</sub> (CO) <sub>30</sub> ].[NEt <sub>4</sub> ] <sub>2</sub> .[CH <sub>3</sub> CN]} <sup>2-</sup>
1103	{[Ni <sub>22</sub> P <sub>2</sub> (CO) <sub>29</sub> ].[CH <sub>3</sub> CN]} <sup>2-</sup>
1089	{[Ni <sub>22</sub> P <sub>2</sub> (CO) <sub>28</sub> ].[CH <sub>3</sub> CN]} <sup>2-</sup>
1047	{[Ni <sub>22</sub> P <sub>2</sub> (CO) <sub>25</sub> ].[CH <sub>3</sub> CN]} <sup>2-</sup>
1033	{[Ni <sub>22</sub> P <sub>2</sub> (CO) <sub>24</sub> ].[CH <sub>3</sub> CN]} <sup>2-</sup>
838	{[Ni <sub>23</sub> P <sub>2</sub> (CO) <sub>30</sub> ].[NEt <sub>4</sub> ] <sub>2</sub> } <sup>3-</sup>
829	{[Ni <sub>23</sub> P <sub>2</sub> (CO) <sub>29</sub> ].[NEt <sub>4</sub> ] <sub>2</sub> } <sup>3-</sup>
819	{[Ni <sub>23</sub> P <sub>2</sub> (CO) <sub>28</sub> ].[NEt <sub>4</sub> ] <sub>2</sub> } <sup>3-</sup>
810	{[Ni <sub>23</sub> P <sub>2</sub> (CO) <sub>27</sub> ].[NEt <sub>4</sub> ] <sub>2</sub> } <sup>3-</sup>
800	{[Ni <sub>23</sub> P <sub>2</sub> (CO) <sub>26</sub> ].[NEt <sub>4</sub> ] <sub>2</sub> } <sup>3-</sup>
(*) 720	{[Ni <sub>11</sub> P(CO) <sub>18</sub> ].[NEt <sub>4</sub> ] <sub>2</sub> } <sup>2-</sup>
(*) 707	{[Ni <sub>11</sub> P(CO) <sub>17</sub> ].[NEt <sub>4</sub> ] <sub>2</sub> } <sup>2-</sup>
(*) 575	{[Ni <sub>11</sub> P(CO) <sub>17</sub> ]} <sup>2-</sup>
(*) 532	{[Ni <sub>11</sub> P(CO) <sub>16</sub> ]} <sup>2-</sup>
(*) 314	{[Ni <sub>5</sub> (CO) <sub>12</sub> ]} <sup>2-</sup>
(*) 200	{[Ni <sub>3</sub> (CO) <sub>8</sub> ]} <sup>2-</sup>

Table 5.4 - Values of the characterised peaks and species to which they have been associated to during the interpretation of the ESI mass spectrum of [Ni<sub>23-x</sub>P<sub>2</sub>(CO)<sub>30-x</sub>]<sup>4-</sup>.

(\*) Indicates fragments that originated from severe fragmentation processes.

\*\*\*

It would have been interesting to perform a <sup>31</sup>P NMR spectroscopy analysis on [Ni<sub>23-x</sub>P<sub>2</sub>(CO)<sub>30-x</sub>]<sup>4-</sup>, since its nuclearity could have allowed to record a spectrum.

Unfortunately, this proved not to be the case. The other aforementioned analytical characterisation techniques were successfully employed since they are usually performed on very diluted solutions or single-crystals. On the contrary, NMR analyses require samples whose concentration is rather high. The scarce availability of this species in crystalline form excluded this possibility, as it proved to be extremely unlikely to obtain the cluster in large quantities with the required purity degree.



## **Reactivity tests**

The behaviour of  $[\text{Ni}_{23-x}\text{P}_2(\text{CO})_{30-x}]^{4+}$  towards reducing agents has already been outlined. In addition, oxidation trials were performed to control the potential redox behaviour of this compound.

Cluster solutions just as obtained at the end of the synthesis were used for all the reactions, since it had not been possible to obtain adequate amounts of crystalline samples.

### **♦ Reduction and oxidation**

As aforementioned, for the reduction tests  $[\text{Ni}_{23-x}\text{P}_2(\text{CO})_{30-x}]^{4+}$  was treated with a freshly-prepared solution of sodium methoxide.

Although this anion could take part in a ligand-exchange process with carbonyl complexes of electron-poor transition metals,<sup>1</sup> this is not common to happen for carbonyl clusters. The methoxide ion usually induces an electronic loss or - whenever possible - a protonic loss, since it can act as a reducing agent as well as a base.

During this trial the sodium methoxide was freshly prepared. The reaction between metallic sodium and methanol was performed, the thus obtained sodium methoxide was dried under vacuum until obtaining a white powder, then redissolved in acetonitrile in order to obtain a diluted solution. Small aliquots of the reducing agent were drop-wise added to the cluster solution in acetonitrile, checking the progress of the reaction via IR spectroscopy. As expected, the IR absorption frequencies gradually decreased, down to 1985s, 1848m  $\text{cm}^{-1}$  (Figure 5.11).

When working towards crystallisation, reduced clusters generally need to be precipitated with an aqueous solution of cation, with the aim of compensating for the lack of counter-ions. Despite that, in this case crystallisation was straightaway attempted, by layering diisopropyl ether over the cluster solution through a thin film of hexane. The aqueous treatment was not performed in order to avoid a pos-

---

<sup>1</sup> A. Bates, M. T. Muraoka, R. J. Trautman; *Inorg. Chem.*, **1993** (32) 2651-2656

sible partial re-oxidation of the cluster. As mentioned in the previous chapter, by following this procedure it was eventually possible to obtain a crystalline sample. Despite the poor quality of the crystals it was possible to structurally characterise the cluster as the  $[\text{Ni}_{23-x}\text{P}_2(\text{CO})_{30-x}]^{6-}$  hexa-anion.

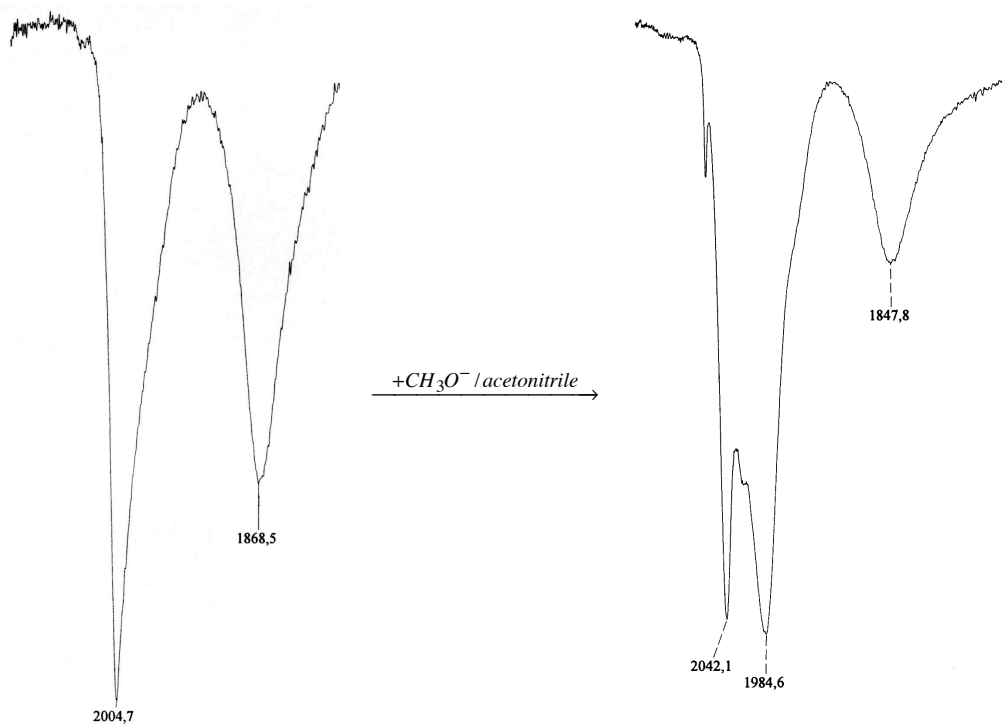


Figure 5.11 - IR spectra in acetonitrile of the  $[\text{Ni}_{23-x}\text{P}_2(\text{CO})_{30-x}]^{4-}$  tetra-anion and of the related  $[\text{Ni}_{23-x}\text{P}_2(\text{CO})_{30-x}]^{6-}$  hexa-anion, before and after the reduction reaction.

\*\*\*

After the remarkable results obtained during the reduction trials, oxidation tests were performed as well. First, a 1:100  $\text{m}/\text{v}$  diluted solution of tropilium tetrafluoroborate was used. Proceeding with an analogous approach, the oxidising reactant was drop-wise added to the cluster solution, after having confirmed via IR spectroscopy the quality of the starting sample.

The recorded IR absorption frequencies rose up to 2024s, 1876m  $\text{cm}^{-1}$ . At the end of the reaction crystallisation was endeavoured, unfortunately without results. It was not possible to collect any crystal, and this unknown compound was tenta-

tively formulated as  $[Ni_{23-x}P_2(CO)_{30-x}]^{2-}$ .

In order to structurally characterise the oxidised derivative of this nickel-phosphorus cluster, other reactants were used. Amongst the others, bismuth(III) triflate -  $Bi(OSO_2CF_3)_3$  - was employed. This unusual choice was made considering that this bismuth(III) salt had never been used with nickel or phosphorus clusters, therefore an unprecedented reactivity could have ensued.

An acetonitrile solution of  $[Ni_{23-x}P_2(CO)_{30-x}]^{4-}$  was prepared and analysed through IR spectroscopy. At the same time, a 1:100 m/v solution of bismuth triflate was prepared, and then it was drop-wise added to the cluster solution.

Since this was a completely novel trial, the advancement of the reaction was carefully followed through IR spectroscopy analysis. As expected, the IR absorption frequencies progressively rose to higher values, nonetheless it was also possible to witness to a shape-shift of the peaks. Interestingly, at the end of the reaction the spectrum was superimposable to that of  $[Ni_{14}P_2(CO)_{22}]^{2-}$  -  $\nu_{CO}$  equal to 2025vs, 2000s, 1865m, 1831mw  $cm^{-1}$  in acetonitrile (Figure 5.12).

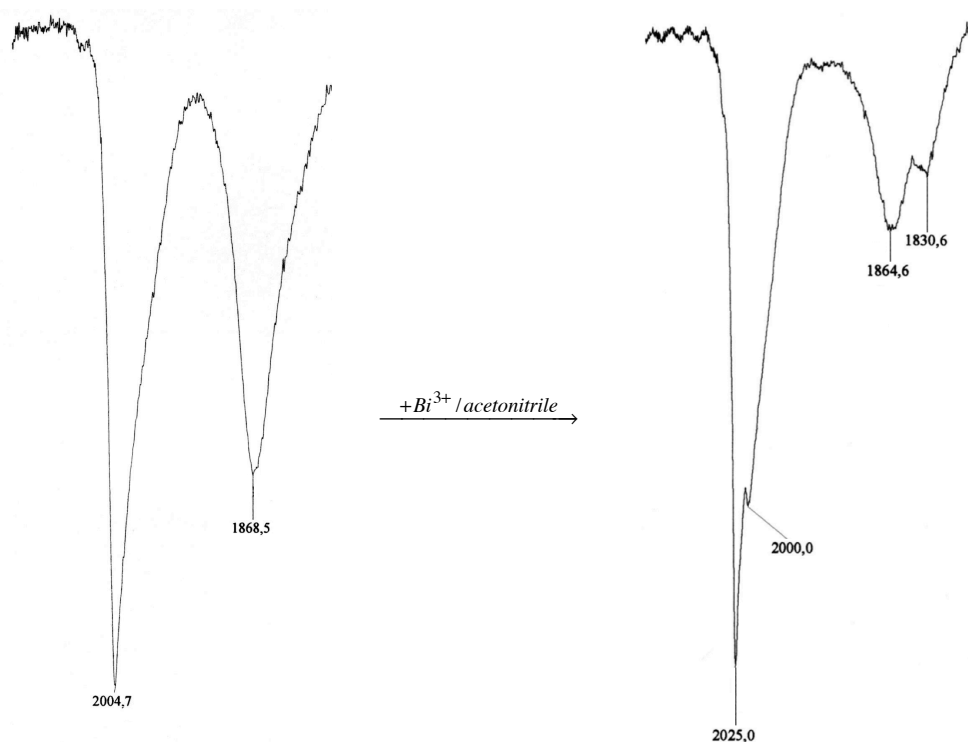


Figure 5.12 - IR spectra in acetonitrile of  $[Ni_{23-x}P_2(CO)_{30-x}]^{4-}$  - before the oxidation reaction - and of  $[Ni_{14}P_2(CO)_{22}]^{2-}$  - after the oxidation reaction.

To confirm the hypothesised oxidation of  $[\text{Ni}_{23-x}\text{P}_2(\text{CO})_{30-x}]^{4-}$  to  $[\text{Ni}_{14}\text{P}_2(\text{CO})_{22}]^{2-}$ , a crystallisation attempt was made. Owing to the proneness of the latter cluster towards crystallisation, it was possible to confirm the assumption. Well-shaped crystals formed via slow diffusion of diisopropyl ether through a thin film of hexane inside the acetonitrile solution. Not only their distinctive greenish colour, but also an X-ray diffraction analysis confirmed that the oxidation of  $[\text{Ni}_{23-x}\text{P}_2(\text{CO})_{30-x}]^{4-}$  with bismuth(III) triflate actually led to the formation of the  $[\text{Ni}_{14}\text{P}_2(\text{CO})_{22}]^{2-}$  di-anion (Figure 5.13).

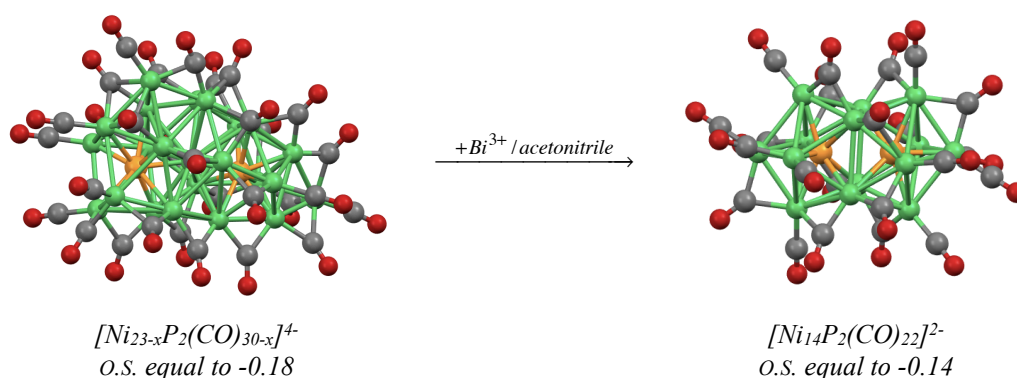


Figure 5.13 - Reaction scheme illustrating that  $[\text{Ni}_{23-x}\text{P}_2(\text{CO})_{30-x}]^{4-}$  is oxidised to  $[\text{Ni}_{14}\text{P}_2(\text{CO})_{22}]^{2-}$  when in presence of bismuth(III) triflate. Nickel atoms are represented in green, phosphorus atoms in orange, carbon atoms in grey, and oxygen atoms in red.

Oxidation reactions are usually employed to obtain larger structures from low-nuclearity or medium-nuclearity precursors. It may therefore seem odd to oxidise a cluster with higher nuclearity as  $[\text{Ni}_{23-x}\text{P}_2(\text{CO})_{30-x}]^{4-}$  to a cluster with lower nuclearity as  $[\text{Ni}_{14}\text{P}_2(\text{CO})_{22}]^{2-}$ . Yet, the former cluster bears a more negative delocalised charge than the latter, thus validating the observed reaction pathway.

#### ♦ *Controlled decompositions*

A further reactivity test was conducted in degrading environment, in order to verify the stability of the cluster. The trial was performed with triphenylphosphine, as this compound displays a high affinity towards nickel atom and its pres-

ence typically triggers the detachment of nickel-carbonyl fragments.

A diluted solution of triphenylphosphine in acetonitrile was prepared, and then drop-wise added to a solution of  $[Ni_{23-x}P_2(CO)_{30-x}]^{4-}$ . While proceeding with the additions it was possible to witness the formation of peaks at the characteristic IR absorption frequencies of different  $Ni(CO)_x(PPh_3)_{4-x}$  complexes -  $\nu_{CO}$  of  $Ni(CO)_3(PPh_3)$  equal to 2070s, 1990vs  $cm^{-1}$ ,  $\nu_{CO}$  of  $Ni(CO)_2(PPh_3)_2$  equal to 2000s, 1940vs  $cm^{-1}$ .

Once all the cluster had reacted, the reaction mixture was dried and then thoroughly washed with toluene in order to eliminate the neutral nickel-carbonyl-triphenylphosphine complexes. At the end of the process it was possible to extract the product of the reaction with acetonitrile, whose IR absorption frequencies were equal to 1980, 1850m  $cm^{-1}$ . These IR absorption frequencies were remarkably similar to those of  $[Ni_{11}P(CO)_{18}]^{3-}$  -  $\nu_{CO}$  equal to 1982, 1847m  $cm^{-1}$  - and the shapes of the two spectra were consistent as well.

It was therefore assumed that the detachment of several nickel-carbonyl fragments from the skeleton of  $[Ni_{23-x}P_2(CO)_{30-x}]^{4-}$  could have triggered a structural rearrangement that led to the formation of  $[Ni_{11}P(CO)_{18}]^{3-}$ . Also, it is worth to mention that within the structure of the larger cluster it was possible to individuate a  $Ni_{11}(\mu_{10}-P)$  moiety whose shape was closely related to that of the smaller cluster (Figure 5.14, Figure 5.15).

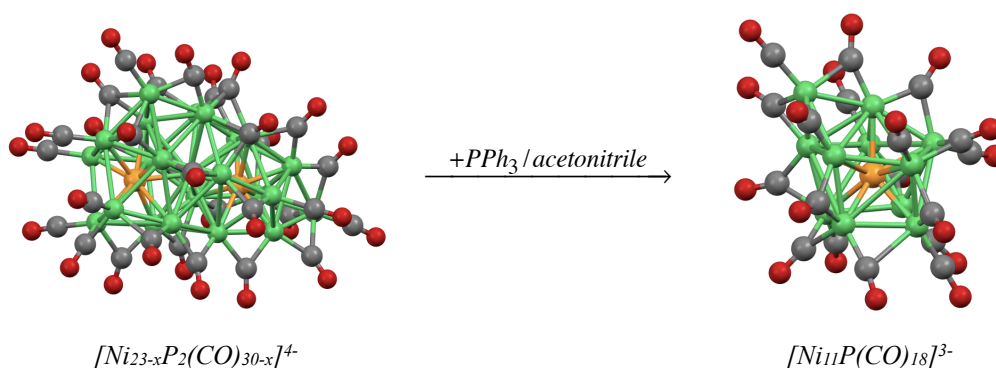


Figure 5.14 - Reaction scheme illustrating that  $[Ni_{23-x}P_2(CO)_{30-x}]^{4-}$  is transformed into  $[Ni_{11}P(CO)_{18}]^{3-}$  when treated with triphenylphosphine. Nickel atoms are represented in green, phosphorus atoms in orange, carbon atoms in grey, and oxygen atoms in red.

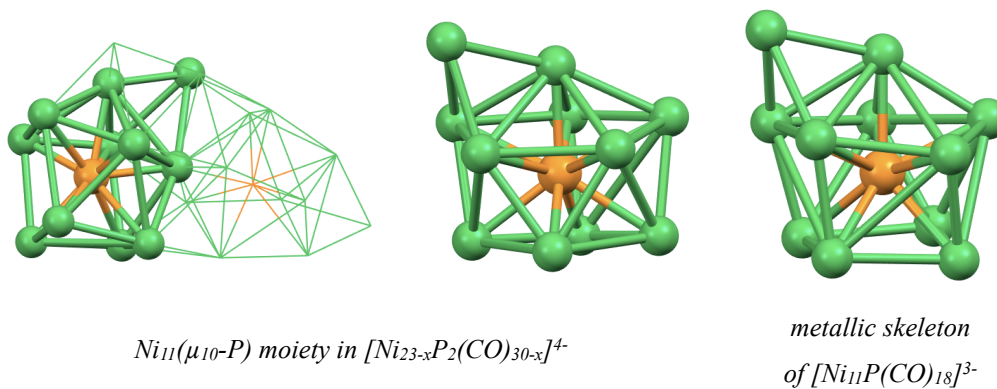


Figure 5.15 - Comparison between the  $Ni_{11}(\mu_{10}-P)$  moiety in the  $[Ni_{23-x}P_2(CO)_{30-x}]^{4-}$  cluster and the  $Ni_{11}(\mu_{10}-P)$  metallic skeleton of  $[Ni_{11}P(CO)_{18}]^{3-}$ . The position of the moiety within the cluster has been highlighted in the left image. Nickel atoms are represented in green, phosphorus atoms in orange.

## Other nickel-phosphorus carbonyl clusters

In the previous chapters the syntheses, the characterisations, and the reactivities of several new nickel-phosphorus carbonyl clusters have been reported. Still, it is worth to mention that  $[\text{Ni}_{11}\text{P}(\text{CO})_{18}]^{3-}$ ,  $[\text{Ni}_{14}\text{P}_2(\text{CO})_{22}]^{2-}$ ,  $[\text{Ni}_{23-x}\text{P}_2(\text{CO})_{30-x}]^{4-}$  ( $x = 0, 1$ ),  $[\text{Ni}_{23-x}\text{P}_2(\text{CO})_{30-x}]^{6-}$  ( $x = 0, 1$ ),  $[\text{HNi}_{31}\text{P}_4(\text{CO})_{39}]^{5-}$ , and  $[\text{H}_2\text{Ni}_{31}\text{P}_4(\text{CO})_{39}]^{4-}$  were not the only species that had been structurally characterised.

Throughout the numerous reactions that were performed by using  $[\text{Ni}_6(\text{CO})_{12}]^{2-}$  and  $\text{PCl}_3$  or  $\text{POCl}_3$  it was possible to detect other species, whose IR absorption frequencies were not corresponding to those of any other known nickel carbonyl cluster. Numerous attempts were made with the aim of characterising those species and of individuating a reproducible synthetic pathway.

In few cases it was possible to obtain some good-quality crystals, allowing a structural characterisation and the identification of the corresponding characteristic IR spectrum. In particular, these further clusters were  $[\text{Ni}_{29}\text{P}_5(\text{PO})(\text{CO})_{36}]^{4-}$  and  $[\text{Ni}_{39}\text{P}_3(\text{CO})_{44}]^{6-}$ .

Unfortunately, despite the efforts made it was neither possible to reproduce the reactions from which they were obtained, nor to individuate an alternative synthetic pathway for these species.

In the following chapters the reactions from which  $[\text{Ni}_{29}\text{P}_5(\text{PO})(\text{CO})_{36}]^{4-}$  and  $[\text{Ni}_{39}\text{P}_3(\text{CO})_{44}]^{6-}$  had originated will be described, and their full structural characterisation will be reported.

## **[Ni<sub>29</sub>P<sub>5</sub>(PO)(CO)<sub>36</sub>]<sup>4-</sup> Synthesis and partial characterisation**

### *Synthesis*

This cluster was obtained throughout a multistage and therefore complicated reaction pathway, whose first step consisted in the reaction between [Ni<sub>6</sub>(CO)<sub>12</sub>]<sup>2-</sup> and PCl<sub>3</sub> in tetrahydrofuran. Tri-methyl-octyl-ammonium was used as counter-ion for the nickel cluster precursor. The reaction was carried out by adding a diluted solution of phosphorus trichloride to a concentrated solution of the nickel cluster precursor. The reaction was concluded when the IR absorption frequencies of [Ni<sub>6</sub>(CO)<sub>12</sub>]<sup>2-</sup> were no longer detectable in the IR spectrum.

At the end of the process the reaction mixture was treated as usual, by removing the solvent under vacuum and then by washing the solid residue with water. Due to the nature of the cation that had been used, [Ni<sub>14</sub>P<sub>2</sub>(CO)<sub>22</sub>]<sup>2-</sup> was extracted with dichloromethane -  $\nu_{\text{CO}}$  equal to 2032vs, 1872m, 1864m cm<sup>-1</sup> - along with an unknown oily product. The oil was separated from the solution, washed accurately, and subjected to metathesis with the aim to dissolve it and then characterise it. The cation was changed to tetra-ethyl-ammonium and the product was dissolved in acetone -  $\nu_{\text{CO}}$  equal to 2011s, 1873m cm<sup>-1</sup> - yet it was not possible to obtain crystals. At that point, the unknown product was used for some reactivity trials, with the aim to structurally characterise a derivative form of the cluster.

First, a diluted solution of (Ph<sub>3</sub>P)AuCl was used - the gold(I) complex could have triggered a mild oxidation, a loss of nickel-carbonyl fragments, or an attachment of gold-phosphine appendices. By following the reaction through IR spectroscopy analyses, it was possible to witness to a moderate rise of the IR absorption frequencies from 2011s, 1873m cm<sup>-1</sup> to 2017s, 1880m cm<sup>-1</sup>. Crystallisation was attempted to no avail.

Then, a diluted solution of [AuBr<sub>2</sub>]<sup>-</sup> was used. By using this reactant the IR absorption frequencies shifted more sensibly towards higher values, rising up to 2028s, 1886m, 1830sh cm<sup>-1</sup>. At this point, by layering hexane over the acetone



solution of the cluster it was eventually possible to obtain a good-quality crystalline sample, and through an X-ray diffraction analysis the  $[Ni_{29}P_5(PO)(CO)_{36}]^{4-}$  tetra-anion was structurally characterised. Unfortunately, the crystalline sample deteriorated shortly after.

Due to the complexity of the process (Table 6.1) that ultimately led to the formation of this cluster, to date it has neither been possible to reproduce it, nor to observe the characteristic IR absorption frequencies of this species again. It was initially presumed that by using  $POCl_3$  rather than  $PCl_3$  the formation of  $[Ni_{29}P_5(PO)(CO)_{36}]^{4-}$  could have been favoured - due to the presence of a phosphorus-oxygen double-bond in the reactant itself. Unfortunately, the hypothesis have been disproved due to lack of positive results.

The development of this distinctive phosphoryl group may have risen after an atmosphere contamination, as it is not possible for minimal air infiltrations to be completely excluded.

<i>reactants</i>	<i><math>\nu_{CO}</math> (<math>cm^{-1}</math>)</i>	<i>product</i>	<i><math>\nu_{CO}</math> (<math>cm^{-1}</math>)</i>
$[Ni_6(CO)_{12}]^{2-} + PCl_3$ <i>in THF</i>	1980s 1820m 1790w	$[Ni_{14}P_2(CO)_{22}]^{2-} + [A]^{n-(oil)}$ <i>in <math>CH_2Cl_2</math></i>	2032vs 1872m 1864m
$[A]^{n-} + (Ph_3P)AuCl$ <i>in acetone</i>	2011s 1873m	$[A']^{m-}$ <i>in acetone</i>	2017s 1880m
$[A']^{m-} + [AuBr_2]^-$ <i>in acetone</i>	2017s 1880m	$[Ni_{29}P_5(PO)(CO)_{36}]^{4-}$ <i>in acetone</i>	2028s 1886m 1830sh

Table 6.1 - List of the reactants and of the products of the reactions that were performed before obtaining  $[Ni_{29}P_5(PO)(CO)_{36}]^{4-}$  as final product. After the metathesis process the unknown species labeled as  $[A]^{n-}$  was soluble in acetone and therefore not an oil anymore.

### **Structural characterisation**

By slow diffusion of hexane into the acetone solution of the cluster it was possible to obtain dark, good-quality crystals. Through an X-ray diffraction analysis the molecular structure of  $[Ni_{29}P_5(PO)(CO)_{36}]^{4-}$  was determined (Figure 6.1). The

most interesting feature of the structure of this cluster was the presence of a double-bonded phosphorus-oxygen fragment, *i.e.* a phosphoryl group.

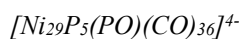
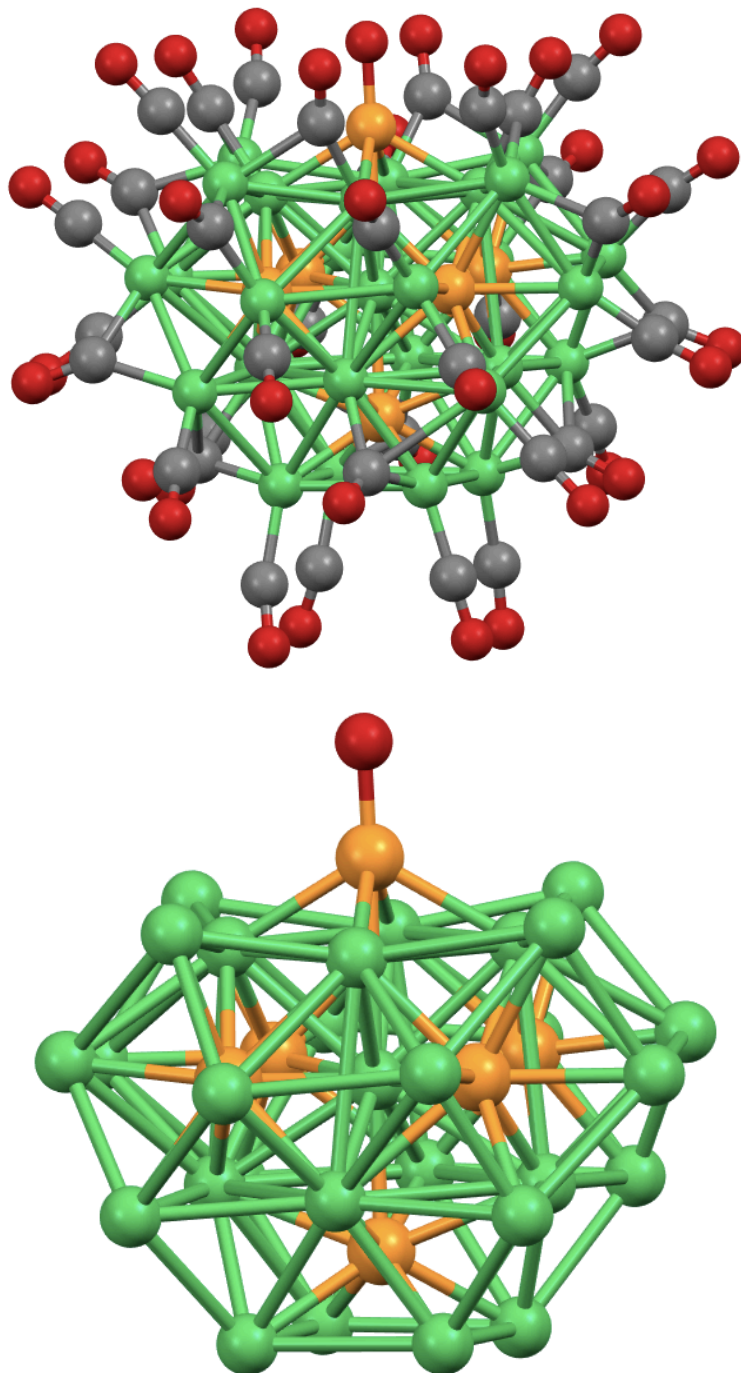
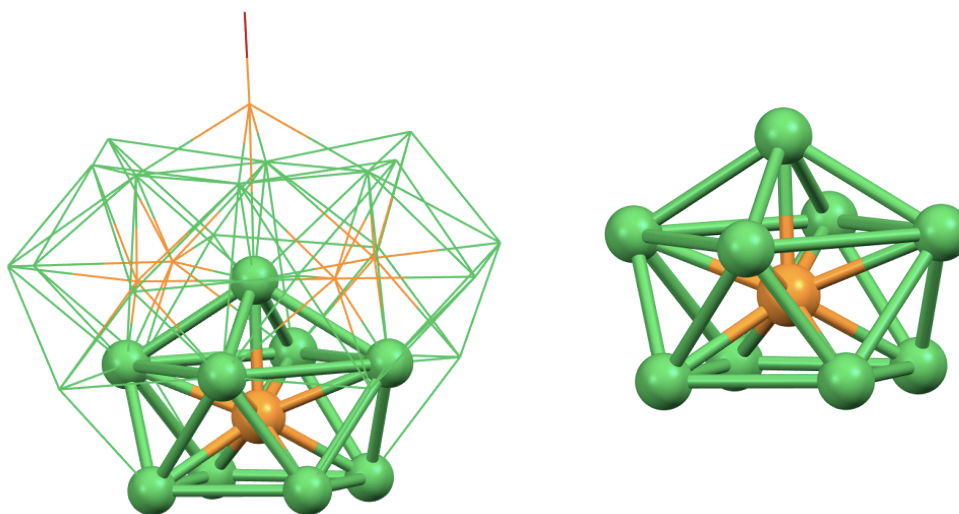


Figure 6.1 - Molecular structure and metallic skeleton of  $[\text{Ni}_{29}\text{P}_5(\text{PO})(\text{CO})_{36}]^{4-}$ . The position of the phosphoryl group is clearly visible in the upper region. Nickel atoms are represented in green, phosphorus atoms in orange, carbon atoms in grey, and oxygen atoms in red.

As usual, the carbonyl ligands surrounded the metallic skeleton, and completed the coordination sphere. The thirty-six COs were varyingly coordinated. Twenty carbonyl ligands were singularly bonded to a nickel atoms, fifteen were bridging over a nickel-nickel edge, and one was bridging over a triangular nickel face. It is worth to mention that in proximity of the phosphorus-oxygen bond the carbonyl shell was relatively loose. Therefore, the phosphorus atom was partially exposed.

The molecular structure of this cluster was not symmetrical. Nonetheless, a significant regularity emerged. Each phosphorus atom - except for the phosphorus belonging to the phosphoryl group - was at the centre of a nine-membered nickel cage. Interestingly, each of these five phosphorus-hosting nickel cavities (Figure 6.2) displayed the same geometry, and they all were shaped as mono-capped squared anti-prisms. The same type of nickel-phosphorus moieties had already been seen in the molecular structures of  $[\text{Ni}_{14}\text{P}_2(\text{CO})_{22}]^{2-}$  and  $[\text{H}\text{Ni}_{31}\text{P}_4(\text{CO})_{39}]^{5-}$ .



*Ni<sub>9</sub>(μ<sub>9</sub>-P) moiety*

*Figure 6.2 - Structure of the only type of phosphorus-hosting cavity within the metallic skeleton of  $[\text{Ni}_{29}\text{P}_5(\text{PO})(\text{CO})_{36}]^{4-}$ . On the left the position of one of these moieties has been highlighted. Nickel atoms are represented in green, phosphorus atoms in orange, oxygen atoms in red.*

All the five  $\text{Ni}_9(\mu_9\text{-P})$  fragments that were individuated inside the  $[\text{Ni}_{29}\text{P}_5(\text{PO})(\text{CO})_{36}]^{4-}$  cluster shared the capping nickel atom, that therefore was in interstitial position and at the centre of a hypothetical octahedron of phosphorus

atoms. However, it is important to note that there were no direct phosphorus-phosphorus interactions. Moreover, the five nickel cages shared the edges of the capped squared bases, one with each adjacent cage. These shared nickel edges formed a distorted cube, that in turn was interpenetrating with the octahedron of phosphorus atoms (Figure 6.3). Therefore, the interstitial nickel atom had a coordination number equal to fourteen.

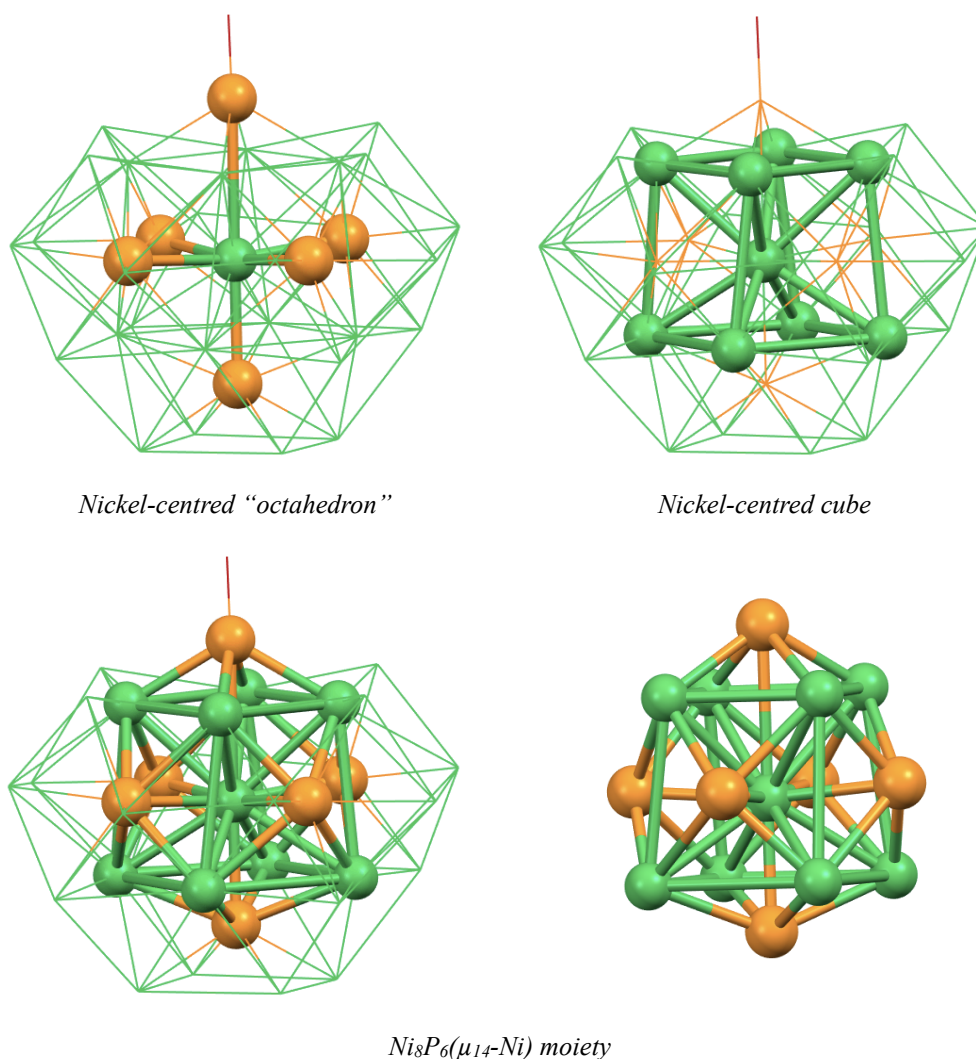


Figure 6.3 - Schematic representation of the structure of the nickel-hosting cavity within the metallic skeleton of  $[Ni_{29}P_5(PO)(CO)_{36}]^{4-}$ . In the upper figure the two different sub-cages that surrounded the interstitial nickel atom have been highlighted. In the lower left figure, the position of the moiety within the metallic skeleton has been highlighted. Nickel atoms are represented in green, phosphorus atoms in orange, oxygen atoms in red.

From another point of view, the structure of the cluster could have been seen as

developing from that single interstitial nickel atom. This metallic atom was at the centre of a nickel cube, which was in turn enclosed by a larger phosphorus octahedron. Therefore, each face of the nickel cube was capped by an heteroatom. The remaining metallic atoms completed the coordination sphere of the phosphorus atoms by forming mono-capped squared anti-prisms that enclosed five out of the six phosphorus atoms. The last heteroatom was bonded to the oxygen atom, forming the characteristic phosphoryl group.

On one hand, the interstitial atom displayed the same coordination number of those seen in the other clusters - *i.e.* fourteen. On the other hand, the resulting  $Ni_8P_6(\mu_{14}-Ni)$  moiety was far richer in phosphorus, and its geometry was completely different from those of the other nickel-centred moieties.

To conclude, the structure of  $[Ni_{29}P_5(PO)(CO)_{36}]^{4-}$  displayed just one type of coordination for the heteroatoms, which was already seen in other nickel-phosphorus clusters - in  $[Ni_{14}P_2(CO)_{22}]^{2-}$  and in  $[HNi_{31}P_4(CO)_{39}]^{5-}$ . Yet, the interconnections between these cages and the presence of a phosphorus-oxygen double-bond were distinctive features which to date have never been observed in other nickel-phosphorus structures.

A selection of the crystal data that were collected for this cluster have been reported (Table 6.2). The unit cell of  $[Ni_{29}P_5(PO)(CO)_{36}]^{4-}$  belonged to the Cc space group of the monoclinic crystal system.

<i>a</i> (Å)	26.674(16)	<i>α</i> (°)	90	<i>c.s.</i>	<i>monoclinic</i>
<i>b</i> (Å)	15.922(10)	<i>β</i> (°)	95.893(8)	<i>space group</i>	<i>Cc</i>
<i>c</i> (Å)	25.555(15)	<i>γ</i> (°)	90	<i>U</i> (Å <sup>3</sup> )	10796.2

Table 6.2 - Selected crystal data collected for  $[Ni_{29}P_5(PO)(CO)_{36}]^{4-}$ .

## **[Ni<sub>39</sub>P<sub>3</sub>(CO)<sub>44</sub>]<sup>6-</sup> Synthesis and partial characterisation**

### *Synthesis*

[Ni<sub>39</sub>P<sub>3</sub>(CO)<sub>44</sub>]<sup>6-</sup> was once obtained while trying to synthesise the aforementioned [Ni<sub>23-x</sub>P<sub>2</sub>(CO)<sub>30-x</sub>]<sup>4-</sup>. In accord with the previously described reaction, [Ni<sub>6</sub>(CO)<sub>12</sub>]<sup>2-</sup> was treated with a diluted solution of POCl<sub>3</sub>, and tetrahydrofuran was used as solvent. The IR spectroscopy analyses did not reveal any consistent difference when compared to the data of reference. In fact, by conducting the reaction in tetrahydrofuran it is only possible to record the gradually decreasing intensities of the IR signals of the precursor. It was therefore initially assumed that the synthesis of the cluster product of interest, [Ni<sub>23-x</sub>P<sub>2</sub>(CO)<sub>30-x</sub>]<sup>4-</sup>, had been successful.

Once the defined stoichiometric ratio had been reached - in that case *circa* 1 to 0.8 - the reaction mixture was treated as usual. The solvent and Ni(CO)<sub>4</sub> were eliminated in vacuum, and the solid was then thoroughly washed with water. It is worth to mention that the aqueous solution displayed an intense greenish colour, fact that may denote decomposition processes.

As expected, traces of [Ni<sub>6</sub>(CO)<sub>12</sub>]<sup>2-</sup> and [Ni<sub>9</sub>(CO)<sub>18</sub>]<sup>2-</sup> were extracted with tetrahydrofuran. On the contrary, a novel and unlooked-for species was extracted with acetone. The IR absorption frequencies -  $\nu_{\text{CO}}$  equal to 1998s, 1868ms cm<sup>-1</sup> - were not those characteristic of any known nickel-phosphorus carbonyl cluster, and therefore a crystallisation attempt was made.

It was eventually possible to obtain a crystalline sample that was suitable for an X-ray diffraction analysis. The analysis allowed to identify the new cluster as [Ni<sub>39</sub>P<sub>3</sub>(CO)<sub>44</sub>]<sup>6-</sup>. The dissolution of few crystals in acetonitrile allowed to record a reference IR spectrum, whose  $\nu_{\text{CO}}$  were coherent to those of the extracted solution. Due to the exceptional molecular structure and to the high nuclearity of this cluster, countless tentatives were made in order to develop a reproducible synthesis for this species. Unfortunately, to date no attempt gave the hoped results.

This problem was probably caused by the similarities between this sought-after synthesis and that of  $[Ni_{23-x}P_2(CO)_{30-x}]^{4-}$ . Both clusters were obtained by using the same reactants in a comparable stoichiometric ratio. A still unknown factor must have played a vital role throughout the reaction, which led to the formation of one species rather than the other.

### ***Structural characterisation***

The X-ray diffraction analysis was performed on dark, well-shaped crystals, that were obtained through slow diffusion of diisopropyl ether through a thin film of hexane into an acetonitrile solution of the cluster. This allowed to determine the molecular structure of  $[Ni_{39}P_3(CO)_{44}]^{6-}$ , which displayed unique and exceptional features. Firstly, the  $[Ni_{39}P_3(CO)_{44}]^{6-}$  hexa-anion had the highest nuclearity and the highest symmetry that had been seen that far for nickel-phosphorus clusters. Secondly, and most importantly, the first proof of the possible existence of icosahedral coordinations in nickel-phosphorus homoleptic carbonyl clusters was found within its metallic skeleton.

As aforementioned, the metallic skeleton of this cluster displayed unprecedented features (Figure 6.4). Unlike other symmetrical nickel-phosphorus clusters - that were formed by no more than two symmetrical sub-units - the molecular structure of  $[Ni_{39}P_3(CO)_{44}]^{6-}$  was composed by three identical sub-units, each of which was a phosphorus-centred fragment. The forty-four carbonyl ligands that completed the coordination sphere of the cluster were varyingly coordinated. Six COs were terminally bonded to a single nickel atom, thirty-two were bridging over a nickel-nickel edge, and six were bridging over a triangular nickel face.

The three heteroatoms were enclosed within symmetrical and therefore identical nickel cages. The most interesting feature of these  $Ni_{14}(\mu_{12}-P)$  moieties was their shape, which was completely different from those already described. Not only the phosphorus atoms had a higher coordination number - C.N. equal to twelve - but for the first time the phosphorus-hosting nickel cages were neither

squared anti-prisms nor related structures. In fact, each symmetrical  $\text{Ni}_{14}(\mu_{12}\text{-P})$  sub-unit was formed by a phosphorus-centred icosahedron of nickel atoms, completed by two additional metallic atoms which were capping two adjacent triangular faces of the icosahedron (Figure 6.5).

There also were three symmetrical interstitial nickel atoms in the structure. Interestingly, these metallic atoms were inside icosahedral environments as well, and their coordination number was equal to twelve (Figure 6.6). Each interstitial nickel atom was enclosed within an heteroatomical cage, forming a  $\text{Ni}_{10}\text{P}_2(\mu_{12}\text{-Ni})$  moiety. The two heteroatoms were in apical position, whilst the pentagonal bases were formed by nickel atoms.

So, in the molecular structure of  $[\text{Ni}_{39}\text{P}_3(\text{CO})_{44}]^{6-}$  there were not only three symmetrical phosphorus-centred icosahedra, but also three symmetrical nickel-centred icosahedra. These types of coordinations are actually common for nickel clusters with other group-15 elements, but had never been seen before in nickel-phosphorus homoleptic carbonyl clusters.

Eventually, the molecular structure of  $[\text{Ni}_{39}\text{P}_3(\text{CO})_{44}]^{6-}$  confirmed the possible existence of icosahedral structures in nickel-phosphorus homoleptic carbonyl clusters. Both phosphorus-centred and nickel-centred icosahedra were individuated inside its metallic skeleton, whose importance will be later highlighted.

A selection of the crystal data that were collected for this cluster have been reported (Table 6.3). The unit cell of  $[\text{Ni}_{39}\text{P}_3(\text{CO})_{44}]^{6-}$  belonged to the  $P6_3$  space group of the hexagonal crystal system. To date, this is the nickel-phosphorus homoleptic carbonyl cluster with the highest symmetry.

$a$ (Å)	25.283(7)	$\alpha$ (°)	90	<i>c.s.</i>	<i>hexagonal</i>
$b$ (Å)	25.283(7)	$\beta$ (°)	90	<i>space group</i>	$P6_3$
$c$ (Å)	15.616(4)	$\gamma$ (°)	120	$U$ (Å <sup>3</sup> )	8644.43

Table 6.3 - Selected crystal data collected for  $[\text{Ni}_{39}\text{P}_3(\text{CO})_{44}]^{6-}$ .



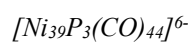
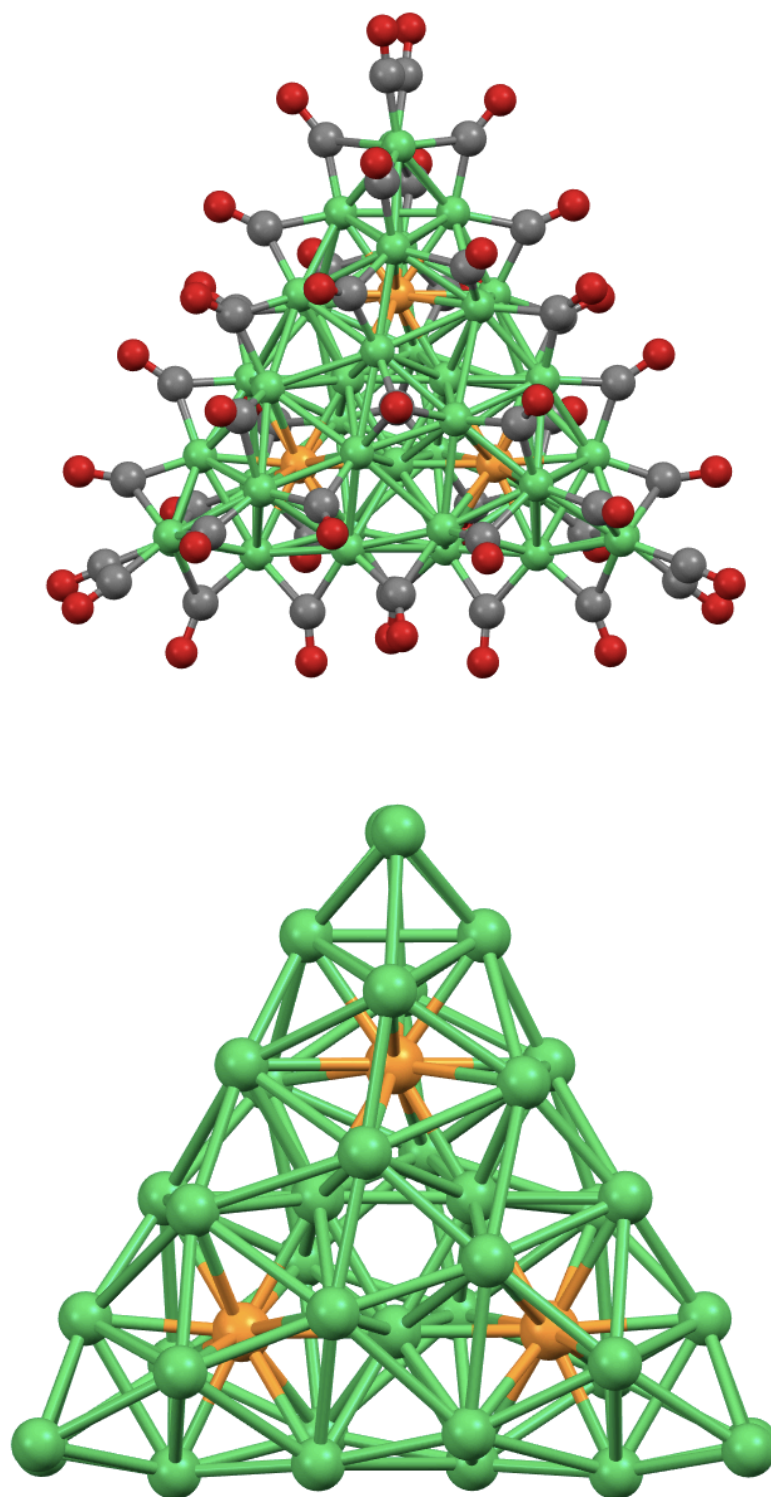
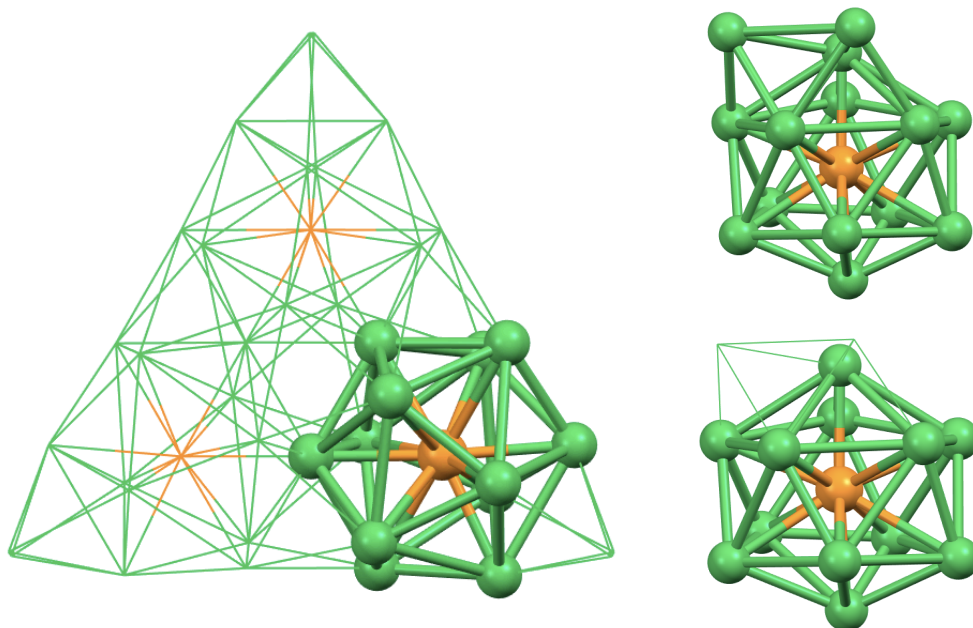
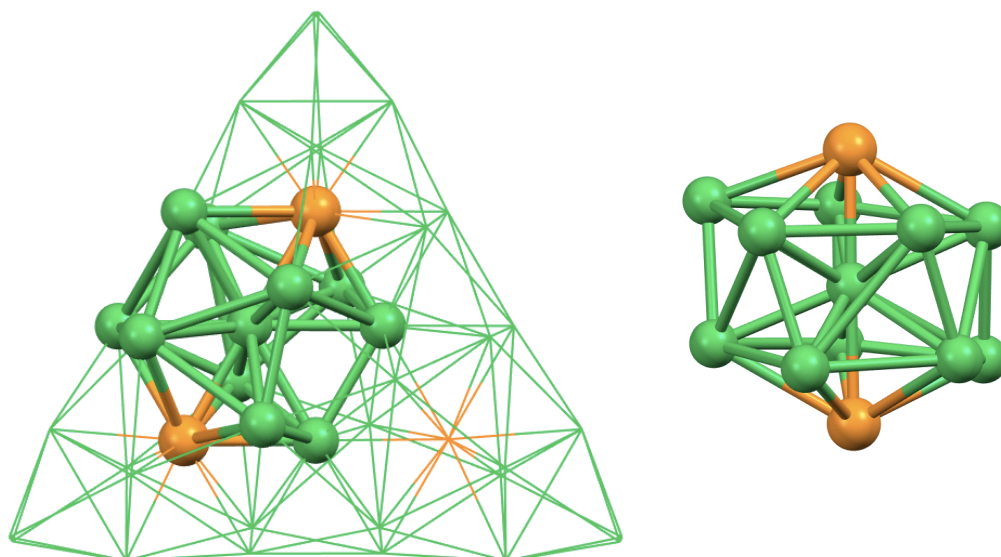


Figure 6.4 - Molecular structure and metallic skeleton of  $[\text{Ni}_{39}\text{P}_3(\text{CO})_{44}]^{6-}$ . Nickel atoms are represented in green, phosphorus atoms in orange, carbon atoms in grey, oxygen atoms in red.



$Ni_{14}(\mu_{12}\text{-P})$  moiety

Figure 6.5 - Structure of the only type of phosphorus-hosting cavity within the metallic skeleton of  $[Ni_{39}P_3(CO)_{44}]^{6-}$ . In the left figure the position of one of the moieties has been highlighted. In the lower right figure the phosphorus-centred icosahedron has been highlighted. Nickel atoms are represented in green, phosphorus atoms in orange.



$Ni_{10}P_2(\mu_{12}\text{-Ni})$  moiety

Figure 6.6 - Structure of the only type of nickel-hosting cavity within the metallic skeleton of  $[Ni_{39}P_3(CO)_{44}]^{6-}$ . In the left figure the position of one of the moieties has been highlighted. Nickel atoms are represented in green, phosphorus atoms in orange.

## Structural analyses and comparisons

The structures of several new nickel-phosphorus carbonyl clusters - *i.e.*  $[\text{Ni}_{11}\text{P}(\text{CO})_{18}]^{3-}$ ,  $[\text{Ni}_{14}\text{P}_2(\text{CO})_{22}]^{2-}$ ,  $[\text{Ni}_{23-x}\text{P}_2(\text{CO})_{30-x}]^{4-}$  ( $x = 0, 1$ ) and the corresponding hexa-anion,  $[\text{HNi}_{31}\text{P}_4(\text{CO})_{39}]^{5-}$  and the corresponding di-hydride tetra-anion,  $[\text{Ni}_{29}\text{P}_5(\text{PO})(\text{CO})_{36}]^{4-}$ , and  $[\text{Ni}_{39}\text{P}_3(\text{CO})_{44}]^{6-}$  - have been illustrated in the previous chapters. In the following sections comprehensive analyses and a comparisons of their molecular structures and characteristic sub-units will be proposed.

Further investigations will be focused on the different types of coordination of the phosphorus atoms, on the bond lengths within the phosphorus-hosting cavities, and on the bond lengths within the nickel-hosting cavities. The collected data will be used to compare these structures to those of other nickel-pnictogen carbonyl clusters and to those of other metal-phosphorus carbonyl clusters.

Before proceeding, in the ensuing sections a reference set of values had been used as comparison for the evaluation of the calculated average bond lengths. For the nickel-phosphorus bond lengths, the reference mean value was calculated from the entire set of nickel-phosphorus interactions. For the nickel-nickel bond lengths, the reference mean value was calculated from the data sets of  $[\text{Ni}_6(\text{CO})_{12}]^{2-}$  and  $[\text{Ni}_9(\text{CO})_{18}]^{2-}$ , in order to avoid any possible interference.

Moreover, an evaluation of the elongation of the bonds was attempted. For an interaction to be considered as elongated, the limit was set by considering the average bond length plus its difference from the minimum bond length.

In the following table the calculated average, the experimental minimum, and the calculated maximum bond lengths have been reported (Table 7.1). These data will be referred to and used as reference values in the following sections.

<i>bond type</i>	<i>calculated average (Å)</i>	<i>experimental minimum (Å)</i>	<i>calculated maximum (Å)</i>
<i>nickel-phosphorus</i>	2.33 ± 0.09	2.15	2.51
<i>nickel-nickel</i>	2.61 ± 0.11	2.37	2.85

Table 7.1 - Set of reference values for the nickel-phosphorus and the nickel-nickel bond lengths.

## ***Phosphorus-hosting cavities***

In the aforementioned clusters - despite the different nickel-phosphorus ratios and nuclearities - a characteristic behaviour emerged regarding the phosphorus atoms. In fact, the cavities in which the heteroatoms were located displayed comparable geometries in all but one species -  $[\text{Ni}_{39}\text{P}_3(\text{CO})_{44}]^{6-}$ . In the first part of this chapter these similar cages will be compared, and then the characteristic sub-structure of  $[\text{Ni}_{39}\text{P}_3(\text{CO})_{44}]^{6-}$  will be presented *per se*.

As aforementioned, in all nickel-phosphorus clusters the heteroatoms were in interstitial position, and in most cases their coordination number was equal to nine, or ten. In both cases the phosphorus-hosting nickel cages displayed very similar geometries. Therefore, it was assumed that the most common behaviour for the phosphorus atoms was to be hosted inside mono-capped prismatic nickel cages - with varying degrees of distortion.

In the following sections the different nickel-phosphorus sub-structures will be classified accordingly to their coordination number.

### **♦ *Ten-membered nickel cages - $\text{Ni}_{10}(\mu_{10}\text{-P})$***

Whenever the phosphorus atoms displayed a coordination number equal to ten, the surrounding cages always presented the same arrangement. In these cases the nickel environments were prismatic, and the prisms had one squared base and one mono-capped pentagonal base.

This coordination appeared in three of the characterised molecular structures - those of  $[\text{Ni}_{11}\text{P}(\text{CO})_{18}]^{3-}$ ,  $[\text{Ni}_{23-x}\text{P}_2(\text{CO})_{30-x}]^{4-}$ , and the related  $[\text{Ni}_{23-x}\text{P}_2(\text{CO})_{30-x}]^{6-}$ . In each of these clusters it was possible to individuate one phosphorus atom within such nickel environment (Figure 7.1). It is worth to mention that, in the first case, the whole metallic skeleton of the cluster was mainly formed by the phosphorus-hosting cage itself, and just a single nickel atom was not coordinated to the heteroatom.

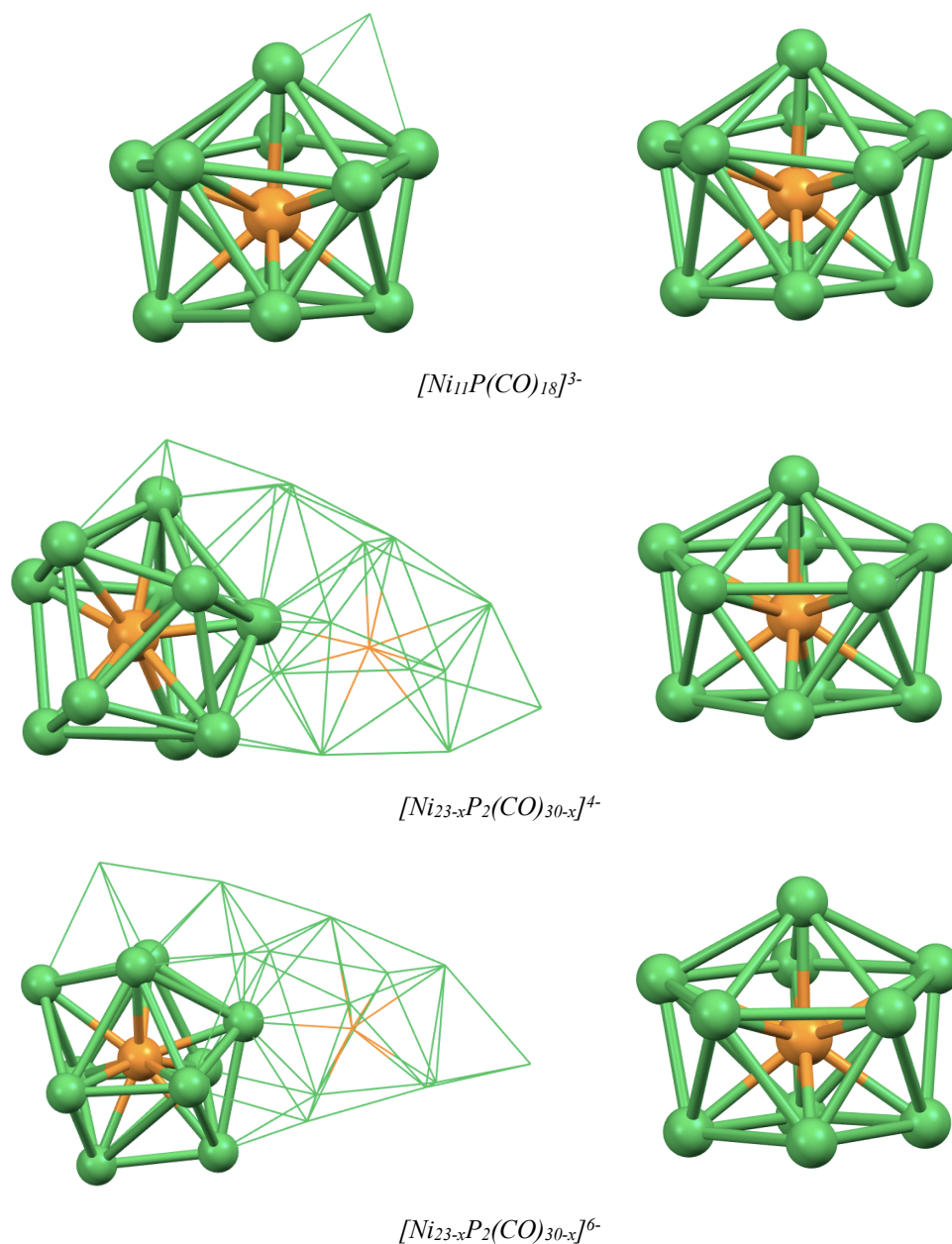


Figure 7.1 -  $Ni_{10}(\mu_{10-P})$  moieties and metallic skeletons of the clusters containing them. On the left the position of the moieties has been highlighted, on the right the structures of the moieties have been enlarged. Nickel atoms are represented in green, phosphorus atoms in orange.

\*\*\*

The values of the nickel-phosphorus bond lengths within these structure were coherent with the reference value. Interestingly, the data were narrowly dispersed and no single nickel-phosphorus bond was elongated over the previously defined threshold (Table 7.2).

<i>cluster containing the Ni<sub>10</sub>(μ<sub>10</sub>-P) fragment</i>	<i>nickel-phosphorus bond lengths (Å)</i>		
	<i>average value</i>	<i>minimum value</i>	<i>maximum value</i>
<i>all clusters</i>	2.36 ± 0.05	2.19	2.50
<i>[Ni<sub>11</sub>P(CO)<sub>18</sub>]<sup>3-</sup></i>	2.35 ± 0.03	2.31	2.44
<i>[Ni<sub>23-x</sub>P<sub>2</sub>(CO)<sub>30-x</sub>]<sup>4-</sup></i>	2.36 ± 0.06	2.19	2.47
<i>[Ni<sub>23-x</sub>P<sub>2</sub>(CO)<sub>30-x</sub>]<sup>6-</sup></i>	2.35 ± 0.07	2.20	2.50

Table 7.2 - Set of values referred to the nickel-phosphorus bonds within the Ni<sub>10</sub>(μ<sub>10</sub>-P) moieties.

A first analysis on these data implied that this type of coordination could fairly stabilise the interstitial heteroatom, despite it not being the most recurrent one.

Furthermore, the behaviours of the tetra-anionic and of the hexa-anionic form of the same cluster - [Ni<sub>23-x</sub>P<sub>2</sub>(CO)<sub>30-x</sub>]<sup>4-</sup> and [Ni<sub>23-x</sub>P<sub>2</sub>(CO)<sub>30-x</sub>]<sup>6-</sup> - were compared. In fact, it could have been possible for the more reduced cluster - *i.e.* the cluster that was bearing a more negative charge - to display shorter bond lengths. In fact, it is known that a higher electronic density strengthens the metallic bonds, and thus shortens the metallic bond lengths. However, in this case it was not possible to notice this behaviour, probably due to the nuclearity of the cluster that delocalised the anionic charge.

\*\*\*

For the analysis of the nickel-nickel bond lengths it had been useful to separate the bonds into distinct categories. The average intra-base, inter-base, and capping bond lengths were individually evaluated, in accord to the other structural analyses available for nickel-pnictogen species in the literature.

The data were in accord with those of the nickel-phosphorus bonds (Table 7.3). Except for the average inter-base bond lengths, the values of the bond distances were quite narrowly dispersed. It worth to mention that [Ni<sub>23-x</sub>P<sub>2</sub>(CO)<sub>30-x</sub>]<sup>4-</sup> and [Ni<sub>23-x</sub>P<sub>2</sub>(CO)<sub>30-x</sub>]<sup>6-</sup> displayed similar average values for all the types of bonds. On the contrary, in [Ni<sub>11</sub>P(CO)<sub>18</sub>]<sup>3-</sup> the inter-base interactions were considerably longer than those of the other two clusters.

Still, all the average nickel-nickel bond lengths were within the expected range

of values. This indicated that the prismatic coordination characteristic of the  $\text{Ni}_{10}(\mu_{10}\text{-P})$  moieties could properly stabilise the phosphorus atom without compromising the effectiveness of the nickel-nickel interactions.

Moreover, just few bonds were elongated, and most were in the inter-base region - as also reflected by the broadly dispersed data. This was probably due to the arrangement of the bases of the prisms. In each pentagonal base there was one nickel-nickel interaction that was remarkably longer than the others, which on the contrary were rather similar to each other.

Finally, it would have been more appropriate to describe the squared bases as tetragonal or rectangular bases, as the bond lengths were not uniform. Both these aspects induced a mild distortion towards the bases, which was in turn reflected on the irregular and sometimes-elongated inter-base interactions.

<i>cluster containing the <math>\text{Ni}_{10}(\mu_{10}\text{-P})</math> fragment</i>	<i>nickel-nickel bond lengths (<math>\text{\AA}</math>)</i>		
	<i>average value</i>	<i>minimum value</i>	<i>maximum value</i>
<i>all clusters</i>	$2.62 \pm 0.12$	2.38	3.14
$[\text{Ni}_{11}\text{P}(\text{CO})_{18}]^{3-}$	$2.64 \pm 0.16$	2.38	3.14
$[\text{Ni}_{23-x}\text{P}_2(\text{CO})_{30-x}]^{4-}$	$2.60 \pm 0.09$	2.43	2.76
$[\text{Ni}_{23-x}\text{P}_2(\text{CO})_{30-x}]^{6-}$	$2.62 \pm 0.11$	2.41	2.85

	<i>average nickel-nickel bond lengths (<math>\text{\AA}</math>)</i>		
	<i>intra-base</i>	<i>inter-base</i>	<i>capping</i>
<i>all clusters</i>	$2.63 \pm 0.07$	$2.59 \pm 0.19$	$2.65 \pm 0.07$
$[\text{Ni}_{11}\text{P}(\text{CO})_{18}]^{3-}$	$2.60 \pm 0.07$	$2.7 \pm 0.3$	$2.68 \pm 0.11$
$[\text{Ni}_{23-x}\text{P}_2(\text{CO})_{30-x}]^{4-}$	$2.65 \pm 0.09$	$2.56 \pm 0.15$	$2.65 \pm 0.04$
$[\text{Ni}_{23-x}\text{P}_2(\text{CO})_{30-x}]^{6-}$	$2.65 \pm 0.06$	$2.53 \pm 0.11$	$2.62 \pm 0.04$

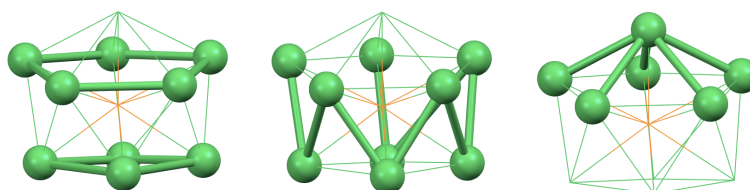


Table 7.3 - Set of values referred to the nickel-nickel bonds within the  $\text{Ni}_{10}(\mu_{10}\text{-P})$  moieties. As example, the fragment within  $[\text{Ni}_{23-x}\text{P}_2(\text{CO})_{30-x}]^{4-}$  has been reported.

To conclude, the shape of these prisms was peculiar, mostly because one base was larger than the other, as well as capped. It was possible to hypothesise that the presence of the capped five-membered ring had been required in order to maximise the nickel-heteroatom interactions and to stabilise the phosphorus-hosting moieties. Still, it was evident that the reduced dimensions of the nickel atoms had an impact that could not be completely overcome. Further considerations will ensue after the description of the other types of nickel-phosphorus interactions.

♦ ***Nine-membered nickel cages - Ni<sub>9</sub>(μ<sub>9</sub>-P)***

The previously described Ni<sub>10</sub>(μ<sub>10</sub>-P) fragments were closely related to the Ni<sub>9</sub>(μ<sub>9</sub>-P) ones. While the former prisms had one squared base and one capped pentagonal base, the latter anti-prisms had two squared bases - one of which was capped. Fundamentally, the capped bases within the cages of Ni<sub>9</sub>(μ<sub>9</sub>-P) were smaller than those of Ni<sub>10</sub>(μ<sub>10</sub>-P) and formed by four atoms instead of five.

This category comprehends the majority of the nickel-phosphorus moieties. In fact, the heteroatoms had a coordination number equal to nine in all but four of the twenty-two different phosphorus-hosting cavities.

For comprehension purposes, this large group of alike structures had been further divided into two sub-categories. One included less distorted, closed anti-prismatic cages. The other group included open cages, whose main structure was nonetheless coherent to that of a mono-capped squared anti-prism.

♦ ***Closed nine-membered nickel cages***

This sub-group is the most numerous one. Of the eighteen Ni<sub>9</sub>(μ<sub>9</sub>-P) phosphorus-hosting cavities, ten belonged to this category. Such shaped moieties had been individuated within [Ni<sub>14</sub>P<sub>2</sub>(CO)<sub>22</sub>]<sup>2-</sup>, [Ni<sub>29</sub>P<sub>5</sub>(PO)(CO)<sub>36</sub>]<sup>4-</sup>, and [HNi<sub>31</sub>P<sub>4</sub>(CO)<sub>39</sub>]<sup>5-</sup> (Figure 7.2).

As aforementioned, the first cluster was symmetrical, and formed by the merg-



ing of two of these moieties. In the second cluster there was no symmetry, so each of its five  $\text{Ni}_9(\mu_9\text{-P})$  fragments was independent. Concerning the last cluster, it had been structurally characterised in three different occasions and in each molecular structure at least one closed  $\text{Ni}_9(\mu_9\text{-P})$  sub-unit was present.

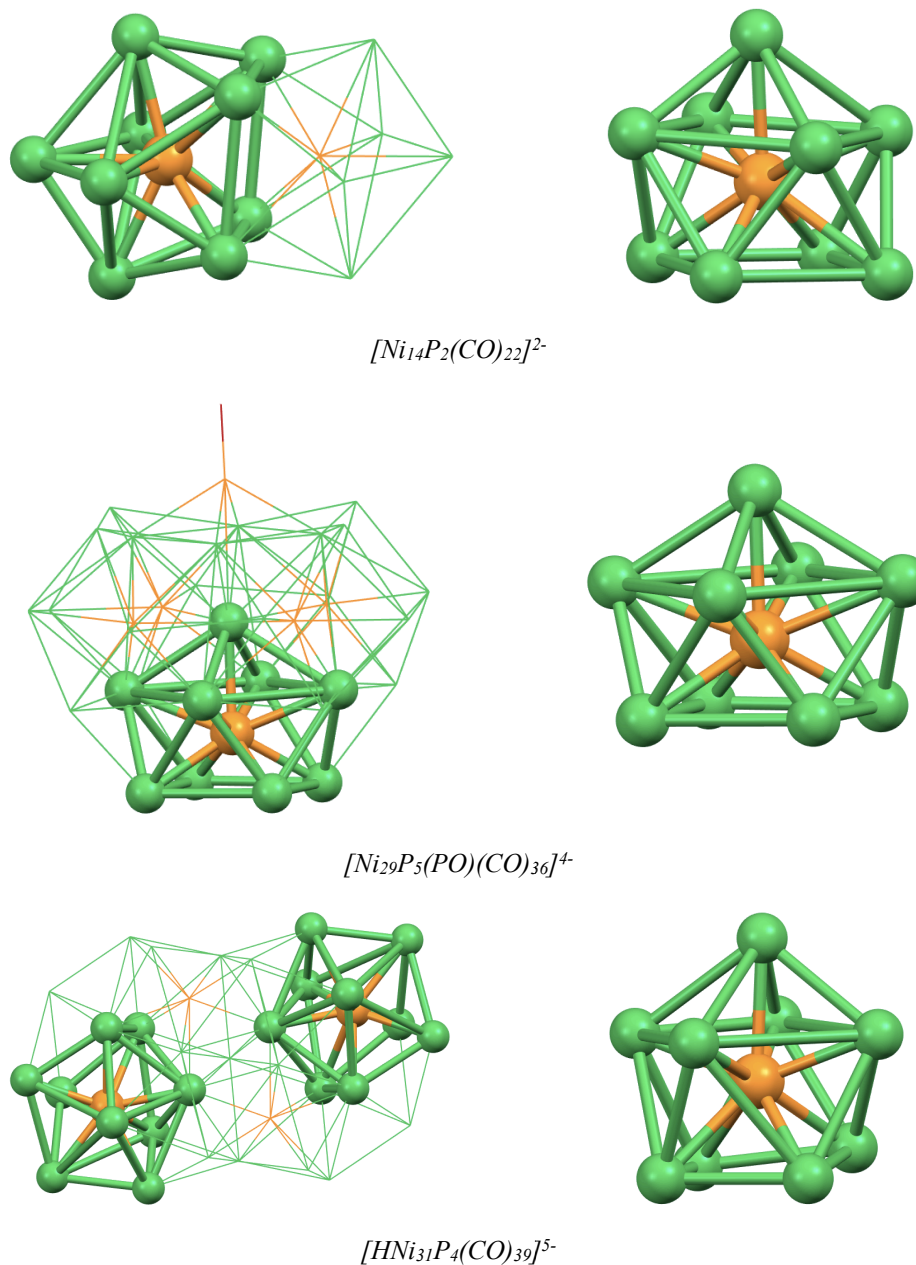


Figure 7.2 - Closed  $\text{Ni}_9(\mu_9\text{-P})$  moieties and metallic skeletons of the clusters containing them. On the left the position of the moieties has been highlighted, on the right the structures of the moieties have been enlarged. Nickel atoms are represented in green, phosphorus atoms in orange. For clarity purposes, just one example have been represented for each cluster.

The average nickel-phosphorus bond lengths were within the defined range (Table 7.4). Still, in a minority of these closed  $Ni_9(\mu_9-P)$  structure it was possible to individuate a longer nickel-phosphorus bond. The elongation extents were minimal, and did not affect the overall average values.

<i>cluster containing the closed <math>Ni_9(\mu_9-P)</math> fragment</i>	<i>nickel-phosphorus bond lengths (<math>\text{\AA}</math>)</i>		
	<i>average value</i>	<i>minimum value</i>	<i>maximum value</i>
<i>all clusters</i>	$2.31 \pm 0.08$	2.15	2.53
<i><math>[Ni_{14}P_2(CO)_{22}]^{2-}</math></i>	$2.30 \pm 0.08$	2.20	2.53
<i><math>[Ni_{29}P_5(PO)(CO)_{36}]^{4-}</math></i>	$2.32 \pm 0.07$	2.20	2.47
	$2.32 \pm 0.09$	2.20	2.52
	$2.32 \pm 0.07$	2.22	2.51
	$2.32 \pm 0.08$	2.21	2.49
	$2.32 \pm 0.07$	2.19	2.41
<i><math>[HNi_{31}P_4(CO)_{39}]^{5-}</math></i>	$2.30 \pm 0.09$	2.15	2.49
	$2.29 \pm 0.07$	2.15	2.44
	$2.30 \pm 0.08$	2.15	2.47
	$2.30 \pm 0.08$	2.16	2.52

Table 7.4 - Set of values referred to the heteroatomical bonds in the closed  $Ni_9(\mu_9-P)$  moieties.

The average nickel-phosphorus bond lengths were shorter than those of the previous case - by nearly the 2%. This phenomenon was clearly due to the lower number of nickel atoms that were surrounding the phosphorus atom. A lower coordination number resulted in a smaller nickel cage, thus shortened the metal-heteroatom interactions. However, the collected values were narrowly dispersed, therefore suggesting that this type of coordination was well-fitting for the phosphorus atoms.

\*\*\*

Regarding the nickel-nickel interactions, the geometry of these cages was homogeneous. In all cases the nine nickel atoms that were surrounding the phosphorus atom were arranged to form a mono-capped squared anti-prism. These structures seemed to be quite regular as well, but a more attentive analysis revealed that the reduced coordination number induced a remarkable elongation on these

cages. This could be deduced by observing the mean values of the nickel-nickel interactions, which appeared to be longer than the overall average values. The intra-base, inter-base, and capping bond distances have been reported (Table 7.5).

<i>cluster containing the closed Ni<sub>9</sub>(μ<sub>9</sub>-P) fragment</i>	<i>nickel-nickel bond lengths (Å)</i>		
	<i>average value</i>	<i>minimum value</i>	<i>maximum value</i>
<i>all clusters</i>	2.72 ± 0.14	2.40	3.21
<i>[Ni<sub>14</sub>P<sub>2</sub>(CO)<sub>22</sub>]<sup>2-</sup></i>	2.71 ± 0.15	2.42	3.05
<i>[Ni<sub>29</sub>P<sub>5</sub>(PO)(CO)<sub>36</sub>]<sup>4-</sup></i>	2.75 ± 0.18	2.40	3.20
	2.75 ± 0.17	2.46	3.20
	2.76 ± 0.18	2.44	3.21
	2.75 ± 0.17	2.44	3.21
	2.73 ± 0.18	2.41	3.16
<i>[HNi<sub>31</sub>P<sub>4</sub>(CO)<sub>39</sub>]<sup>5-</sup></i>	2.69 ± 0.11	2.42	3.10
	2.68 ± 0.09	2.45	3.04
	2.69 ± 0.10	2.42	3.12
	2.67 ± 0.09	2.43	2.94

	<i>average nickel-nickel bond lengths (Å)</i>		
	<i>intra-base</i>	<i>inter-base</i>	<i>capping</i>
<i>all clusters</i>	2.8 ± 0.2	2.68 ± 0.09	2.63 ± 0.05
<i>[Ni<sub>14</sub>P<sub>2</sub>(CO)<sub>22</sub>]<sup>2-</sup></i>	2.88 ± 0.10	2.59 ± 0.10	2.61 ± 0.13
<i>[Ni<sub>29</sub>P<sub>5</sub>(PO)(CO)<sub>36</sub>]<sup>4-</sup></i>	2.8 ± 0.3	2.73 ± 0.11	2.629 ± 0.011
	2.8 ± 0.2	2.72 ± 0.11	2.616 ± 0.005
	2.8 ± 0.3	2.74 ± 0.12	2.622 ± 0.010
	2.8 ± 0.3	2.72 ± 0.11	2.635 ± 0.010
	3.0 ± 0.2	2.56 ± 0.13	2.626 ± 0.012
<i>[HNi<sub>31</sub>P<sub>4</sub>(CO)<sub>39</sub>]<sup>5-</sup></i>	2.72 ± 0.16	2.70 ± 0.06	2.63 ± 0.09
	2.73 ± 0.17	2.67 ± 0.03	2.63 ± 0.09
	2.73 ± 0.17	2.69 ± 0.03	2.63 ± 0.09
	2.66 ± 0.12	2.69 ± 0.08	2.64 ± 0.09

Table 7.5 - Set of values referred to the nickel-nickel bonds within the closed Ni<sub>9</sub>(μ<sub>9</sub>-P) moieties.

The data highlighted that these closed Ni<sub>9</sub>(μ<sub>9</sub>-P) fragments were substantially different from the Ni<sub>10</sub>(μ<sub>10</sub>-P) fragments, despite having a similar structural ar-

rangement. In the previous case just few bonds in the inter-base zone were elongated, to a moderate extent too. Considering the closed  $\text{Ni}_9(\mu_9\text{-P})$  moieties instead, in most cases the average inter-base bond distances were longer than the average nickel-nickel interaction.

Moreover, in these fragments the intra-base interactions were sensibly elongated compared to the average nickel-nickel interaction - by more than 7%. Besides, the elongation appeared even more significant by considering only the bonds within the mono-capped squared bases. In that category, three out of four bonds were significantly elongated. On the contrary, in the non-capped bases the nickel-nickel bond distances were within the normal range.

Concerning the capping bond lengths, the mean values were surprisingly close to the overall average value, as well as narrowly dispersed. The remarkable elongation observed for the bonds within the capped bases could have suggested a scarce interaction with the above nickel atoms, yet the capping bond lengths indicated the opposite.

\*\*\*

To conclude, the  $\text{Ni}_9(\mu_9\text{-P})$  mono-capped squared anti-prisms were actually affected by elongation effects, presumably because of the reduced coordination number of the heteroatom.

On one hand the mean values of the nickel-phosphorus bond lengths were close to the overall average value, thus indicating a good interaction with the heteroatom. On the other hand, a large number of nickel-nickel bonds was elongated.

This phenomenon was not unexpected due to the lower coordination number, and it would have been otherwise atypical. A commentary on this behaviour and further considerations will follow in the dedicated section.

#### ✦ *Open nine-membered nickel cages*

In this group of open  $\text{Ni}_9(\mu_9\text{-P})$  fragments the general shape was still that of a

mono-capped squared anti-prism. However, one nickel-nickel bond was missing from the capped bases, and therefore the capped four-membered rings were open. Due to this, on the sides of these prisms there were larger squared or pentagonal faces along with the triangular ones. Eight examples were individuated, in the molecular structures of  $[\text{Ni}_{23-x}\text{P}_2(\text{CO})_{30-x}]^{4-}$ ,  $[\text{Ni}_{23-x}\text{P}_2(\text{CO})_{30-x}]^{6-}$ ,  $[\text{HNi}_{31}\text{P}_4(\text{CO})_{39}]^{5-}$ , and  $[\text{H}_2\text{Ni}_{31}\text{P}_4(\text{CO})_{39}]^{4-}$  (Figure 7.3).

\*\*\*

The heteroatoms could be considered as interstitial as they were not exposed, despite the lateral apertures. The average nickel-phosphorus bond lengths were close to the expected values, and only in some of the open  $\text{Ni}_9(\mu_9\text{-P})$  sub-units there was a single elongated nickel-phosphorus bond. However, these interactions did not affect the overall average values (Table 7.6).

<i>cluster containing the open <math>\text{Ni}_9(\mu_9\text{-P})</math> fragment</i>	<i>nickel-phosphorus bond lengths (<math>\text{\AA}</math>)</i>		
	<i>average value</i>	<i>minimum value</i>	<i>maximum value</i>
<i>all clusters</i>	$2.32 \pm 0.08$	2.15	2.68
<i><math>[\text{Ni}_{23-x}\text{P}_2(\text{CO})_{30-x}]^{4-}</math></i>	$2.31 \pm 0.08$	2.16	2.45
<i><math>[\text{Ni}_{23-x}\text{P}_2(\text{CO})_{30-x}]^{6-}</math></i>	$2.31 \pm 0.08$	2.17	2.51
<i><math>[\text{HNi}_{31}\text{P}_4(\text{CO})_{39}]^{5-}</math></i>	$2.32 \pm 0.08$	2.17	2.57
	$2.33 \pm 0.09$	2.18	2.64
	$2.33 \pm 0.09$	2.18	2.63
	$2.33 \pm 0.10$	2.17	2.68
<i><math>[\text{H}_2\text{Ni}_{31}\text{P}_4(\text{CO})_{39}]^{4-}</math></i>	$2.32 \pm 0.08$	2.17	2.55
	$2.29 \pm 0.08$	2.15	2.44

Table 7.6 - Set of values referred to the nickel-phosphorus bonds in the open  $\text{Ni}_9(\mu_9\text{-P})$  moieties.

The average nickel-phosphorus bond lengths of the open  $\text{Ni}_9(\mu_9\text{-P})$  moieties were similar to those of the closed  $\text{Ni}_9(\mu_9\text{-P})$  fragments, and accordingly they were shorter than those of  $\text{Ni}_{10}(\mu_{10}\text{-P})$  moieties. This indicated that, despite the openness and the higher distortion of these structures, the phosphorus atoms retained a good interaction with the surrounding metallic atoms.

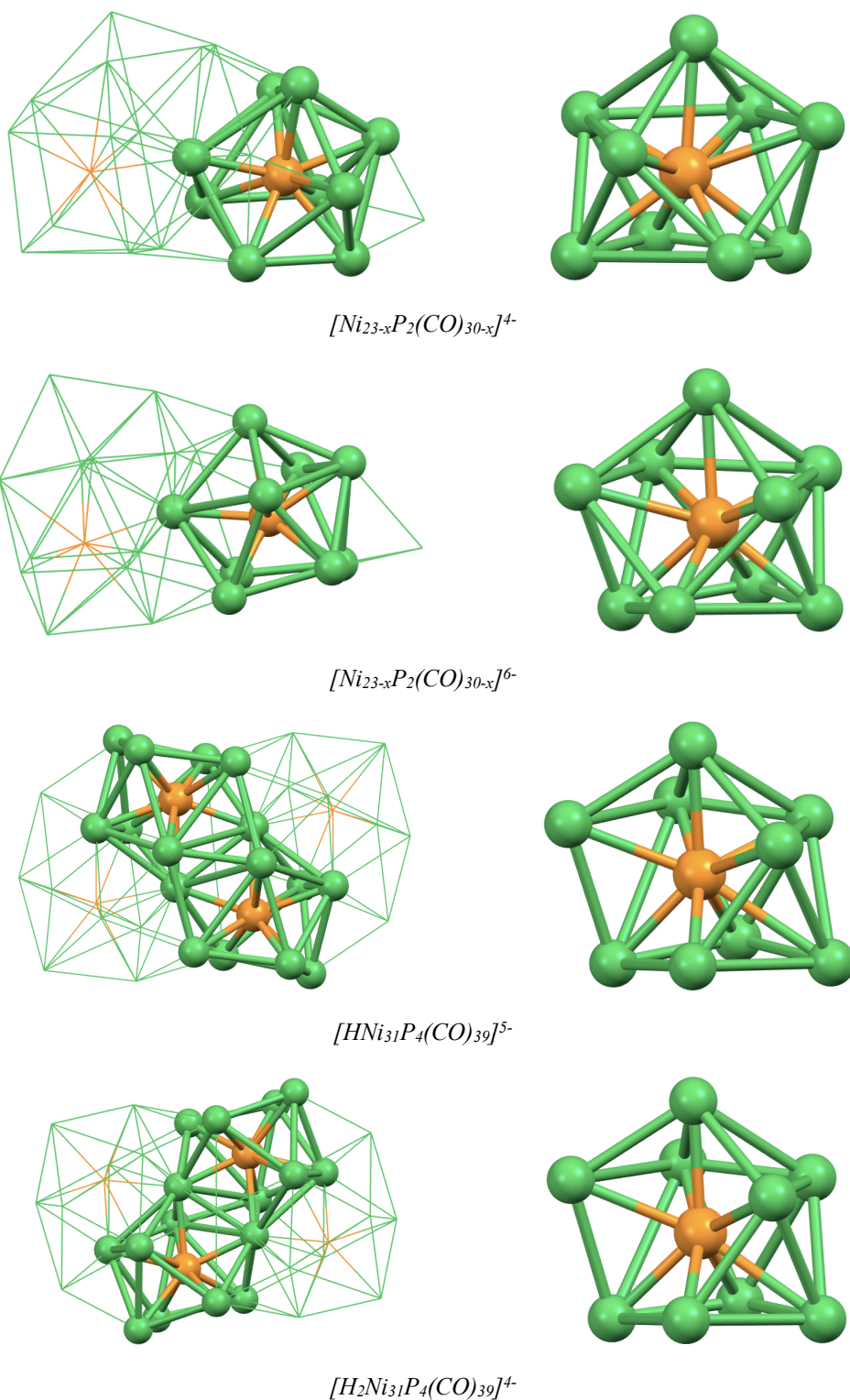


Figure 7.3 - Open  $Ni_9(\mu_9-P)$  moieties and metallic skeletons of the clusters containing them. On the left the position of the moieties has been highlighted, on the right the structures of the moieties have been enlarged. Nickel atoms are represented in green, phosphorus atoms in orange. For clarity purposes, just one example have been represented for each cluster.

\*\*\*

For what concerns the nickel-nickel interactions and the resulting cages, the data were less uniform. It was still possible to consider the nickel cavities as mono-capped anti-prisms, yet with a certain degree of distortion due to the opening of the capped squared bases.

Surprisingly, the misshaping had a beneficial effect on the overall structures. It had been previously shown that in the closed  $\text{Ni}_9(\mu_9\text{-P})$  moieties a remarkable traction induced a severe elongation onto the nickel-nickel bonds, particularly in the inter-base region. On the contrary, in these open cages fewer bond distances were affected, although it was still possible to individuate some elongations - mainly in the intra-base and inter-base zone. Nonetheless, the average values were closer to the expected values (Table 7.7).

Interestingly, the mean values of the capping bond lengths suggested that the capped bases were well-coordinated to the atom above, despite the openness of the bases themselves.

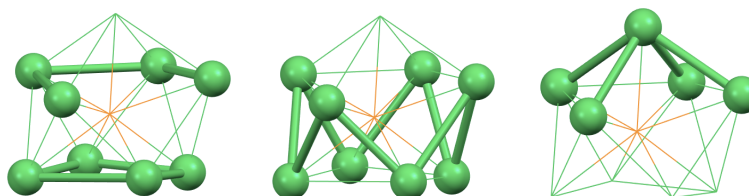
Moreover, the number of elongated bonds as well as the intensity of the elongation itself were limited, and thus had a lesser effect on the average values of the nickel-nickel bond distances.

\*\*\*

To conclude, it was clear that the higher distortion that occurred in the open  $\text{Ni}_9(\mu_9\text{-P})$  fragments actually enhanced the nickel-phosphorus and the nickel-nickel interactions. Despite the irregular structures of the nickel cages, the values of all the average bond distances were within the expected range of values. Whereas the same number of nickel atoms was arranged in a more regular, closed shape - as in the closed  $\text{Ni}_9(\mu_9\text{-P})$  moieties - the elongations were more consistent, and affected a greater number of bonds. On the contrary, in these open structures there were generally better interactions, which were granted by a loss in terms of uniformity.

cluster containing the open Ni <sub>9</sub> (μ <sub>9</sub> -P) fragment	nickel-nickel bond lengths (Å)		
	average value	minimum value	maximum value
<i>all clusters</i>	2.64 ± 0.09	2.39	3.04
[Ni <sub>23-x</sub> P <sub>2</sub> (CO) <sub>30-x</sub> ] <sup>4-</sup>	2.66 ± 0.12	2.39	2.90
[Ni <sub>23-x</sub> P <sub>2</sub> (CO) <sub>30-x</sub> ] <sup>6-</sup>	2.65 ± 0.12	2.43	3.03
[HNi <sub>31</sub> P <sub>4</sub> (CO) <sub>39</sub> ] <sup>5-</sup>	2.64 ± 0.08	2.50	2.99
	2.64 ± 0.08	2.50	2.93
	2.63 ± 0.07	2.51	2.81
	2.63 ± 0.07	2.51	2.75
[H <sub>2</sub> Ni <sub>31</sub> P <sub>4</sub> (CO) <sub>39</sub> ] <sup>4-</sup>	2.62 ± 0.07	2.47	2.87
	2.68 ± 0.09	2.43	3.04

	average nickel-nickel bond lengths (Å)		
	<i>intra-base</i>	<i>inter-base</i>	<i>capping</i>
<i>all clusters</i>	2.67 ± 0.06	2.63 ± 0.07	2.63 ± 0.10
[Ni <sub>23-x</sub> P <sub>2</sub> (CO) <sub>30-x</sub> ] <sup>4-</sup>	2.67 ± 0.14	2.65 ± 0.10	2.67 ± 0.11
[Ni <sub>23-x</sub> P <sub>2</sub> (CO) <sub>30-x</sub> ] <sup>6-</sup>	2.68 ± 0.15	2.64 ± 0.09	2.65 ± 0.11
[HNi <sub>31</sub> P <sub>4</sub> (CO) <sub>39</sub> ] <sup>5-</sup>	2.68 ± 0.10	2.61 ± 0.06	2.62 ± 0.10
	2.68 ± 0.10	2.61 ± 0.05	2.61 ± 0.09
	2.65 ± 0.06	2.62 ± 0.06	2.62 ± 0.10
	2.65 ± 0.07	2.62 ± 0.05	2.62 ± 0.09
[H <sub>2</sub> Ni <sub>31</sub> P <sub>4</sub> (CO) <sub>39</sub> ] <sup>4-</sup>	2.66 ± 0.07	2.60 ± 0.06	2.59 ± 0.09
	2.71 ± 0.17	2.67 ± 0.02	2.62 ± 0.08

Table 7.7 - Set of values referred to the nickel-nickel bonds within the open Ni<sub>9</sub>(μ<sub>9</sub>-P) moieties.

\*\*\*

Before analysing the last typology of nickel-phosphorus moieties, it would be useful to compare the two categories of Ni<sub>9</sub>(μ<sub>9</sub>-P) sub-structures - open and closed (Table 7.8). For what concerns the similarities, both types shared the same formula and roughly the same arrangement. The nickel-phosphorus interactions were alike, and their average values were as well similar.



Nonetheless there were significant differences, especially regarding the nickel-nickel bonds that formed the metallic cages. By comparing the nickel-nickel bond lengths it was evident that the closed cages were subjected to higher elongations.

On average, interactions within the closed nickel anti-prisms were longer by about the 3% than those within open structures. Moreover, the relative difference rose up to about the 5% by comparing only the intra-base interactions. This further indicated that the distortion was localised in the intra-base region of the moiety. This could also explain the fact that all the open  $\text{Ni}_9(\mu_9\text{-P})$  moieties had a missing nickel-nickel interaction in that region.

$\text{Ni}_9(\mu_9\text{-P})$	average nickel-phosphorus bond length ( $\text{\AA}$ )	average nickel-nickel bond lengths ( $\text{\AA}$ )		
		<i>intra-base</i>	<i>inter-base</i>	<i>capping</i>
<i>closed</i>	$2.31 \pm 0.08$	$2.8 \pm 0.2$	$2.68 \pm 0.09$	$2.63 \pm 0.05$
<i>open</i>	$2.32 \pm 0.08$	$2.67 \pm 0.11$	$2.63 \pm 0.07$	$2.63 \pm 0.10$

Table 7.8 - Set of values referred to the interactions in the different  $\text{Ni}_9(\mu_9\text{-P})$  moieties.

♦ **Twelve-membered nickel cages -  $\text{Ni}_{12}(\mu_{12}\text{-P})$**

Three symmetrical and interconnected  $\text{Ni}_{12}(\mu_{12}\text{-P})$  icosahedral moieties had been individuated within the molecular structure of  $[\text{Ni}_{39}\text{P}_3(\text{CO})_{44}]^{6-}$ . (Figure 7.4).

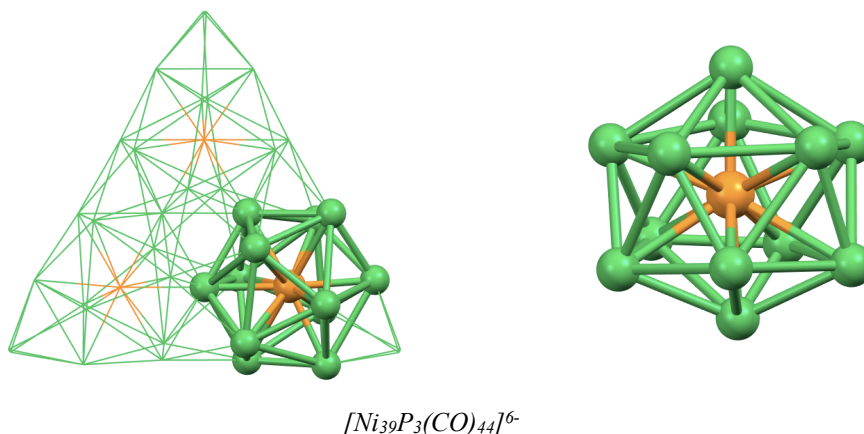


Figure 7.4 - Icosahedral  $\text{Ni}_{12}(\mu_{12}\text{-P})$  moiety and metallic skeleton of the cluster containing it. Nickel atoms are represented in green, phosphorus atoms in orange.

\*\*\*

Although the least common, this type of coordination was the most interesting amongst those displayed by nickel and phosphorus in homoleptic carbonyl clusters. In this unique fragment the coordination number of the phosphorus was higher, and equal to twelve. The nickel-phosphorus bond lengths were severely affected by the increased amount of metallic atoms that were coordinated to the heteroatom (Table 7.9).

<i>cluster containing the Ni<sub>12</sub>(μ<sub>12</sub>-P) fragment</i>	<i>nickel-phosphorus bond lengths (Å)</i>		
	<i>average value</i>	<i>minimum value</i>	<i>maximum value</i>
<i>[Ni<sub>39</sub>P<sub>3</sub>(CO)<sub>44</sub>]<sup>6-</sup></i>	2.46 ± 0.10	2.29	2.68

Table 7.9 - Set of values referred to the nickel-phosphorus bonds in the Ni<sub>12</sub>(μ<sub>12</sub>-P) moiety.

In this fragment the average nickel-phosphorus bond length was significantly longer than the reference average bond length - 2.33 Å. Moreover, one third of the interactions was sensibly elongated, and their length exceeded the given threshold - 2.51 Å.

All these phenomena were a clear indication of a poor nickel-phosphorus interaction, clearly due to the higher coordination number. The increased number of surrounding atoms enlarged the nickel cage, thus loosening the bonds with the interstitial heteroatom. Considering these data, it appeared clear that for the phosphorus atom it was difficult to be fitting inside a icosahedral nickel environment.

\*\*\*

Compared to the nickel-phosphorus interactions, the nickel-nickel interactions were oppositely affected by the higher coordination number.

Consistently with the previously reported analyses, the bonds have been classified as inter-pentagonal, intra-pentagonal, and capping. Interestingly, the average values for each type of bond were within the expected range of values (Table

7.10). Therefore, the icosahedral cage was remarkably stabilised and the metal-metal interactions were neither elongated nor strained.

By comparing these values to those of the smaller cages, it was evident that the presence of a greater number of nickel atoms allowed to completely eliminate any structural distress from the metallic cage. This phenomenon was consistent with the typical behaviour displayed by other heteroatomical nickel clusters, in which the metallic atoms often form icosahedral geometries.

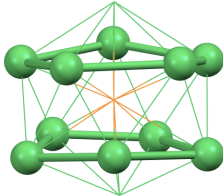
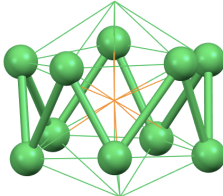
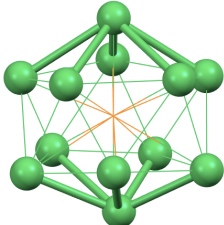
<i>cluster containing the Ni<sub>12</sub>(μ<sub>12</sub>-P) fragment</i>	<i>nickel-nickel bond lengths (Å)</i>		
	<i>average value</i>	<i>minimum value</i>	<i>maximum value</i>
<i>[Ni<sub>39</sub>P<sub>3</sub>(CO)<sub>44</sub>]<sup>6-</sup></i>	2.59 ± 0.12	2.31	2.89
	<i>average nickel-nickel bond lengths (Å)</i>		
			
	<i>intra-pentagonal</i>	<i>inter-pentagonal</i>	<i>capping</i>
<i>[Ni<sub>39</sub>P<sub>3</sub>(CO)<sub>44</sub>]<sup>6-</sup></i>	2.57 ± 0.15	2.61 ± 0.11	2.61 ± 0.09

Table 7.10 - Set of values referred to the nickel-nickel bonds within the Ni<sub>12</sub>(μ<sub>12</sub>-P) moiety.

\*\*\*

To conclude, by surveying this unique Ni<sub>12</sub>(μ<sub>12</sub>-P) sub-unit it was possible to identify two divergent main features.

On one hand, the analysis of the nickel-nickel bond lengths confirmed that this metal is extremely prone to form icosahedral cages in heteroatomical clusters. No metal-metal interaction was elongated, thus suggesting the own intrinsic strength and stability of this type of nickel framework.

On the other hand, the nickel-phosphorus interactions had been severely affected by the higher coordination number. Whenever the heteroatom was hosted inside smaller cages its interactions were within the expected range of values. On

the contrary, in this case the nickel-phosphorus bonds were sensibly longer. This indicated that the phosphorus atoms were not prone to being hosted inside that type of environment since they could not be properly stabilised.

This phenomenon was peculiar yet not completely unexpected - it was assessed that the respective covalent radii of the nickel and the phosphorus atoms were not suitable for the stabilisation of a phosphorus-centred icosahedral environment.

### ***Nickel-hosting cavities***

In the formerly introduced nickel-phosphorus clusters the heteroatoms were always located in interstitial positions. It was clear that that could not be the case for the metallic atoms, as they primarily form the skeletons of the clusters. Nonetheless, within some medium-nuclearity and high-nuclearity cluster species it has been possible to individuate some interstitial nickel atoms as well.

Different examples have been found, in the structures of  $[\text{Ni}_{23-x}\text{P}_2(\text{CO})_{30-x}]^{4-}$ ,  $[\text{Ni}_{23-x}\text{P}_2(\text{CO})_{30-x}]^{6-}$ ,  $[\text{Ni}_{29}\text{P}_5(\text{PO})(\text{CO})_{36}]^{4-}$ ,  $[\text{H}_2\text{Ni}_{131}\text{P}_4(\text{CO})_{39}]^{4-}$ ,  $[\text{HNi}_{131}\text{P}_4(\text{CO})_{39}]^{5-}$ , and  $[\text{Ni}_{39}\text{P}_3(\text{CO})_{44}]^{6-}$ . The geometries of the nickel-hosting cavities were less homogeneous than those of the phosphorus-hosting cavities, and in most cases they were distorted. Still, it has been possible to individuate some commonly shared features. First, all the interstitial nickel atoms were within heteroatomical environments. Second, in the majority of cases the cavities did not display a clear structural arrangement and due to their distortion it has been difficult to rationalise a methodology to compare their structures. It was eventually decided to separately consider the nickel-hosting cavities that displayed more regular geometries. The other sub-units were severely misshapen, yet have been tentatively compared as they shared the same coordination number and the same rough arrangement.

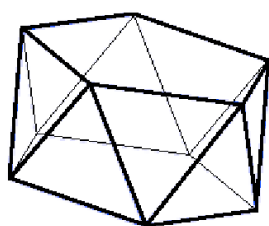
In the ensuing sections the reference set of values that had been reported in the previous chapter will be used as comparison for the evaluation of the calculated average bond lengths (Table 7.11).

The calculated average, the experimental minimum, and the calculated maximum bond lengths have been reported again for clarity purposes. These data will be referred to and used as reference values.

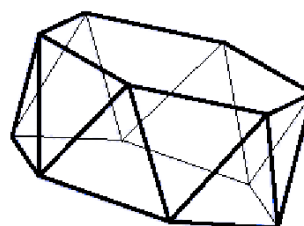
<i>bond type</i>	<i>calculated average (Å)</i>	<i>experimental minimum (Å)</i>	<i>calculated maximum (Å)</i>
<i>nickel-phosphorus</i>	2.33 ± 0.09	2.15	2.51
<i>nickel-nickel</i>	2.61 ± 0.11	2.37	2.85

Table 7.11 - Reference values for the nickel-phosphorus and the nickel-nickel bond lengths.

As previously suggested, in the following sections the different nickel-hosting sub-structures will be classified according to their structural arrangement, *e.g.* the coordination number of the interstitial atom. Apart from few examples, the nickel-hosting fragments displayed a coordination number equal to fourteen. This might have suggested the existence of icosahedron-related environments - by substitution of the pentagonal bases with hexagonal bases (Figure 7.5). However, this was only partially true. It was indeed possible to individuate two capped six-membered rings in the majority of the structures, yet most were extremely distorted and non-planar, and only in part related to bi-capped hexagonal anti-prisms.



*Pentagonal anti-prism*



*Hexagonal anti-prism*

Figure 7.5 - Comparison between anti-prisms with pentagonal or hexagonal bases. The capping atoms have not been represented for clarity purposes.

♦ **Fourteen-membered heteroatomical cages**

It has been said that interstitial nickel atoms had a coordination number equal to fourteen in the majority of cases. Eight of the nickel-centred fragments that had been individuated fit into this group, yet the corresponding polyhedra displayed different degrees of distortion and it has not been possible to determine a comprehensive structural model.

Therefore, the diverse compositions of the heteroatomical fragments have been considered as additional parameter.  $\text{Ni}_{11}\text{P}_3(\mu_{14}\text{-Ni})$  and  $\text{Ni}_{12}\text{P}_2(\mu_{14}\text{-Ni})$  structures were consequently divided into two further sub-categories.

There also were some exceptions. First, due to some structural similarities, the  $\text{Ni}_{10}\text{P}_3(\mu_{13}\text{-Ni})$  moiety has been included in the second sub-group despite the different coordination number. Second, the phosphorus-rich  $\text{Ni}_8\text{P}_6(\mu_{14}\text{-Ni})$  moiety of  $[\text{Ni}_{29}\text{P}_5(\text{PO})(\text{CO})_{36}]^{4-}$  was separately considered as it was not comparable to any other group of nickel-hosting structures.

♦ **Fourteen-membered heteroatomical cages -  $\text{Ni}_{11}\text{P}_3(\mu_{14}\text{-Ni})$**

The most numerous sub-group included the  $\text{Ni}_{11}\text{P}_3(\mu_{14}\text{-Ni})$  moieties. Four different nickel-hosting cavities belonging to this category have been individuated, within the molecular structures of the  $[\text{H}_2\text{Ni}_{13}\text{P}_4(\text{CO})_{39}]^{4-}$  and the  $[\text{HNi}_{13}\text{P}_4(\text{CO})_{39}]^{5-}$  clusters (Figure 7.6).

In the following section these fragments will be proposed as bi-capped hexagonal anti-prisms - *i.e.* icosahedra with hexagonal rather than pentagonal bases. Still, all the structures were subjected to severe distortion, especially in the central region, and in fact the hexagonal bases were neither regular nor planar. This irregularity was primarily due to the heteroatomic nature of the six-membered rings. In other heteroatomical nickel-centred structures with group-15 elements the heteroatoms generally tend to be in apical positions, yet in these cases the phosphorus atoms acted differently. The consequences will be discussed in the following paragraphs.

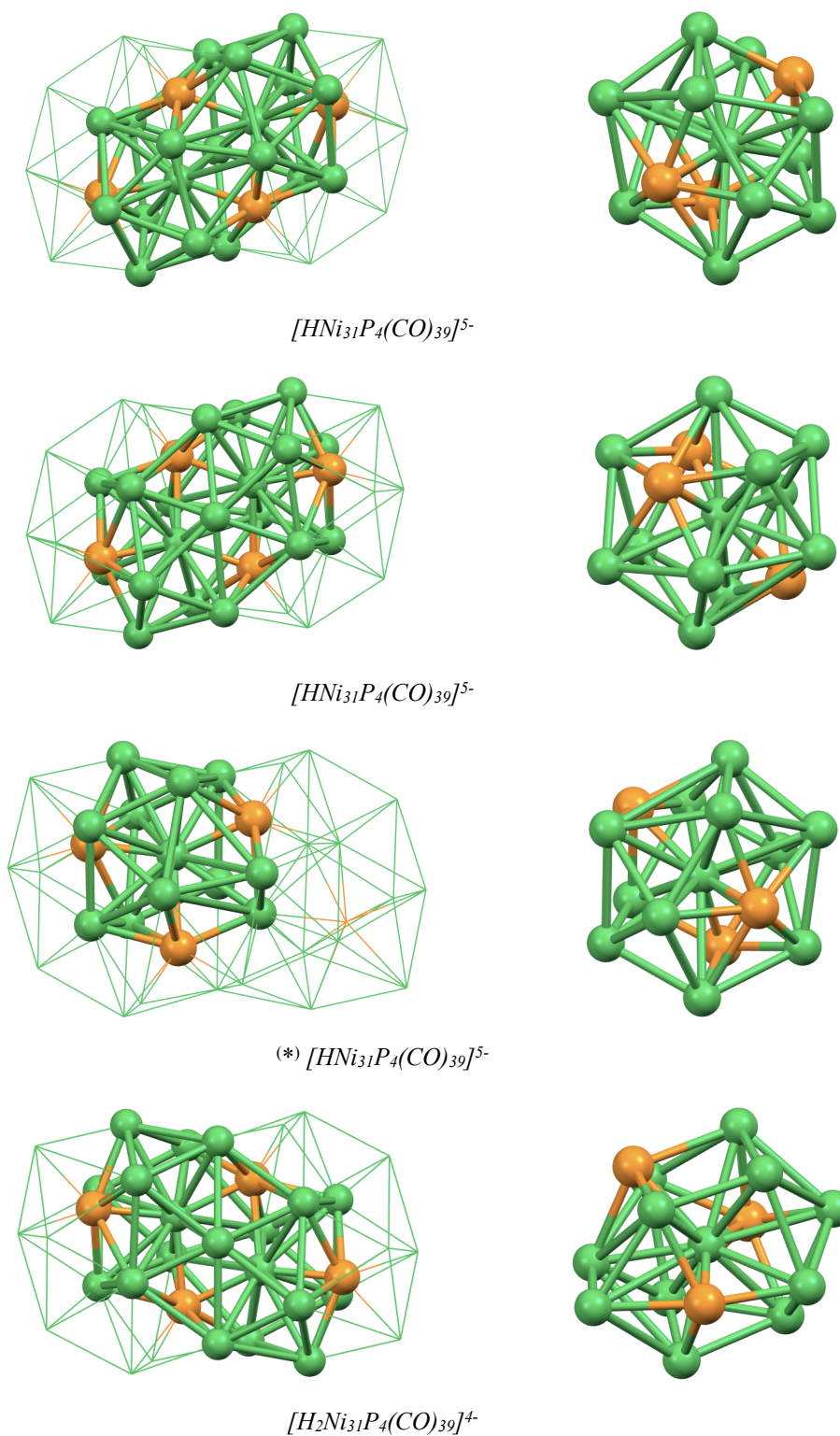


Figure 7.6 -  $Ni_{11}P_3(\mu_{14}\text{-Ni})$  moieties and metallic skeletons of the clusters containing them. On the left the position of the moieties has been highlighted. Nickel atoms are represented in green, phosphorus atoms in orange.

(\*) Non-symmetrical metallic skeleton of  $[HNi_{31}P_4(CO)_{39}]^{5-}$ , which only contained one  $Ni_{11}P_3(\mu_{14}\text{-Ni})$  moiety. The second nickel-hosting moiety had a different formula and will be later introduced.

\*\*\*

First, the interactions between the central nickel atoms and its surrounding cage have been considered. For comprehension purposes the nickel-nickel and the nickel-phosphorus interactions have been separately examined (Table 7.12).

Surprisingly, the average values of the nickel-phosphorus bond lengths were lower than the reference average values, whilst the values of the mean homometallic bond distances were close to it. Few nickel-nickel interactions were elongated, and therefore they did not affect the averages.

<i>cluster containing the Ni<sub>11</sub>P<sub>3</sub>(μ<sub>14</sub>-Ni) fragment</i>	<i>average value</i>	<i>minimum value</i>	<i>maximum value</i>
<i>interstitial nickel-phosphorus bond lengths (Å)</i>			
<i>all clusters</i>	2.21 ± 0.07	2.15	2.32
<i>[HNi<sub>31</sub>P<sub>4</sub>(CO)<sub>39</sub>]<sup>5-</sup></i>	2.21 ± 0.06	2.15	2.30
	2.21 ± 0.06	2.15	2.31
	2.21 ± 0.07	2.16	2.32
<i>[H<sub>2</sub>Ni<sub>31</sub>P<sub>4</sub>(CO)<sub>39</sub>]<sup>4-</sup></i>	2.21 ± 0.07	2.15	2.31
<i>interstitial nickel-nickel bond lengths (Å)</i>			
<i>all clusters</i>	2.65 ± 0.08	2.51	2.86
<i>[HNi<sub>31</sub>P<sub>4</sub>(CO)<sub>39</sub>]<sup>5-</sup></i>	2.65 ± 0.09	2.51	2.86
	2.65 ± 0.08	2.54	2.80
	2.65 ± 0.08	2.54	2.85
<i>[H<sub>2</sub>Ni<sub>31</sub>P<sub>4</sub>(CO)<sub>39</sub>]<sup>4-</sup></i>	2.64 ± 0.09	2.51	2.86

Table 7.12 - Set of values referred to the bonds involving the interstitial nickel atoms within the Ni<sub>11</sub>P<sub>3</sub>(μ<sub>14</sub>-Ni) moieties.

The data revealed that the interstitial nickel atoms were well fitting in this type of cage, despite the irregular structure. In fact, few bonds were elongated and the average bond distances were within the expected range of values.

Nonetheless, the shortness of the interstitial nickel-phosphorus interactions was unexpected. The contraction was probably due to the heteroatomical nature of the cage that was surrounding the interstitial metallic atom.



\*\*\*

The bonds that were constituting the heteroatomical cage have been further classified as intra-base, inter-base, and capping distances (Table 7.13). However, it is important to remember that the cages were strongly misshapen and therefore the classification of the bonds was sometimes ambiguous.

<i>cluster containing the Ni<sub>11</sub>P<sub>3</sub>(μ<sub>14</sub>-Ni) fragment</i>	<i>average value</i>	<i>minimum value</i>	<i>maximum value</i>
	<i>nickel-phosphorus bond lengths (Å)</i>		
<i>all clusters</i>	2.35 ± 0.09	2.17	2.68
<i>[HNi<sub>31</sub>P<sub>4</sub>(CO)<sub>39</sub>]<sup>5-</sup></i>	2.35 ± 0.08	2.18	2.64
	2.36 ± 0.09	2.18	2.63
	2.36 ± 0.10	2.17	2.68
<i>[H<sub>2</sub>Ni<sub>31</sub>P<sub>4</sub>(CO)<sub>39</sub>]<sup>4-</sup></i>	2.34 ± 0.08	2.17	2.55
<i>nickel-nickel bond lengths (Å)</i>			
<i>all clusters</i>	2.62 ± 0.10	2.38	2.99
<i>[HNi<sub>31</sub>P<sub>4</sub>(CO)<sub>39</sub>]<sup>5-</sup></i>	2.62 ± 0.10	2.40	2.99
	2.63 ± 0.10	2.41	2.98
	2.62 ± 0.10	2.42	2.92
<i>[H<sub>2</sub>Ni<sub>31</sub>P<sub>4</sub>(CO)<sub>39</sub>]<sup>4-</sup></i>	2.61 ± 0.10	2.38	2.90
<i>average nickel-phosphorus bond lengths (Å)</i>			
	<i>intra-base</i>	<i>inter-base</i>	<i>capping</i>
<i>all clusters</i>	2.28 ± 0.06	2.35 ± 0.06	2.49 ± 0.09
<i>[HNi<sub>31</sub>P<sub>4</sub>(CO)<sub>39</sub>]<sup>5-</sup></i>	2.28 ± 0.06	2.35 ± 0.05	2.49 ± 0.10
	2.28 ± 0.06	2.36 ± 0.05	2.50 ± 0.09
	2.27 ± 0.06	2.36 ± 0.05	2.53 ± 0.10
<i>[H<sub>2</sub>Ni<sub>31</sub>P<sub>4</sub>(CO)<sub>39</sub>]<sup>4-</sup></i>	2.31 ± 0.04	2.31 ± 0.09	2.45 ± 0.07
<i>average nickel-nickel bond lengths (Å)</i>			
<i>all clusters</i>	2.59 ± 0.10	2.59 ± 0.06	2.67 ± 0.13
<i>[HNi<sub>31</sub>P<sub>4</sub>(CO)<sub>39</sub>]<sup>5-</sup></i>	2.58 ± 0.09	2.60 ± 0.06	2.67 ± 0.15
	2.59 ± 0.10	2.60 ± 0.07	2.68 ± 0.13
	2.60 ± 0.11	2.59 ± 0.07	2.65 ± 0.11
<i>[H<sub>2</sub>Ni<sub>31</sub>P<sub>4</sub>(CO)<sub>39</sub>]<sup>4-</sup></i>	2.57 ± 0.10	2.58 ± 0.05	2.67 ± 0.12

Table 7.13 - Set of values referred to the different types of bonds within the cages that surrounded the interstitial nickel atoms in the Ni<sub>11</sub>P<sub>3</sub>(μ<sub>14</sub>-Ni) moieties.

The data showed that the elongations were concentrated in the capping regions. In the whole cages there were not many elongated bonds, nonetheless most of them involved the capping nickel atoms. This behaviour affected the mean capping bonds lengths, which were longer than expected.

However, the extent of the elongation was not particularly severe, despite the evident deformation of the structures. The coordination number of the nickel atoms - equal to fourteen - was higher than expected, as interstitial nickel atoms in carbonyl clusters are commonly found within icosahedral environments.

Still, the bonding analyses strongly suggested that the conformation of these  $\text{Ni}_{11}\text{P}_3(\mu_{14}\text{-Ni})$  sub-units provided a suitable stabilisation to the interstitial nickel atoms, as well as to the cavities that hosted them.

\*\*\*

Further validation for this hypothesis was provided by considering other nickel-pnictogen carbonyl cluster. Notwithstanding the peculiarity of this type of sub-structure, a relatable geometry had been individuated in a nickel-antimony species -  $[\text{Ni}_{31}\text{Sb}_4(\text{CO})_{40}]^{6-}$  (Figure 7.7). In its metallic skeleton there were two symmetrical  $\text{Ni}_{11}\text{Sb}_3(\mu_{14}\text{-Ni})$  sub-units, similar to  $\text{Ni}_{11}\text{P}_3(\mu_{14}\text{-Ni})$ . The nickel-antimony moieties were shaped as bi-capped hexagonal anti-prisms, yet were far more regular in shape. Further information will ensue in the dedicated chapter.

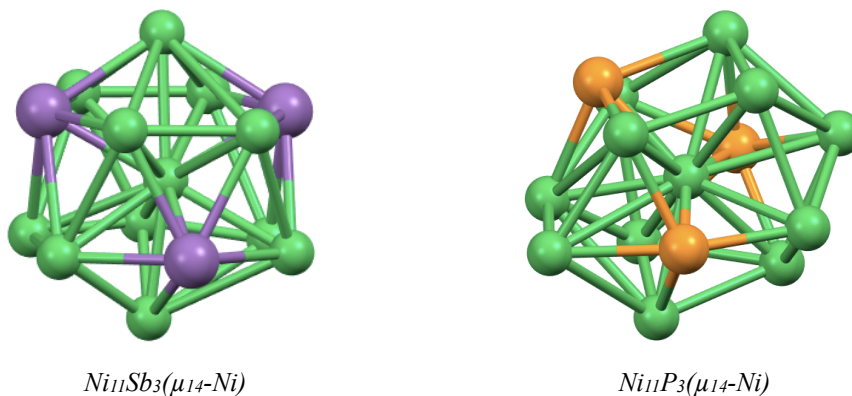


Figure 7.7 -  $\text{Ni}_{11}\text{E}_3(\mu_{14}\text{-Ni})$  moieties. Nickel atoms are represented in green, antimony atoms in purple, phosphorus atoms in orange.

★ **Fourteen-membered heteroatomical cages -  $\text{Ni}_{12}\text{P}_2(\mu_{14}\text{-Ni})$ ,  $\text{Ni}_{10}\text{P}_3(\mu_{13}\text{-Ni})$**

Another type of nickel-centred moieties in which the interstitial atoms displayed a coordination number equal to fourteen appeared to be closely related to  $\text{Ni}_{11}\text{P}_3(\mu_{14}\text{-Ni})$ .  $\text{Ni}_{12}\text{P}_2(\mu_{14}\text{-Ni})$  fragments had been identified in two separate instances, within  $[\text{Ni}_{23-x}\text{P}_2(\text{CO})_{30-x}]^{4-}$  and  $[\text{Ni}_{23-x}\text{P}_2(\text{CO})_{30-x}]^{6-}$  (Figure 7.8).

On one hand, the presence of only two phosphorus atoms could have suggested their positioning in reciprocal, apical sites. On the other hand, structures similar to those of  $\text{Ni}_{11}\text{P}_3(\mu_{14}\text{-Ni})$  could have occurred, due to the similar formulae. Eventually, neither the first nor the second hypothesis applied to the structures of these fragments.

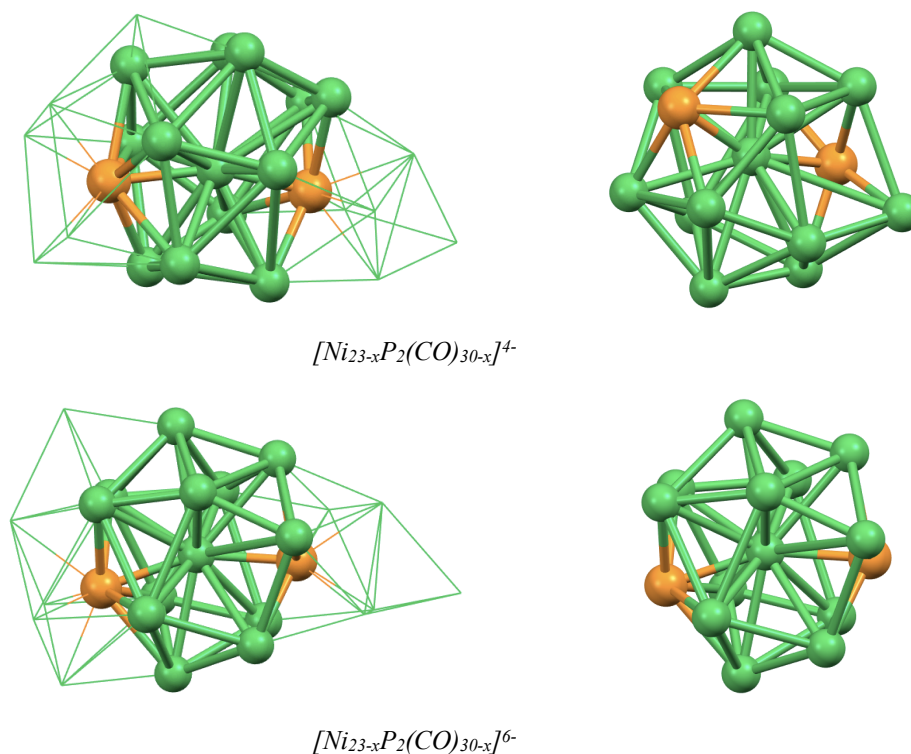


Figure 7.8 -  $\text{Ni}_{12}\text{P}_2(\mu_{14}\text{-Ni})$  moieties and metallic skeletons of the clusters containing them. On the left the position of the moieties has been highlighted, on the right the structures of the moieties have been enlarged. Nickel atoms are represented in green, phosphorus atoms in orange.

The  $\text{Ni}_{12}\text{P}_2(\mu_{14}\text{-Ni})$  moieties were even more misshapen than the  $\text{Ni}_{11}\text{P}_3(\mu_{14}\text{-Ni})$  moieties, and their structural configuration was even less clear. In order to evaluate their structures, it has been eventually decided to formally ignore the atoms

whose position was exceedingly in disarray. It will be shown that such arbitrary conjecture allowed to speculate that both the  $\text{Ni}_{12}\text{P}_2(\mu_{14}\text{-Ni})$  sub-units could be derived from nickel-centred icosahedra (Figure 7.9).

One nickel and one phosphorus atom have been excluded during the evaluation of the geometry of both the  $\text{Ni}_{12}\text{P}_2(\mu_{14}\text{-Ni})$  sub-units. The stemming moieties could have been considered like cleaved icosahedra, since the two resulting pentagonal bases were angled and divergent.

At this point, an interesting similarity between these  $\text{Ni}_{12}\text{P}_2(\mu_{14}\text{-Ni})$  moieties and the  $\text{Ni}_{10}\text{P}_3(\mu_{13}\text{-Ni})$  moiety - that had been individuated within the asymmetrical molecular structures of  $[\text{HNi}_{31}\text{P}_4(\text{CO})_{39}]^{5-}$  - emerged. In fact, by excluding a nickel atom from the structure of  $\text{Ni}_{10}\text{P}_3(\mu_{13}\text{-Ni})$  it was possible to individuate a cleaved icosahedron as well.

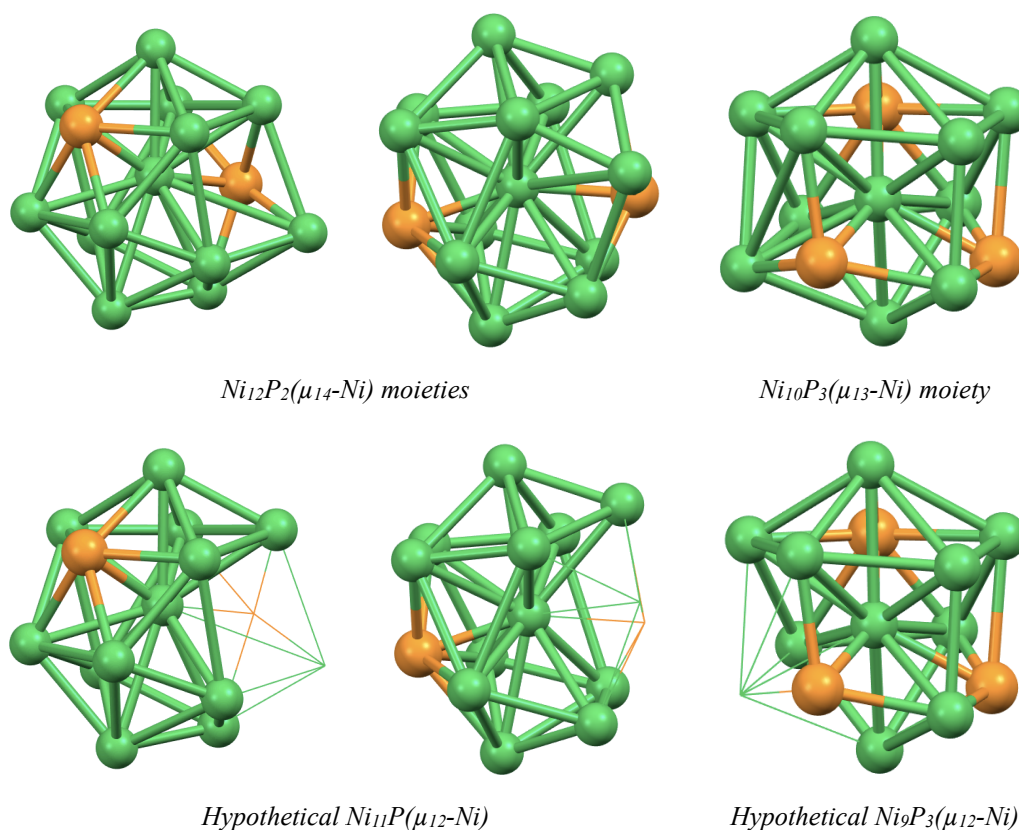


Figure 7.9 -  $\text{Ni}_{12}\text{P}_2(\mu_{14}\text{-Ni})$  moieties and  $\text{Ni}_{10}\text{P}_3(\mu_{13}\text{-Ni})$  moiety. The complete structure of the nickel-hosting fragments have been reported in the upper figures. In the lower figures, the disarrayed atoms have been faded in order to highlight the resulting cleaved icosahedra. Nickel atoms are represented in green, phosphorus atoms in orange.

It is important to notice that all interactions - also those involving the atoms that had been excluded in the structural description - have been considered in the following analyses of the bond lengths. The aforementioned exclusions were just aimed to the simplification of the arrangement of the moieties and to the identification of a structural model.

\*\*\*

The interstitial nickel atoms in  $\text{Ni}_{12}\text{P}_2(\mu_{14}\text{-Ni})$  and  $\text{Ni}_{10}\text{P}_3(\mu_{13}\text{-Ni})$  displayed a similar behaviour to those previously described. Despite the distortion of the cavities the interactions were not elongated, except for those involving the disarranged atoms. As a result, the average bond distances were within the expected range of values. This indicated that the nickel atoms were well-fitting in these cavities.

Interestingly, the mean values of the nickel-phosphorus bond lengths were shorter than average, as in the related  $\text{Ni}_{11}\text{P}_3(\mu_{14}\text{-Ni})$  sub-units (Table 7.14).

<i>cluster containing the <math>\text{Ni}_{12}\text{P}_2(\mu_{14}\text{-Ni})</math> or the <math>\text{Ni}_{10}\text{P}_3(\mu_{13}\text{-Ni})</math> fragment</i>	<i>average value</i>	<i>minimum value</i>	<i>maximum value</i>
<i>interstitial nickel-phosphorus bond lengths (Å)</i>			
<i>all clusters</i>	2.19 ± 0.04	2.15	2.32
(*) $[\text{Ni}_{23-x}\text{P}_2(\text{CO})_{30-x}]^{4-}$	2.19 ± 0.02	2.17	2.20
(*) $[\text{Ni}_{23-x}\text{P}_2(\text{CO})_{30-x}]^{6-}$	2.18 ± 0.01	2.16	2.19
(§) $[\text{HNi}_{31}\text{P}_4(\text{CO})_{39}]^{5-}$	2.21 ± 0.07	2.15	2.32
<i>interstitial nickel-nickel bond lengths (Å)</i>			
<i>all clusters</i>	2.64 ± 0.08	2.48	2.87
(*) $[\text{Ni}_{23-x}\text{P}_2(\text{CO})_{30-x}]^{4-}$	2.63 ± 0.08	2.48	2.87
(*) $[\text{Ni}_{23-x}\text{P}_2(\text{CO})_{30-x}]^{6-}$	2.64 ± 0.07	2.49	2.80
(§) $[\text{HNi}_{31}\text{P}_4(\text{CO})_{39}]^{5-}$	2.65 ± 0.08	2.53	2.84

Table 7.14 - Set of values referred to the bonds involving the interstitial nickel atoms within the  $\text{Ni}_{12}\text{P}_2(\mu_{14}\text{-Ni})$  (\*) and the  $\text{Ni}_{10}\text{P}_3(\mu_{13}\text{-Ni})$  (§) moieties.

\*\*\*

For what concerns the bonds that were constituting the cages, the nickel-phosphorus bonds and the nickel-nickel bonds have been further classified as intra-base, inter-base, and capping (Table 7.15). The bonds involving the formally excluded nickel atoms from  $\text{Ni}_{11}\text{P}_3(\mu_{14}\text{-Ni})$  have only been considered in the general analysis, as they did not fit in any further category.

cluster containing the $\text{Ni}_{12}\text{P}_2(\mu_{14}\text{-Ni})$ or the $\text{Ni}_{10}\text{P}_3(\mu_{13}\text{-Ni})$ fragment	average value	minimum value	maximum value
	<i>nickel-phosphorus bond lengths (Å)</i>		
<i>all clusters</i>	$2.37 \pm 0.08$	2.17	2.57
(*) $[\text{Ni}_{23-x}\text{P}_2(\text{CO})_{30-x}]^{4-}$	$2.40 \pm 0.05$	2.34	2.50
(*) $[\text{Ni}_{23-x}\text{P}_2(\text{CO})_{30-x}]^{6-}$	$2.40 \pm 0.05$	2.32	2.47
(§) $[\text{H}\text{Ni}_{31}\text{P}_4(\text{CO})_{39}]^{5-}$	$2.35 \pm 0.09$	2.17	2.57
<i>nickel-nickel bond lengths (Å)</i>			
<i>all clusters</i>	$2.61 \pm 0.12$	2.31	3.08
(*) $[\text{Ni}_{23-x}\text{P}_2(\text{CO})_{30-x}]^{4-}$	$2.60 \pm 0.12$	2.31	3.00
(*) $[\text{Ni}_{23-x}\text{P}_2(\text{CO})_{30-x}]^{6-}$	$2.61 \pm 0.15$	2.35	3.08
(§) $[\text{H}\text{Ni}_{31}\text{P}_4(\text{CO})_{39}]^{5-}$	$2.61 \pm 0.10$	2.41	2.74
	<i>intra-base</i>	<i>inter-base</i>	<i>capping</i>
<i>average nickel-phosphorus bond lengths (Å)</i>			
<i>all clusters</i>	$2.35 \pm 0.09$	$2.39 \pm 0.08$	$2.38 \pm 0.05$
(*) $[\text{Ni}_{23-x}\text{P}_2(\text{CO})_{30-x}]^{4-}$	$2.46 \pm 0.03$	$2.36 \pm 0.02$	/
(*) $[\text{Ni}_{23-x}\text{P}_2(\text{CO})_{30-x}]^{6-}$	$2.38 \pm 0.04$	$2.38 \pm 0.05$	/
(§) $[\text{H}\text{Ni}_{31}\text{P}_4(\text{CO})_{39}]^{5-}$	$2.30 \pm 0.08$	$2.41 \pm 0.12$	$2.35 \pm 0.04$
<i>average nickel-nickel bond lengths (Å)</i>			
<i>all clusters</i>	$2.59 \pm 0.15$	$2.68 \pm 0.11$	$2.59 \pm 0.10$
(*) $[\text{Ni}_{23-x}\text{P}_2(\text{CO})_{30-x}]^{4-}$	$2.61 \pm 0.15$	$2.78 \pm 0.15$	$2.58 \pm 0.09$
(*) $[\text{Ni}_{23-x}\text{P}_2(\text{CO})_{30-x}]^{6-}$	$2.55 \pm 0.16$	$2.62 \pm 0.07$	$2.59 \pm 0.12$
(§) $[\text{H}\text{Ni}_{31}\text{P}_4(\text{CO})_{39}]^{5-}$	$2.62 \pm 0.11$	$2.64 \pm 0.08$	$2.59 \pm 0.09$

Table 7.15 - Set of values referred to the different types of bonds within the cage that surrounded the interstitial nickel atoms in the  $\text{Ni}_{12}\text{P}_2(\mu_{14}\text{-Ni})$  (\*) and the  $\text{Ni}_{10}\text{P}_3(\mu_{13}\text{-Ni})$  (§) moieties.

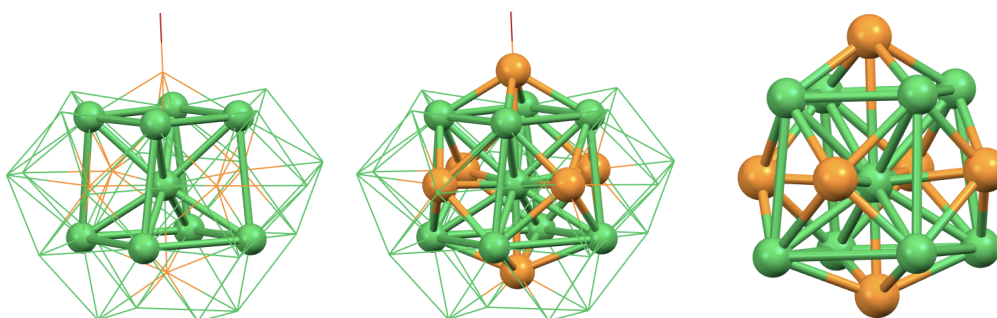
The data showed that the nickel-nickel and the nickel-phosphorus bonds within the cages behaved similarly. In both cases the average values of the bond lengths were within the set threshold, and few interactions were elongated.

Therefore, the bonding analyses strongly suggested that the conformation of the  $\text{Ni}_{12}\text{P}_2(\mu_{14}\text{-Ni})$  and the  $\text{Ni}_{10}\text{P}_3(\mu_{13}\text{-Ni})$  sub-units provided a suitable stabilisation to the interstitial nickel atoms, as well as to the cavities that hosted them, despite the structural distortion.

♦ **Fourteen-membered heteroatomical cages -  $\text{Ni}_8\text{P}_6(\mu_{14}\text{-Ni})$**

Finally, it would be interesting to mention one last interstitial nickel atom that was hosted inside a fourteen-membered heteroatomical cavity. The corresponding moiety was individuated within the molecular structure of  $[\text{Ni}_{29}\text{P}_5(\text{PO})(\text{CO})_{36}]^{4+}$ . This was the most phosphorus-rich nickel-centred fragment, as the nickel atom was enclosed in a  $\text{Ni}_8\text{P}_6$  structure, forming a  $\text{Ni}_8\text{P}_6(\mu_{14}\text{-Ni})$  sub-unit.

The whole fragment was shaped as a centred cube of nickel atoms, whose squared faces were capped by one phosphorus atom each (Figure 7.10). All heteroatoms were coordinated to the interstitial nickel atom as well, except for the phosphorus belonging to the phosphoryl group.



$[\text{Ni}_{29}\text{P}_5(\text{PO})(\text{CO})_{36}]^{4+}$

Figure 7.10 -  $\text{Ni}_8\text{P}_6(\mu_{14}\text{-Ni})$  moiety and metallic skeleton of the cluster containing it. The position of the nickel-centred cube of nickel atoms (left) and the position of the whole moiety (middle) have been highlighted. Nickel atoms are represented in green, phosphorus atoms in orange, oxygen atoms in red.

\*\*\*

For what concerns the interstitial nickel atom, the values of the average bond distances were within the expected range of values (Table 7.16). Moreover, the values of the bond lengths were narrowly dispersed, and no bond was elongated. These observations suggested that the interstitial metallic atom was well-stabilised by this environment, despite its peculiar arrangement.

<i>type of bond</i>	<i>bond lengths (Å)</i>		
	<i>average value</i>	<i>minimum value</i>	<i>maximum value</i>
<i>nickel-phosphorus</i>	2.35 ± 0.04	2.25	2.40
<i>nickel-nickel</i>	2.63 ± 0.01	2.61	2.65

Table 7.16 - Set of values referred to the bonds involving the interstitial nickel atom within the  $Ni_8P_6(\mu_{14}-Ni)$  moiety.

\*\*\*

For what concerns the  $Ni_8P_6$  cage, it has been useful to separate the nickel-nickel interactions within the  $Ni_8$  cube from the nickel-phosphorus interactions involving the face-capping phosphorus atoms (Table 7.17). For the latter type of bond, the average values for the interactions over each face have been reported.

<i>type of bond</i>	<i>bond lengths (Å)</i>		
	<i>average value</i>	<i>minimum value</i>	<i>maximum value</i>
<i>face-capping nickel-phosphorus</i>	2.34 ± 0.09		
	2.33 ± 0.11		
	2.35 ± 0.12		
	2.35 ± 0.11	2.20	2.52
	2.35 ± 0.11		
	2.39 ± 0.02		
	2.24 ± 0.01		
<i>nickel-nickel</i>	3.0 ± 0.2	2.72	3.21

Table 7.17 - Set of values referred to the bonds within the cage that surrounded the interstitial nickel atom in the  $Ni_8P_6(\mu_{14}-Ni)$  moieties.



At this point the weakness of the cage became apparent, since the majority of the nickel-nickel interactions that formed the metallic cube were severely elongated. Only one out of the six squared faces of the cube was formed by four non-elongated - yet still longer than average - bonds.

In light of this it was possible to assume that the metallic cube was loose. However, the capping phosphorus atoms were well-coordinated to their respective squared nickel faces, and they probably had a stabilising effect. Due to this, it was presumed that the  $\text{Ni}_8\text{P}_6(\mu_{14}\text{-Ni})$  fragment would not have subsisted without the balancing effect of the six capping heteroatoms.

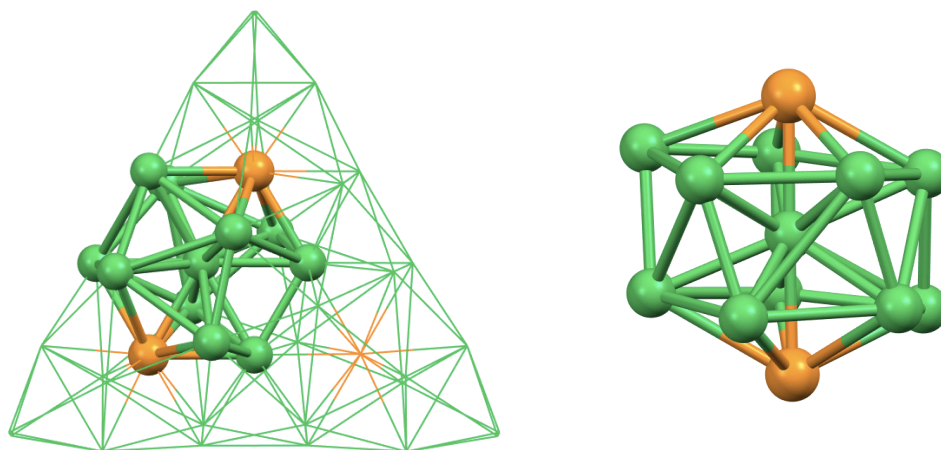
This phenomenon was clearly attributable to the nature of the interstitial atom. Nickel atoms are too bulky to be hosted inside a cube of alike atoms. Its presence therefore tended to enlarge the metallic structure, and sensibly elongated the nickel-nickel bonds of the cage. The elongation was partly counterbalanced by the presence of the six phosphorus atoms, which provided the necessary stabilisation by capping and strengthening the enlarged faces of the cube.

Still, the structure of this moiety had obvious limitations - unsurprisingly, similar arrangements had not been identified in any other nickel-phosphorus clusters.

✦ ***Twelve-membered heteroatomical cages -  $\text{Ni}_{10}\text{P}_2(\mu_{12}\text{-P})$***

Although in a single case, an interstitial nickel atom has been identified inside a smaller heteroatomical cage. This extremely significant example was identified within the molecular structure of  $[\text{Ni}_{39}\text{P}_3(\text{CO})_{44}]^{6-}$ . The arrangement of its  $\text{Ni}_{10}\text{P}_2(\mu_{12}\text{-Ni})$  moiety was unique - so far it is the only example of a nickel-centred icosahedron with two apical phosphorus atoms in homoleptic carbonyl clusters (Figure 7.11).

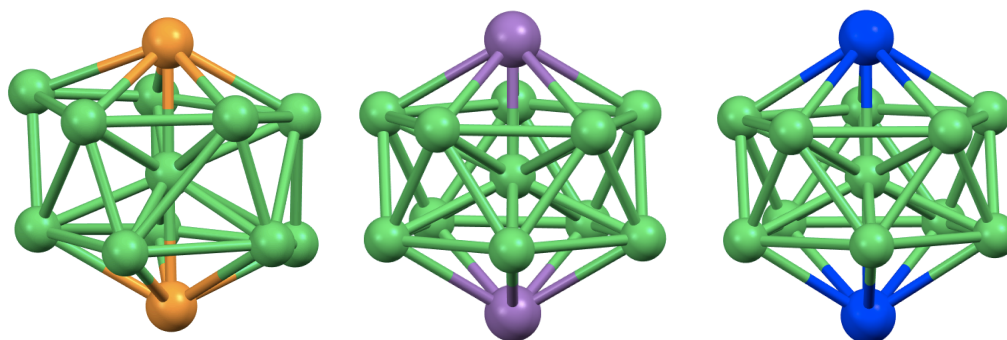
This fragment displayed remarkable features, in sharp contrast with those previously described. The heteroatomical nickel-hosting cage was far more regular in shape than the others, and the phosphorus atoms were in apical positions rather than within the bases of the prismatic structure.



$Ni_{10}P_2(\mu_{12}\text{-Ni})$  in  $[Ni_{39}P_3(CO)_{44}]^{6-}$

Figure 7.11 -  $Ni_{10}P_2(\mu_{12}\text{-Ni})$  moiety and metallic skeleton of the cluster containing it. On the left the position of the icosahedral fragment has been highlighted. On the right the structure of the fragment has been enlarged. Nickel atoms are represented in green, phosphorus atoms in orange.

The structural arrangement of the  $Ni_{10}P_2(\mu_{12}\text{-Ni})$  sub-unit was actually more similar to the structures of other nickel-pnictogen carbonyl cluster than to those of other nickel-phosphorus species (Figure 7.12). This phenomenon will be further discussed in the dedicated chapter.



$Ni_{10}E_2(\mu_{12}\text{-Ni})$

Figure 7.12 -  $Ni_{10}E_2(\mu_{12}\text{-Ni})$  moieties with phosphorus atoms (within  $[Ni_{39}P_3(CO)_{44}]^{6-}$ ), antimony atoms (within  $[Ni_{11}Sb_2(CO)_{18}]^{3-}$ ), and bismuth atoms (within  $[Ni_{11}Bi_2(CO)_{18}]^{2-}$ ) in apical positions. Despite all being structured as nickel-centred icosahedra, the nickel-antimony and the nickel-bismuth fragments are more regular in terms of configuration than the nickel-phosphorus fragment. Nickel atoms are reported in green, phosphorus atoms in orange, antimony atoms in purple, bismuth atoms in blue.

\*\*\*

The central nickel atom was well coordinated to the two nickel pentagonal bases, and to the apical phosphorus atoms as well (Table 7.18), as evinced by the analysis of the interactions that involved the interstitial atom.

<i>type of bond</i>	<i>bond lengths (Å)</i>		
	<i>average value</i>	<i>minimum value</i>	<i>maximum value</i>
<i>nickel-phosphorus</i>	2.30 ± 0.01	(*)	(*)
<i>nickel-nickel</i>	2.53 ± 0.14	2.31	2.89

Table 7.18 - Set of values referred to the bonds involving the interstitial nickel atom within the  $Ni_{10}P_2(\mu_{12}-Ni)$  moiety.

(\*) The minimum and maximum values for the nickel-phosphorus interactions have not been reported as only two values, one for each apical heteroatom, were available.

The data, along with the fact that a limited number of bonds was elongated, could have suggested that this type of icosahedral structure was well-stabilised. Yet, it is possible to notice that the average value of the nickel-nickel interactions was fairly lower than the reference value - 2.61 Å. This implied that the pentagonal nickel rings had shrank, and that the bases had been brought closer to the interstitial atom probably because of the presence of the smaller phosphorus atoms in apical positions.

\*\*\*

The stress that characterised this structural arrangement became more evident by considering the bonds that were constituting the icosahedral cage (Table 7.19). In the  $Ni_{10}P_2$  cage all the intra-pentagonal and the inter-pentagonal bonds were nickel-nickel bonds, while all the capping bonds were nickel-phosphorus bonds.

Considering the fact that almost all the nickel-phosphorus bonds - *i.e.* the bonds in the capping region - were elongated, this type of coordination could not be considered as well-fitting for an interstitial nickel atom.

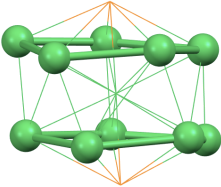
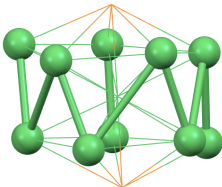
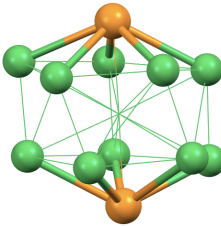
<i>average bond length (Å)</i>			
			
<i>intra-pentagonal nickel-nickel</i>	<i>inter-pentagonal nickel-nickel</i>	<i>capping nickel-phosphorus</i>	
$2.65 \pm 0.08$	$2.56 \pm 0.19$	$2.54 \pm 0.11$	
<i>bond lengths (Å)</i>			
<i>type of bond</i>	<i>average value</i>	<i>minimum value</i>	<i>maximum value</i>
<i>nickel-phosphorus</i>	$2.54 \pm 0.11$	2.29	2.68
<i>nickel-nickel</i>	$2.61 \pm 0.15$	2.31	3.02

Table 7.19 - Set of values referred to the bonds in the  $Ni_{10}P_2$  cage of the  $Ni_{10}P_2(\mu_{12}-Ni)$  moiety.

More in detail, these data highlighted two characteristic phenomena. The average value of the nickel-nickel bond distances was slightly lower - yet still comparable - to the reference average value. On the contrary, the average nickel-phosphorus bond length was significantly longer than expected, and most nickel-phosphorus interactions were elongated nonetheless. These two behaviours were clearly correlated and due to the small dimensions of the heteroatoms.

Considering their apical position, each phosphorus atom had to be coordinated to the five nickel atoms of the corresponding pentagonal base. So, on one hand the nickel-nickel interactions tended to shorten, in order to reduce the dimensions of the ring and to promote its interaction with the overlying phosphorus atom. On the other hand the pentagonal bases could not shrink beyond a certain threshold, because of the presence of the interstitial nickel atom. Therefore, the nickel-phosphorus interactions were elongated - and as a result weakened - whilst the nickel-nickel interactions were oppositely affected.

This behaviour was in accord with that displayed by the aforementioned phosphorus hosting cages, and further supported the hypothesis for which icosahedral environments were not suitable for the stabilisation of an homoleptic nickel-phosphorus species.

## ***Elongations***

In the previous sections the nickel-hosting cavities and the phosphorus-hosting cavities have been thoroughly investigated. In both cases the available molecular structures provided a fair amount of examples. The different types of moieties have already been divided in categories and described, yet a comprehensive comparison should be useful.

In the introduction it was argued that the presence of icosahedral arrangements could be expected. Heteroatomical nickel carbonyl clusters with post-transition elements frequently display such geometries - both centred and non-centred - with the heteroatoms in central or in apical positions. It was therefore reasonable to assume that nickel-phosphorus homoleptic carbonyl clusters would have engaged in the same type of structures.

In spite of that, experimental data revealed an opposite behaviour. Very few icosahedral sub-units have been individuated, and they were clearly subjected to distortions and elongations. In the following discussion a comparison between the different types of arrangements and further considerations on their internal degree of elongation will ensue.

Phosphorus-hosting cavities and nickel-hosting cavities will be separately considered. The number of elongated bonds will be counted and compared, in order to evaluate the degrees of distortion that affected the different structures.

### ***✦ Elongation in phosphorus-hosting cavities***

Twenty-two phosphorus-hosting cavities were individuated and characterised, and then classified into four groups accordingly to their coordination number and their structural arrangement.

In summary, it has been previously determined that the phosphorus atoms were always interstitial and enclosed in nickel cages. The most common coordination number for the heteroatoms was equal to nine or ten, and the nickel cages were shaped as mono-capped squared anti-prisms. It was still possible for the phospho-

rus atoms to be at the centre of a nickel icosahedron, yet just one example had been found. So, the categories of the phosphorus-hosting moieties were closed  $\text{Ni}_9(\mu_9\text{-P})$ , open  $\text{Ni}_9(\mu_9\text{-P})$ ,  $\text{Ni}_{10}(\mu_{10}\text{-P})$ , and  $\text{Ni}_{12}(\mu_{12}\text{-P})$  (Figure 7.13).

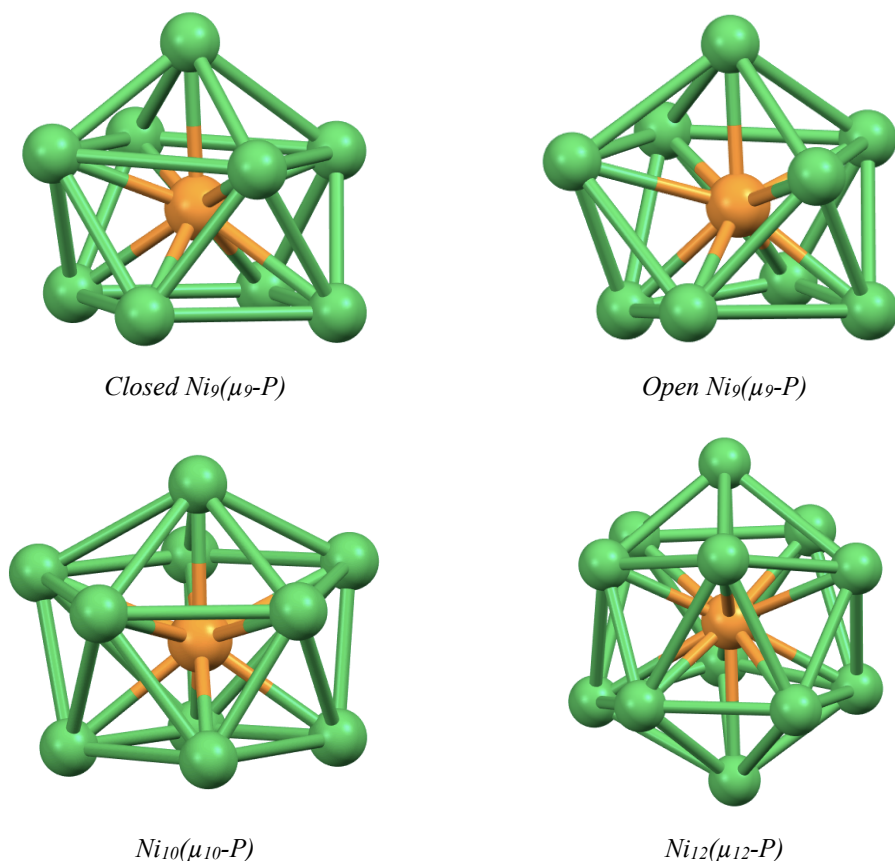


Figure 7.13 - Representation of each type of phosphorus-hosting cavity that had been identified. From the upper left, the moieties that are reported are those in the molecular structures of  $[\text{Ni}_{14}\text{P}_2(\text{CO})_{22}]^{2-}$ ,  $[\text{Ni}_{23-x}\text{P}_2(\text{CO})_{30-x}]^{4-}$ ,  $[\text{Ni}_{23-x}\text{P}_2(\text{CO})_{30-x}]^{6-}$ , and  $[\text{Ni}_{39}\text{P}_3(\text{CO})_{44}]^{6-}$ . Nickel atoms are represented in green, phosphorus atoms in orange.

A statistical analysis on the number of elongated interactions was attempted, in order to compare these structures in terms of intrinsic stability. A higher percentage of elongated bonds would have indicated a lower stability for the corresponding structural arrangement.

In the following data (Table 7.20) two different types of percentages will be reported. The local percentage was calculated by considering the number of elongated bonds over the total number of bonds within a specific region of the prismatic structure - interstitial, intra-base, inter-base, and capping (Figure 7.14). The

total percentage considered the number of strained bonds over the total number of bonds, for the whole moiety. This further distinction had been done in order to individuate any preferentially unstable region within the fragments.

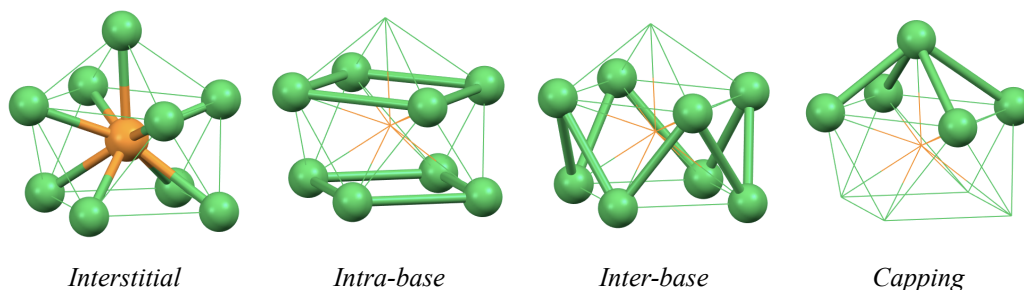


Figure 7.14 - In each image one different region has been highlighted. From the left, the interstitial interactions, the intra-base interactions, the inter-base interactions, and the capping interactions have been accentuated. The  $Ni_9(\mu_9-P)$  moiety within  $[Ni_{14}P_2(CO)_{22}]^{2-}$  has been used as example. Nickel atoms are represented in green, phosphorus atoms in orange.

	<i>closed <math>Ni_9(\mu_9-P)</math></i>	<i>open <math>Ni_9(\mu_9-P)</math></i>	<i><math>Ni_{10}(\mu_{10}-P)</math></i>	<i><math>Ni_{12}(\mu_{12}-P)</math></i>
<i>c.N.</i>	9	9	10	12
<i>instances</i>	<i>ten instances</i>	<i>eight instances</i>	<i>three instances</i>	<i>one instance</i>
<i>elongated bonds (%)</i>				
<i>all regions</i>	13.0	6.1	5.3	14.3
(*) <i>interstitial</i>	2.2	6.9	0	33.3
(§) <i>intra-base</i>	34.7	14.8	0	20.0
(§) <i>inter-base</i>	11.3	0	18.2	0
(§) <i>capping</i>	0	0	6.7	0

Table 7.20 - Total (all regions) and local percentages of elongated bonds in the different types of phosphorus-hosting cavities, referred to the whole structures and to each region.

(\*) All the bonds involving the interstitial atoms are nickel-phosphorus bonds.

(§) All the bonds in the intra-base, inter-base, and capping regions are nickel-nickel bonds.

\*\*\*

These statistics revealed some interesting behaviours.

Considering first the phosphorus-centred icosahedron, the data clearly ex-

plained the reason why this type of structure was rare - even unique - as that geometry had the highest total percentage of elongated bonds. On one hand, the nickel icosahedral cage was well-stabilised and most nickel-nickel interactions were within the expected range of values. On the other hand, the majority of the elongated bonds involved the interstitial heteroatom, and more than the 30% of the nickel-phosphorus interactions were severely elongated.

This evidently indicated that the nickel icosahedral cavity was too large to host the phosphorus atom, despite the metallic atoms being well-arranged in an icosahedral structure. The reduced dimensions of the heteroatom inhibited the effectiveness of its interactions with the surrounding metallic cage. These observations allowed to explain the rarity of an otherwise common type of coordination for heteroatomical nickel and group-15 elements structures.

\*\*\*

For what concerns the other moieties, the data were less unambiguous. In most cases the phosphorus atoms were within closed nine-membered nickel cages, shaped as mono-capped squared anti-prisms and forming closed  $\text{Ni}_9(\mu_9\text{-P})$  moieties. However, in this type of sub-structures there was a rather high percentage of elongated bonds - particularly in the intra-base region, where more than the 30% of the interactions were elongated. This evidence suggested that the squared bases of the anti-prisms were subjected to enlargement. Because of this, it appeared clear that a squared nickel anti-prism was too small to host a phosphorus atoms without being subjected to distortion, even when a capping atom was present.

This was further supported by considering the related open  $\text{Ni}_9(\mu_9\text{-P})$  structures. Those belonged to the second most numerous sub-group of phosphorus-hosting cages, and had the same structure of the closed  $\text{Ni}_9(\mu_9\text{-P})$  moieties except for the presence of a lateral opening. The cleavage enlarged the nickel cages, and therefore there was a lower percentage of elongated bonds. The elongated interactions were preferentially located in the intra-base region of these structures - and in particular in the closed, non-capped bases. It was therefore possible to assume that the lateral opening of the cages allowed to partly reduce the extent of the



elongations in the upper region of the moieties.

Eventually, the statistics concerning the ten-membered phosphorus-hosting cages were contradictory. In the  $\text{Ni}_{10}(\mu_{10}\text{-P})$  moieties the metallic cages were shaped as prisms, with one squared and one capped pentagonal base. Despite their peculiar arrangement, these sub-structures had the lowest percentage of elongated bonds, thus indicating a good degree of stabilisation.

By recalling the previously stated considerations, it was clear that the addition of one nickel atom within the capped base enlarged the phosphorus-hosting cavity, and therefore further enhanced the nickel-nickel interactions as well as the nickel-phosphorus interactions. However, the presence of a larger pentagonal base affected the inter-base interactions. Still, more occurrences of  $\text{Ni}_{10}(\mu_{10}\text{-P})$  sub-structures would have been expected due to their apparent stability. However, only three examples had been characterised.

#### ♦ *Elongation in nickel-hosting cavities*

The nickel-hosting cavities were less homogeneous than the phosphorus-hosting ones. Indeed the majority of the interstitial nickel atoms displayed the same coordination number - C.N. equal to fourteen - yet the resulting structures were heavily distorted.

In order to evaluate the number of elongated bonds in the different regions of the fragments, different models had to be taken into account. In accord to the previously proposed structural analysis, in the following survey  $\text{Ni}_{11}\text{P}_3(\mu_{14}\text{-Ni})$  have been considered as bi-capped hexagonal anti-prisms,  $\text{Ni}_{12}\text{P}_2(\mu_{14}\text{-Ni})$  and  $\text{Ni}_{10}\text{P}_3(\mu_{13}\text{-Ni})$  as icosahedron-related structures,  $\text{Ni}_{10}\text{P}_2(\mu_{12}\text{-Ni})$  as an icosahedron, and  $\text{Ni}_8\text{P}_6(\mu_{14}\text{-Ni})$  as a face-capped cube (Figure 7.15).

This allowed to subdivide the interactions into interstitial, intra-base, inter-base, and capping categories (Figure 7.16) for all but the latter moiety. As in the previous analysis, the local and the total percentages of elongated bonds have been calculated (Table 7.21). For what concerns the icosahedron-related  $\text{Ni}_{12}\text{P}_2(\mu_{14}\text{-Ni})$  moieties, it is worth to mention that the bonds that were previously

described as disarranged were only considered in the evaluation of the total percentage of strained bonds, as they did not fit in any other category.

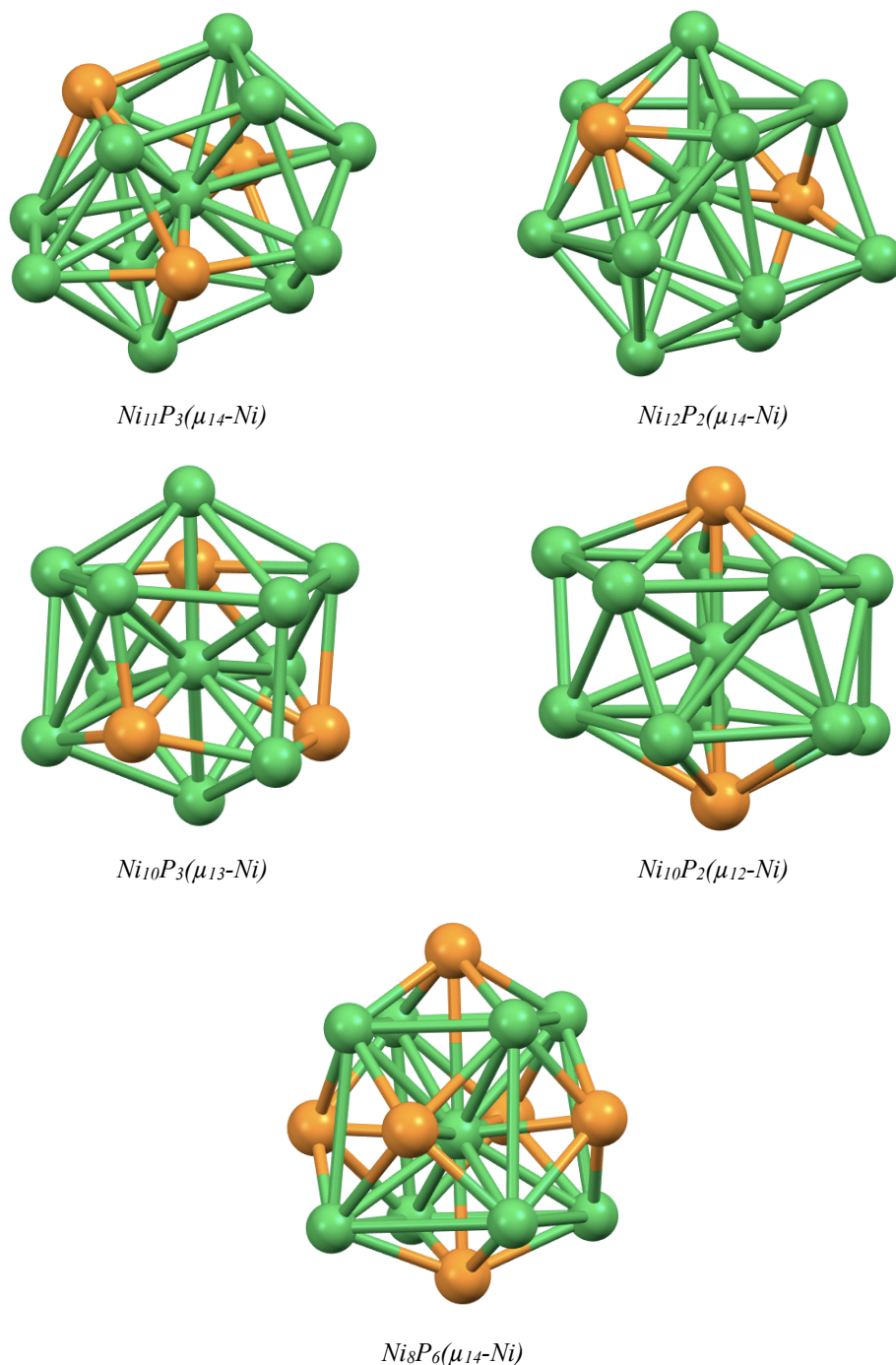


Figure 7.15 - Examples for each type of nickel-hosting cavity that had been identified. From the upper left, the moieties are those within  $[H_2Ni_{31}P_4(CO)_{39}]^+$ ,  $[Ni_{23-x}P_2(CO)_{30-x}]^+$ ,  $[HNi_{31}P_4(CO)_{39}]^5-$ ,  $[Ni_{39}P_3(CO)_{44}]^6-$ , and  $[Ni_{29}P_5(PO)(CO)_{36}]^4-$ . Nickel atoms are represented in green, phosphorus atoms in orange.

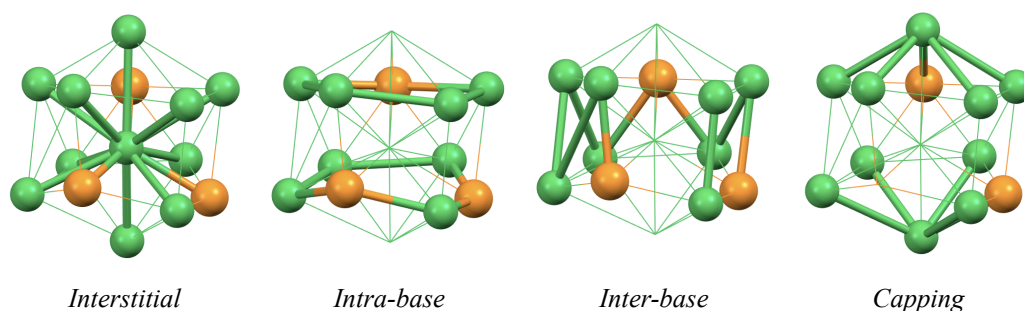


Figure 7.16 - In each image one different region has been highlighted. From the left, the interstitial interactions, the intra-base interaction, the inter-base interactions, and the capping interactions have been accentuated. The  $Ni_{10}P_3(\mu_{13}-P)$  moiety within  $[HNi_{31}P_4(CO)_{39}]^{5-}$  has been used as example. Nickel atoms are represented in green, phosphorus atoms in orange.

	$Ni_{11}P_3(\mu_{14}-Ni)$	$Ni_{12}P_2(\mu_{14}-Ni)$	$Ni_8P_6(\mu_{14}-Ni)$	$Ni_{10}P_3(\mu_{13}-Ni)$	$Ni_{10}P_2(\mu_{12}-Ni)$
<b>C.N.</b>	14	14	14	13	12
<b>instances</b>	four instances	two instances	one instance	one instance	one instance
<b>elongated bonds (%)</b>					
<b>all bonds</b>	6.6	4.9	25.0	2.8	25.0
<b>interstitial</b>	5.8	3.8	0	0	16.7
<b>intra-base</b>	0	9.5	(*) 66.7	0	10.0
<b>inter-base</b>	0	6.3		14.3	12.5
<b>capping</b>	22.0	0	(§) 4.2	0	60.0

Table 7.21 - Total (all regions) and local percentages of elongated bonds in the different types of nickel-hosting cavities, referred to the whole structures and to each region.

(\*) Percentage referred to the elongated bonds amongst those constituting the  $Ni_8$  cube.

(§) Percentage referred to the elongated bonds amongst those capping the faces of the cube.

\*\*\*

The most affected types of nickel-hosting moieties will be considered at first.

For what concerns the icosahedral geometry, just one  $Ni_{10}P_2(\mu_{12}-Ni)$  sub-unit had been individuated, despite nickel-centred - as well as non-centred - icosahedra being well-known in heteroatomical nickel clusters with group-15 elements.

In fact, the data highlighted that this structure was subjected to considerable elongations. In  $Ni_{10}P_2(\mu_{12}-Ni)$  the 25% of the bonds was elongated. The capping

region of the icosahedral skeleton was particularly affected, as suggested by the fact that the 60% of the capping nickel-phosphorus bonds was elongated. This indicated that the apical positions of a nickel icosahedron were not suitable for the phosphorus atoms in a carbonyl-stabilised environment - because of their reduced dimensions. It is actually important to remember that these considerations are solely valid for nickel-phosphorus homoleptic carbonyl clusters, since the presence of alkyl or aryl ligands coordinated to the phosphorus atoms can provide further stabilisation, as will be discussed in the dedicated chapter.

The same total percentage of elongated bonds - equal to the 25% - was found in the  $\text{Ni}_8\text{P}_6(\mu_{14}\text{-Ni})$  moiety. As in the icosahedron, also in this structure it was possible to individuate a region within which the elongated bonds were preferentially located. In fact, in this nickel-hosting moiety nearly the 70% of the bonds that were constituting the inner nickel cube was subjected to elongation. It was therefore possible to assume that a cubic structure of nickel atoms was not large enough in order to host a further nickel atom. Accordingly, the whole moiety was probably stabilised by the presence of the six capping phosphorus atoms above the nickel faces of the cube.

Despite being extremely different in terms of shape, as well as in terms of nickel-phosphorus ratio, the icosahedral  $\text{Ni}_{10}\text{P}_2(\mu_{12}\text{-Ni})$  moiety and the cubic  $\text{Ni}_8\text{P}_6(\mu_{14}\text{-Ni})$  moiety behaved similarly. Both displayed much more regular structures than the other nickel-hosting moieties, and in both cases the phosphorus atoms were located in specific regions of the structures - apical or face-capping, respectively.

However, their regular arrangements have proved to be subjected to intense elongations when thoroughly investigated, thus further highlighting the principal limitation of nickel-phosphorus structures. In the first case the elongation was due to the fact that the icosahedral cage was too large for the apical phosphorus atom. In the second case the elongation was due to the fact that the nickel cube was too small to host the interstitial nickel atom. So, this was an additional validation that suggested the vital role of the respective dimensions of nickel and phosphorus atoms.

\*\*\*

Interestingly,  $\text{Ni}_{11}\text{P}_3(\mu_{14}\text{-Ni})$ ,  $\text{Ni}_{12}\text{P}_2(\mu_{14}\text{-Ni})$ , and  $\text{Ni}_{10}\text{P}_3(\mu_{13}\text{-Ni})$  displayed relatively similar behaviours, despite being arranged as sensibly distorted structures. All these moieties were, to some extent, relatable to bi-capped anti-prismatic structures. As aforementioned, the  $\text{Ni}_{11}\text{P}_3(\mu_{14}\text{-Ni})$  moieties could be considered as bi-capped hexagonal anti-prisms, whilst  $\text{Ni}_{12}\text{P}_2(\mu_{14}\text{-Ni})$  and  $\text{Ni}_{10}\text{P}_3(\mu_{13}\text{-Ni})$  could be considered as derived from icosahedral geometries.

However, in these structures the heteroatoms were not in apical positions - as in  $\text{Ni}_{10}\text{P}_2(\mu_{12}\text{-Ni})$  - but rather within the bases of the anti-prisms. On one hand, this evidently distorted the heteroatomical cages. On the other hand, the structures were more stabilised, since the percentages of elongated bonds were much lower.

The inclusion of the smaller heteroatoms within the bases of the anti-prisms probably allowed to better distribute the effects of their small dimensions, therefore reducing the number of elongated bonds.

## Comparisons with other structures

It has been said that these new nickel-phosphorus homoleptic carbonyl clusters displayed unique features, and that their structural arrangement was unexpected. In the following sections the nickel-phosphorus moieties will be compared to those of other known clusters, in order to identify any possible common feature and to better understand their behaviour.

First, a comparison with the structures of other heteroatomical nickel and group-15 elements clusters will ensue. When possible, the various nickel-pnictogen species known in the literature will be structurally compared to these new nickel-phosphorus clusters.

Then, the same approach will be used to compare nickel-phosphorus clusters to other transition metal-phosphorus clusters, and to nickel-phosphorus binary phases.

### *Comparison with other heteroatomical nickel structures*

Despite their peculiar structural arrangements, nickel-phosphorus clusters actually had features in common with other heteroatomical nickel clusters. A particular focus will be put on nickel and group-15 elements, since phosphorus belongs to that group along with arsenic, antimony and bismuth.

\*\*\*

As it was already mentioned, most nickel-pnictogen clusters displayed related molecular structures that were based on icosahedral geometries.

However, amongst them only one heteroatom-centred icosahedron was present, within the structure of  $[\text{Ni}_{15}(\mu_{12}\text{-Sb})(\text{CO})_{24}]^{2-}$ . The same type of coordination was rare in nickel-phosphorus clusters as well, and only one phosphorus-centred icosahedron had been individuated, within the structure of  $[\text{Ni}_{13}\text{P}_3(\text{CO})_{44}]^{6-}$ . The rarity of these heteroatom-centred nickel icosahedra suggests that this type of coor-

dination does not provide a suitable degree of stabilisation, as will be investigated in the following sections.

On the contrary, most nickel-pnictogen clusters known in the literature displayed icosahedral structures in which the heteroatoms occupied the apical positions of the cages. This type of heteroatomical icosahedra occurred as nickel-centred and as non-centred, yet in both cases the structures were similar. Also, by considering heteroleptic carbonyl clusters it was possible to individuate at least one heteroatomical nickel icosahedron -  $\text{Ni}_{10}\text{E}_2$  - for all the group-15 elements.

Homoleptic nickel-phosphorus carbonyl clusters behaved differently, and just one heteroatomical nickel-centred moiety with the phosphorus atoms in apical position had been individuated, within  $[\text{Ni}_{39}\text{P}_3(\text{CO})_{44}]^{6-}$ . This unexpected behaviour will be analysed in the following sections as well.

Finally,  $[\text{Ni}_{31}\text{Sb}_4(\text{CO})_{40}]^{6-}$  will be considered *per se* and compared to the closely related  $[\text{HNi}_{31}\text{P}_4(\text{CO})_{39}]^{5-}$ . In fact, the nickel-antimony species not only had an almost identical formula to that of the nickel-phosphorus species, but both clusters shared some interesting structural features that will be further investigated.

#### ♦ *Heteroatom-centred nickel icosahedra*

In nickel and group-15 elements clusters there is a low tendency for the heteroatoms to occupy the interstitial positions of icosahedral environments. The  $\text{Ni}_{12}(\mu_{12}\text{-P})$  fragment that was observed within  $[\text{Ni}_{39}\text{P}_3(\text{CO})_{44}]^{6-}$  had just one reliable structure, since only in the di-anionic  $[\text{Ni}_{15}(\mu_{12}\text{-Sb})(\text{CO})_{24}]^{2-}$  there was a comparable  $\text{Ni}_{12}(\mu_{12}\text{-Sb})$  moiety (Figure 8.1).

Despite including the same nickel-pnictogen moiety, these clusters presented extremely different molecular structures. The nickel-phosphorus species had a high nuclearity, as well as a rather symmetrical structure. Within its metallic skeleton there were three identical  $\text{Ni}_{14}(\mu_{12}\text{-P})$  - *i.e.* three icosahedral fragments with two additional capping atoms. On the contrary, the nickel-antimony species had a medium-low nuclearity, and its metallic skeleton was mainly formed by the

nickel icosahedron. It is interesting to notice that the remaining metallic atoms were capping over three adjacent triangular faces of the icosahedron, as in the phosphorus-centred one.

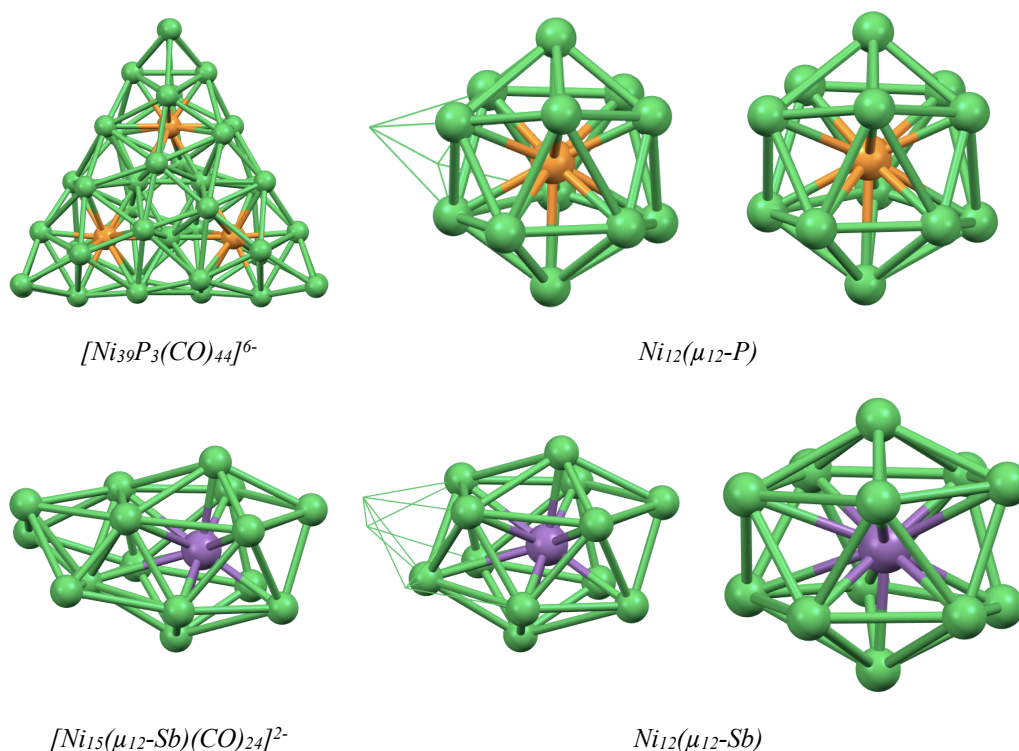


Figure 8.1 - Heteroatom-centred nickel icosahedra and metallic skeletons of the cluster containing them. On the left, the metallic skeletons of the clusters have been reported. On the right, the phosphorus-centred and the antimony-centred icosahedra have been highlighted. Nickel atoms are represented in green, phosphorus atoms in orange, antimony atoms in purple.

In order to compare these icosahedra, their bond lengths have been classified as intra-pentagonal, inter-pentagonal, and capping nickel-nickel interactions, and interstitial heteroatom-nickel interactions (Table 8.1).

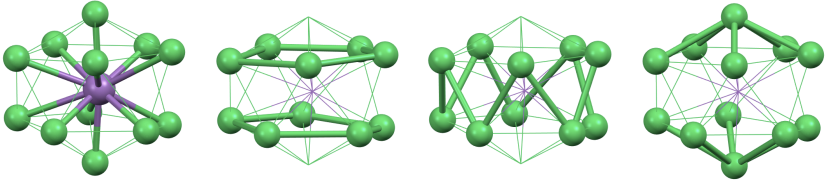
By observing the data it was clear that the bulkier antimony atom triggered an opposite effect on the icosahedral structure, compared to the phosphorus atom.

In fact, the presence of the larger antimony atom tended to enlarge the whole nickel cage, as revealed by the average nickel-nickel bonds. Within the metallic cage of  $Ni_{12}(\mu_{12}-Sb)$  most nickel-nickel bonds were longer than average, particularly in the intra-pentagonal region. On the contrary, in the metallic cage of  $Ni_{12}(\mu_{12}-P)$  the average values of the nickel-nickel bond distances were close to



the expected average value - 2.61 Å, as reported before. The nickel-phosphorus bonds were the most affected by elongations.

*average bond lengths (Å)*



<i>icosahedral moiety</i>	<i>interstitial</i>	<i>intra-pentagonal</i>	<i>inter-pentagonal</i>	<i>capping</i>
<i>Ni<sub>12</sub>(μ<sub>12</sub>-P)</i>	2.46 ± 0.10	2.57 ± 0.15	2.61 ± 0.11	2.61 ± 0.09
<i>Ni<sub>12</sub>(μ<sub>12</sub>-Sb)</i>	2.64 ± 0.18	2.86 ± 0.12	2.65 ± 0.14	2.73 ± 0.19

Table 8.1 - Set of values referred to the heteroatom-centred nickel icosahedra, Ni<sub>12</sub>(μ<sub>12</sub>-P) within [Ni<sub>39</sub>P<sub>3</sub>(CO)<sub>44</sub>]<sup>6-</sup> and Ni<sub>12</sub>(μ<sub>12</sub>-Sb) within [Ni<sub>15</sub>Sb(CO)<sub>24</sub>]<sup>2-</sup>. The Ni<sub>12</sub>(μ<sub>12</sub>-Sb) moiety within [Ni<sub>15</sub>Sb(CO)<sub>24</sub>]<sup>2-</sup> has been used as example. Nickel atoms are represented in green, antimony atoms in purple.

By comparing the two structures, it was therefore evident that they were oppositely affected. The average nickel-phosphorus bond distances indicated a loose interaction between the heteroatom and its surrounding atoms. On the contrary, the mean value of the antimony-nickel bond length was close to the expected value - 2.63 Å, calculated from the covalent radii of the elements - thus indicating a good interaction with the nickel cage. Yet, the nickel-nickel interactions within Ni<sub>12</sub>(μ<sub>12</sub>-Sb) were elongated, indicating that the antimony-centred icosahedron was poorly stabilised, particularly in the intra-pentagonal region.

It was therefore reasonable to assume that neither the phosphorus nor the antimony atom were suitable to be hosted inside an icosahedral nickel cage. The lighter pnictogen is probably too small to achieve an adequate interaction with its surroundings, and the heavier pnictogen is too bulky not to trigger a destabilising enlargement of the metallic cage.

These observations allowed to explain the scarce presence of such types of coordination in other nickel-pnictogen clusters, as well as the presence of further metallic atoms on the sides of the metallic icosahedral cages.

### ♦ *Heteroatomical icosahedra*

In the previous section it has been shown that heteroatom-centred nickel icosahedra were not common. On the contrary, icosahedral environments were more recurrent whenever the heteroatoms were occupying the apical positions of an icosahedron.

There were several examples of both nickel-centred and non-centred icosahedra, with each group-15 element in apical positions. Different  $\text{Ni}_{10}\text{E}_2$  and  $\text{Ni}_{10}\text{E}_2(\mu_{12}\text{-Ni})$  metallic skeletons were known in the literature, from both heteroleptic and homoleptic carbonyl clusters.

Considering as examples  $[\text{Ni}_{10}(\text{PMe})_2(\text{CO})_{18}]^{2-}$ ,  $[\text{Ni}_{10}(\text{AsMe})_2(\text{CO})_{18}]^{2-}$ ,  $[\text{Ni}_{10}(\text{SbMe})_2(\text{CO})_{18}]^{2-}$ ,  $[\text{Ni}_{10}(\text{BiMe})_2(\text{CO})_{18}]^{2-}$ ,  $[\text{Ni}_{10}\text{Sb}_2(\mu_{12}\text{-Ni})(\text{CO})_{18}]^{3-}$ ,  $[\text{Ni}_{12}\text{Sb}_2(\mu_{12}\text{-Ni})(\text{CO})_{24}]^{3-}$ , and  $[\text{Ni}_{10}\text{Bi}_2(\mu_{12}\text{-Ni})(\text{CO})_{18}]^{2-}$ , all present similar structural features that appear to be related to those of the nickel-centred icosahedral moiety within  $[\text{Ni}_{39}\text{P}_3(\text{CO})_{44}]^{6-}$  (Figure 8.2, Figure 8.3).

Interestingly, the two types of icosahedral framework that can be individuated - non-centred and nickel-centred - appeared to be linked to the nature of the cluster itself. In fact, all the heteroleptic species displayed non-centred icosahedral structures, whilst all the homoleptic species displayed nickel-centred icosahedral structures. It was therefore supposed that both the alkyl ligands and the interstitial nickel atoms were present in order to provide further stabilisation to the basic  $\text{Ni}_{10}\text{E}_2$  icosahedral framework.

Despite these differences,  $\text{Ni}_{10}\text{E}_2$  and  $\text{Ni}_{10}\text{E}_2(\mu_{12}\text{-Ni})$  moieties will be considered as a single group of structures, since the presence or the absence of the interstitial metallic atom only trivially altered the icosahedral cages. In fact, it will be highlighted that the nature of the heteroatom was the most important parameter.

In the following section  $\text{Ni}_{10}\text{E}_2$  and  $\text{Ni}_{10}\text{E}_2(\mu_{12}\text{-Ni})$  icosahedral sub-units will be compared, in order to individuate any common behaviour or tendency in terms of bond lengths. Still, it is important to remember that the  $\text{Ni}_{10}\text{P}_2(\mu_{12}\text{-Ni})$  moiety within  $[\text{Ni}_{39}\text{P}_3(\text{CO})_{44}]^{6-}$  was part of a much larger metallic skeleton. On the contrary, all the other heteroatomical icosahedra embodied the whole cluster skeletons.

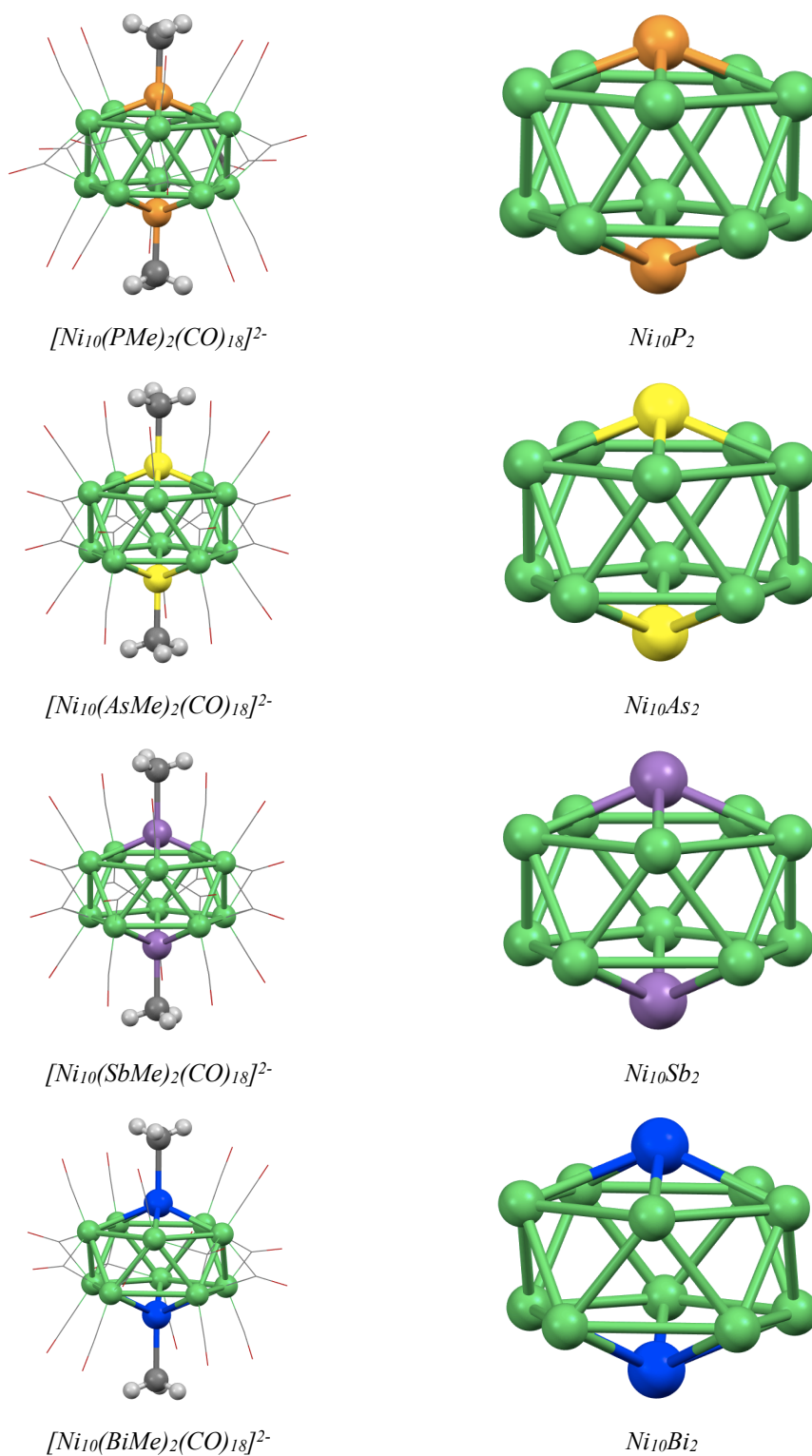


Figure 8.2 - Non-centred  $Ni_{10}E_2$  icosahedra and metallic skeletons of the heteroleptic clusters containing them. On the left, the metallic skeletons of clusters have been reported, and the alkyl ligands have been highlighted along with the icosahedral frameworks. On the right, the icosahedral cages have been enlarged. Nickel atoms are represented in green, phosphorus atoms in orange, arsenic atoms in yellow, antimony atoms in purple, bismuth atoms in blue, carbon atoms in grey, oxygen atoms in red, hydrogen atoms in light grey.

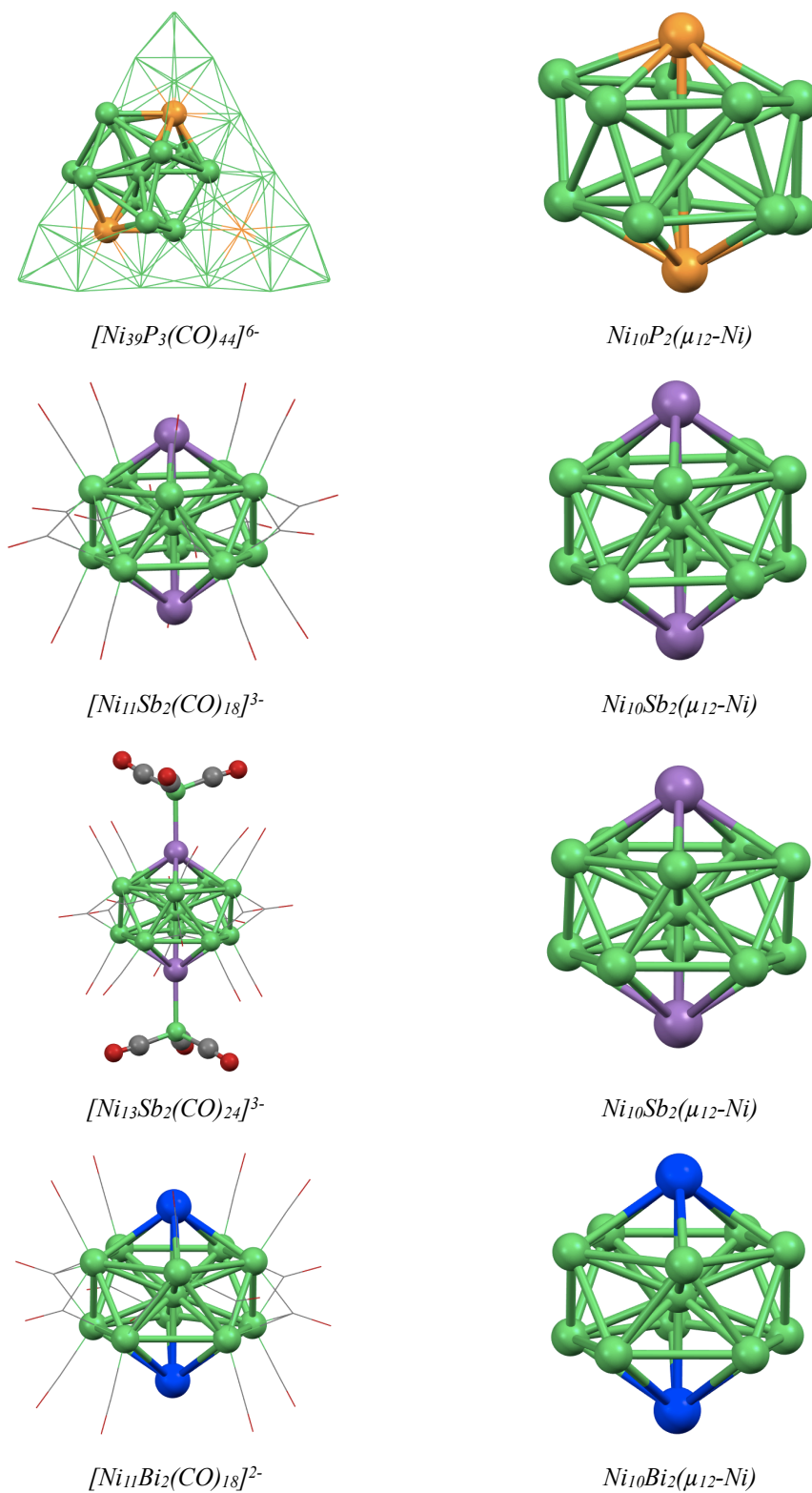


Figure 8.3 - Nickel-centred  $Ni_{10}E_2(\mu_{12}-Ni)$  icosahedra and metallic skeletons of the homoleptic clusters containing them. On the left, the position of the icosahedral sub-units within the metallic skeletons of clusters have been highlighted. On the right, the icosahedral cages have been enlarged. Nickel atoms are represented in green, phosphorus atoms in orange, antimony atoms in purple, bismuth atoms in blue, carbon atoms in grey, oxygen atoms in red.

In order to compare these structures the average bond lengths have been divided in intra-pentagonal, inter-pentagonal, and capping categories (Table 8.2). The latter category included only nickel-heteroatom bonds, and the others included only nickel-nickel bonds. The clusters corresponding to each moiety were explicitly indicated.

<i>average bond lengths (Å)</i>			
<i>Ni<sub>10</sub>E<sub>2</sub></i>	<i>intra-pentagonal</i>	<i>inter-pentagonal</i>	<i>capping</i>
<i>[Ni<sub>10</sub>(PMe)<sub>2</sub>(CO)<sub>18</sub>]<sup>2-</sup></i>	2.61 ± 0.03	2.49 ± 0.03	2.35 ± 0.02
<i>[Ni<sub>10</sub>(AsMe)<sub>2</sub>(CO)<sub>18</sub>]<sup>2-</sup></i>	2.69 ± 0.05	2.49 ± 0.03	2.43 ± 0.02
<i>[Ni<sub>10</sub>(SbMe)<sub>2</sub>(CO)<sub>18</sub>]<sup>2-</sup></i>	2.81 ± 0.07	2.49 ± 0.03	2.59 ± 0.02
<i>[Ni<sub>10</sub>(BiMe)<sub>2</sub>(CO)<sub>18</sub>]<sup>2-</sup></i>	2.88 ± 0.11	2.50 ± 0.04	2.63 ± 0.02
<i>Ni<sub>10</sub>E<sub>2</sub>(μ<sub>12</sub>-Ni)</i>			
<i>[Ni<sub>39</sub>P<sub>3</sub>(CO)<sub>44</sub>]<sup>6-</sup></i>	2.65 ± 0.08	2.56 ± 0.14	2.54 ± 0.11
<i>[Ni<sub>11</sub>Sb<sub>2</sub>(CO)<sub>18</sub>]<sup>3-</sup></i>	2.78 ± 0.05	2.52 ± 0.01	2.74 ± 0.02
<i>[Ni<sub>13</sub>Sb<sub>2</sub>(CO)<sub>24</sub>]<sup>3-</sup></i>	2.77 ± 0.08	2.51 ± 0.05	2.73 ± 0.02
<i>[Ni<sub>11</sub>Bi<sub>2</sub>(CO)<sub>18</sub>]<sup>2-</sup></i>	2.81 ± 0.06	2.50 ± 0.01	2.82 ± 0.03

Table 8.2 - Set of values referred to the Ni<sub>10</sub>E<sub>2</sub> and the Ni<sub>10</sub>E<sub>2</sub>(μ<sub>12</sub>-Ni) moieties. The icosahedral structure of [Ni<sub>10</sub>(AsMe)<sub>2</sub>(CO)<sub>18</sub>]<sup>2-</sup> has been used as example. Nickel atoms are represented in green, arsenic atoms in yellow.

The data showed that the behaviour of the newly discovered Ni<sub>10</sub>P<sub>2</sub>(μ<sub>12</sub>-Ni) - that was within the high-nuclearity [Ni<sub>39</sub>P<sub>3</sub>(CO)<sub>44</sub>]<sup>6-</sup> cluster - was in accord with those of the other considered icosahedra. In other words, the data followed the same trend as those of the other fragments. Still, there were some divergences. Due to this, it would be useful to make some general considerations concerning the whole set of structures (Figure 8.4).

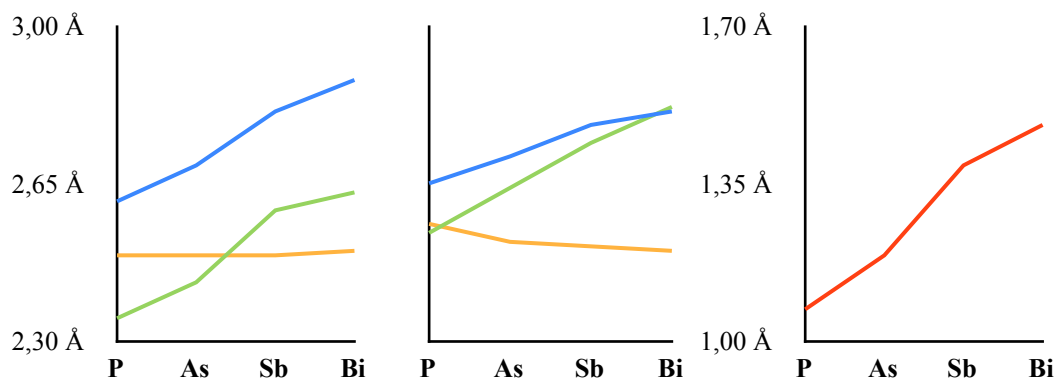


Figure 8.4 - Plots showing the variation of the mean distances as a function of the congeneric element for the four members of the group-15 series (P, As, Sb, Bi) for each of the three kinds of edges in the  $Ni_{10}E_2$  (left) and the  $Ni_{10}E_2(\mu_{12}-Ni)$  (middle) icosahedral cages. Plot showing the trend of the covalent radii of the heteroatoms (right). All the ordinate axes are reported with the same scale. The intra-pentagonal interactions are reported in blue, the inter-pentagonal interactions in orange, the capping interactions in green, the covalent radii in red.

As shown in the plots, the intra-pentagonal interactions and the capping interactions tended to lengthen when considering moieties with heavier congeneric elements of the group-15 series - *i.e.* from phosphorus to bismuth. This clearly happened because of the progressively bulkier nature of the heteroatoms, as further demonstrated by the fact that the experimental covalent radii of the elements followed the same trend.

Interestingly, the inter-pentagonal distances did not follow this trend. On the contrary, the inter-pentagonal interactions displayed consistent values within all the  $Ni_{10}E_2$  and the  $Ni_{10}E_2(\mu_{12}-Ni)$  icosahedra. These values were independent of the nature of the involved heteroatom as well as of the presence of the interstitial nickel atoms or of the alkyl ligands.

These phenomena denoted that the size of the capping heteroatoms affected the dimensions of the pentagonal nickel bases, but not the distance amongst them. For what concerns the trend followed by the capping interactions, the data had minor importance as it is evident that the length of an heteroatomical bond rises along with the dimensions of the involved atoms.

It was also interesting to notice that the presence of a nickel atom in interstitial position did not have considerable effects on the trends followed by the bond lengths. However, the average values of the bond lengths were moderately af-

fect, except for those of the inter-pentagonal interactions. It was possible to notice that within the  $\text{Ni}_{10}\text{E}_2(\mu_{12}\text{-Ni})$  structures the values of the intra-pentagonal interactions were slightly lower compared to those within  $\text{Ni}_{10}\text{E}_2$ . Moreover, the capping interactions in  $\text{Ni}_{10}\text{E}_2(\mu_{12}\text{-Ni})$  were longer than those within  $\text{Ni}_{10}\text{E}_2$ .

Therefore, it was assumed that the presence of the interstitial nickel atom prevented a further approaching of the capping heteroatoms towards the pentagonal bases, and therefore the capping bond distances were longer. At the same time, its presence strengthened the metallic framework, thus the slight reduction of the intra-pentagonal bond distances.

\*\*\*

The data collected for the new  $\text{Ni}_{10}\text{P}_2(\mu_{12}\text{-Ni})$  fragment were actually following these general trends. Still, for this moiety it was possible to notice that all the average bond distances were slightly longer than expected - except for those in the capping region, whose elongation was possibly due to the presence of the interstitial nickel atom.

In particular, the value of the average inter-pentagonal bond length was the most deviating from the series of otherwise consistent values. This unexpected phenomenon was probably due to the inclusion of the  $\text{Ni}_{10}\text{P}_2(\mu_{12}\text{-Ni})$  fragment within a much larger cluster. On the contrary, the other  $\text{Ni}_{10}\text{E}_2$  and  $\text{Ni}_{10}\text{E}_2(\mu_{12}\text{-Ni})$  structures constituted the whole skeletons of the clusters themselves. This possibly caused a trivial yet detectable deviation from the expected average bond distances.

However, by considering the whole group of  $\text{Ni}_{10}\text{E}_2$  and  $\text{Ni}_{10}\text{E}_2(\mu_{12}\text{-Ni})$  icosahedral moieties it was not clear what induced the rarity of this type of structural configuration in nickel-phosphorus carbonyl clusters. To further investigate on this issue, a comparison between  $\text{Ni}_{10}\text{P}_2$  within  $[\text{Ni}_{10}(\text{PMe})_2(\text{CO})_{18}]^{2-}$  and  $\text{Ni}_{10}\text{P}_2(\mu_{12}\text{-Ni})$  within  $[\text{Ni}_{39}\text{P}_3(\text{CO})_{44}]^{6-}$  was attempted (Table 8.3, Figure 8.5).

By drawing attention to these two data-sets alone, the limitations of the  $\text{Ni}_{10}\text{P}_2(\mu_{12}\text{-Ni})$  icosahedron became evident. Although in both fragments the average values of the nickel-nickel interactions belonged to the expected range of values, the nickel-phosphorus interaction behaved differently. In  $\text{Ni}_{10}\text{P}_2$  the average

value - 2.35 Å - was close to the expected reference value - 2.33 Å - whilst the nickel-phosphorus interactions in  $\text{Ni}_{10}\text{P}_2(\mu_{12}\text{-Ni})$  were remarkably longer, and therefore indicated a less effective interaction of the heteroatoms towards the metallic framework.

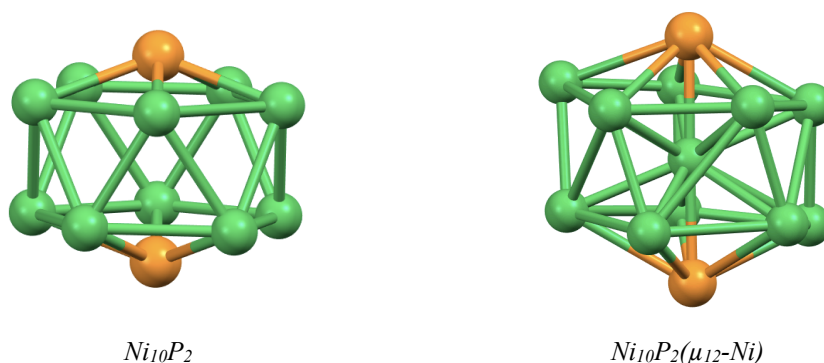


Figure 8.5 - Non-centred  $\text{Ni}_{10}\text{P}_2$  and nickel-centred  $\text{Ni}_{10}\text{P}_2(\mu_{12}\text{-Ni})$  icosahedra. By comparing these structures, it was even more evident to what extent the newly discovered  $\text{Ni}_{10}\text{P}_2(\mu_{12}\text{-Ni})$  was distorted. Nickel atoms are represented in green, phosphorus atoms in orange.

<i>average bond lengths (Å)</i>			
<i>type of moiety</i>	<i>intra-pentagonal</i>	<i>inter-pentagonal</i>	<i>capping</i>
$\text{Ni}_{10}\text{P}_2$	$2.61 \pm 0.03$	$2.49 \pm 0.03$	$2.35 \pm 0.02$
$\text{Ni}_{10}\text{P}_2(\mu_{12}\text{-Ni})$	$2.65 \pm 0.08$	$2.56 \pm 0.14$	$2.54 \pm 0.11$

Table 8.3 - Set of values referred to the  $\text{Ni}_{10}\text{P}_2$  and the  $\text{Ni}_{10}\text{P}_2(\mu_{12}\text{-Ni})$  moieties. The icosahedral sub-structure within  $[\text{Ni}_{39}\text{P}_3(\text{CO})_{44}]^{6-}$  has been used as example. Nickel atoms are represented in green, phosphorus atoms in orange.

Therefore, it was possible to assume that for nickel-phosphorus icosahedra the presence of two additional alkyl ligands was more stabilising than the presence of one interstitial nickel atom, which even destabilised the framework. On the contrary, in nickel-antimony and nickel-bismuth species the two types of stabilisation were comparably effective.

As aforementioned, these problems were probably related to the relative di-



mensions of the nickel and the phosphorus atoms. In the  $\text{Ni}_{10}\text{P}_2(\mu_{12}\text{-Ni})$  icosahedron, the presence of two small phosphorus atoms in apical positions would have caused a shortening of the capping interactions. However, the presence of the interstitial nickel atom inhibited the displacement of the heteroatoms toward the pentagonal nickel bases, thus elongating the capping interactions. Also, this probably induced the trivial lengthening of the inter-pentagonal interactions, in a counterbalancing endeavour.

♦  $[\text{Ni}_{31}\text{Sb}_4(\text{CO})_{40}]^{6-}$  - sub-structures

In the ensuing section the structure of the nickel-antimony  $[\text{Ni}_{31}\text{Sb}_4(\text{CO})_{40}]^{6-}$  cluster will be compared to those of the nickel-phosphorus clusters. To begin with, this nickel-antimony species shared an almost identical molecular formula with  $[\text{HNi}_{31}\text{P}_4(\text{CO})_{39}]^{5-}$ , as these two species differed just for one carbonyl ligand. Therefore, the two clusters were almost isoelectronic, and their C.V.E. - cluster valence electrons - counts only differed by two valence electrons.

At first sight,  $[\text{HNi}_{31}\text{P}_4(\text{CO})_{39}]^{5-}$  and  $[\text{Ni}_{31}\text{Sb}_4(\text{CO})_{40}]^{6-}$  did not share any other feature, as their molecular structures seemed to be quite different. Nonetheless, by proceeding with a more detailed structural analysis on  $[\text{Ni}_{31}\text{Sb}_4(\text{CO})_{40}]^{6-}$  it was actually possible to individuate some interesting features, that were relatable to those of the nickel-phosphorus clusters. Before illustrating them, a description of the molecular structure of this nickel-antimony cluster will ensue.

The metallic skeleton of the heteroatomical  $[\text{Ni}_{31}\text{Sb}_4(\text{CO})_{40}]^{6-}$  (Figure 8.6) was formed by two *quasi*-symmetrical halves. The forty carbonyl ligand completed the coordination shell of the cluster and were varyingly coordinated. The four heteroatoms were in semi-interstitial positions, a type of coordination that to date is exclusive to this species amongst all nickel-pnictogen clusters. The antimony atoms were exposed on the surface of the metallic skeleton. Two heteroatoms had a coordination number equal to ten, and formed two  $\text{Ni}_{10}(\mu_{10}\text{-Sb})$  fragments. The other two heteroatoms had a coordination number equal to eight, and formed two  $\text{Ni}_8(\mu_8\text{-Sb})$  fragments (Figure 8.6). Eventually, there also were two interstitial

nickel atoms, and each was within a fourteen-membered heteroatomal cavity - forming two  $\text{Ni}_{11}\text{Sb}_3(\mu_{14}\text{-Ni})$  sub-structures (Figure 8.6).

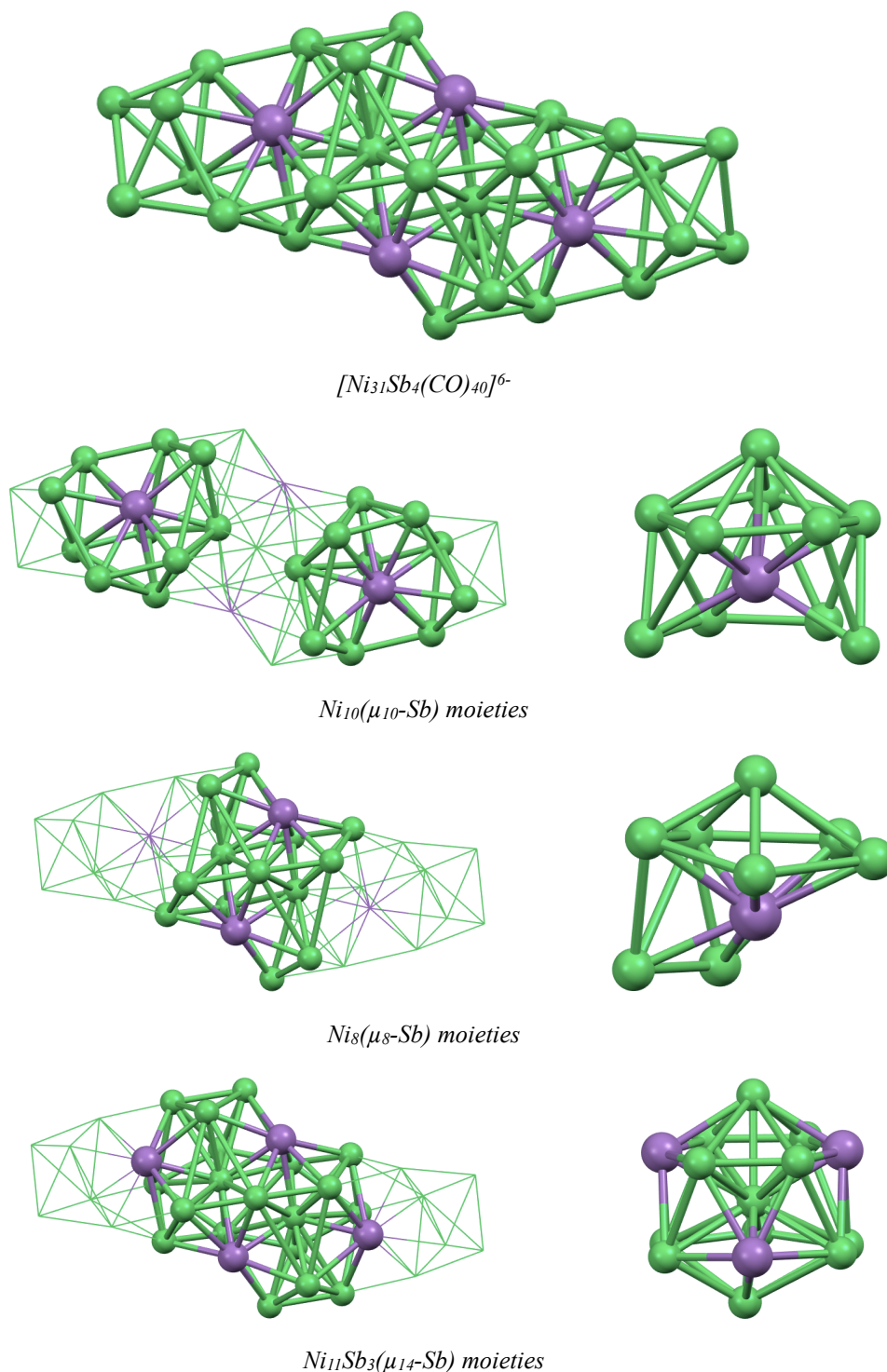
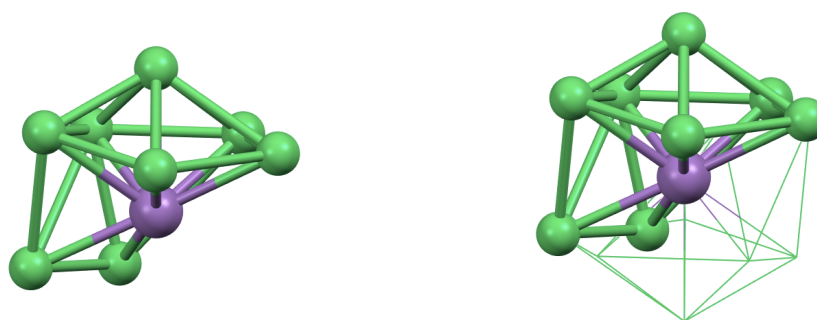


Figure 8.6 - Metallic skeleton of the high-nuclearity  $[\text{Ni}_{31}\text{Sb}_4(\text{CO})_{40}]^{6-}$  nickel-antimony cluster, and structures of the different types of antimony-hosting and nickel-hosting moieties within its molecular structure. On the left the position of the moieties has been highlighted. Nickel atoms are represented in green, antimony atoms in purple.

Before proceeding, it would be interesting to briefly describe the  $\text{Ni}_8(\mu_8\text{-Sb})$  moieties - the  $\text{Ni}_{10}(\mu_{10}\text{-Sb})$  and the  $\text{Ni}_{11}\text{Sb}_3(\mu_{14}\text{-Sb})$  moieties will be later thoroughly discussed. In these nickel-antimony fragments the heteroatom was particularly exposed, nonetheless the most interesting feature of this moiety was the conformation of the metallic framework. In fact,  $\text{Ni}_8(\mu_8\text{-Sb})$  could be interpreted as a halved icosahedron (Figure 8.7).



$\text{Ni}_8(\mu_8\text{-Sb})$

Figure 8.7 - Graphical representation of the icosahedral structure that could be visualised from  $\text{Ni}_8(\mu_8\text{-Sb})$ . The figure was obtained by inverting and superimposing a copy of the original framework over itself. Nickel atoms are represented in green, antimony atoms in purple.

\*\*\*

By comparing the overall structure of this nickel-antimony species to that of the similar  $[\text{HNi}_{31}\text{P}_4(\text{CO})_{39}]^{5-}$  cluster, the arrangement of the former appeared more elongated, whilst the latter seemed rather compact. Still, it was evident that a couple of the sub-units within  $[\text{Ni}_{31}\text{Sb}_4(\text{CO})_{40}]^{6-}$  were closely related to those seen in nickel-phosphorus clusters. In particular, both the  $\text{Ni}_{10}(\mu_{10}\text{-Sb})$  antimony-hosting and the  $\text{Ni}_{11}\text{Sb}_3(\mu_{14}\text{-Ni})$  nickel-hosting cavities were similar in terms of coordination number, nickel-heteroatom ratio, and structural arrangement.

In fact, the  $\text{Ni}_{10}(\mu_{10}\text{-Sb})$  fragment and the  $\text{Ni}_{11}\text{Sb}_3(\mu_{14}\text{-Ni})$  fragment were analogous to  $\text{Ni}_{10}(\mu_{10}\text{-P})$  and  $\text{Ni}_{11}\text{P}_3(\mu_{14}\text{-Ni})$ , which were individuated in different nickel-phosphorus species. In the following paragraphs the structures of these types of sub-units will be compared, in order to identify any possible similarity or difference.

First, the semi-interstitial antimony atoms and the corresponding  $\text{Ni}_{10}(\mu_{10}\text{-Sb})$  sub-units will be considered and compared to the analogous nickel-phosphorus ones (Figure 8.8). Three independent  $\text{Ni}_{10}(\mu_{10}\text{-P})$  fragments had been previously described, within the metallic skeletons of  $[\text{Ni}_{11}\text{P}(\text{CO})_{18}]^{3-}$ ,  $[\text{Ni}_{23-x}\text{P}_2(\text{CO})_{30-x}]^{4-}$ , and  $[\text{Ni}_{23-x}\text{P}_2(\text{CO})_{30-x}]^{6-}$ .

It has already been said that the antimony atoms in  $\text{Ni}_{10}(\mu_{10}\text{-Sb})$  were not completely enclosed by their surrounding nickel atoms - unlike the phosphorus atoms. Nonetheless, the structural arrangement of these two types of sub-units was surprisingly similar.

The structure of this type of nickel-phosphorus moiety had already been thoroughly described in the dedicated chapter. To recapitulate, the metallic cages were shaped as prisms, with one squared and one capped pentagonal base. Moreover, the analysis performed on the bonding lengths revealed that this structural arrangement was the less affected by elongation effects amongst all the phosphorus-hosting cavities.

Interestingly the nickel-antimony fragments displayed a comparable geometry - the only difference consisted in a significant opening located on the four-membered non-capped ring. In other words, the open antimony-hosting nickel cages were formed by one capped pentagonal ring, and by an open four-membered “base”. If the latter had been closed it would have formed a squared base, and therefore the structure of  $\text{Ni}_{10}(\mu_{10}\text{-Sb})$  would have been identical to that of the  $\text{Ni}_{10}(\mu_{10}\text{-P})$  fragments.

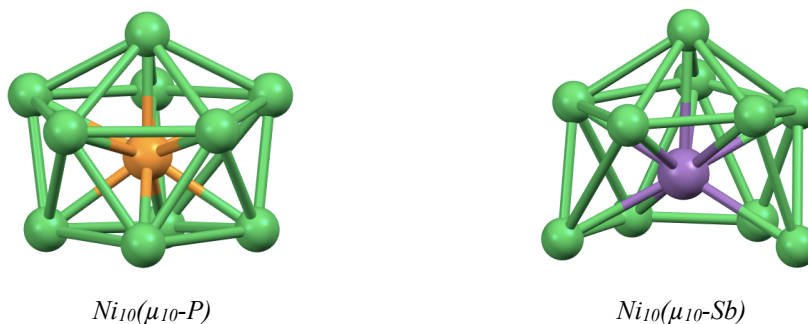


Figure 8.8 - Ten-membered heteroatom-hosting nickel cages,  $\text{Ni}_{10}(\mu_{10}\text{-P})$  (from the structure of  $[\text{Ni}_{23-x}\text{P}_2(\text{CO})_{30-x}]^{4-}$ ) and  $\text{Ni}_{10}(\mu_{10}\text{-Sb})$ . The upper sections of the moieties are remarkably similar. Nickel atoms are represented in green, phosphorus atoms in orange, antimony atoms in purple.

With the aim to individuate any other common behaviour, an analysis on the bond lengths was performed (Table 8.4). The heteroatom-nickel bonds and the nickel-nickel bonds have been separately considered. The latter have been further divided in intra-base, inter-base, and capping interactions as usual.

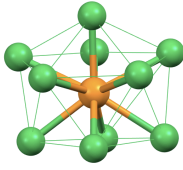
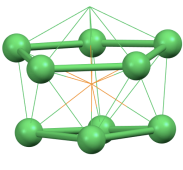
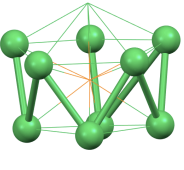
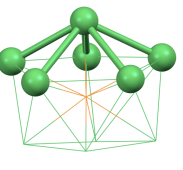
<i>average bond lengths (Å)</i>				
<i>type of moiety</i>	<i>interstitial</i>	<i>intra-base</i>	<i>inter-base</i>	<i>capping</i>
				
	$2.36 \pm 0.05$	$2.63 \pm 0.07$	$2.59 \pm 0.19$	$2.65 \pm 0.07$
<i>Ni<sub>10</sub>(μ<sub>10</sub>-P)</i>	$2.35 \pm 0.03$	$2.60 \pm 0.07$	$2.7 \pm 0.3$	$2.68 \pm 0.11$
	$2.36 \pm 0.06$	$2.65 \pm 0.09$	$2.56 \pm 0.15$	$2.65 \pm 0.04$
	$2.35 \pm 0.07$	$2.65 \pm 0.06$	$2.53 \pm 0.11$	$2.62 \pm 0.04$
<i>Ni<sub>10</sub>(μ<sub>10</sub>-Sb)</i>	$2.63 \pm 0.05$	$2.66 \pm 0.16$	$2.79 \pm 0.13$	$2.70 \pm 0.13$
	$2.62 \pm 0.04$	$2.62 \pm 0.16$	$2.92 \pm 0.16$	$2.68 \pm 0.08$
	$2.63 \pm 0.05$	$2.69 \pm 0.17$	$2.73 \pm 0.10$	$2.71 \pm 0.17$

Table 8.4 - Set of values referred to the different types of bonds within the Ni<sub>10</sub>(μ<sub>10</sub>-P) and the Ni<sub>10</sub>(μ<sub>10</sub>-Sb) moieties. In both cases, the overall average value has been reported along with the average values calculated for each single Ni<sub>10</sub>(μ<sub>10</sub>-E) moiety.

The data revealed that Ni<sub>10</sub>(μ<sub>10</sub>-P) and Ni<sub>10</sub>(μ<sub>10</sub>-Sb) differed the most in terms of heteroatom-nickel bond distance. This behaviour was expected, and was clearly related to the different dimensions of the heteroatoms. Apart from that, the Ni<sub>10</sub>(μ<sub>10</sub>-E) moieties displayed very similar average values for all the types of nickel-nickel interaction but the inter-base interactions. The intra-base and the capping average bond distances were, in both cases, comparable to the reference nickel-nickel average bond length - 2.61 Å. However, it was possible to notice that in both structures the inter-base interactions were slightly elongated.

By taking these considerations into account it was possible to hypothesise that if the nickel-antimony sub-unit had been closed then Ni<sub>10</sub>(μ<sub>10</sub>-Sb) would have had the same dimensions as Ni<sub>10</sub>(μ<sub>10</sub>-P), and therefore the nickel cage would have not been large enough to host the bulkier antimony atom. The opening of the metallic

cages of  $\text{Ni}_{10}(\mu_{10}\text{-Sb})$  - and the resulting semi-interstitial position of the antimony atoms - was therefore due to the larger covalent radius of the heteroatom.

\*\*\*

The molecular structure of the  $[\text{Ni}_{31}\text{Sb}_4(\text{CO})_{40}]^{6-}$  hexa-anion presented another feature that was comparable to those seen in nickel-phosphorus carbonyl clusters. As aforementioned, within its metallic skeleton there were two fully-interstitial nickel atoms, which were enclosed inside fourteen-membered heteroatomical cavities. The two corresponding  $\text{Ni}_{11}\text{Sb}_3(\mu_{14}\text{-Ni})$  moieties were very similar to each other, and in part related to the  $\text{Ni}_{11}\text{P}_3(\mu_{14}\text{-Ni})$  ones - that had been individuated in the molecular structures of  $[\text{H}_2\text{Ni}_{31}\text{P}_4(\text{CO})_{39}]^{4-}$  and  $[\text{HNi}_{31}\text{P}_4(\text{CO})_{39}]^{5-}$ .

In terms of coordination number and structural arrangement, the two types of nickel-hosting cavities were almost matching. In both cases the interstitial nickel atoms were within heteroatomical cages, shaped as bi-capped hexagonal antiprisms. The heteroatoms were not in apical position, and instead were within the hexagonal rings - one  $\text{Ni}_4\text{E}_2$  and one  $\text{Ni}_5\text{E}$  - of the prismatic structures. It is worth to highlight that the geometries of the nickel-antimony sub-structures were far more regular than those of the nickel-phosphorus ones (Figure 8.9).

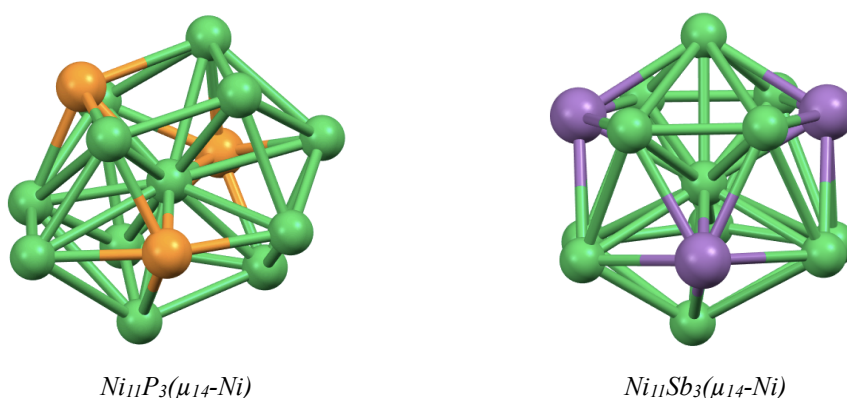


Figure 8.9 - Fourteen-membered nickel-hosting cages,  $\text{Ni}_{11}\text{P}_3(\mu_{14}\text{-Ni})$  (from the structure of  $[\text{H}_2\text{Ni}_{31}\text{P}_4(\text{CO})_{39}]^{4-}$ ) and  $\text{Ni}_{11}\text{Sb}_3(\mu_{14}\text{-Ni})$ . The nickel-phosphorus fragment is far more distorted than the nickel-antimony one. Nickel atoms are represented in green, phosphorus atoms in orange, antimony atoms in purple.

Moreover, the couple of moieties that was present in each molecular structure was interpenetrating into very similar macro-fragments (Figure 8.10). In  $[\text{Ni}_{31}\text{Sb}_4(\text{CO})_{40}]^{6-}$ ,  $[\text{HNi}_{31}\text{P}_4(\text{CO})_{39}]^{5-}$ , and  $[\text{H}_2\text{Ni}_{31}\text{P}_4(\text{CO})_{39}]^{4-}$  it was possible to individuate the larger  $\text{Ni}_{17}\text{Sb}_4(\mu_{14}\text{-Ni})_2$  and  $\text{Ni}_{17}\text{P}_4(\mu_{14}\text{-Ni})_2$  sub-units, respectively - still, in one of the characterised molecular structures of  $[\text{HNi}_{31}\text{P}_4(\text{CO})_{39}]^{5-}$  a  $\text{Ni}_{17}\text{P}_4(\mu_{14}\text{-Ni})(\mu_{13}\text{-Ni})$  moiety was present.

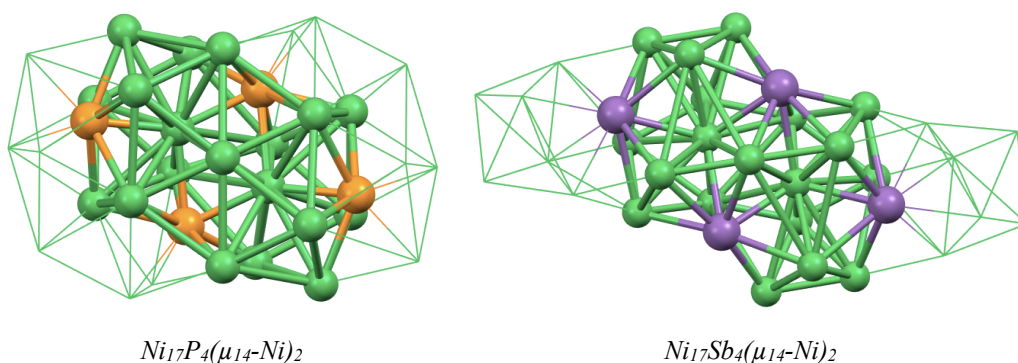
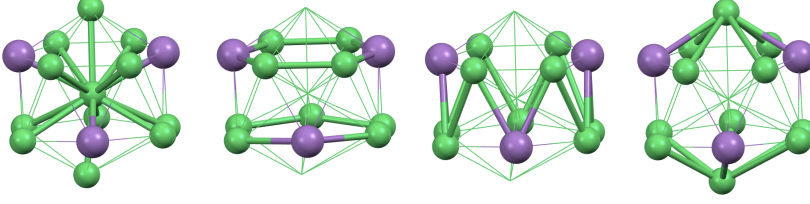


Figure 8.10 - Macro-fragments derived from the interpenetration of two  $\text{Ni}_{11}\text{P}_3(\mu_{14}\text{-Ni})$  or two  $\text{Ni}_{11}\text{Sb}_3(\mu_{14}\text{-Ni})$ . The nickel-phosphorus structure is one of those of  $[\text{HNi}_{31}\text{P}_4(\text{CO})_{39}]^{5-}$ . Nickel atoms are represented in green, phosphorus atoms in orange, antimony atoms in purple.

In order to compare these nickel-centred cavities the bond distances have been analysed (Table 8.5). The heteroatom-nickel bonds and the nickel-nickel bonds have been separately considered. In both cases the interactions have been further divided in intra-base, inter-base, and capping interactions as usual.

By comparing these data-sets it was possible to understand for what reason the nickel-phosphorus and the nickel-antimony polyhedra had such different shapes, despite sharing the same structural arrangement.

As expected, the nickel-nickel bond lengths displayed similar average values in  $\text{Ni}_{11}\text{P}_3(\mu_{14}\text{-Ni})$  and  $\text{Ni}_{11}\text{Sb}_3(\mu_{14}\text{-Ni})$  - yet in the nickel-antimony moieties they were slightly longer, apart from those in the intra-hexagonal region. Moreover, by considering the nickel-heteroatom bond distances it was possible to notice that the average values were different as they were clearly depending on the characteristic dimensions of the involved atoms.



<i>type of moiety</i>	<i>interstitial</i>	<i>intra-base</i>	<i>inter-base</i>	<i>capping</i>
	<i>average nickel-heteroatom bond lengths (Å)</i>			
	2.21 ± 0.07	2.28 ± 0.06	2.35 ± 0.06	2.49 ± 0.09
<i>Ni<sub>11</sub>P<sub>3</sub>(μ<sub>14</sub>-Ni)</i>	2.21 ± 0.06	2.28 ± 0.06	2.35 ± 0.05	2.49 ± 0.10
	2.21 ± 0.06	2.28 ± 0.06	2.36 ± 0.05	2.50 ± 0.09
	2.21 ± 0.07	2.27 ± 0.06	2.36 ± 0.05	2.53 ± 0.10
	2.21 ± 0.07	2.31 ± 0.04	2.31 ± 0.09	2.45 ± 0.07
<i>Ni<sub>11</sub>Sb<sub>3</sub>(μ<sub>14</sub>-Ni)</i>	2.57 ± 0.07	2.56 ± 0.03	2.68 ± 0.06	2.67 ± 0.07
	2.56 ± 0.07	2.56 ± 0.03	2.68 ± 0.05	2.67 ± 0.08
	2.57 ± 0.07	2.55 ± 0.03	2.69 ± 0.06	2.67 ± 0.06
	<i>average nickel-nickel bond lengths (Å)</i>			
	2.65 ± 0.08	2.59 ± 0.10	2.59 ± 0.06	2.67 ± 0.13
<i>Ni<sub>11</sub>P<sub>3</sub>(μ<sub>14</sub>-Ni)</i>	2.65 ± 0.09	2.58 ± 0.09	2.60 ± 0.06	2.67 ± 0.15
	2.65 ± 0.08	2.59 ± 0.10	2.60 ± 0.07	2.68 ± 0.13
	2.65 ± 0.08	2.60 ± 0.11	2.59 ± 0.07	2.65 ± 0.10
	2.64 ± 0.09	2.57 ± 0.10	2.58 ± 0.05	2.67 ± 0.12
<i>Ni<sub>11</sub>Sb<sub>3</sub>(μ<sub>14</sub>-Ni)</i>	2.76 ± 0.16	2.42 ± 0.07	2.75 ± 0.12	2.74 ± 0.16
	2.77 ± 0.16	2.42 ± 0.07	2.75 ± 0.12	2.74 ± 0.16
	2.76 ± 0.15	2.42 ± 0.07	2.74 ± 0.11	2.74 ± 0.16

Table 8.5 - Set of values referred to the different types of bonds within the  $Ni_{11}P_3(\mu_{14}-Ni)$  and the  $Ni_{11}Sb_3(\mu_{14}-Ni)$  moieties. In both cases, the overall average value has been reported along with the average values calculated for each single  $Ni_{11}E_3(\mu_{14}-Ni)$  moiety.  $[Ni_{13}Sb_4(CO)_{40}]^{6-}$  has been used as example to highlight the different regions of the moieties. Nickel atoms are represented in green, antimony atoms in purple.

Interestingly, in  $Ni_{11}Sb_3(\mu_{14}-Ni)$  the average nickel-antimony bond lengths were comparable to the average nickel-nickel bond distances, regardless of the position within the anti-prism. Therefore, the two types of interactions - nickel-antimony and nickel-nickel - that formed the structure of  $Ni_{11}Sb_3(\mu_{14}-Ni)$  were more homogeneous in terms of length than those forming the structure of  $Ni_{11}P_3(\mu_{14}-Ni)$ .

This phenomenon probably allowed to reduce the distortion within the former



nickel-hosting cavity, and therefore its shape was more regular than that of the latter. The presence of shorter nickel-phosphorus bonds within the hexagonal rings of the anti-prisms actually distorted the bases, and restrained them from being either planar or regular. This misshaping had an effect also on the other regions of the cage of  $\text{Ni}_{11}\text{P}_3(\mu_{14}\text{-Ni})$ , thus its peculiar shape.

### ***Comparison with other heteroatomical transition metals structures***

When first advancing hypotheses on the possible structural arrangement of nickel-phosphorus homoleptic carbonyl clusters, it had been assumed that their structures would have been comparable to those of other known nickel-pnictogen carbonyl clusters. Indeed, in that family of compounds most species shared similar structural features and so it would have been reasonable to discover analogous structure.

However, as shown in the previous sections, despite there being some common features between nickel-phosphorus and nickel-pnictogen clusters, they were minor. Most nickel-pnictogen clusters known in the literature had icosahedral structures, whilst just the high-nuclearity  $[\text{Ni}_{39}\text{P}_3(\text{CO})_{44}]^{6-}$  displayed that type of coordination. At the same time, only within the molecular structure of  $[\text{Ni}_{31}\text{Sb}_4(\text{CO})_{40}]^{6-}$  it was possible to individuate sub-structures that were relatable to those of nickel-phosphorus homoleptic carbonyl clusters.

With the aim to better investigate the relationships between this novel class of compounds and other clusters, the focus was shifted to different types of carbonyl species. In particular, transition metal-phosphorus carbonyl clusters were taken into account.

Interestingly, it emerged that other VIII group-transition metals - *i.e.* metals belonging to the iron, the cobalt, and the nickel groups - formed phosphido clusters that shared structural features with nickel-phosphorus species. More in detail, cobalt-phosphorus, ruthenium-phosphorus, and rhodium-phosphorus clusters displayed relatable arrangements to those of nickel-phosphorus clusters. It might even be possible to consider nickel-phosphorus species to be more similar to these

heteroatomical transition metal clusters rather than to nickel-pnictogen compounds.

In the ensuing section these species will be thoroughly described. However, it is worth to mention that all the phosphorus atoms in these clusters displayed a coordination number equal to eight, despite being enclosed in larger metallic cages. No phosphorus atom in nickel environments had been observed having a coordination number equal to eight, yet the phosphorus-hosting cages of these cobalt, ruthenium, and rhodium species were extremely similar to those of the nickel-phosphorus clusters.

#### ♦ *Squared anti-prismatic metallic cages*

In this chapter transition metal-phosphorus clusters will be introduced - cobalt-phosphorus clusters as  $[\text{Co}_9\text{P}(\text{CO})_{21}]^{2-}$  and  $[\text{Co}_{10}\text{P}(\text{CO})_{22}]^{3-}$ ,<sup>1</sup> ruthenium-phosphorus clusters as  $[\text{Ru}_8\text{P}(\text{CO})_{22}]^-$ ,<sup>2</sup> and rhodium-phosphorus clusters as  $[\text{Rh}_9\text{P}(\text{CO})_{21}]^{2-}$  and  $[\text{Rh}_{10}\text{P}(\text{CO})_{22}]^{3-}$ .<sup>3,4</sup>

All these species displayed low-nuclearities. Due to this, their metallic skeletons were almost coincident with the phosphorus-hosting moieties. A brief description of their metallic frameworks will ensue, and since all these carbonyl clusters displayed extremely similar molecular structures (Figure 8.11) they will be compared.

Considering the  $[\text{Ru}_8\text{P}(\text{CO})_{22}]^-$  mono-anion, its metallic skeleton was shaped as a fairly regular phosphorus-centred squared anti-prism, and the coordination number of the phosphorus atom was equal to eight. The metallic cage of ruthenium atoms will be taken as reference, as the other cobalt-phosphorus and rhodium-phosphorus species displayed derivative structures.

---

<sup>1</sup> G. Ciani, A. Sironi, S. Martinengo, L. Garlaschelli, R. Della Pergola, P. Zanello, F. Laschi, N. Masciocchi; *Inorg. Chem.*, **2001** (40) 3905-3911

<sup>2</sup> M. D. Randles, A. C. Willis, M. P. Cifuentes, M. G. Humphrey; *Acta Cryst.*, **2006** (E62) m2350-m2351

<sup>3</sup> J. L. Vidal, W. E. Walker, R. L. Pruett, R. C. Schoening; *Inorg. Chem.*, **1979** (18) 129-136

<sup>4</sup> J. L. Vidal, W. E. Walker, R. C. Schoening; *Inorg. Chem.*, **1981** (20) 238-242

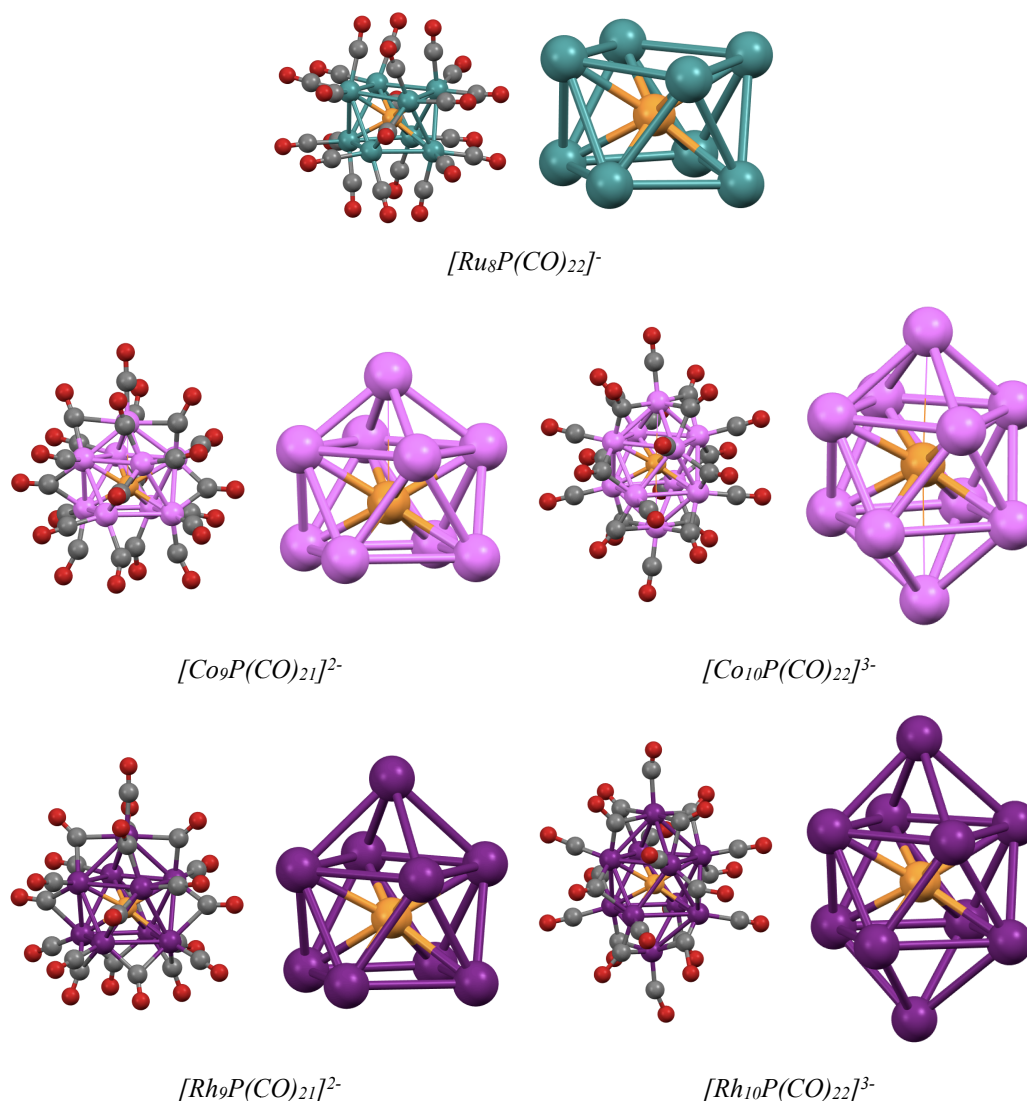


Figure 8.11 - Molecular structures and metallic skeletons of cobalt-phosphorus, ruthenium-phosphorus, and rhodium-phosphorus carbonyl clusters. Cobalt atoms are represented in pink, ruthenium atoms in petrol-blue, rhodium atoms in violet, phosphorus atoms in orange, carbon atoms in grey, oxygen atoms in red.

For what concerns  $[Co_9P(CO)_{21}]^{2-}$  and  $[Rh_9P(CO)_{21}]^{2-}$ , these two clusters were isoelectronic as well as isostructural. The metallic cages of cobalt or rhodium atoms were shaped as mono-capped squared anti-prisms, centred by the heteroatom. Compared to  $[Ru_8P(CO)_{22}]^-$ , these species only differed for a single capping atom.

Finally,  $[Co_{10}P(CO)_{22}]^{3-}$  and  $[Rh_{10}P(CO)_{22}]^{3-}$  were isoelectronic and isostructural as well. Their metallic cages were shaped as phosphorus-centred bi-capped squared anti-prisms. Compared to  $[Ru_8P(CO)_{22}]^-$ , they displayed caps on both bases of the metallic anti-prisms.

Before proceeding, it is important to highlight that in all these newly introduced carbonyl compounds the coordination number of the phosphorus atoms was equal to eight, regardless of the nuclearity of the cluster. In fact, there was no interaction between the capping metal atoms and the interstitial phosphorus atoms. In light of this, it was possible to consider the phosphorus-hosting moieties as follows:  $\text{Ru}_8(\mu_8\text{-P})$ ,  $\text{Co}_9(\mu_8\text{-P})$ ,  $\text{Co}_{10}(\mu_8\text{-P})$ ,  $\text{Rh}_9(\mu_8\text{-P})$ , and  $\text{Rh}_{10}(\mu_8\text{-P})$ .

By observing the structures of these moieties, it appeared clear that they were not only similar to each other, but that they were also closely related to the previously introduced  $\text{Ni}_9(\mu_9\text{-P})$  moieties, and in particular to the closed  $\text{Ni}_9(\mu_9\text{-P})$  fragments (Figure 8.12).

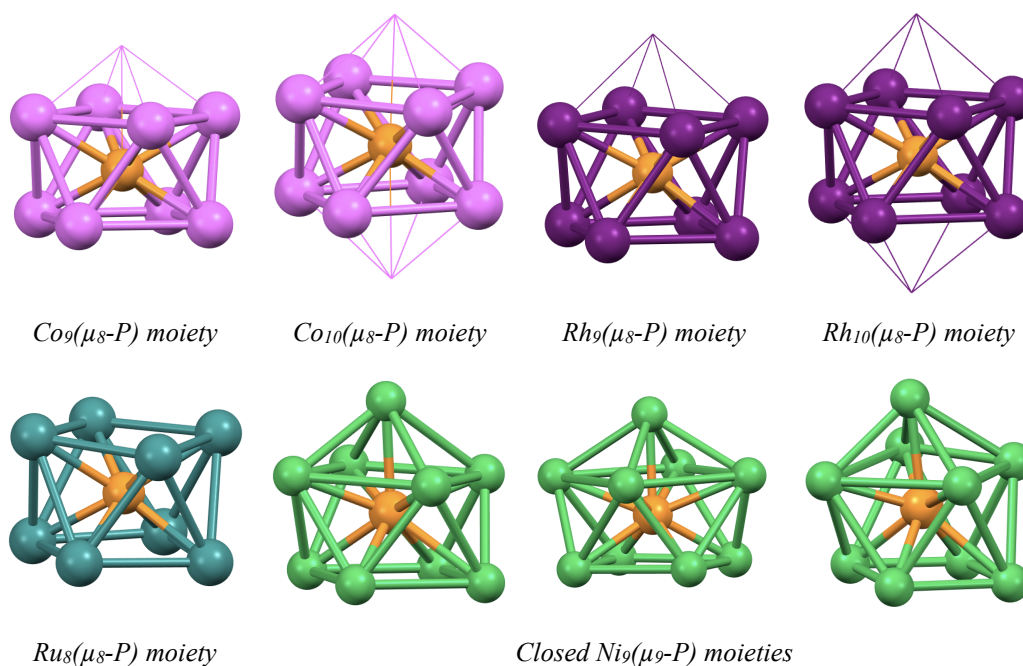


Figure 8.12 - Cobalt, ruthenium, rhodium, and nickel phosphorus-hosting cages. Cobalt atoms are represented in pink, nickel atoms in green, ruthenium atoms in petrol-blue, rhodium atoms in violet, phosphorus atoms in orange.

By comparing these metallic cages it was possible to notice that cobalt, ruthenium, and rhodium atoms formed more regular structures, whilst on the contrary nickel cages were occasionally distorted. Moreover, the capping atoms of the nickel moieties were directly bonded to the interstitial heteroatom.

A comparison between the bond lengths within  $\text{Ni}_9(\mu_9\text{-P})$  and those within  $\text{Co}_9(\mu_8\text{-P})$ ,  $\text{Co}_{10}(\mu_8\text{-P})$ ,  $\text{Ru}_8(\mu_8\text{-P})$ ,  $\text{Rh}_9(\mu_8\text{-P})$ , and  $\text{Rh}_{10}(\mu_8\text{-P})$  has been reported.

The phosphorus-metal bonds and the metal-metal bonds have been separately considered. The latter have been further divided in intra-base, inter-base, and capping interactions as usual (Table 8.6, Figure 8.13). Despite the non-coordinative role of the capping cobalt and rhodium atoms towards the heteroatoms, the corresponding bonds have been considered for consistency purposes.

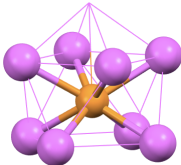
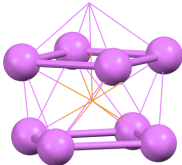
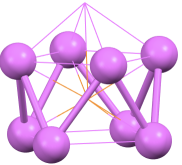
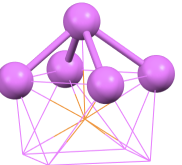
		<i>average bond lengths (Å)</i>			
					
<i>type of moiety</i>		<i>interstitial</i>	<i>intra-base</i>	<i>inter-base</i>	<i>capping</i>
<i>closed Ni<sub>9</sub>(μ<sub>9</sub>-P)</i>		$2.31 \pm 0.08$	$2.8 \pm 0.2$	$2.68 \pm 0.09$	$2.63 \pm 0.05$
		$2.30 \pm 0.08$	$2.88 \pm 0.10$	$2.59 \pm 0.10$	$2.61 \pm 0.13$
		$2.32 \pm 0.07$	$2.8 \pm 0.3$	$2.73 \pm 0.11$	$2.629 \pm 0.011$
		$2.32 \pm 0.09$	$2.8 \pm 0.2$	$2.72 \pm 0.11$	$2.616 \pm 0.005$
		$2.32 \pm 0.07$	$2.8 \pm 0.3$	$2.74 \pm 0.12$	$2.622 \pm 0.010$
		$2.32 \pm 0.08$	$2.8 \pm 0.3$	$2.72 \pm 0.11$	$2.635 \pm 0.010$
		$2.32 \pm 0.07$	$3.0 \pm 0.2$	$2.56 \pm 0.13$	$2.626 \pm 0.012$
		$2.30 \pm 0.09$	$2.72 \pm 0.16$	$2.70 \pm 0.06$	$2.63 \pm 0.09$
		$2.29 \pm 0.07$	$2.73 \pm 0.17$	$2.67 \pm 0.03$	$2.63 \pm 0.09$
		$2.30 \pm 0.08$	$2.73 \pm 0.17$	$2.69 \pm 0.03$	$2.63 \pm 0.09$
	$2.30 \pm 0.08$	$2.66 \pm 0.12$	$2.69 \pm 0.08$	$2.64 \pm 0.09$	
<i>Co<sub>9</sub>(μ<sub>8</sub>-P) and Co<sub>10</sub>(μ<sub>8</sub>-P)</i>		$2.26 \pm 0.02$	$2.81 \pm 0.03$	$2.63 \pm 0.05$	$2.55 \pm 0.06$
		$2.260 \pm 0.010$	$2.81 \pm 0.03$	$2.63 \pm 0.06$	$2.59 \pm 0.03$
		$2.26 \pm 0.02$	$2.81 \pm 0.02$	$2.63 \pm 0.04$	$2.47 \pm 0.06$
<i>Ru<sub>8</sub>(μ<sub>8</sub>-P)</i>		$2.407 \pm 0.009$	$2.948 \pm 0.018$	$2.89 \pm 0.04$	/
<i>Rh<sub>9</sub>(μ<sub>8</sub>-P) and Rh<sub>10</sub>(μ<sub>8</sub>-P)</i>		$2.43 \pm 0.03$	$3.00 \pm 0.03$	$2.86 \pm 0.03$	$2.87 \pm 0.03$
		$2.42 \pm 0.02$	$2.98 \pm 0.02$	$2.883 \pm 0.011$	$2.880 \pm 0.009$
		$2.43 \pm 0.04$	$3.02 \pm 0.02$	$2.84 \pm 0.03$	$2.87 \pm 0.07$

Table 8.6 - Set of values referred to the different bonds within  $\text{Ni}_9(\mu_9\text{-P})$ ,  $\text{Co}_9(\mu_8\text{-P})$ ,  $\text{Co}_{10}(\mu_8\text{-P})$ ,  $\text{Ru}_8(\mu_8\text{-P})$ ,  $\text{Rh}_9(\mu_8\text{-P})$ , and  $\text{Rh}_{10}(\mu_8\text{-P})$ . In all cases, the overall average value has been reported along with the average values calculated for each single moiety.  $[\text{Co}_9\text{P}(\text{CO})_{21}]^{2-}$  has been used as example to highlight the different regions of the moieties. Cobalt atoms are represented in pink, phosphorus atoms in orange.

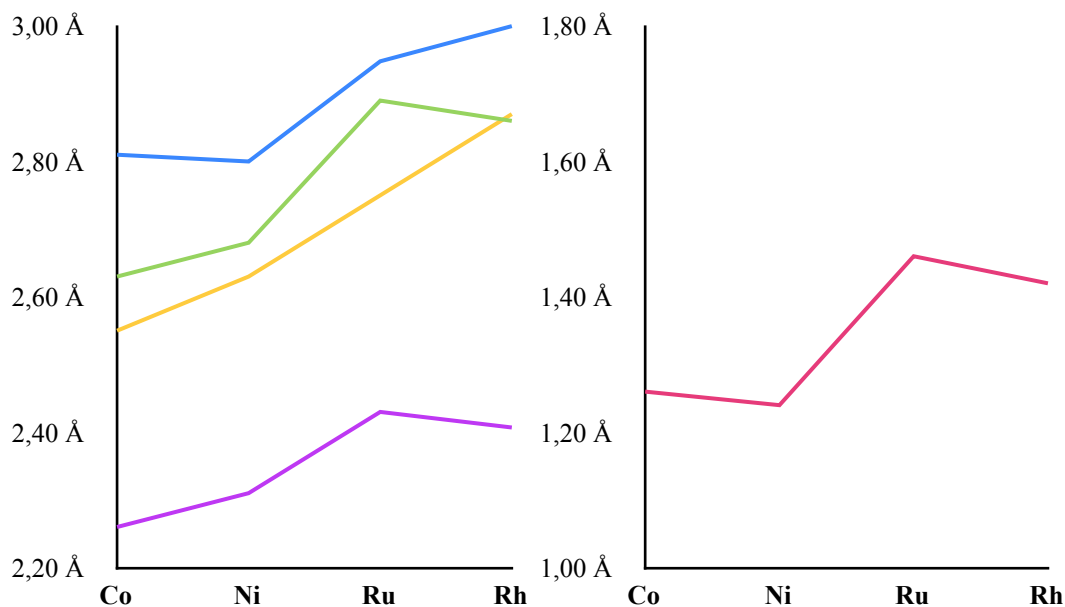


Figure 8.13 - On the left, plot showing the variation of the mean distances as a function of the metallic element - cobalt, nickel, ruthenium, rhodium - for each of the three kinds of edges in the  $Co_9(\mu_8-P)$ ,  $Co_{10}(\mu_8-P)$ ,  $Ni_9(\mu_9-P)$ ,  $Ru_8(\mu_8-P)$ ,  $Rh_9(\mu_8-P)$  and in the  $Rh_{10}(\mu_8-P)$  moieties. On the right, plot showing the trend of the covalent radii of the metallic elements. The intra-pentagonal interactions are reported in blue, the inter-pentagonal interactions in green, the capping interactions in orange, the metal-phosphorus interactions in purple, the covalent radii in red.

The data revealed some unforeseen behaviours. First, the values of the cobalt-cobalt, ruthenium-ruthenium, and rhodium-rhodium bond distances were narrowly dispersed, in contrast to those of the nickel-nickel interactions which were widely dispersed.

Eventually, further interesting behaviours emerged. First, it was possible to notice that for these metal-phosphorus clusters there was a looser-than-usual correlation between the trend followed by the metallic covalent radii and those followed by the average bond lengths within the structures. Indeed, the first-series transition metals displayed smaller covalent radii than the second-series transition metals, and so formed shorter in-cluster interactions. However, by comparing cobalt and nickel, it emerged that the slightly larger cobalt atoms exhibited shorter bond lengths in the interstitial, inter-base, and capping regions of the moieties. Analogously, by comparing ruthenium and rhodium, it emerged that the larger ruthenium atoms formed shorter interactions in the inter-base region of the moieties. However, in all cases these deviations from the expected trend were moderate and

could be associated with the different dimensions of the metallic cages.

Besides, it was noted that in  $\text{Co}_9(\mu_8\text{-P})$ ,  $\text{Co}_{10}(\mu_8\text{-P})$ , and  $\text{Ni}_9(\mu_9\text{-P})$  the intra-base bonds were quite elongated and their average values were *circa* 7% higher than those in the intra-base and capping regions of the cages. A similar phenomenon occurred in  $\text{Ru}_8(\mu_8\text{-P})$ ,  $\text{Rh}_9(\mu_8\text{-P})$ , and  $\text{Rh}_{10}(\mu_8\text{-P})$ , yet to a minor extent - their average intra-base bond distances were less than 5% longer than the other ruthenium-ruthenium and rhodium-rhodium bonds.

Still, in all the phosphorus-hosting moieties the mean intra-base interactions were longer than the other types of interactions, regardless of the nature of the metallic atom. Considering that in  $\text{Ru}_8(\mu_8\text{-P})$  the difference between intra-base and inter-base interactions was minimal, it was presumed that the presence of the capping atoms could have influenced the other moieties. This hypothesis was further supported by the fact that the difference between intra-base and inter-base interactions was maximum in  $\text{Ni}_9(\mu_9\text{-P})$  - the only type of moiety in which the phosphorus atom was actually interacting with the metallic capping atom.

Having said that, the characteristics of the nickel-phosphorus moieties still appeared not entirely fitting with those of the other metal-phosphorus ones. First, the  $\text{Ni}_9(\mu_9\text{-P})$  moieties were irregularly shaped. Second, the values of their bond lengths were not narrowly dispersed. Third, the extent of the elongation of their intra-base interactions was the most severe. If these structures had been compared to  $\text{Ru}_8(\mu_8\text{-P})$ ,  $\text{Rh}_9(\mu_8\text{-P})$ , and  $\text{Rh}_{10}(\mu_8\text{-P})$  only, the above-listed dissimilarities would have been attributed to the smaller dimensions of the nickel atoms compared to those of the second-series transition metals. However, this hypothesis was rebutted by the existence of two cobalt-phosphorus moieties whose characteristics were well-fitting with those of the ruthenium-phosphorus and the rhodium-phosphorus moieties. It was therefore supposed that the differences were due to the coordination number of the heteroatoms, which was equal to eight in all moieties except for the nickel-phosphorus ones.

It was nonetheless clear that, despite somewhat minor discrepancies, the characteristic geometric model of transition metal-phosphorus clusters was more ap-

appropriate to describe nickel-phosphorus clusters than the geometric model of nickel-pnictogen clusters - based on icosahedral structures.

### ***Comparison with nickel-phosphorus binary phases***

Numerous nickel-phosphorus binary phases had been listed in the introduction. Besides, the diverse types of connectivity displayed by the nickel and the phosphorus atoms have been briefly described, considering the few data available.

For instance, it was said that in  $\text{Ni}_5\text{P}_4$  the phosphorus atoms displayed four different and rather complex types of connectivity, and were inside heteroatomical macro-cages (Figure 8.14). These coordination polyhedra were interestingly shaped, yet their structures did not correlate to those of nickel-phosphorus homoleptic carbonyl clusters.

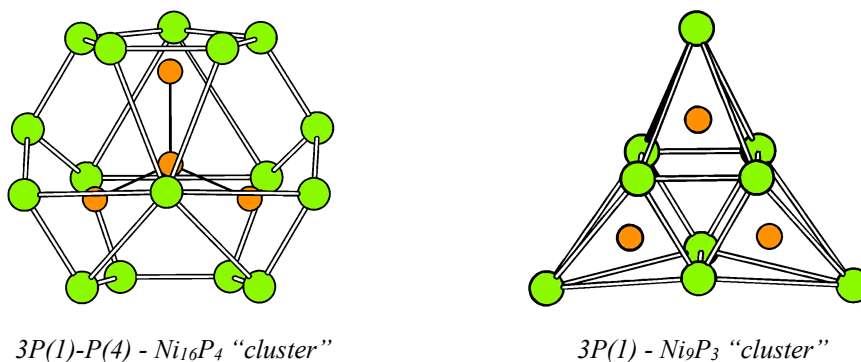


Figure 8.14 - Graphical representation of the “clusters” resulting from the interpenetration of coordination polyhedra of nickel and phosphorus atoms in the  $\text{Ni}_5\text{P}_4$  binary phase. It is interesting to notice that in  $\text{Ni}_{16}\text{P}_4$  (on the left) there are direct interactions between phosphorus atoms, whilst in  $\text{Ni}_9\text{P}_3$  (on the right) there is none. Nickel atoms are represented in green, phosphorus atoms in orange.

$\text{Ni}_5\text{P}_2$  has two structures and exists both as LT- $\text{Ni}_5\text{P}_2$  and HT- $\text{Ni}_5\text{P}_2$  - low and high temperature, respectively. Both displayed only three different coordination sites available for the phosphorus atoms. In the former phase it was possible to identify three completely different types of coordination. In the latter phase there was more homogeneity, as all the phosphorus atoms were inside similar polyhe-



dra. In  $LT-Ni_5P_2$  as well as in  $HT-Ni_5P_2$  there were no direct phosphorus-phosphorus interactions. Due to the characteristics that will be highlighted in the ensuing section, these coordination polyhedra have been tentatively compared to the moieties that were within nickel-phosphorus carbonyl clusters.

♦ ***Coordination polyhedra of  $LT-Ni_5P_2$  and  $HT-Ni_5P_2$***

For what concerns  $LT-Ni_5P_2$ , it presented three different types of coordination for the phosphorus atoms (Figure 8.15). Their structures were far more simple than those seen in  $Ni_5P_4$ , and were based on prismatic arrangements.

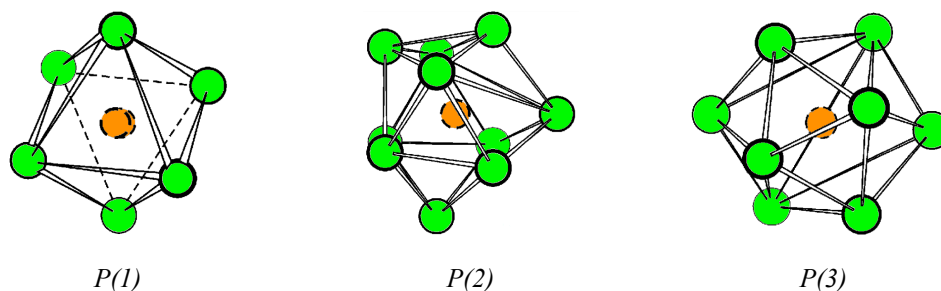


Figure 8.15 - Graphical representation of the three coordination polyhedra of phosphorus atoms in  $LT-Ni_5P_2$ .  $P(1)$  is inside an octahedral polyhedron.  $P(2)$  is inside a bi-capped tetragonal anti-prism.  $P(3)$  is inside a bi-capped triangular prism. Nickel atoms are represented in green, phosphorus atoms in orange.

The first type of phosphorus atoms -  $P(1)$  - was inside a nickel octahedron, the second type -  $P(2)$  - was inside a bi-capped tetragonal anti-prism, and the third type -  $P(3)$  - was inside a bi-capped trigonal prism. Clearly,  $P(1)$  and  $P(3)$  were not related to any of the previously described nickel-phosphorus moieties, yet the coordination polyhedra of  $P(2)$  presented some interesting structural features that were further investigated.

For what concerns  $HT-Ni_5P_2$ , in this binary phase the three different types of coordination were more homogeneous. In fact, all the coordination polyhedra were shaped as bi-capped tetragonal anti-prisms, and therefore they were not only similar to each other but similar to the  $P(2)$ -polyhedron of  $LT-Ni_5P_2$  as well.

It appeared clear that these configurations - the  $P(2)$  polyhedron of  $LT-Ni_5P_2$ , and the three polyhedra of  $HT-Ni_5P_2$ , which further on will be all addressed to as  $P(2)$ -configurations - shared some features with the previously described nickel-phosphorus moieties. Despite their evident distortion,  $P(2)$ -configurations were based on a tetragonal anti-prismatic geometry that could be compared to the squared anti-prismatic geometry observed in many nickel-phosphorus carbonyl clusters. Bearing in mind that these  $P(2)$ -configurations were found in binary phases, which are completely different from carbonyl clusters, a comparison between the nickel-phosphorus interactions has been proposed (Table 8.7).

<i>type of moiety or polyhedron</i>	<i>nickel-phosphorus bond lengths (Å)</i>	
	<i>average value</i>	<i>minimum value</i>
<i>cluster moieties</i>	$2.33 \pm 0.09$	2.15
<i>LT-Ni<sub>5</sub>P<sub>2</sub> polyhedra</i>	$2.35 \pm 0.07$	2.22
<i>HT-Ni<sub>5</sub>P<sub>2</sub> polyhedra</i>	$2.34 \pm 0.08$	2.20

Table 8.7 - Set of values referred to the nickel-phosphorus bonds within the phosphorus-hosting nickel cages of clusters and within the coordination polyhedra of selected binary phases.

The data revealed that the interactions occurring between nickel atoms and phosphorus atoms within these two environments were comparable. Therefore it was possible to assume that nickel-phosphorus carbonyl clusters shared some structural features with nickel-phosphorus binary phases, in terms of not only structural configurations but of bond lengths as well.

However, due to the intrinsic difference of these two nickel-phosphorus systems and due to the scarcity of available data, this comparison should be carefully considered.

# Summary and conclusions

In the ensuing sections the most important features that had been listed in the previous chapters will be summarised and proposed in a more organic fashion. The information that had been gathered regarding the behaviour of nickel-phosphorus homoleptic carbonyl clusters were remarkable, yet to understand their relationship with other cluster species was challenging.

First, the most significant features of this new family of cluster compounds will be reported. Then, the most relevant characteristics that were discovered for each species will be summarised. Any common trait with already known groups of carbonyl clusters will be further highlighted. Finally, the collected knowledge will be used in order to draw some conclusions.

## Summary

The formerly introduced nickel-phosphorus carbonyl clusters proved to have interesting and novel characteristics. In the following section a brief account of their properties and a comparison with those of other nickel-pnictogen clusters and transition metal-phosphorus carbonyl clusters will be proposed.

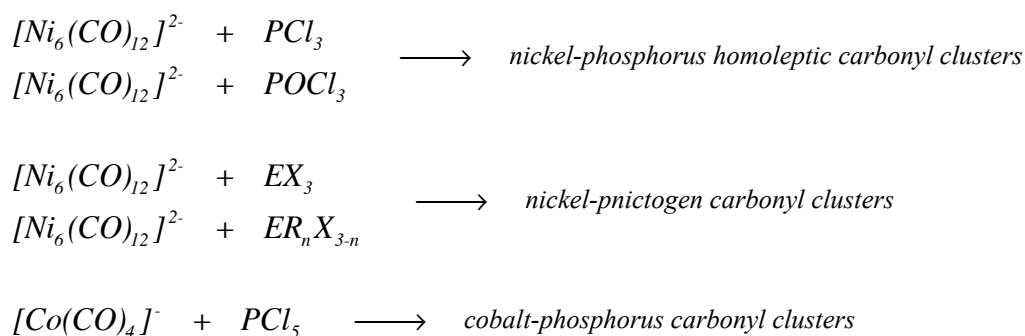
This discussion will separately account for synthetic strategies, structural features as nuclearity and other characteristics, and reactivity.

## *Syntheses*

Concerning the syntheses that had been described for nickel-phosphorus homoleptic carbonyl cluster (Scheme 9.1), they were in accord with the reactions reported in the literature for other nickel-pnictogen clusters and transition metal-phosphorus clusters.

In fact, most nickel and group-15 elements clusters can be obtained by carrying out the reaction between a nickel cluster precursor -  $[\text{Ni}_6(\text{CO})_{12}]^{2-}$  - and an appro-

appropriate pnictogen halide -  $EX_3$  or  $ER_nX_{3-n}$  (Scheme 9.1).<sup>1</sup> Analogously, some transition metal-phosphorus clusters can be synthesised through similar processes. For instance, cobalt-phosphorus carbonyl clusters are formed when  $[Co(CO)_4]^-$  is oxidised by  $PCl_5$  (Scheme 9.1).<sup>2</sup> However, the syntheses that are reported in the literature for this group of clusters are less homogeneous and often require to use exotic reactants or catalysts. For example, rhodium-phosphorus clusters can be obtained in presence of caesium benzoate.<sup>3, 4</sup>



Scheme 9.1 - Representation of the basic syntheses for different families of carbonyl clusters.

Interestingly, all the newly discovered clusters shared remarkably similar synthetic pathways and just by changing the operative conditions it was possible to tune the processes and to obtain the selected species (Table 9.1).

For what concerns the processes known by the literature, in most cases it was necessary to use different reactants to obtain different species. However, another sub-group of nickel-pnictogen clusters displayed a behaviour that was analogous to that of nickel-phosphorus homoleptic carbonyl clusters - *i.e.* nickel-antimony clusters.<sup>5, 6, 7</sup>

- 
- <sup>1</sup> P. D. Mlynek; L. F. Dahl; *Organometallics*, **1997** (16) 1655-1667
  - <sup>2</sup> G. Ciani, A. Sironi, S. Martinengo, L. Garlaschelli, R. Della Pergola, P. Zanello, F. Laschi, N. Masciocchi; *Inorg. Chem.*, **2001** (40) 3905-3911
  - <sup>3</sup> J. L. Vidal, W. E. Walker, R. L. Pruett, R. C. Schoening; *Inorg. Chem.*, **1979** (18) 129-136
  - <sup>4</sup> J. L. Vidal, W. E. Walker, R. C. Schoening; *Inorg. Chem.*, **1981** (20) 238-242
  - <sup>5</sup> V. G. Albano, F. Demartin, M. C. Iapalucci, F. Laschi, G. Longoni, A. Sironi, P. Zanello; *J. Chem. Soc., Dalton Trans.*, **1991** (S) 739-748
  - <sup>6</sup> V. G. Albano, F. Demartin, C. Femoni, M. C. Iapalucci, G. Longoni, M. Monari, P. Zanello; *Journal of Organometallic Chemistry*, **2000** (593-594) 325-334
  - <sup>7</sup> C. Femoni, M. C. Iapalucci, G. Longoni, P. H. Svensson; *Chem. Commun.*, **2000** (8) 655-656

In fact,  $[\text{Ni}_{13}\text{Sb}_2(\text{CO})_{24}]^{3-}$ ,  $[\text{Ni}_{11}\text{Sb}_2(\text{CO})_{18}]^{3-}$ ,  $[\text{Ni}_{15}\text{Sb}(\text{CO})_{24}]^{2-}$ , and  $[\text{Ni}_{31}\text{Sb}_4(\text{CO})_{40}]^{6-}$  can be obtained by using the same reactants with different stoichiometric ratios.

	$[\text{Ni}_{11}\text{P}(\text{CO})_{18}]^{3-}$	$[\text{Ni}_{14}\text{P}_2(\text{CO})_{22}]^{2-}$	$[\text{Ni}_{23-x}\text{P}_2(\text{CO})_{30-x}]^{4-}$
<i>solvent</i>	THF	dichloromethane	THF or acetonitrile
<i>reactant</i>	$\text{PCl}_3$	$\text{PCl}_3$	$\text{POCl}_3$
<i>S. R.</i>	1 : 0.5	1 : 0.5	1 : 0.8
<i>counter-ion</i>	$[\text{NEt}_4]^+$	$[\text{NBu}_4]^+$	$[\text{NEt}_4]^+$
	$[\text{Ni}_{29}\text{P}_5(\text{PO})(\text{CO})_{36}]^{5-}$	$[\text{HNi}_{31}\text{P}_4(\text{CO})_{39}]^{5-}$	$[\text{Ni}_{39}\text{P}_3(\text{CO})_{44}]^{6-}$
<i>solvent</i>	THF, acetone	THF or acetonitrile	THF
<i>reactant</i>	$\text{PCl}_3$ , Au(I) salts	$\text{PCl}_3$	$\text{POCl}_3$
<i>S. R.</i>	unknown	1 : 0.7	unknown
<i>counter-ion</i>	$[\text{NMe}_3\text{Oct}]^+$ , $[\text{NEt}_4]^+$	$[\text{NEt}_4]^+$	$[\text{NEt}_4]^+$

Table 9.1 - Different operative conditions lead to the formation of different cluster products, even by using the same nickel and phosphorus reactants. The S.R. is referred to  $[\text{Ni}_6(\text{CO})_{12}]^{2-}$ .

Therefore, in terms of synthetic pathways it was possible to consider the new group of nickel-phosphorus homoleptic carbonyl clusters to be well-fitting in the larger family of the nickel-pnictogen carbonyl clusters.

In fact, it has been shown that transition metal-phosphorus clusters are synthesised through different and heterogenous reactions. On the contrary, all nickel-pnictogen species are formed via analogous reactions, that also corresponded to those with which nickel-phosphorus homoleptic carbonyl compounds were obtained. Moreover, the behaviour of the nickel-antimony sub-group of clusters was surprisingly similar to that of this newly presented family of species.

### ***Nuclearities***

It was possible to notice that these new nickel-phosphorus homoleptic carbonyl species displayed quite a wide range of nuclearities - *i.e.* number of metallic at-

oms. Low-nuclearity, medium-nuclearity, and high-nuclearity clusters belonging to this family of compounds existed - *e.g.*  $[\text{Ni}_{14}\text{P}_2(\text{CO})_{22}]^{2-}$ ,  $[\text{Ni}_{23-x}\text{P}_2(\text{CO})_{30-x}]^{4-}$ , and  $[\text{HNi}_{31}\text{P}_4(\text{CO})_{39}]^{5-}$  (Figure 9.1).

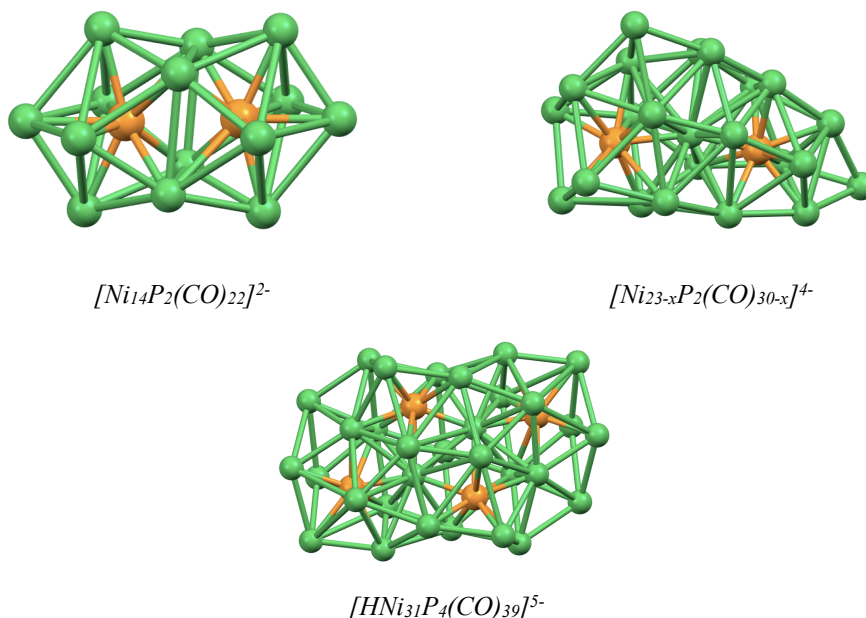


Figure 9.1 - Metallic skeletons of nickel-phosphorus carbonyl clusters with different nuclearities. Examples of low-nuclearity, medium-nuclearity, and high-nuclearity species have been reported. Nickel atoms are represented in green, phosphorus atoms in orange.

However, whilst it had been possible to individuate a correspondence in terms of syntheses between these species and nickel-pnictogen clusters, for what concerns the nuclearity their behaviour is rather different from that reported in the literature for related cluster compounds.

In fact, other nickel-pnictogen clusters known in the literature displayed low nuclearities, whose values ranged between ten<sup>1</sup> and fifteen<sup>2</sup> (Figure 9.2) - except for that of  $[\text{Ni}_{31}\text{Sb}_4(\text{CO})_{40}]^{6-}$ . On the contrary, most nickel-phosphorus homoleptic carbonyl clusters had larger metallic skeletons. Only two out of the six newly individuated species presented a comparable nuclearity - *i.e.*  $[\text{Ni}_{11}\text{P}(\text{CO})_{18}]^{3-}$  and  $[\text{Ni}_{14}\text{P}_2(\text{CO})_{22}]^{2-}$ .

<sup>1</sup> P. D. Mlynek; L. F. Dahl; *Organometallics*, **1997** (16) 1655-1667

<sup>2</sup> V. G. Albano, F. Demartin, C Femoni, M. C. Iapalucci, G. Longoni, M. Monari, P. Zanello; *Journal of Organometallic Chemistry*, **2000** (593-594) 325-334

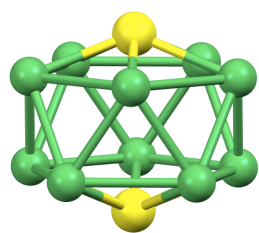
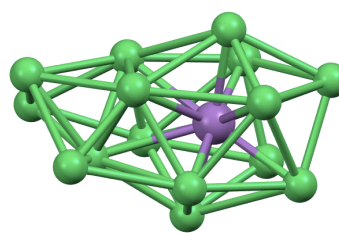

 $[Ni_{10}(AsMe)_2(CO)_{18}]^{2-}$ 

 $[Ni_{15}Sb(CO)_{24}]^{2-}$ 

Figure 9.2 - Metallic skeletons of two low-nuclearity nickel-pnictogen clusters. On the left, one of the nickel-pnictogen species with the lowest nuclearity has been reported. On the right, the nickel-pnictogen species with the second-highest nuclearity has been reported. Nickel atoms are represented in green, arsenic atoms in yellow, antimony atoms in purple.

At the same time, other transition metal-phosphorus clusters known in the literature displayed an even narrower range of nuclearities, going from eight<sup>1</sup> to ten<sup>2</sup> (Figure 9.3). By comparing nickel-phosphorus homoleptic carbonyl clusters to these species, it appeared evident that all had larger metallic skeletons and that only the small  $[Ni_{11}P(CO)_{18}]^{3-}$  tri-anion displayed a comparable nuclearity.

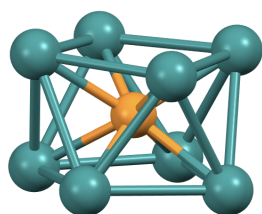
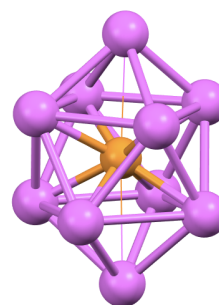

 $[Ru_8P(CO)_{22}]^{-}$ 

 $[Co_{10}P(CO)_{22}]^{3-}$ 

Figure 9.3 - Metallic skeletons of two low-nuclearity transition metal-phosphorus clusters. On the left, the transition metal-phosphorus species with the lowest nuclearity has been reported. On the right, one of the transition metal-phosphorus species with the highest nuclearity has been reported. Cobalt atoms are represented in pink, ruthenium atoms in petrol-blue, phosphorus atoms in orange.

<sup>1</sup> M. D. Randles, A. C. Willis, M. P. Cifuentes, M. G. Humphrey; *Acta Cryst.*, **2006** (E62) m2350-m2351

<sup>2</sup> J. L. Vidal, W. E. Walker, R. C. Schoening; *Inorg. Chem.*, **1981** (20) 238-242

In light of this, it was not possible for nickel-phosphorus homoleptic carbonyl clusters to be regarded as well-fitting in either of these two larger families of cluster compounds. This newly presented group of clusters displayed a much wider range of nuclearities, whilst the other species reported in the literature usually did not grow above a quite reduced number of metallic atoms.

Still, their behaviour was to a certain extent more similar to that of nickel-pnictogen clusters, due to the existence of the high-nuclearity  $[\text{Ni}_{31}\text{Sb}_4(\text{CO})_{40}]^{6-}$ .

### ***Structural characteristics***

In the previous sections it has been shown that nickel-phosphorus carbonyl clusters were rather similar to nickel-pnictogen clusters. They were fitting in that larger group of cluster compounds both in terms of synthesis and of nuclearity. However, their structural characteristics were quite different.

A comprehensive structural comparison between the new nickel-phosphorus homoleptic carbonyl species and other cluster compounds has already been profiled in the previous chapter. In the following paragraphs the most relevant points will be re-proposed.

Briefly, it had been shown that all the metallic skeletons of this family of compounds - except for that of  $[\text{Ni}_{39}\text{P}_3(\text{CO})_{44}]^{6-}$  - were based on the merging of mono-capped anti-prismatic moieties (Figure 9.4). The heteroatoms were in interstitial positions and their C.N. was equal to nine or ten.

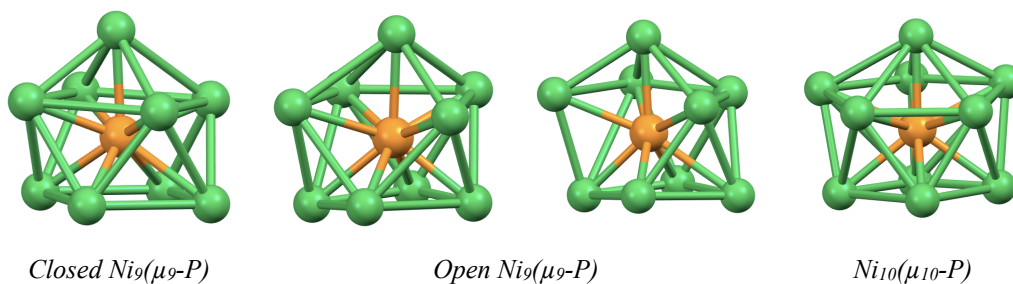


Figure 9.4 - Typical structures of the moieties that were individuated within the metallic skeletons of most nickel-phosphorus homoleptic carbonyl clusters. Nickel atoms are represented in green, phosphorus atoms in orange.



On the contrary, the structures of nickel and group-15 elements clusters - even those of nickel-phosphorus heteroleptic carbonyl clusters - were based on a completely different type of geometry. In most cases the heteroatoms were in apical positions, and the metallic skeletons formed icosahedral structures, both centred and non-centred (Figure 9.5).

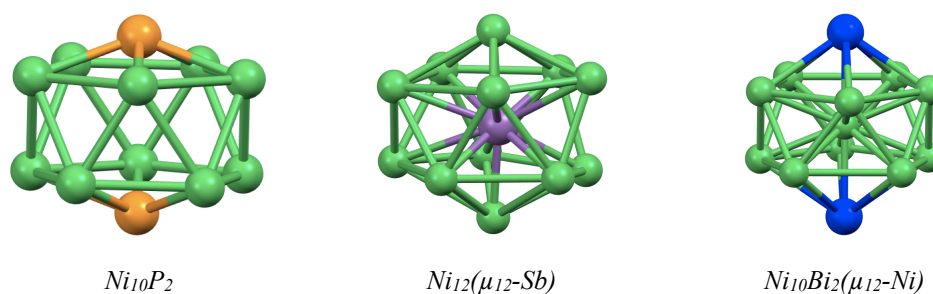


Figure 9.5 - Typical structures of the metallic skeletons of nickel-pnictogen clusters. From left to right, a non-centred framework, an heteroatom-centred framework, and a nickel-centred framework have been reported. Nickel atoms are represented in green, phosphorus atoms in orange, antimony atoms in purple, bismuth atoms in blue.

Furthermore, it had been shown that transition metal-phosphorus species displayed structures that were related to those of nickel-phosphorus homoleptic carbonyl clusters (Figure 9.6). In fact, the metallic frameworks of cobalt-phosphorus, ruthenium-phosphorus, and rhodium-phosphorus clusters were all based on squared anti-prismatic geometries.

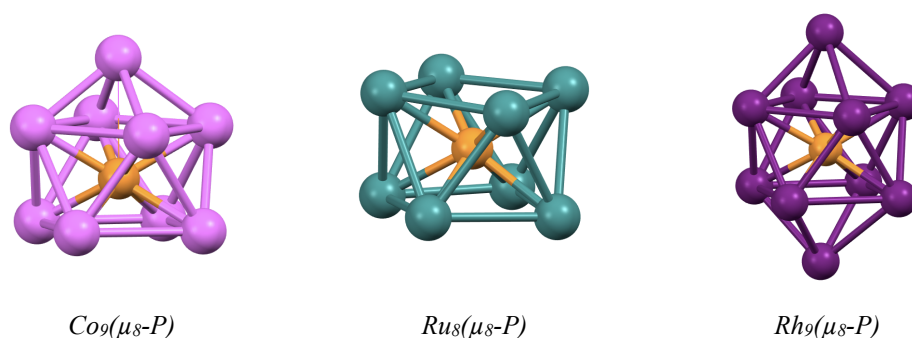


Figure 9.6 - Typical metallic skeletons of transition metal-phosphorus clusters, shaped as squared anti-prisms. From left to right, a mono-capped framework, a non-capped framework, and a bi-capped framework have been reported. Cobalt atoms are represented in pink, ruthenium atoms in petrol-blue, rhodium atoms in violet, phosphorus atoms in orange.

In light of this it was determined that, despite being similar in terms of synthetic approach and nuclearity, nickel-phosphorus homoleptic carbonyl clusters were hardly comparable to other nickel-pnictogen clusters in structural terms.

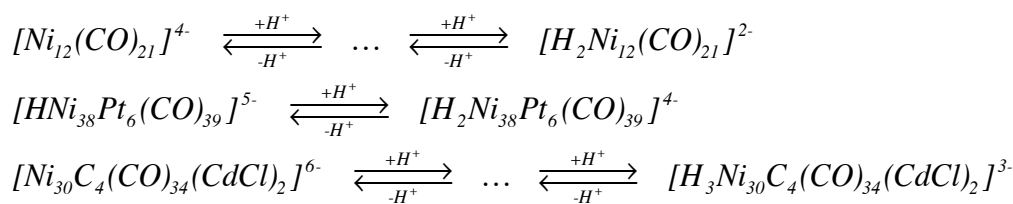
On the contrary, this new group of clusters was closely related to that of transition metal-phosphorus clusters. Due to this, it was possible to assume that the phosphorus atoms had a more significant influence on the structures of the clusters than the nickel atoms.

### Reactivity

For what concerns the reactivity of nickel-phosphorus homoleptic carbonyl clusters, their behaviour will not be only compared to that of nickel-pnictogen or transition metal-phosphorus clusters. A more general report concerning the typical characteristics of carbonyl clusters will be presented.

In particular, it is known that many medium-nuclearity and high-nuclearity carbonyl clusters share some characteristics, as acid-base and redox properties.

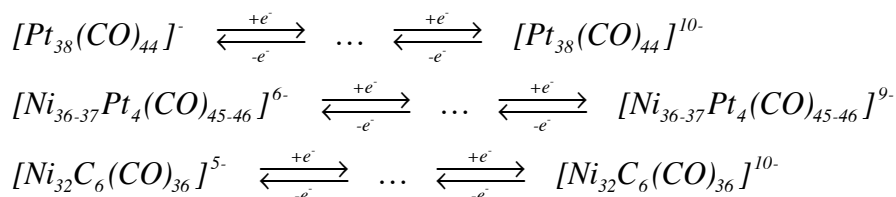
For example, it is common for cluster compounds to exist as distinct polyhydride forms of the same species. This behaviour is featured by different types of clusters - *e.g.* homo-metallic,<sup>1</sup> bi-metallic,<sup>2</sup> and heteroatomical<sup>3</sup> carbonyl clusters (Scheme 9.2).



Scheme 9.2 - Examples of different types of carbonyl clusters that display acid-base properties.

- 
- <sup>1</sup> A. Ceriotti, P. Chini, R. Della Pergola, G. Longoni; *Inorg. Chem.*, **1983** (22) 1595-1598
- <sup>2</sup> A. Ceriotti, F. Dernartin, G. Longoni, M. Manassero, M. Marchionna, G. Piva, M. Sansoni; *Angew. Chem. Int. Ed. Engl.*, **1985** (24) 697-698
- <sup>3</sup> A. Bernardi, C. Femoni, M. C. Iapalucci, G. Longoni, F. Ranuzzi, S. Zacchini, P. Zanello, S. Fedi; *Chem. Eur. J.*, **2008** (14) 1924-1934

Analogously, many cluster compounds are known for their redox properties. It is not unusual for a carbonyl species to bear different anionic charges - *i.e.* to display different oxidation states. As well as for the acid-base properties, redox properties are not linked to a specific category of clusters, and are common for homo-metallic,<sup>1</sup> bi-metallic,<sup>2</sup> and heteroatomical<sup>3</sup> species (Scheme 9.3).

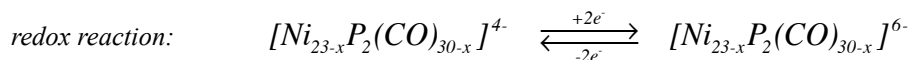
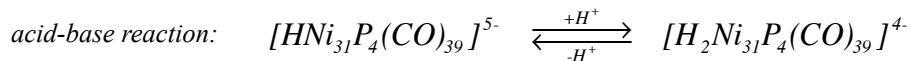


Scheme 9.3 - Examples of different types of carbonyl clusters that display redox properties.

Considering these two aspects, it was possible to notice that nickel-phosphorus homoleptic carbonyl clusters displayed a behaviour that was in accord with what would have been expected. In fact, some of these new clusters manifested acid-base and redox properties, as was shown in the previous discussion.

Most importantly, in few cases these features were not only deduced via IR spectroscopy analyses but confirmed via X-ray diffraction analyses (Scheme 9.4). As was thoroughly described in the foregoing chapters, it had been possible to obtain and to structurally characterise the  $[Ni_{23-x}P_2(CO)_{30-x}]^{6-}$  hexa-anion by reducing the corresponding  $[Ni_{23-x}P_2(CO)_{30-x}]^{4-}$  tetra-anion. It had also been possible to obtain and to structurally characterise the  $[H_2Ni_{131}P_4(CO)_{39}]^{4-}$  di-hydride by protonating the corresponding  $[HNi_{131}P_4(CO)_{39}]^{5-}$  mono-hydride. In both cases the progression of the reactions and the shifts of the recorded IR absorption frequencies were coherent with those generally displayed by carbonyl clusters.

- 
- <sup>1</sup> J. D. Roth, G. J. Lewis, L. K. Safford, X. Jiang, L. F. Dahl, M. J. Weaver; *J. Am. Chem. Soc.*, **1992** (114) 6159-6169
  - <sup>2</sup> F. Demartin, F. Fabrizi de Biani, C. Femoni, M. C. Iapalucci, G. Longoni, P. Macchi, P. Zanello; *Journal of Cluster Science*, **2001** (12) 61-74
  - <sup>3</sup> F. Calderoni, F. Demartin, F. Fabrizi de Biani, C. Femoni, M. C. Iapalucci, G. Longoni, P. Zanello; *Eur. J. Inorg. Chem.*, **1999** (4) 663-671



Scheme 9.4 - Reactions of two nickel-phosphorus homoleptic carbonyl clusters that displayed acid-base or redox properties. In these cases the processes were unequivocally confirmed through X-ray diffraction analyses, and the products were structurally characterised.

Therefore, it was assessed that nickel-phosphorus homoleptic carbonyl clusters behaved accordingly to carbonyl clusters in general terms of reactivity. As most carbonyl species, they were proved to have acid-base and redox properties. Despite these not being unusual results, the reported information were still significant as it was actually possible to ascertain that this new family of compounds did actually display some of the typical characteristics of carbonyl clusters.

\*\*\*

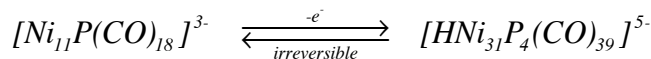
Besides, these new clusters were subjected to a wide range of reactivity trials with the aim to further investigate their characteristics and to better understand their behaviour. In the following paragraphs the more relevant results that were obtained for each specimen will be separately reported.

♦  $[\text{Ni}_{11}\text{P}(\text{CO})_{18}]^{3-}$

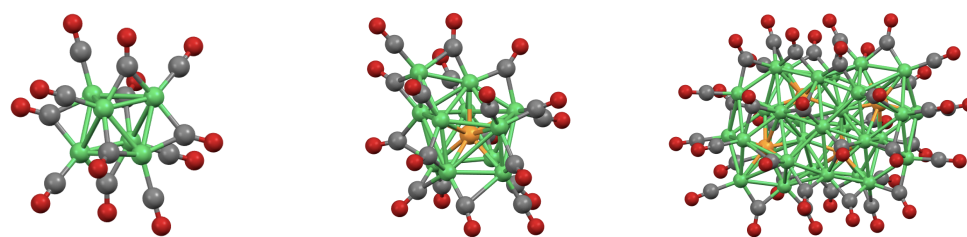
The reactivity of this cluster had been the least investigated, since it proved to be extremely difficult to obtain this species with an adequate purity degree. Just one reactivity trial was performed, yet the results proved to be highly significant. In fact, it was demonstrated that this carbonyl cluster was the intermediate product of the reaction between  $[\text{Ni}_6(\text{CO})_{12}]^{2-}$  and  $\text{PCl}_3$  - reaction that ultimately leads to the formation of  $[\text{HNi}_{31}\text{P}_4(\text{CO})_{39}]^{5-}$ .

In other words, this tri-anion was poorly stable in solution and could be easily oxidised by  $\text{PCl}_3$  itself or other mild oxidants. However, the oxidation process did

not change the anionic charge of the carbonyl cluster, but rather resulted in the formation of a different species (Scheme 9.5, Figure 9.7).



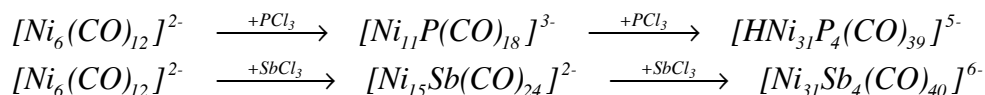
Scheme 9.5 - The reaction illustrates the irreversible oxidation process through which  $[\text{Ni}_{11}\text{P}(\text{CO})_{18}]^{3-}$  is transformed into  $[\text{HNi}_{31}\text{P}_4(\text{CO})_{39}]^{5-}$ .



$[\text{Ni}_6(\text{CO})_{12}]^{2-}$  - reagent       $[\text{Ni}_{11}\text{P}(\text{CO})_{18}]^{3-}$  - intermediate       $[\text{HNi}_{31}\text{P}_4(\text{CO})_{39}]^{5-}$  - product

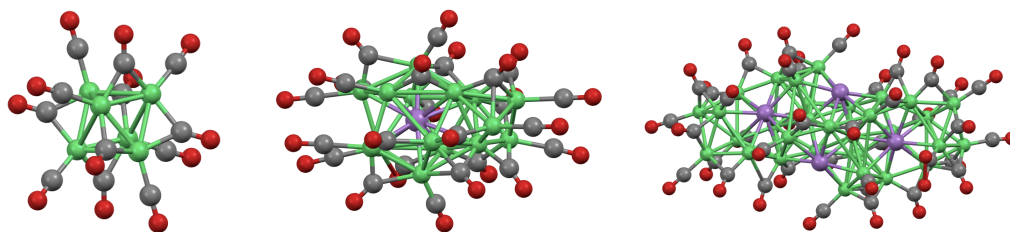
Figure 9.7 - Molecular structures of the three nickel-phosphorus cluster species that are involved in the reaction with  $\text{PCl}_3$ . Nickel atoms are represented in green, phosphorus atoms in orange, carbon atoms in grey, oxygen atoms in red.

Through this reactivity trial it was possible to confirm the previously hypothesised mechanism of the reaction between the nickel cluster precursor and  $\text{PCl}_3$ . Interestingly, a similar mechanism was reported in the literature concerning the consecutive syntheses of a couple of nickel-antimony carbonyl clusters.<sup>1</sup> It is in fact known that the reaction between  $[\text{Ni}_6(\text{CO})_{12}]^{2-}$  and  $\text{SbCl}_3$  follows an analogous pathway - first  $[\text{Ni}_{15}\text{Sb}(\text{CO})_{24}]^{2-}$  is formed, followed by  $[\text{Ni}_{31}\text{Sb}_4(\text{CO})_{40}]^{6-}$  (Scheme 9.6, Figure 9.8).



Scheme 9.6 - The reactions illustrate the analogous pathways of the reactions between the same nickel cluster precursor and two different group-15 element chlorides,  $\text{PCl}_3$  and  $\text{SbCl}_3$ .

<sup>1</sup> C. Femoni, M. C. Iapalucci, G. Longoni, P. H. Svensson; *Chem. Commun.*, **2000** (8) 655-656



$[Ni_6(CO)_{12}]^{2-}$  - reagent     $[Ni_{15}Sb(CO)_{24}]^{2-}$  - intermediate     $[Ni_{31}Sb_4(CO)_{40}]^{6-}$  - product

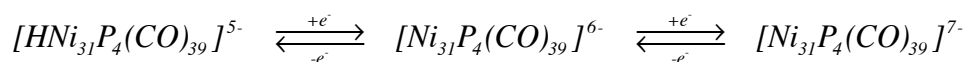
Figure 9.8 - Molecular structures of the three nickel-antimony cluster species involved in the reaction with  $SbCl_3$ . Nickel atoms are represented in green, antimony atoms in purple, carbon atoms in grey, oxygen atoms in red.

✦  $[HNi_{31}P_4(CO)_{39}]^{5-}$

This penta-anionic cluster was subjected to a comprehensive set of reactivity trials. Most importantly, it was possible to investigate its acid-base and redox properties.

The results concerning its acid-base behaviour have already been described in the previous section of this chapter - by protonating the mono-hydride  $[HNi_{31}P_4(CO)_{39}]^{5-}$  penta-anion it was possible to obtain the di-hydride  $[H_2Ni_{31}P_4(CO)_{39}]^{4-}$  tetra-anion.

Furthermore, this cluster displayed an interesting redox behaviour. It was indeed possible to reduce this carbonyl compound, yet the product of the reaction was not its precursor -  $[Ni_{11}P(CO)_{18}]^{3-}$ . The reduction of the  $[HNi_{31}P_4(CO)_{39}]^{5-}$  penta-anion followed a more common pathway. At first the cluster allegedly lost the hydride, and then the corresponding hepta-anion was obtained (Scheme 9.7). Moreover, by using a mild oxidant it was possible to revert the reduction process (Scheme 9.7). It is important to notice that during the oxidation reaction it was not possible to witness to the formation of the tetra-anion - *i.e.* it was not possible to further oxidise the penta-anion.

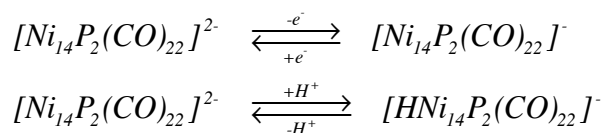


Scheme 9.7 - The alleged poly-anions involved in the reversible redox processes are reported.

♦  $[\text{Ni}_{14}\text{P}_2(\text{CO})_{22}]^{2-}$

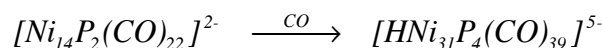
By investigating the reactivity of  $[\text{Ni}_{14}\text{P}_2(\text{CO})_{22}]^{2-}$  it was possible to uncover some interesting features. Despite its reduced nuclearity, this carbonyl species supposedly displayed mild redox and acid-base properties.

Unfortunately, the IR spectra that were recorded throughout the reduction and the deprotonation reactions were not clear enough to tentatively identify the derivative species. On the contrary, the oxidation and the protonation processes were less ambiguous, and had comparable outcomes. It was supposed that the  $[\text{Ni}_{14}\text{P}_2(\text{CO})_{22}]^-$  and the  $[\text{HNi}_{14}\text{P}_2(\text{CO})_{22}]^-$  mono-anions had formed (Scheme 9.8).

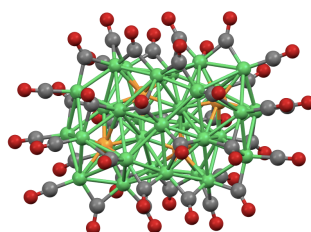


Scheme 9.8 - The alleged products of the redox and acid-base processes have been reported.

For what concerns the other reaction, interesting results were obtained throughout a controlled decomposition trial. In fact, it was observed that by setting  $[\text{Ni}_{14}\text{P}_2(\text{CO})_{22}]^{2-}$  under CO atmosphere it was possible to obtain the  $[\text{HNi}_{31}\text{P}_4(\text{CO})_{39}]^{5-}$  penta-anion (Scheme 9.9, Figure 9.9).

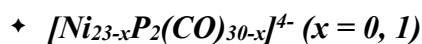


Scheme 9.9 - Controlled decomposition of  $[\text{Ni}_{14}\text{P}_2(\text{CO})_{22}]^{2-}$  under CO atmosphere.



$[\text{HNi}_{31}\text{P}_4(\text{CO})_{39}]^{5-}$

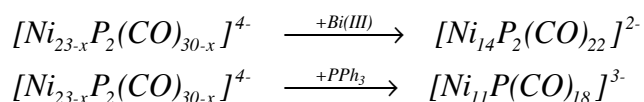
Figure 9.9 - Molecular structure of the cluster that can be obtained from  $[\text{Ni}_{14}\text{P}_2(\text{CO})_{22}]^{2-}$ . Nickel atoms are represented in green, phosphorus atoms in orange, carbon atoms in grey, oxygen atoms in red.



This species was used to perform a wide set of reactivity tests.

The results concerning its redox properties have already been described in the previous section of this chapter - by reducing the  $[Ni_{23-x}P_2(CO)_{30-x}]^{4-}$  tetra-anion it was possible to obtain the  $[Ni_{23-x}P_2(CO)_{30-x}]^{6-}$  hexa-anion.

Interestingly, this cluster displayed an unexpected behaviour when treated with less conventional reactants (Scheme 9.10, Figure 9.10). In fact, by oxidising it with a bismuth(III) salt it was possible to obtain  $[Ni_{14}P_2(CO)_{22}]^{2-}$ . Moreover, by treating it with a  $PPh_3$  solution it was possible to obtain  $[Ni_{11}P(CO)_{18}]^{3-}$ .



Scheme 9.10 - By treating  $[Ni_{23-x}P_2(CO)_{30-x}]^{4-}$  with different reactants it was possible to obtain other nickel-phosphorus homoleptic carbonyl clusters.

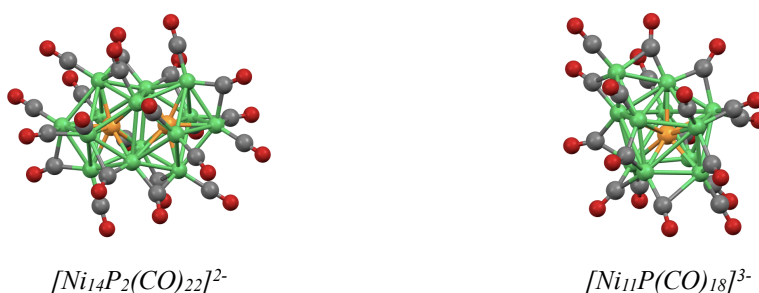


Figure 9.10 - Molecular structures of the clusters that can be obtained from  $[Ni_{23-x}P_2(CO)_{30-x}]^{4-}$ . Nickel atoms are represented in green, phosphorus atoms in orange, carbon atoms in grey, oxygen atoms in red.

\*\*\*

Due to these results, it was possible to assume that nickel-phosphorus carbonyl clusters followed the same general reactivity pattern of carbonyl clusters - in accord with their nuclearities and oxidation states.

Still, these new family of compounds also displayed a further set of characteristic reactions. It was in fact possible to discover that these clusters can transform



into one another. This behaviour was unexpected, as neither nickel-pnictogen nor transition metal-phosphorus clusters manifested it - except for nickel-antimony species, although to a minor extent.<sup>1,2</sup>

It is known that  $[\text{Ni}_{11}\text{Sb}_2(\text{CO})_{18}]^{3-}$  can be obtained by treating  $[\text{Ni}_{13}\text{Sb}_2(\text{CO})_{24}]^{3-}$  with  $\text{PPh}_3$ . Moreover,  $[\text{Ni}_{31}\text{Sb}_4(\text{CO})_{40}]^{6-}$  can be obtained by oxidising  $[\text{Ni}_{15}\text{Sb}(\text{CO})_{24}]^{2-}$ . However, the former reaction merely consists in the detachment of two  $\text{Ni}(\text{CO})_3$  appendices. Therefore, the latter remains the only example of reactivity trial that can be compared to those of homoleptic nickel-phosphorus carbonyl clusters.

## Conclusions

In the introduction it had been said that the aim of this work was to explore the chemistry of nickel and phosphorus in new heteroatomical molecular compounds - nickel-phosphorus homoleptic carbonyl clusters. This type of carbonyl clusters had never been reported in the scientific literature before, and therefore their syntheses, their characterization, and the study of their reactivity had been investigated.

As was illustrated in the previous chapters, these objectives were achieved. Six new species belonging to the family of nickel-phosphorus homoleptic carbonyl clusters were structurally characterised - *i.e.*  $[\text{Ni}_{11}\text{P}(\text{CO})_{18}]^{3-}$ ,  $[\text{Ni}_{14}\text{P}_2(\text{CO})_{22}]^{2-}$ ,  $[\text{Ni}_{23-x}\text{P}_2(\text{CO})_{30-x}]^{4-}$ ,  $[\text{Ni}_{29}\text{P}_5(\text{PO})(\text{CO})_{36}]^{4-}$ ,  $[\text{HNi}_{31}\text{P}_4(\text{CO})_{39}]^{5-}$ , and  $[\text{Ni}_{39}\text{P}_3(\text{CO})_{44}]^{6-}$  (Figure 9.11). For four of them it has also been possible to individuate a reproducible synthetic pathway, thus enabling to perform comprehensive characterisations and reactivity studies.

The thus obtained information allowed to better understand the behaviour of these species, and some distinctive properties were recognised. At the same time, it appeared clear that this type of carbonyl clusters were remarkably different from

<sup>1</sup> V. G. Albano, F. Demartin, C. Femoni, M. C. Iapalucci, G. Longoni, M. Monari, P. Zanello; *Journal of Organometallic Chemistry*, **2000** (593-594) 325-334

<sup>2</sup> C. Femoni, M. C. Iapalucci, G. Longoni, P. H. Svensson; *Chem. Commun.*, **2000** (8) 655-656

any other akin species. As was previously stated, it had been supposed that this new family of clusters could fit in that of nickel-pnictogen clusters, or that of transition metal-phosphorus clusters.

However, nickel-phosphorus carbonyl clusters did not appear to strictly belong to any of those two groups. Some of their characteristics were comparable to those of nickel-pnictogen clusters, yet others were comparable to those of transition metal-phosphorus clusters.

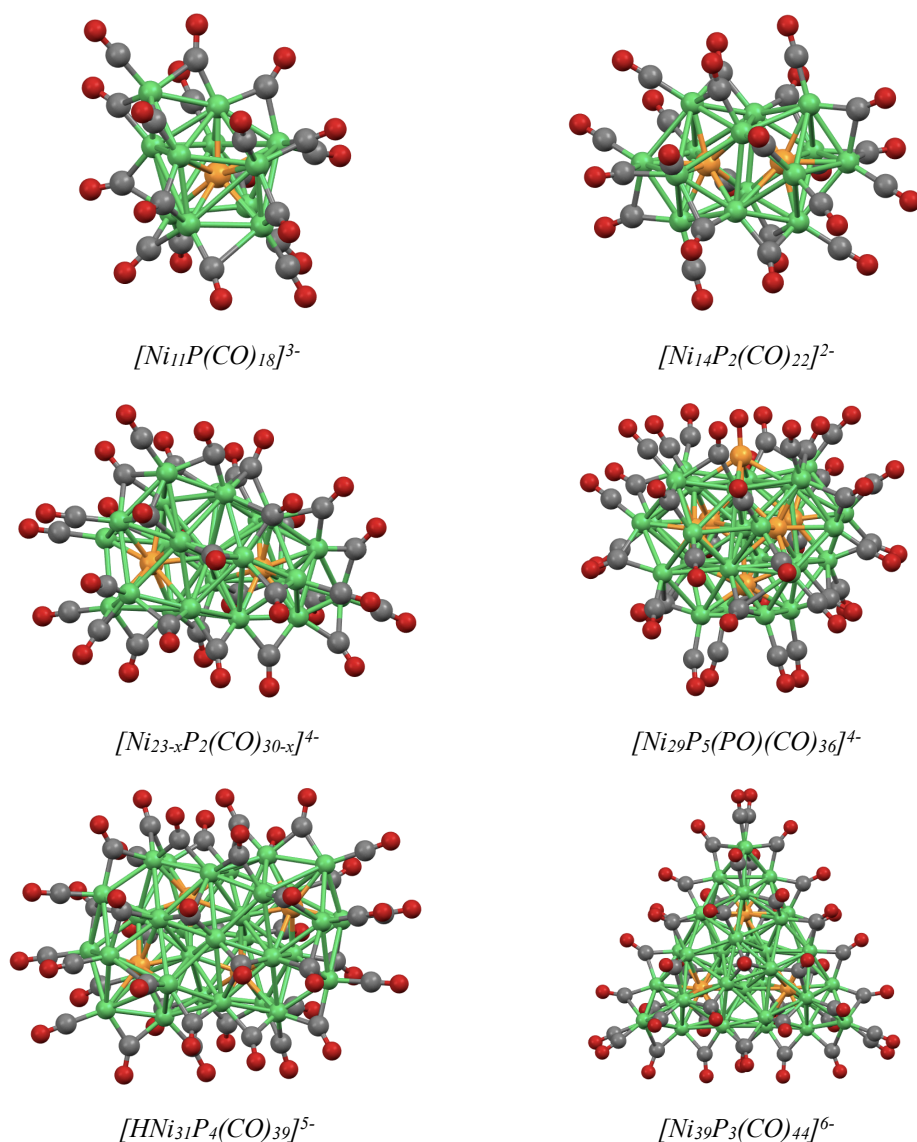


Figure 9.11 - Molecular structures of the clusters belonging to the new family of nickel-phosphorus homoleptic carbonyl clusters that were identified throughout this work. The species have been reported in order of nuclearity. Nickel atoms are represented in green, phosphorus atoms in orange, carbon atoms in grey, oxygen atoms in red.

Their syntheses were similar to those of nickel-pnictogen clusters, and in particular to those of nickel-antimony homoleptic carbonyl clusters.

Both groups involved syntheses between  $[\text{Ni}_6(\text{CO})_{12}]^{2-}$  and  $\text{PCl}_3$  or  $\text{SbCl}_3$ , and by simply varying the operative conditions it was possible to obtain different cluster products. Moreover, it was shown that some of the clusters belonging to both of these group could react and transform into one another.

However, the similarities end here. The divergence between the structures of nickel-phosphorus homoleptic carbonyl clusters and those of other nickel-pnictogen clusters was evident. The latter were characterised by a remarkably uniform structural pattern, and icosahedral frameworks were predominant. On the contrary, it was shown that the metallic skeletons of all nickel-phosphorus homoleptic carbonyl clusters were formed by similar building-blocks (Figure 9.12) based on squared anti-prismatic geometries. The same structural pattern was actually characteristic of the family of transition metal-phosphorus clusters.

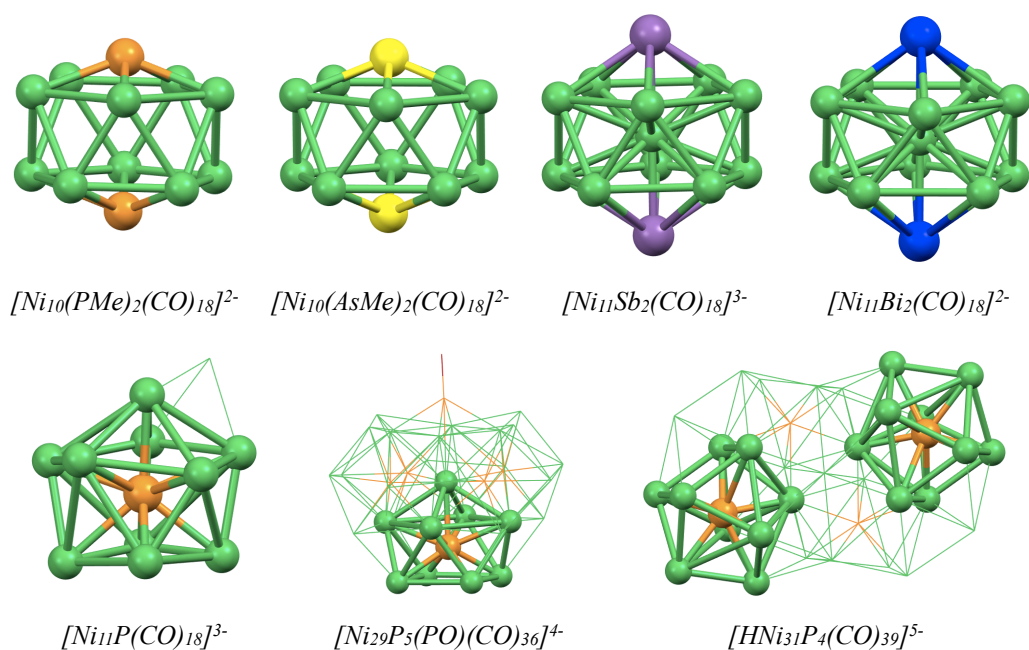


Figure 9.12 - In the upper row, the metallic skeletons of nickel-pnictogen carbonyl clusters have been reported. Their structures are based on icosahedral geometries: from left to right it is possible to see two non-centred icosahedra and two nickel-centred icosahedra. In the lower row, the metallic skeletons of nickel-phosphorus homoleptic carbonyl clusters have been reported. Their structures are formed by similar building-blocks, shaped as mono-capped anti-prisms. Nickel atoms are represented in green, phosphorus atoms in orange, antimony atoms in purple.

\*\*\*

It is easy to understand why it was difficult to rationalise the bivalent behaviour of nickel-phosphorus homoleptic carbonyl clusters. These carbonyl species appeared to belong to a group of their own, and this complexity is in part corresponding to that of the nickel-phosphorus binary phases.

On these bases, it seemed as the combination of these two elements - in molecular compounds as well as in the solid state - could trigger unexpected results.

This intuition was confirmed by the extensive structural analysis that was made concerning the bond lengths and the apparent distortions that affected the metallic skeletons of these clusters.

It was possible to demonstrate that phosphorus atoms could hardly enable for nickel atoms to be arranged in an icosahedral fashion.

First, it was shown that homo-metallic nickel cages were too large to be properly interacting with an interstitial phosphorus atom. The only  $\text{Ni}_{12}(\mu_{12}\text{-P})$  fragment that was individuated - within  $[\text{Ni}_{139}\text{P}_3(\text{CO})_{44}]^{6-}$  - suffered from severe elongation concerning the nickel-phosphorus bonds (Figure 9.13).

Then, it was shown that heteroatomical nickel icosahedral environments required to be stabilised by further factors, such as interstitial nickel atoms or non-carbonyl ligands. However, neither possibility was feasible. It was demonstrated that nickel-phosphorus icosahedral cages were too small to properly host a nickel atom. The only  $\text{Ni}_{10}\text{P}_2(\mu_{12}\text{-Ni})$  fragment that was individuated - within  $[\text{Ni}_{139}\text{P}_3(\text{CO})_{44}]^{6-}$  - suffered from severe elongation in the apical regions (Figure 9.13). For what concerns the presence of non-carbonyl ligands, it would have invalidated the aim of this work, that was focused on homoleptic cluster compounds. Still, in the literature there exist proof for alkyl-stabilised nickel-phosphorus icosahedral carbonyl clusters (Figure 9.13), as was previously reported.

Therefore, it was possible to assume that the almost null correlation between the structures of nickel-phosphorus and nickel-pnictogen carbonyl clusters was related to the relative atomic dimensions of nickel and phosphorus.

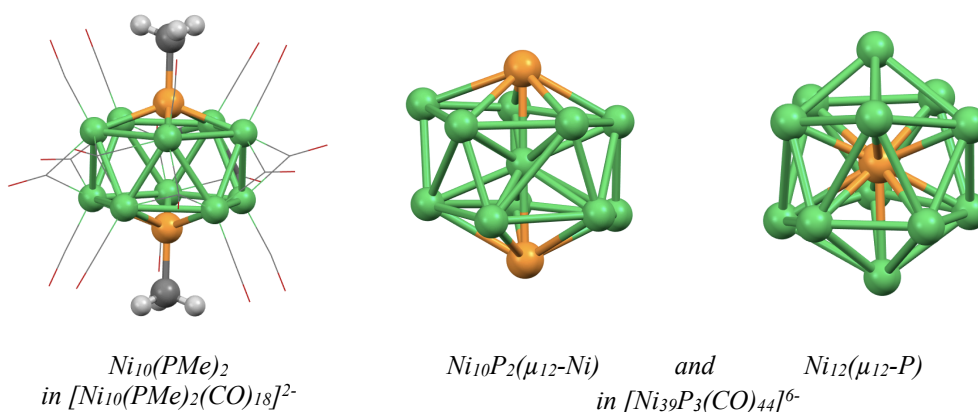


Figure 9.13 - Nickel-phosphorus icosahedral moieties. On the left, an alkyl-stabilised framework. On the right, two poorly stabilised frameworks that appear distorted. Nickel atoms are represented in green, phosphorus atoms in orange, carbon atoms in grey, hydrogen atoms in light grey, oxygen atoms in red.

However, other considerations emerged throughout the structural analyses, with somewhat ambiguous results. On one hand, it emerged that transition metal-phosphorus clusters were closely related to nickel-phosphorus homoleptic carbonyl clusters in structural terms. Clusters belonging to both groups displayed geometries that were based on squared or tetragonal anti-prisms (Figure 9.14).

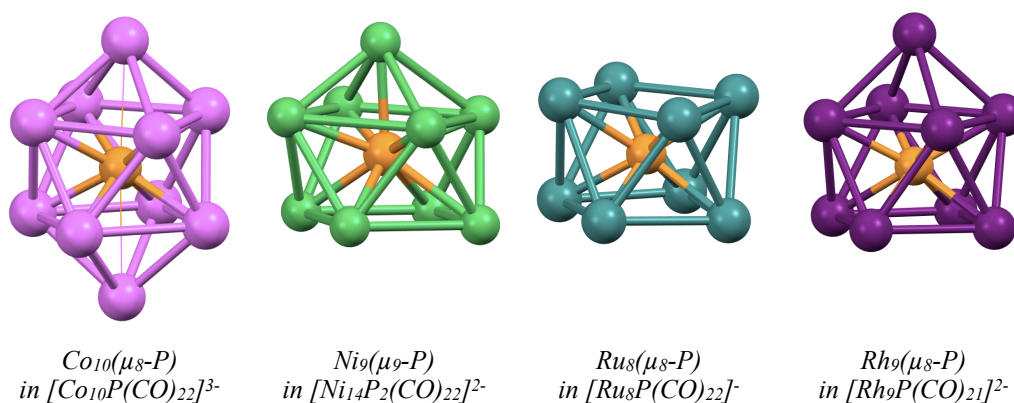


Figure 9.14 - Transition metal-phosphorus squared anti-prismatic moieties. From the left, a bi-capped framework, a mono-capped framework, a non-capped framework, and another mono-capped framework. Cobalt atoms are represented in pink, nickel atoms in green, ruthenium atoms in petrol-blue, rhodium atoms in violet, phosphorus atoms in orange.

Due to this, it appeared clear that phosphorus atoms in transition metal frameworks preferred lower coordinations, and adopted squared anti-prismatic geome-

tries. However, some details were contradictory.

In fact, in all but the nickel cages the phosphorus atoms displayed a coordination number equal to eight, regardless of the presence of the capping atoms. Moreover, the cobalt, the ruthenium, and the rhodium cages were remarkably regular in shape. On the contrary, the C.N. of phosphorus atoms in nickel cages was usually equal to nine or even ten, and the cages displayed slightly different configurations (Figure 9.15).

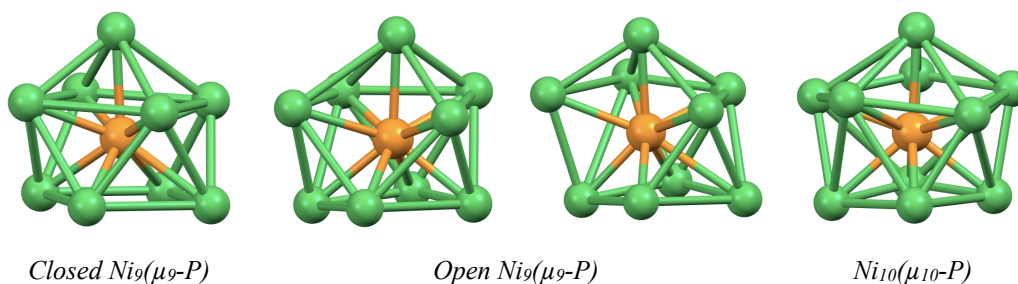


Figure 9.15 - Different types of nickel-phosphorus anti-prismatic moieties. Nickel atoms are represented in green, phosphorus atoms in orange.

Were it not for the existence of cobalt-phosphorus species, these discrepancies could have been attributed to the different dimensions of the metallic atoms. Nickel is a first-series transition metal -  $r_M$  equal to 1.24 Å - whilst ruthenium and rhodium are second-series transition metals -  $r_M$  equal to 1.46 Å and 1.42 Å, respectively. However, cobalt is a first-series transition metal as well -  $r_M$  equal to 1.26 Å - yet the structures of cobalt-phosphorus clusters did not display any of the deviances found in nickel-phosphorus clusters.

As a consequence of these considerations, it appeared even more clear that not only the relative dimensions of nickel and phosphorus atoms, but just the combination of these two elements could trigger unexpected results.

\*\*\*

In conclusion, this study allowed to identify and characterise a considerable number of new species. Due to this, to date the family of nickel-phosphorus ho-

moleptic carbonyl clusters is the most numerous one - amongst nickel-pnictogen or transition metal-phosphorus clusters.

These results left many future prospects and possibilities open for further investigations. In fact, by studying these new nickel-phosphorus species it was indeed possible to understand that these two elements behave in unique and sometimes unanticipated ways. This novel group of carbonyl species represents an interesting and promising conjunction between cluster compounds and binary phases.

In light of this, it was possible to presume that some of these clusters could be used as catalysts, just as nickel phosphides do. An early investigation showed that some of these nickel-phosphorus homoleptic carbonyl clusters could actually be used as precursors for heteroatomical nanoparticles.

$[\text{Ni}_{23-x}\text{P}_2(\text{CO})_{30-x}]^{4+}$  and  $[\text{HNi}_{131}\text{P}_4(\text{CO})_{39}]^{5-}$  were selected, due to their straightforward syntheses and their fair stability. Considering the procedures reported in the literature,<sup>1</sup> two different preliminary approaches were defined.

$[\text{Ni}_{23-x}\text{P}_2(\text{CO})_{30-x}]^{4+}$  was supported on silica, and then chemically decomposed in controlled acidic conditions.  $[\text{HNi}_{131}\text{P}_4(\text{CO})_{39}]^{5-}$  was not supported, and was thermally decomposed under reflux in DMF. In both cases it was possible to obtain heteroatomical nanoparticles, as confirmed via transmission electron microscopy - TEM - analyses (Figure 9.16).

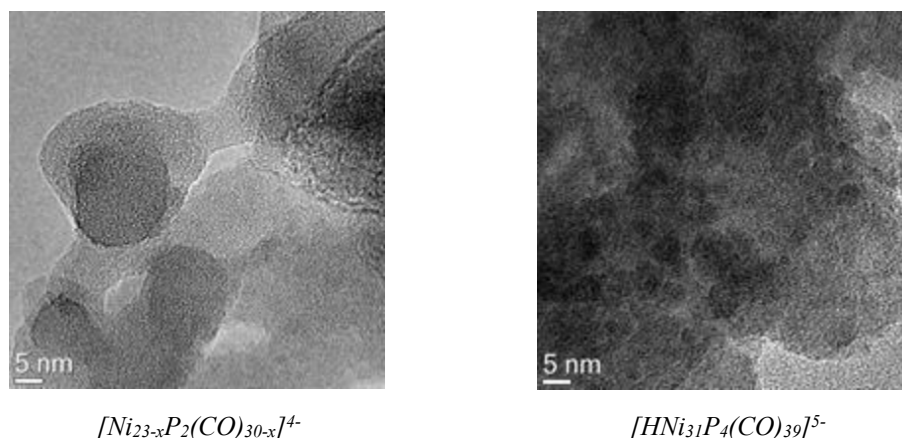


Figure 9.16 - TEM images of the samples obtained through controlled decomposition processes.

<sup>1</sup> S. Albonetti, R. Bonelli, J. E. Mengou, C. Femoni, C. Tiozzo, S. Zacchini, F. Trifirò; *Catalysis Today*, **2000** (137) 483-488

These significant results are nonetheless partial, and still non-conclusive. It was indeed possible to obtain nickel-phosphorus nanoparticles - both supported and non-supported - by decomposing nickel-phosphorus homoleptic carbonyl clusters, yet it will be necessary to repeat the tests in order to validate the processes. Besides, the limited data available did not allow to determine the composition of the nanoparticles that had been obtained. It was only possible to assess that the materials contained nickel as well as phosphorus. With further analyses it might be possible to discover which nickel phosphides had been obtained and their stoichiometric ratio.

Moreover, while it seems highly probable to be able to define a procedure with which to obtain nanoparticles from these clusters, their supposed catalytic behaviour has yet to be confirmed. A valid onset would be that of considering the usage of these nanoparticles as catalysts in hydrogen-involving reactions. In fact, most nickel-phosphorus nanoparticles and binary phases are used as hydroprocessing catalysts.

On these bases, it would be interesting to forward this catalytic project. In the future, the possible use of these new nickel-phosphorus carbonyl clusters as precursor for catalytic heteroatomical nanoparticles could be investigated. To date, the most common syntheses for nickel phosphides are simple,<sup>1,2,3,4,5</sup> yet there is little control on the final size and composition of the products. By using clusters as precursors, it could be possible to better control the nickel-phosphorus ratio of the obtained nanoparticles.

The development of a catalysis-oriented project based on the species individuated in this work would highlight new, interdisciplinary prospects. The future studies on nickel-phosphorus carbonyl clusters could therefore possibly focus on

---

<sup>1</sup> N. Grobert, K. Mandel, F. Dillon, A. A. Koos, Z. Aslam, K. Jurkschat, F. Cullen, A. Crossley, H. Bishop, K. Moh, C. Cavelius, E. Arzt; *Chem Commun.*, **2011** (47) 4108-4110

<sup>2</sup> D. Dong, X. H. Chen, W. T. Xiao, G. B. Yang, P. Y. Zhang; *Applied Surface Science*, **2009** (255) 7051-7055

<sup>3</sup> H. Zhang, Y. Lu, C. D. Gu, X. L. Wang, J. P. Tu; *Cryst. Eng. Comm.*, **2012** (14) 7942-7950

<sup>4</sup> L. Feng, H. Vrabel, M. Bensimon, X. Hu; *Phys. Chem. Chem. Phys.*, **2014** (16) 5917-5921

<sup>5</sup> S. Wie, M. Qiao, W. Zhou, G. Lu, H. He, K. Fan, T. Zhao, W. Yuan; *J. Phys. Chem. B*, **2005** (109) 24361-24368



these aspects, as well as on the completion of the characterisations that were reported in the previous chapters.



## **Experimental section**

All reactions were carried out by using Schlenk lines and related techniques, under inert atmosphere of nitrogen. All solvents and all solutions were dehydrated and de-gassed before use. Tetrahydrofuran was refluxed with sodium benzophenone and distilled, in order to obtain it anhydrous as well as oxygen-free.  $\text{PCl}_3$  was stocked under nitrogen in sealed, small-scaled custom test-tubes, in order to better preserve it. Once opened, the test-tubes were kept under nitrogen inside a larger Schlenk flask and consumed as soon as possible.

The reported IR spectra were recorded by a Perkin-Elmer Spectrum One FT-IR interferometer. The sensibility of the instrument was set at  $1\text{ cm}^{-1}$ . The cells were made of 1 mm thick fluorite.

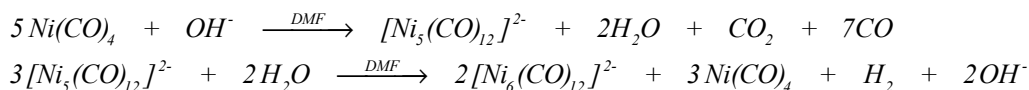
The reported ESI mass spectra were recorded by a Waters ZQ-4000 instrument, whose resolution was equal to 1000.

The reported  $^1\text{H}$  NMR spectra were recorded by a 600 MHz Varian instrument.

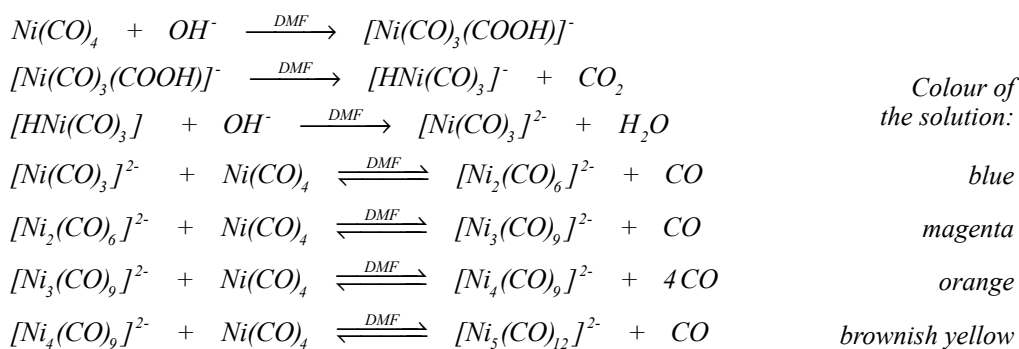
The reported  $^{31}\text{P}$  NMR spectra were recorded by a 400 MHz Varian instrument.

## Synthesis of $[NEt_4]_2[Ni_6(CO)_{12}]$

$[Ni_6(CO)_{12}]^{2-}$  is the most used precursor in the chemistry of nickel clusters. Its synthesis involves the reduction of nickel tetracarbonyl, performed with soda in anhydrous dimethylformamide. The reduction reaction evolves through numerous subsequent steps, and then hydrolysis is performed (Scheme 10.1, Scheme 10.2).



Scheme 10.1 - Reduction reaction and hydrolysis reaction.



Scheme 10.2 - Step by step reduction process. It is interesting to notice that each condensation step is characterised by a bright colour that appears in solution. This allows to easily follow the reaction progress just by observing the coloration of the reaction mixture.

To carry out this reaction, it is useful to saturate DMF with an excess of soda. This will provide a more basic and anhydrous solvent, and will rise the yield of the reaction.

A solution of *circa* 20 mL of  $Ni(CO)_4$  - PM = 170.73 g/mol,  $\rho = 1.319$  g/mL - is prepared in 100 mL of dimethylformamide, inside a 500 mL two-neck round flask. The round flask is provided with a cryostat set at -25 °C, and after cooling 10 g of NaOH - PM = 40.00 g/mol - are added to the solution. The so-prepared reaction mixture is stirred for eight hours. It is important to control the flux of produced gas in order to avoid air contamination. Throughout this period of time it is possible to observe that the solution changes in coloration - each colour corresponding to a different intermediate species. From colourless the solution turns blue almost immediately after adding soda. Eventually the solution turns

brownish-yellow, thus indicating the presence of  $[\text{Ni}_5(\text{CO})_{12}]^{2-}$  as well as the end of the reduction reaction.

Before proceeding with the hydrolysis reaction, it is necessary to wait for the gas efflux to cease. 200 mL of  $\text{H}_2\text{O}$  - PM = 18.02 g/mol,  $\rho = 1.00 \text{ g/mL}$  - are added to the solution and the reaction mixture is stirred for twelve hours.

At the end of the reaction  $[\text{Ni}_6(\text{CO})_{12}]^{2-}$  is in solution as sodic salt. It is necessary to perform a metathesis process with  $[\text{NEt}_4]^+$  - PM = 130.25 g/mol - or another organic ammonium cation of choice. An aqueous saturated solution of tetra-ethyl-ammonium chloride is prepared, and then drop-wise added to the vigorously stirred reaction mixture until complete precipitation of the cluster product. Once precipitated the cluster is filtered, and thoroughly washed with  $\text{H}_2\text{O}$  in order to eliminate the exceeding ammonium cation. The filtered solid is dried under vacuum and eventually extracted with acetone.

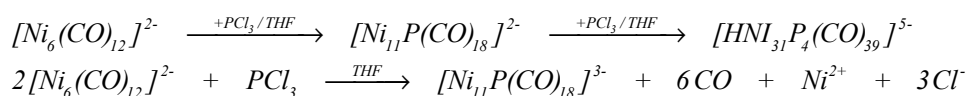
### \_\_\_\_\_ Characteristics

The cluster with this counter-ion is moderately soluble in tetrahydrofuran or methanol, and well soluble in acetone, acetonitrile, and more polar solvents. In solution the cluster displays a characteristic red colour, namely cherry-red.

$\nu_{\text{CO}}$  in acetonitrile - 1980s, 1810m, 1790m  $\text{cm}^{-1}$ .

### **Synthesis of $[\text{NEt}_4]_3[\text{Ni}_{11}\text{P}(\text{CO})_{18}]$**

This cluster is synthesised by oxidising  $[\text{NEt}_4]_2[\text{Ni}_6(\text{CO})_{12}]$  with anhydrous  $\text{PCl}_3$  (Scheme 10.3) in tetrahydrofuran. This cluster actually is an intermediate product of the reaction, therefore the cation and the solvent should not be changed in order to achieve a reasonable yield and an appropriate degree of purity.



*Scheme 10.3 - Representation of the mechanism of the oxidation of  $[\text{Ni}_6(\text{CO})_{12}]^{2-}$  with  $\text{PCl}_3$ , and proposed reaction mechanism for the synthesis of  $[\text{Ni}_{11}\text{P}(\text{CO})_{18}]^{3-}$ .*

In a two-neck round flask 3.42 g of  $[\text{NEt}_4]_2[\text{Ni}_6(\text{CO})_{12}]$  - PM = 948.78 g/mol - are dissolved in the minimum amount of tetrahydrofuran. Considering a stoichiometric ratio of 1 to 0.5 referred to the nickel cluster precursor, a 1:100 V/V solution of  $\text{PCl}_3$  - PM = 137.33 g/mol,  $\rho = 1.574 \text{ g/mL}$  - in tetrahydrofuran is prepared. The reactant solution is drop-wise added to the solution of the nickel cluster, considering aliquots of 1 mL at a time. After each addition it is fundamental to survey the presence of  $\text{Ni}(\text{CO})_4$ , and to apply vacuum in order to eliminate it whenever needed. After reaching the designed stoichiometric ratio the reaction mixture is dried, accurately washed with  $\text{H}_2\text{O}$  - five times, 20 mL per washing - and dried anew. The solid thus obtained is thoroughly washed with THF and then the product of interest  $[\text{NEt}_4]_3[\text{Ni}_{11}\text{P}(\text{CO})_{18}]$  (Figure 10.1) can be extracted with acetone.

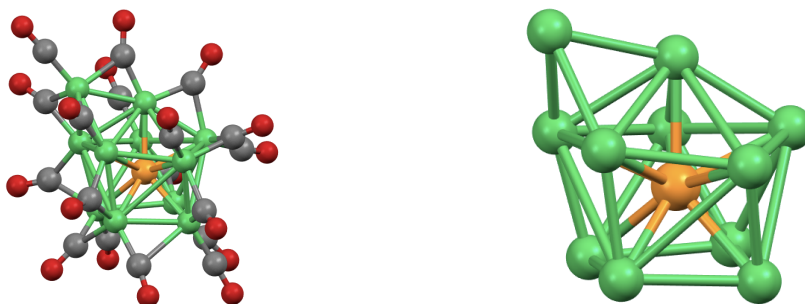


Figure 10.1 - Molecular structure and metallic skeleton of  $[\text{Ni}_{11}\text{P}(\text{CO})_{18}]^{3-}$ . Nickel atoms are represented in green, phosphorus atom in orange, carbon atoms in grey, oxygen atoms in red.

#### Characteristics

The cluster with this counter-ion is poorly soluble in tetrahydrofuran or methanol, and well soluble in acetone, acetonitrile, and more polar solvents. In solution the cluster displays a non-distinctive brown colour.

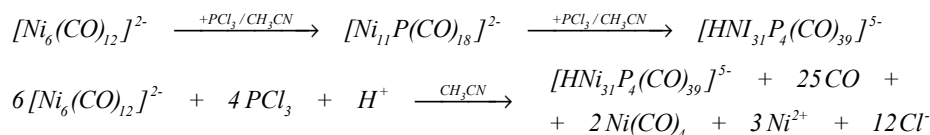
$\nu_{\text{CO}}$  in acetone - 1980s, 1848m  $\text{cm}^{-1}$ .

$\nu_{\text{CO}}$  in acetonitrile - 1982s, 1847m  $\text{cm}^{-1}$ .

#### Synthesis of $[\text{NEt}_4]_5[\text{HNi}_{31}\text{P}_4(\text{CO})_{39}]$

This cluster is synthesised by oxidising  $[\text{NEt}_4]_2[\text{Ni}_6(\text{CO})_{12}]$  with anhydrous  $\text{PCl}_3$  (Scheme 10.4) in acetonitrile. This cluster actually is the final product of

subsequent reactions, therefore the cation and the solvent can be changed without affecting yields or purity.



Scheme 10.4 - Representation of the mechanism of the oxidation of  $[\text{Ni}_6(\text{CO})_{12}]^{2-}$  with  $\text{PCl}_3$ , and proposed reaction mechanism for the synthesis of  $[\text{HNI}_{31}\text{P}_4(\text{CO})_{39}]^{5-}$ .

In a large Schlenk flask 2.24 g of  $[\text{NEt}_4]_2[\text{Ni}_6(\text{CO})_{12}]$  - PM = 948.78 g/mol - are dissolved in the minimum amount of acetonitrile. Considering a stoichiometric ratio of 1 to 0.7 referred to the nickel cluster precursor, a 1:100 up to 1:50 V/V solution of  $\text{PCl}_3$  - PM = 137.33 g/mol,  $\rho = 1.574$  g/mL - in acetonitrile is prepared. The reactant solution is drop-wise added to the solution of the nickel cluster, considering aliquots of 2 mL at a time. After few additions it is fundamental to survey the presence of  $\text{Ni}(\text{CO})_4$ , and to apply vacuum in order to eliminate it whenever needed. After reaching the designed stoichiometric ratio the reaction mixture is dried, accurately washed with  $\text{H}_2\text{O}$  - five times, 20 mL per washing - and dried anew. The solid thus obtained is thoroughly washed with THF and then the product of interest  $[\text{NEt}_4]_5[\text{HNI}_{31}\text{P}_4(\text{CO})_{39}]$  (Figure 10.2) can be extracted with acetone.

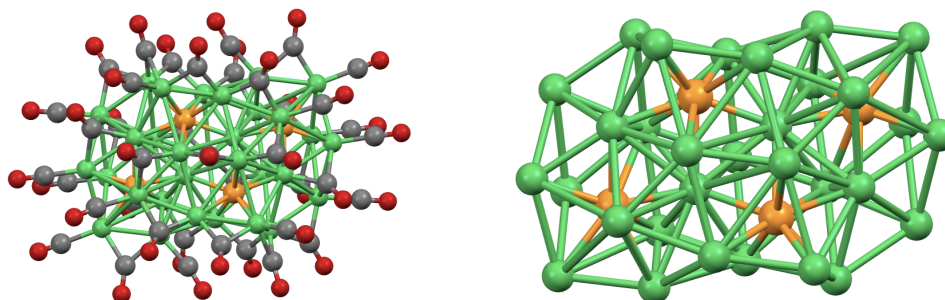


Figure 10.2 - Molecular structure and metallic skeleton of  $[\text{HNI}_{31}\text{P}_4(\text{CO})_{39}]^{5-}$ . Nickel atoms are represented in green, phosphorus atom in orange, carbon atoms in grey, oxygen atoms in red.

### Characteristics

The cluster with this counter-ion is not soluble in THF, and well soluble in ace-

tone, acetonitrile, and more polar solvents. In solution the cluster displays a non-distinctive brown colour, yet a trained eye can discern an orangish hue.

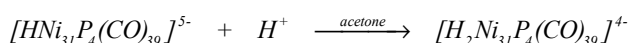
$\nu_{\text{CO}}$  in acetone - 2014s, 1873m  $\text{cm}^{-1}$ .

$\nu_{\text{CO}}$  in acetonitrile - 2013s, 1869m  $\text{cm}^{-1}$ .

$\nu_{\text{CO}}$  in dimethylformamide - 2005s, 1868m  $\text{cm}^{-1}$ .

### ***Synthesis of $[\text{NEt}_4]_4[\text{H}_2\text{Ni}_{31}\text{P}_4(\text{CO})_{39}]$***

This cluster is synthesised by protonating  $[\text{NEt}_4]_5[\text{HNi}_{31}\text{P}_4(\text{CO})_{39}]$  with any mild protic acid, as  $\text{HBF}_4$  (Scheme 10.5) in acetone.



*Scheme 10.5 - Schematic representation of the protonation of  $[\text{HNi}_{31}\text{P}_4(\text{CO})_{39}]^{5-}$ .*

In a small Schlenk flask 0.47 g of  $[\text{NEt}_4]_5[\text{HNi}_{31}\text{P}_4(\text{CO})_{39}]$  are dissolved in 15 mL of acetone. A 1:100  $\text{V}/\text{V}$  solution of  $\text{HBF}_4$  -  $\text{PM} = 87.81 \text{ g}/\text{mol}$ ,  $\rho = 1.18 \text{ g}/\text{mL}$  - in acetone is prepared. The reactant solution is drop-wise added to the solution of the nickel-phosphorus cluster, considering aliquots of no more than five drops at a time. It is fundamental to follow the course of the reaction through frequent IR spectroscopy analyses. The reaction is concluded whenever only the IR absorption frequencies of  $[\text{NEt}_4]_4[\text{H}_2\text{Ni}_{31}\text{P}_4(\text{CO})_{39}]$  (Figure 10.3) can be detected.

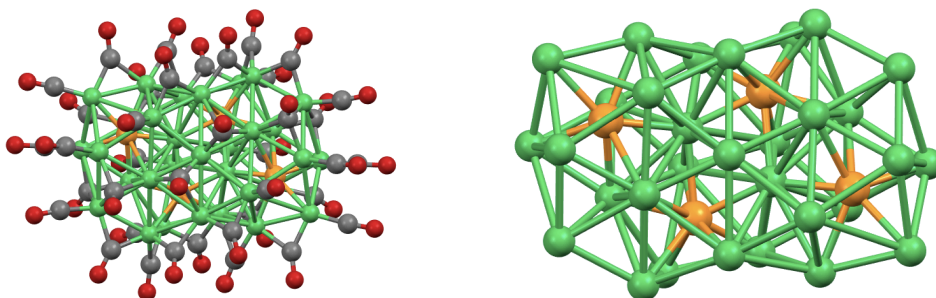


*Figure 10.3 - Molecular structure and metallic skeleton of  $[\text{H}_2\text{Ni}_{31}\text{P}_4(\text{CO})_{39}]^{4-}$ . Nickel atoms are represented in green, phosphorus atom in orange, carbon atoms in grey, oxygen atoms in red.*



Characteristics

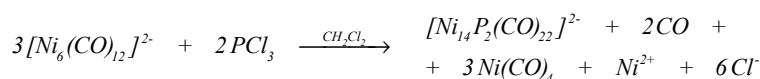
The cluster with this counter-ion is not soluble in THF, and well soluble in acetone, and acetonitrile. It de-protonates in more polar yet basic solvents. In solution the cluster displays the same colour of the penta-anion.

$\nu_{\text{CO}}$  in acetone - 2024s, 1885m  $\text{cm}^{-1}$ .

$\nu_{\text{CO}}$  in acetonitrile - 2022s, 1884m  $\text{cm}^{-1}$ .

**Synthesis of  $[\text{NBu}_4]_2[\text{Ni}_{14}\text{P}_2(\text{CO})_{22}]$** 

This cluster is synthesised by oxidising  $[\text{NBu}_4]_2[\text{Ni}_6(\text{CO})_{12}]$  with anhydrous  $\text{PCl}_3$  (Scheme 10.6) in dichloromethane. It is not possible to obtain this cluster when using different cations or solvents.



*Scheme 10.6 - Proposed reaction mechanism for the synthesis of  $[\text{Ni}_{14}\text{P}_2(\text{CO})_{22}]^{2-}$ .*

In a large Schlenk flask 2.76 g of  $[\text{NBu}_4]_2[\text{Ni}_6(\text{CO})_{12}]$  - PM = 1173.20  $\text{g/mol}$  - are dissolved in the minimum amount of dichloromethane. Considering a stoichiometric ratio of 1 to 0.5 referred to the nickel cluster precursor, a 1:100 up to 1:50  $\text{V/V}$  solution of  $\text{PCl}_3$  - PM = 137.33  $\text{g/mol}$ ,  $\rho = 1.574 \text{ g/mL}$  - in dichloromethane is prepared. The reactant solution is drop-wise added to the solution of the nickel cluster, considering aliquots of 2 mL at a time. It is fundamental to survey the presence of  $\text{Ni}(\text{CO})_4$ , and to apply vacuum in order to eliminate it whenever needed. Due to the volatile nature of the solvent, it is sometimes necessary to replenish it. After reaching the designed stoichiometric ratio the reaction mixture is dried, accurately washed with  $\text{H}_2\text{O}$  - five times, 20 mL per washing - and dried anew. The product of interest  $[\text{NBu}_4]_2[\text{Ni}_{14}\text{P}_2(\text{CO})_{22}]$  (Figure 10.4) can be extracted with  $\text{CH}_2\text{Cl}_2$ .

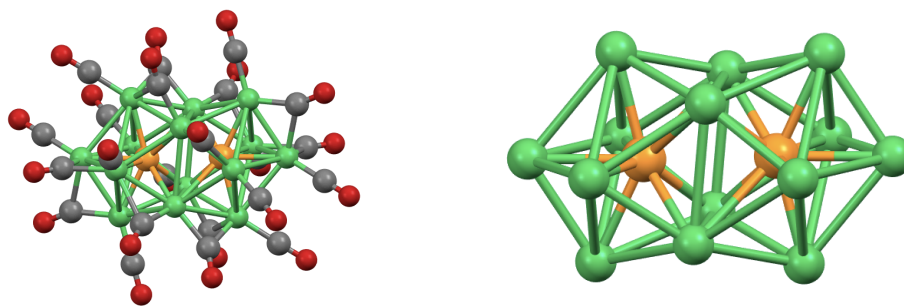


Figure 10.4 - Molecular structure and metallic skeleton of  $[Ni_{14}P_2(CO)_{22}]^{2-}$ . Nickel atoms are represented in green, phosphorus atom in orange, carbon atoms in grey, oxygen atoms in red.

### \_\_\_\_\_ Characteristics

The cluster with this counter-ion is soluble in dichloromethane, THF, and more polar solvents. In solution the cluster displays a non-distinctive brown colour, yet in crystalline form it displays a characteristic greenish hue.

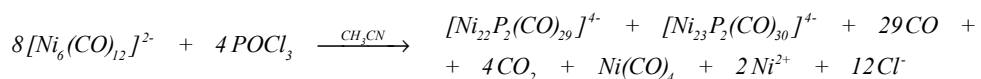
$\nu_{CO}$  in dichloromethane - 2033vs, 1862mw, 1837sh  $cm^{-1}$ .

$\nu_{CO}$  in tetrahydrofuran - 2029vs, 2006m, 1866w, 1843mw  $cm^{-1}$ .

$\nu_{CO}$  in acetonitrile - 2025s, 2000m, 1865mw, 1831w  $cm^{-1}$ .

### **Synthesis of $[NEt_4]_4[Ni_{23-x}P_2(CO)_{30-x}]$ ( $x = 0, 1$ )**

This cluster is synthesised by oxidising  $[NEt_4]_2[Ni_6(CO)_{12}]$  with  $POCl_3$  (Scheme 10.7) in acetonitrile. It is possible to obtain this cluster when using different cations.



Scheme 10.7 - Proposed reaction mechanism for the synthesis of  $[Ni_{23-x}P_2(CO)_{30-x}]^{4+}$  ( $x = 0, 1$ ).

In a large Schlenk flask 2.39 g of  $[NEt_4]_2[Ni_6(CO)_{12}]$  - PM = 948.78  $g/mol$  - are dissolved in the minimum amount of acetonitrile. Considering a stoichiometric ratio of 1 to 0.8 referred to the nickel cluster precursor, a 1:100 up to 1:50  $V/V$  solution of  $POCl_3$  - PM = 153.33  $g/mol$ ,  $\rho = 1.645$   $g/mL$  - in acetonitrile is prepared. The reactant solution is drop-wise added to the solution of the nickel cluster, con-

sidering aliquots of 2 mL at a time. It is fundamental to survey the presence of  $\text{Ni}(\text{CO})_4$ , and to apply vacuum in order to eliminate it whenever needed. After reaching the designed stoichiometric ratio the reaction mixture is dried, washed with  $\text{H}_2\text{O}$  - five times, 20 mL per washing - and dried. The solid thus obtained is thoroughly washed with THF, then  $[\text{NEt}_4]_4[\text{Ni}_{23-x}\text{P}_2(\text{CO})_{30-x}]$  (Figure 10.5) can be extracted with acetone.

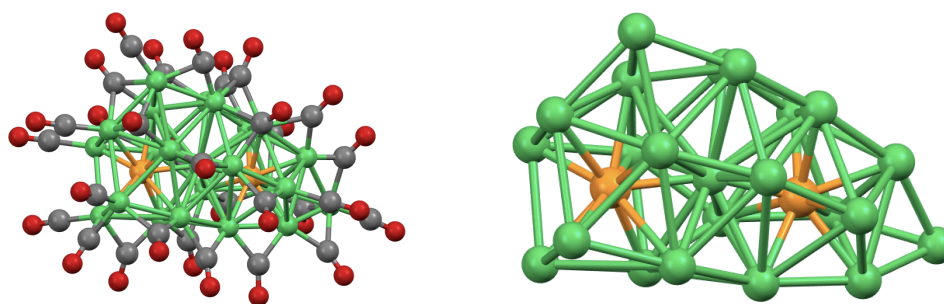


Figure 10.5 - Molecular structure and metallic skeleton of  $[\text{Ni}_{23-x}\text{P}_2(\text{CO})_{30-x}]^{4-}$ . Nickel atoms are represented in green, phosphorus atom in orange, carbon atoms in grey, oxygen atoms in red.

### Characteristics

The cluster with this counter-ion is not soluble in dichloromethane or THF, and well soluble in acetone, acetonitrile, and more polar solvents. In solution the cluster displays a non-distinctive brown colour.

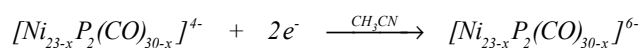
$\nu_{\text{CO}}$  in acetone - 2001s, 1872m  $\text{cm}^{-1}$ .

$\nu_{\text{CO}}$  in acetonitrile - 2005s, 1869m  $\text{cm}^{-1}$ .

$\nu_{\text{CO}}$  in dimethylformamide - 1995s, 1869m  $\text{cm}^{-1}$ .

### Synthesis of $[\text{NEt}_4]_6[\text{Ni}_{23-x}\text{P}_2(\text{CO})_{30-x}]$ ( $x = 0, 1$ )

This cluster is synthesised by reducing  $[\text{NEt}_4]_4[\text{Ni}_{23-x}\text{P}_2(\text{CO})_{30-x}]$  ( $x = 0, 1$ ) with any mild reducing agent, as sodium methoxide (Scheme 10.8) in acetonitrile.



Scheme 10.8 - Schematic representation of the reduction of  $[\text{Ni}_{23-x}\text{P}_2(\text{CO})_{30-x}]^{4-}$ .

In a small Schlenk flask 0.51 g of  $[\text{NEt}_4]_4[\text{Ni}_{23-x}\text{P}_2(\text{CO})_{30-x}]$  ( $x = 0, 1$ ) are dissolved in 15 mL of acetonitrile. A 1:100  $\text{m}/\text{v}$  solution of sodium methoxide -  $\text{Na}[\text{CH}_3\text{O}]$ ,  $\text{PM} = 54.02 \text{ g}/\text{mol}$  - in acetonitrile is prepared. The reactant solution is drop-wise added to the solution of the nickel-phosphorus cluster, considering aliquots of no more than ten drops at a time. The course of the reaction is followed through frequent IR spectroscopy analyses. The reaction is concluded whenever only the characteristic IR absorption frequencies of the  $[\text{NEt}_4]_6[\text{Ni}_{23-x}\text{P}_2(\text{CO})_{30-x}]$  (Figure 10.6) hexa-anion can be detected.

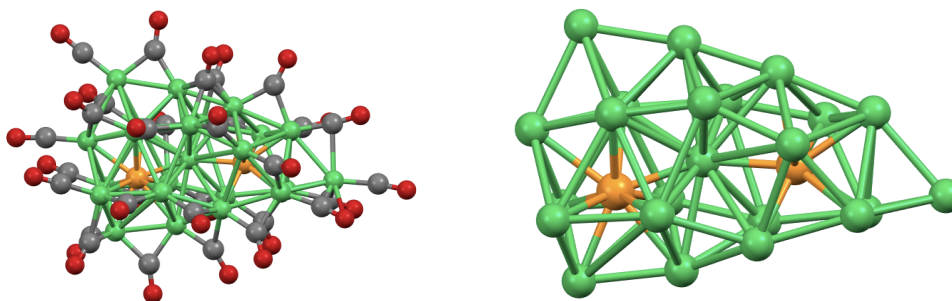


Figure 10.6 - Molecular structure and metallic skeleton of  $[\text{Ni}_{23-x}\text{P}_2(\text{CO})_{30-x}]^{6-}$ . Nickel atoms are represented in green, phosphorus atom in orange, carbon atoms in grey, oxygen atoms in red.

### Characteristics

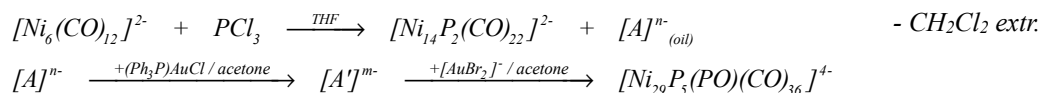
The cluster is not stable in solution, unless an excess of reducing agent is present, and is re-oxidised to its tetra-anionic form. In solution the cluster displays a non-distinctive brown colour.

$\nu_{\text{CO}}$  in acetonitrile - 1985s, 1848m  $\text{cm}^{-1}$ .

### ***Synthesis of $[\text{NEt}_4]_4[\text{Ni}_{29}\text{P}_5(\text{PO})(\text{CO})_{36}]$***

A reproducible and reliable synthesis for this cluster has yet to be tuned. The reactions that led to the formation of  $[\text{Ni}_{29}\text{P}_5(\text{PO})(\text{CO})_{36}]^{4-}$  will be described.

This cluster was synthesised by oxidising  $[\text{NMe}_3\text{Oct}]_2[\text{Ni}_6(\text{CO})_{12}]$  with anhydrous  $\text{PCl}_3$ ,  $(\text{Ph}_3\text{P})\text{AuCl}$ , and  $[\text{AuBr}_2]^-$  (Scheme 10.9) in different solvents.



Scheme 10.9 - Schematisation of the steps that led to the synthesis of  $[\text{Ni}_{29}\text{P}_5(\text{PO})(\text{CO})_{36}]^{4-}$ .

In a large Schlenk flask 4.50 g of  $[\text{NMe}_3\text{Oct}]_2[\text{Ni}_6(\text{CO})_{12}]$  - PM = 1032.94 g/mol - were dissolved in the minimum amount of tetrahydrofuran. A solution of unknown concentration of  $\text{PCl}_3$  - PM = 153.33 g/mol,  $\rho = 1.645$  g/mL - in THF was prepared. The reactant solution was drop-wise added to the solution of the nickel cluster, considering aliquots of few millilitres at a time. Vacuum was applied whenever needed to reduced the presence of  $\text{Ni}(\text{CO})_4$ . After having consumed all the nickel cluster precursor the reaction was deemed concluded, and the reaction mixture was precipitated and accurately washed with  $\text{H}_2\text{O}$ , and then dried anew. The known  $[\text{NMe}_3\text{Oct}]_2[\text{Ni}_{14}\text{P}_2(\text{CO})_{22}]$  was extracted with dichloromethane along with an unknown oily product,  $[\text{NMe}_3\text{Oct}]_n[\text{A}]$ . The oil was dissolved in DMF and underwent metathesis from  $[\text{NMe}_3\text{Oct}]^+$  to  $[\text{NEt}_4]^+$ . A solution of  $[\text{NEt}_4]_n[\text{A}]$  in acetone was treated with  $(\text{Ph}_3\text{P})\text{AuCl}$ , and later with  $[\text{AuBr}_2]^-$ , thus allowing to crystallise  $[\text{NEt}_4]_4[\text{Ni}_{29}\text{P}_5(\text{PO})(\text{CO})_{36}]^{4-}$  (Figure 10.7).

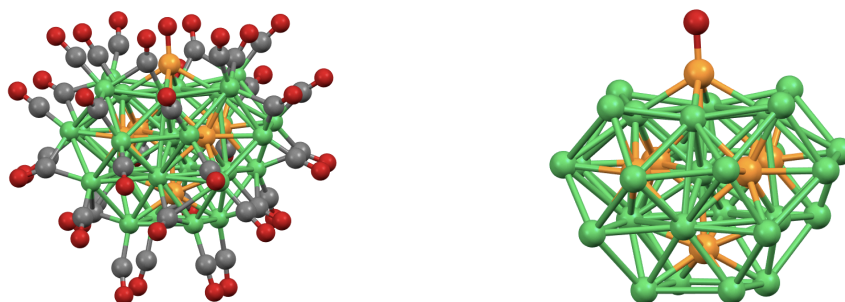


Figure 10.7 - Molecular structure and metallic skeleton of  $[\text{Ni}_{29}\text{P}_5(\text{PO})(\text{CO})_{36}]^{4-}$ . Nickel atoms are represented in green, phosphorus atom in orange, carbon atoms in grey, oxygen atoms in red.

### Characteristics

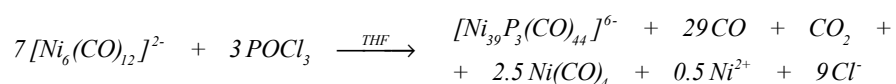
The available crystals deteriorated shortly after having performed the structural analysis, therefore the complete solubility of this cluster is still unknown.

$\nu_{\text{CO}}$  in acetone - 2028s, 1886m, 1830sh  $\text{cm}^{-1}$ .

### ***Synthesis of [NEt<sub>4</sub>]<sub>6</sub>[Ni<sub>39</sub>P<sub>3</sub>(CO)<sub>44</sub>]***

A reproducible and reliable synthesis for this cluster has yet to be tuned, despite the numerous efforts. In this chapter the one reaction that led to the formation of [Ni<sub>39</sub>P<sub>3</sub>(CO)<sub>44</sub>]<sup>6-</sup> will be described.

This cluster was synthesised by oxidising [NEt<sub>4</sub>]<sub>2</sub>[Ni<sub>6</sub>(CO)<sub>12</sub>] with anhydrous POCl<sub>3</sub> (Scheme 10.10) in acetonitrile.



*Scheme 10.10 - Proposed reaction mechanism for the synthesis of [Ni<sub>39</sub>P<sub>3</sub>(CO)<sub>44</sub>]<sup>6-</sup>.*

In a large Schlenk flask 2.39 g of [NEt<sub>4</sub>]<sub>2</sub>[Ni<sub>6</sub>(CO)<sub>12</sub>] - PM = 948.78 g/mol - were dissolved in the minimum amount of tetrahydrofuran. Considering a stoichiometric ratio of 1 to 1 referred to the nickel cluster precursor, a 1:75 V/V solution of POCl<sub>3</sub> - PM = 153.33 g/mol, ρ = 1.645 g/mL - in THF was prepared. The reactant solution was drop-wise added to the solution of the nickel cluster, considering aliquots of 1 mL at a time. Vacuum was not applied as the presence of Ni(CO)<sub>4</sub> was minimal. After reaching a 1 to 0.5 stoichiometric ratio the reaction was deemed concluded, and the reaction mixture was dried, accurately washed with H<sub>2</sub>O - five times, 20 mL per washing - and dried anew. The solid thus obtained was thoroughly washed with THF, acetone, and then the product [NEt<sub>4</sub>]<sub>6</sub>[Ni<sub>39</sub>P<sub>3</sub>(CO)<sub>44</sub>] (Figure 10.8) was extracted with acetonitrile.

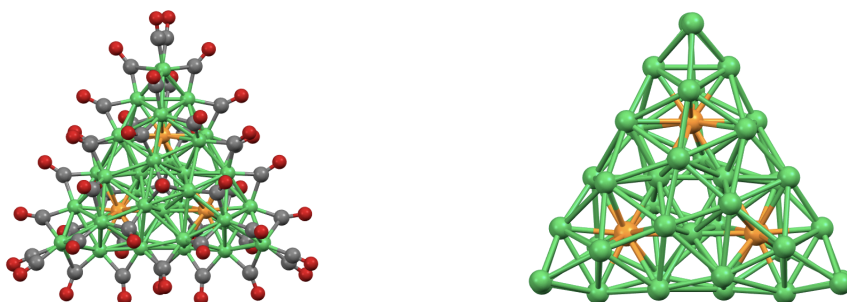


*Figure 10.8 - Molecular structure and metallic skeleton of [Ni<sub>39</sub>P<sub>3</sub>(CO)<sub>44</sub>]<sup>6-</sup>. Nickel atoms are represented in green, phosphorus atom in orange, carbon atoms in grey, oxygen atoms in red.*

\_\_\_\_\_ *Characteristics*

The cluster with this counter-ion is not soluble in THF or acetone, and well soluble in acetonitrile. In solutions the cluster displays a non-distinctive dark, brown colour.

$\nu_{\text{CO}}$  in acetonitrile - 1998s, 1868ms  $\text{cm}^{-1}$ .